Mechanisms of Catalytic Ozonation for the Removal of Low Molecular Weight acids

Author:
Yuan, Yuting

Publication Date:
2021

DOI:
https://doi.org/10.26190/unsworks/4031

Mechanisms of Catalytic Ozonation for the Removal of Low Molecular Weight acids

by

Yuting Yuan

A thesis submitted in fulfilment of the requirements for the degree of

Doctor of Philosophy

School of Civil and Environmental Engineering

Faculty of Engineering

The University of New South Wales

September, 2021

Thesis Title and Abstract | Declarations | Inclusion of Publications Statement | Corrected Thesis and Responses

Thesis Title

Mechanisms of Catalytic Ozonation for the Removal of Low Molecular Weight Acids

Thesis Abstract

Catalytic ozonation has been widely applied for the treatment of municipal and industrial wastewaters. However, the mechanism of catalytic ozonation is still unclear due to the controversial results reported in the literature with this limiting the optimization of this technology. In this study, we extended the mechanistic understanding of catalytic ozonation process via investigation of organic oxidation and O_3 decay in the presence of a wide variety of catalysts including commercially available Fe–impregnated activated carbon, CuO and Cu–Al layered double hydroxides. We also investigated the influence of salinity as well as the matrix on the performance of the catalytic ozonation process.

The Fe–impregnated activated carbon catalyst enhances O_3 decay with this generating hydroxyl which enhanced the formate oxidation at pH 3.0 compared to that observed in the presence of O_3 alone. The involvement of hydroxyl radicals in formate oxidation by the catalytic ozonation process is supported by the observation that the rate and extent of formate oxidation decreases in the presence of *tert*-butanol and Cl^- (which are known bulk hydroxyl radicals scavengers under acidic conditions). Moreover, the oxidation of formate mostly occurs in the solid–liquid interface and/or the bulk solution with adsorption playing no role in the overall oxidation. The catalyst is not active at pH 7.3 and 8.5 suggesting that only the protonated iron oxide surface sites generated strong oxidant(s) on interaction with O_3. A mechanistic kinetic model has been developed to adequately explain O_3 decay and formate oxidation during catalytic ozonation process.

In the presence of CuO and Cu–Al layered double hydroxides, oxidation of oxalate mostly occurs on the catalyst surface via interaction of surface oxalate complexes with surface–located oxidants. In contrast, the oxidation of formate occurs in the bulk solution as well as on the surface of the catalyst. Measurement of O_3 decay kinetics coupled with fluorescence microscopy image analysis corresponding to 7–hydroxycoumarin formation indicates that while surface hydroxyl groups in Cu–Al layered double hydroxides facilitate slow decay of O_3 resulting in the formation of hydroxyl radicals on the surface, CuO rapidly transforms O_3 into surface–located hydroxyl radicals and/or other oxidants. Futile consumption of surface–located oxidants via interaction with the catalyst surface is minimal for Cu–Al layered double hydroxides; however, it becomes significant in the presence of higher CuO dosages. Based on our understanding of the process, a kinetic model has been built and adequately explains the experimental results obtained.

In the study of influence of matrix on performance of ozonation and catalytic ozonation processes, our results reveal that the rate of ozone self–decay is considerably faster in phosphate buffer compared to carbonate buffered solution with this effect stemming from the differing hydroxyl radicals scavenging capacities of the buffering ions. Interestingly, while the nature of the buffer used affects the rate of organic oxidation in conventional ozonation, the overall extent of oxidation of formate and oxalate is the same for different buffering ions. The results obtained also indicate that the carbonate radicals generated as a result of carbonate ion – hydroxyl radical reaction can oxidize formate and oxalate however the oxidation of these organics by phosphate radicals appears to be minimal. The presence of phosphate ions also affects the surface chemistry of the two Cu–based catalysts tested here with phosphate ions inhibiting catalyst mediated O_3 decay and sorption of the target organic compounds on the catalyst surface. This inhibition of organic sorption and O_3 decay decreases the performance of the catalytic ozonation process in the presence of phosphate ions.

The presence of salts (particularly chloride ions) reduces the rate and extent of degradation of humic–like substances and low molecular weight neutrals (typical pollutants present in reverse osmosis concentrates of coal chemical wastewater) during catalytic ozonation using a commercially available Fe–loaded Al_2O_3 catalyst. Scavenging of aqueous O_3 by chloride ions and/or transformation of organics (particularly humics) to more hydrophobic form as a result of charge shielding between adjacent functional groups and/or intramolecular binding by cations inhibits the bulk oxidation of organics to a measurable extent. While the scavenging of aqueous hydroxyl radicals at the salt concentrations investigated here was minimal, the accumulation of chloride ions in the electric double layer near the catalyst surface, particularly when $pH<pH_{pzc}$, results in more significant scavenging of surface associated hydroxyl radicals, thereby decreasing the performance of the catalytic ozonation process.

We also discuss the caveats associated with the application of *tert*-butanol as a hydroxyl radicals scavenger in ozone–related studies. Our results show that *tert*-butanol may not be able to access surface located $^{\cdot}OH$ formed during catalytic ozonation. Furthermore, *tert*-butanol may also interfere with the adsorption of organics on the catalyst surface and decrease the adsorptive as well as concomitant oxidative removal of organics via non radical mediated pathways (if important). In addition, TBA scavenging results are inconclusive for mildly ozone reactive compounds due to switching from $O_3/^{\cdot}OH$ mediated oxidation in the absence of *tert*-butanol to O_3 driven oxidation in the presence of *tert*-butanol. The presence of *tert*-butanol may also decrease the rate of O_3 decay with the increased stability of O_3 in the presence of *tert*-butanol facilitating (i) direct oxidation of ozone–reactive organics in the bulk solution and/or (ii) diffusion of O_3 to the surface and subsequent surface–mediated oxidation of organics.

Overall, the results presented in thesis provide important insights into the catalytic ozonation process. The experimental methods and the kinetic modelling tools developed in this work can be used to gain mechanistic insights into catalytic ozonation process using other catalysts. Furthermore, the kinetic models developed here can be coupled with the hydrodynamics using computational fluid dynamics tools to predict and optimize the performance of full scale catalytic ozonation reactors.

Thesis Title and Abstract | Declarations | Inclusion of Publications Statement | Corrected Thesis and Responses

ORIGINALITY STATEMENT

☑ I hereby declare that this submission is my own work and to the best of my knowledge it contains no materials previously published or written by another person, or substantial proportions of material which have been accepted for the award of any other degree or diploma at UNSW or any other educational institution, except where due acknowledgement is made in the thesis. Any contribution made to the research by others, with whom I have worked at UNSW or elsewhere, is explicitly acknowledged in the thesis. I also declare that the intellectual content of this thesis is the product of my own work, except to the extent that assistance from others in the project's design and conception or in style, presentation and linguistic expression is acknowledged.

COPYRIGHT STATEMENT

AUTHENTICITY STATEMENT

☑ I certify that the Library deposit digital copy is a direct equivalent of the final officially approved version of my thesis.

Thesis Title and Abstract | Declarations | Inclusion of Publications Statement | Corrected Thesis and Responses

UNSW is supportive of candidates publishing their research results during their candidature as detailed in the UNSW Thesis Examination Procedure.

Publications can be used in the candidate's thesis in lieu of a Chapter provided:

- The candidate contributed **greater than 50%** of the content in the publication and are the "primary author", i.e. they were responsible primarily for the planning, execution and preparation of the work for publication.
- The candidate has obtained approval to include the publication in their thesis in lieu of a Chapter from their Supervisor and Postgraduate Coordinator.
- The publication is not subject to any obligations or contractual agreements with a third party that would constrain its inclusion in the thesis.

☑ The candidate has declared that **some of the work described in their thesis has been published and has been documented in the relevant Chapters with acknowledgement**.

A short statement on where this work appears in the thesis and how this work is acknowledged within chapter/s:

> The results from "Mechanistic insights into the catalytic ozonation process using iron oxide-impregnated activated carbon" in Water Research is contained in chapter 4. The results from "Kinetic modelling-assisted mechanistic understanding of the catalytic ozonation process using Cu-Al layered double hydroxides and copper oxide catalysts" in Environmental Science and Technology is contained in chapter 5. The results from "Comparison of performance of conventional ozonation and heterogeneous catalytic ozonation processes in phosphate and bicarbonate buffered solutions" in ACS Environmental Science &Technology Engineering in contained in chapter 6. The results from "Influence of salinity on the heterogeneous catalytic ozonation process: Implications to treatment of high salinity wastewater" in Journal of Hazardous Materials is contained in chapter 7. Acknowledge of each work has been made at the beginning of the relevant chapter.

Candidate's Declaration

I declare that I have complied with the Thesis Examination Procedure.

Abstract

Catalytic ozonation has been widely applied for the treatment of municipal and industrial wastewaters. However, the mechanism of catalytic ozonation is still unclear due to the controversial results reported in the literature with this limiting the optimization of this technology. In this study, we extended the mechanistic understanding of catalytic ozonation process via investigation of organic oxidation and O_3 decay in the presence of a wide variety of catalysts including commercially available Fe–impregnated activated carbon, CuO and Cu–Al layered double hydroxides. We also investigated the influence of salinity as well as the matrix on the performance of the catalytic ozonation process.

The Fe–impregnated activated carbon catalyst enhances O_3 decay with this generating hydroxyl which enhanced the formate oxidation at pH 3.0 compared to that observed in the presence of O_3 alone. The involvement of hydroxyl radicals in formate oxidation by the catalytic ozonation process is supported by the observation that the rate and extent of formate oxidation decreases in the presence of *tert*-butanol and Cl^- (which are known bulk hydroxyl radicals scavengers under acidic conditions). Moreover, the oxidation of formate mostly occurs in the solid–liquid interface and/or the bulk solution with adsorption playing no role in the overall oxidation. The catalyst is not active at pH 7.3 and 8.5 suggesting that only the protonated iron oxide surface sites generated strong oxidant(s) on interaction with O_3. A mechanistic kinetic model has been developed to adequately explain O_3 decay and formate oxidation during catalytic ozonation process.

In the presence of CuO and Cu–Al layered double hydroxides, oxidation of oxalate mostly occurs on the catalyst surface via interaction of surface oxalate complexes with surface−located oxidants. In contrast, the oxidation of formate occurs in the bulk

solution as well as on the surface of the catalyst. Measurement of O_3 decay kinetics coupled with fluorescence microscopy image analysis corresponding to 7−hydroxycoumarin formation indicates that while surface hydroxyl groups in Cu−Al layered double hydroxides facilitate slow decay of O_3 resulting in the formation of hydroxyl radicals on the surface, CuO rapidly transforms O_3 into surface−located hydroxyl radicals and/or other oxidants. Futile consumption of surface−located oxidants via interaction with the catalyst surface is minimal for Cu−Al layered double hydroxides; however, it becomes significant in the presence of higher CuO dosages. Based on our understanding of the process, a kinetic model has been built and adequately explains the experimental results obtained.

In the study of influence of matrix on performance of ozonation and catalytic ozonation processes, our results reveal that the rate of ozone self−decay is considerably faster in phosphate buffer compared to carbonate buffered solution with this effect stemming from the differing hydroxyl radicals scavenging capacities of the buffering ions. Interestingly, while the nature of the buffer used affects the rate of organic oxidation in conventional ozonation, the overall extent of oxidation of formate and oxalate is the same for different buffering ions. The results obtained also indicate that the carbonate radicals generated as a result of carbonate ion – hydroxyl radical reaction can oxidize formate and oxalate however the oxidation of these organics by phosphate radicals appears to be minimal. The presence of phosphate ions also affects the surface chemistry of the two Cu–based catalysts tested here with phosphate ions inhibiting catalyst mediated O_3 decay and sorption of the target organic compounds on the catalyst surface. This inhibition of organic sorption and O_3 decay decreases the performance of the catalytic ozonation process in the presence of phosphate ions.

The presence of salts (particularly chloride ions) reduces the rate and extent of degradation of humic–like substances and low molecular weight neutrals (typical pollutants present in reverse osmosis concentrates of coal chemical wastewater) during catalytic ozonation using a commercially available Fe−loaded Al_2O_3 catalyst. Scavenging of aqueous O_3 by chloride ions and/or transformation of organics (particularly humics) to more hydrophobic form as a result of charge shielding between adjacent functional groups and/or intramolecular binding by cations inhibits the bulk oxidation of organics to a measurable extent. While the scavenging of aqueous hydroxyl radicals at the salt concentrations investigated here was minimal, the accumulation of chloride ions in the electric double layer near the catalyst surface, particularly when $pH<pH_{pzc}$, results in more significant scavenging of surface associated hydroxyl radicals, thereby decreasing the performance of the catalytic ozonation process.

We also discuss the caveats associated with the application of *tert*-butanol as a hydroxyl radicals scavenger in ozone–related studies. Our results show that *tert*-butanol may not be able to access surface located $^{\bullet}OH$ formed during catalytic ozonation. Furthermore, *tert*-butanol may also interfere with the adsorption of organics on the catalyst surface and decrease the adsorptive as well as concomitant oxidative removal of organics via non radical mediated pathways (if important). In addition, TBA scavenging results are inconclusive for mildly ozone reactive compounds due to switching from $O_3/^{\bullet}OH$ mediated oxidation in the absence of *tert*-butanol to O_3 driven oxidation in the presence of *tert*-butanol. The presence of *tert*-butanol may also decrease the rate of O_3 decay with the increased stability of O_3 in the presence of *tert*-butanol facilitating (i) direct oxidation of ozone−reactive organics in the bulk solution and/or (ii) diffusion of O_3 to the surface and subsequent surface−mediated oxidation of organics.

Overall, the results presented in thesis provide important insights into the catalytic ozonation process. The experimental methods and the kinetic modelling tools developed in this work can be used to gain mechanistic insights into catalytic ozonation process using other catalysts. Furthermore, the kinetic models developed here can be coupled with the hydrodynamics using computational fluid dynamics tools to predict and optimize the performance of full scale catalytic ozonation reactors.

Acknowledgments

During my PhD interview, the committee raised a question that what you would feel when working with the project in the the field that you have not stepped into before. My answer was “That must be very interesting and I am quite keen to learn new skills.” Probably due to the positive impression I left on the committee, I was offered a scholarship to conduct my PhD at University of New South Wales (UNSW). However, I started to realise that this was an exact summary of PhD projects after meeting with my supervisor Scientia Prof. T. David Waite on 16th June 2017.

This is the start of my story with the team in Water Research Centre (WRC), School of Civil and Environmental Engineering, UNSW. I feel so grateful to have David as my supervisor who has been strongly supportive both academically and mentally. David is a sharp captain who controls the overall direction of my project and is so sensitive to the research niches where I should head to. It has been joyful to talk to him during our regular meetings when he would provide valuable comments. He would feel excited about my progresses as well as encourage me faithfully when my experiments went wrong with this giving me the confidence to discuss my thoughts and questions with him.

It has been a privilege for me to work closely with my co-supervisors Dr. Shikha Garg and Dr. Jinxing Ma. Their extensive feedbacks and creative ideas would always bring me out from the desperation of my experiments. Shikha gives me constant guidance during my project and responses to any requires as soon as she can. Shikha has contributed essentially to completion of this piece of work and the timely submission of this thesis is owing to her selfless assistance and coherent management. Her dedication to work and intelligence set a good example for me throughout my PhD and would continue to inspire me in the future. Jinxing provides insights from different angles with this furnishing effective solutions for the encountered problems. I would like to thank the two intelligent and dedicated scientists for their help during my PhD.

WRC is a friendly committee where I have benefited loads of help from the lab team including lab managers Dr. Gautam Chattopadhyay and Dr. Nhat Le-Minh, technical officers Dr. Artur Ziolkowski, Mr Chun Ong, Dr. Vivian Xiao and Ms Juee Vorha, and the administrative team including Mr Robert Steel and Ms Uttra Benton.

I deeply appreciate the training guidance from Dr. Richard Collins for radiation lab, Dr. Christopher Miller for UV and fluorescence measurement, Dr. Adele Jones for Fourier transform infrared spectroscopy analysis, Dr. Taehwan Kim for Brunauer–Emmett–Teller surface area measurement, Dr. Changyong Zhang for total organic carbon analysis, Dr Yingying Sun for fluorescent microscope measurement, Dr. Hongyan Rong for hydrogen peroxide measurement, Dr Guowei Xing for assistance in ozonation experiments, Dr Andrew Kinsela for Inductively coupled plasma optical emission spectroscopy analysis and Dr Yuan Wang for the inspiring thoughts and discussion during our technical meetings. Valuable help from technicians (Dr Ruoming Tian, Dr Yu Wang, Dr Yin Yao, Dr Bill Dong, Dr Khorshed Chinu and Dr Martin Bucknall) in Mark Wainwright analytical centre UNSW is gratefully acknowledged.

Great thanks to my friends and colleagues: Jieli Xie, Shaoyue Ma, Zhaozhi Zheng, Lingqi Tan, Zhao Song, Yufan Chen, Jiangzhou Xie, Mahshid Mortazavi, Dr Lily Wang and Dr Yating Tang. Having you as my friends makes me feel less lonely and enjoy the relaxing and pleasant life in Sydney.

In a personal level, I am deeply indebted to my grandmother, parents and my boyfriend. Over the past twelve years, I am not able to repay them with good harvest due to the "endless" study while receiving their continuous trust and unconditional love. At this moment, I dedicate all my achievements to them including this thesis.

In the retrospect, the four-year stay in Sydney has been a wonderful journey, a peaceful and sunny city with beautiful coastal lines and smiling people. It is a bit regretful that we have been in lockdown due to COVID since this June and it would be a permanent loss for me not being able to complete the "100 must-have activities" before leaving Sydney. Hope the COVID epidemic could be under control and people come back to the normal routines as soon as possible.

Yuting Yuan

Sydney, September 2021

Table of Contents

List of figures

List of Tables

Abbreviations

Acetonitrile: ACN

Brunauer–Emmett–Teller: BET

Barrett−Joyner−Halenda: BJH

Beijing OriginWater: BOW

Coal Coal chemical industry: CCI

Chemical Research Institute: CCRI

Coal chemical wastewater: CCW

Computational fluid dynamics: CFD

Chemical oxygen demand: COD

Cu−Al layered double hydroxides: Cu−Al LDHs

Cu oxide: CuO

Electric double layer: EDL

Electron paramagnetic resonance: EPR

Gas chromatography−mass spectrometry: GC−MS

Humic acid: HA

High performance liquid-chromatography: HPLC

Inductively coupled plasma atomic emission spectroscopy: ICP−OES

Kinetic isotope effect: KIE

Liquid chromatography−organic carbon detection: LC−OCD

Low molecular weight: LMW

Milli−Q: MQ

Multiwalled carbon nanotube: MWCNT

Non−reactive products: NRP

Ozone: O_3

Oxygen vacancies: OVs

Heterogeneous catalytic ozonation: HCO

Principal Component Analysis: PCA

para-chlorobenzoic acid: *p*-CBA

Reverse osmosis: RO

RO membrane concentrate: ROC

Reactive oxidative species: ROS

Scanning electron microscopy with energy dispersive X−ray spectroscopy: SEM−EDX

tert-butanol: TBA

Total organic carbon: TOC

X−ray diffraction: XRD

X−ray photoelectron spectroscopy: XPS

Nitric acid: HNO_3

Surface hydroxyl groups: $\equiv^{\bullet}OH$

Point of zero charge: pH_{pzc}

Surface atomic oxygen: O^{*}

Superoxide: $O_2^{\bullet-}$

Lanthanum manganite perovskites: LMO

Singlet oxygen: $^1O_2$

Surface O_3: $\equiv O_3$

Coumarin: COU

7−hydroxyl COU: 7−HC

Nitrone traps such as 5,5−dimethylpyrroline−N−oxide: DMPO

5−*tert*−butoxycarbonyl−5methyl−1−pyrroline−N−oxide: BMPO

Formate: $HCOO^-$ or FA

Oxalate: $C_2O_4^-$ or OA

Hydroxyl ions: OH^-

Deuterated water: D_2O

Sodium hydroxide: NaOH

Hydrophilic fraction: HPI

Hydrophobic fraction: HPO

Transphilic fraction: TPI

Sulfamethoxazole: SMX

1,3 dichlorobenzene: *m*–DCB

5−sulfosalicylic acid: SSal

Rhodamine B: RhB

Chapter 1 Introduction

Ozone (O_3), first discovered in 1839 by the German chemist C. F. Schonbein (1799−1869), is a powerful oxidant with three oxygen atoms in a resonance structure (Fig.1.1).[1] The lack of electrons on the terminal oxygen renders O_3 electrophilic with the excess negative charge on the other oxygen confering nucleophilic character. These properties enable O_3 to be an extremely reactive molecule towards many inorganic and organic compounds.[2-5]

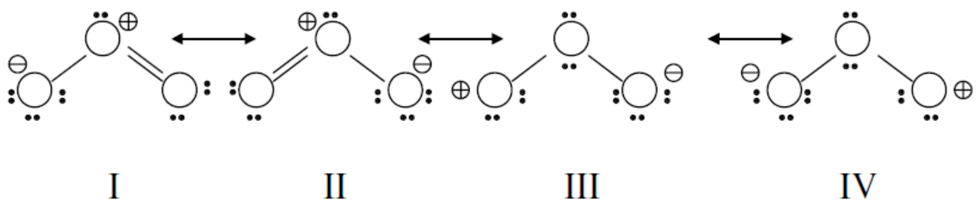

Figure 1.1 Resonance structure of ozone [1]

The oxidation of organic compounds in the ozonation process occurs via (1) direct oxidation by molecular O_3 and (2) indirect oxidation by reactive oxidative species (ROS) such as $^{\bullet}OH$ generated via O_3 decay.[6-10] Conventional ozonation, which mainly relies on the oxidation power of O_3, has been extensively used for wastewater treatment and water purification.[11-17] However, molecular O_3 is quite selective and reacts with compounds characterized with aromatic rings, unsaturated bonds, and electron-rich moieties.[15, 18-20] The generation of organic intermediates, such as aldehydes, ketones and carboxylic acid which are quite ozone-refractory, is often observed during the conventional ozonation process.[12, 18, 21] Complete mineralization of organics is hardly achieved by the conventional ozonation process and tertiary treatment is usually required to further polish the ozonated waters.[22, 23] Although hydroxyl radicals ($^{\bullet}OH$), a powerful and non-selective oxidant, can be generated via O_3 self-decay in the conventional ozonation process, this pathway is favoured under alkaline conditions and/or on activation by specific groups of organics only.[18, 21]

To enhance the oxidation of O_3-resistant organics, heterogeneous catalytic ozonation (HCO) has been developed where the presence of solid catalysts improves the oxidation of target organic compounds. In HCO, O_3 is transformed into ROS, especially $^{\bullet}OH$ which has a higher oxidation potential (2.80 *vs* SHE) compared to the oxidation potential of O_3 (2.08 *vs* SHE).[24] The $^{\bullet}OH$ reacts with most organic compounds with a second order rate constant in the order of $10^8 - 10^{10}$ $M^{-1}\cdot s^{-1}$,[22] thereby increasing the rate and extent of organic mineralization.

In addition to radical mediated ozonation processes, direct oxidation of adsorbed organics by molecular O_3 has been reported to be an alternative for organic oxidation.[25, 26] Usually, adsorption of organics on the surface either improves the reactivity of the organics by forming surface‒organic complexes or enhances the availability of organics towards the surface-generated oxidants.[25, 26] However, it has also been suggested that adsorption of organics may inhibit organic oxidation due to the blockage of surface sites inhibiting O_3‒catalyst interaction and/or due to decrease in the availability of organics if oxidants are mainly present in the bulk solution.[27-29]

According to the brief discussion above, the controversies regarding the mechanisms of HCO inevitably hinders the optimization and application of this technology. In this thesis, we investigated the mechanisms of HCO using carbon, copper and iron-based catalysts using a variety of target organics. We also investigated the influence of both salinity and the matrix composition on ozonation and HCO performance. Based on the results obtained, we provide important insights into the catalytic ozonation process. We also employ kinetic modeling tools to assist with the mechanistic understanding of

HCO. The mathematical kinetic models developed in this work can be used to predict the performance of organic oxidation under a range of conditions and can be employed for optimization of HCO.

The thesis is organized into nine chapters (including this introduction chapter):

(1) Chapter 2 contains a literature review in the field of heterogeneous catalytic ozonation focusing on the interaction of O_3 and organics with the catalysts.

(2) Chapter 3 describes the materials, experimental methods and setup used in this thesis. The kinetic modeling tool used is also described in this chapter.

(3) Chapter 4 investigates the performance of catalytic ozonation using a commercially available iron-impregnated activated carbon. The results obtained in this chapter has been published in the following article:

Yuting Yuan, Guowei Xing, Shikha Garg, Jinxing Ma, Xiangtong Kong, Pan Dai, T. David Waite, Mechanistic insights into the catalytic ozonation process using iron oxide-impregnated activated carbon, Water Research, Volume 177, Pages 115785, 2020.

(4) Chapter 5 explores the mechanisms of catalytic ozonation in the presence of Cu-based catalysts. The results obtained in this chapter has been published in the following article:

Yuting Yuan, Shikha Garg, Jinxing Ma and T. David Waite, Kinetic modelling-assisted mechanistic understanding of the catalytic ozonation process using Cu-Al layered double hydroxides and copper oxide catalysts, Environmental Science and Technology, doi: 10.1021/acs.est.1c03718.

(5) Chapter 6 studies the influences of buffers on the performance of conventional ozonation and catalytic ozonation processes for organic oxidation. The results obtained in this chapter has been published in the following article:

Yuting Yuan, Mahshid Mortazavi, Shikha Garg, Jinxing Ma, and T. David Waite, Comparison of performance of conventional ozonation and heterogeneous catalytic ozonation processes in phosphate and bicarbonate buffered solutions, ACS Environmental Science &Technology Engineering, doi: 10.1021/acsestengg.1c00350

(6) Chapter 7 summarizes the influence of chloride and sulphate on the performance of the commercial Fe-Mn Al_2O_3 catalyst. The results obtained in this chapter has been published in the following article:

Yuting Yuan, Shikha Garg, Yuan Wang, Wenbo Li, Guifeng Chen, Minglong Gao, Jinlong Zhong, Jikun Wang and T. David Waite, Influence of salinity on the heterogeneous catalytic ozonation process: Implications to treatment of high salinity wastewater, Journal of Hazardous Materials (2021), 127255.

(7) Chapter 8 discusses the caveats in use of *tert*-butanol as a hydroxyl radical scavenger in ozonation and catalytic ozonation studies.

(8) Chapter 9 presents the general conclusions and implications obtained in this thesis.

Chapter 2 Literature Review

2.1 Catalyst-O_3 interaction based on active sites

It is envisaged that the interactions of O_3 and/or organics with the catalyst surface are key processes responsible for the primary oxidation capacity in HCO.[30, 31] The catalyst–ozone interaction and concomitant generation of ROS is dependent on the nature of the catalysts, pH as well as the presence of scavengers in the matrix. The following discussion would be focused on the involvement of various surface sites which are reported to play a role in the catalyst–O_3 interaction.

2.1.1 Surface hydroxyl groups

Surface hydroxyl groups (≡OH) are present on the surface and/or formed via hydration of the Lewis acid sites on metal oxides in aqueous solutions.[32] ≡OH have been reported to serve as active sites for O_3 decay (and concomitant generation of ROS) and organic adsorption in HCO. The ≡OH formed at Mn sites in Mn–modified Al_2O_3 adsorb O_3 and catalytically transform O_3 into $^{\bullet}OH$ with these $^{\bullet}OH$ molecules contributing to oxidation of pharmaceuticals in the bulk solution.[33] The removal of phenol in the presence of TiO_2 increased with the concentration of ≡OH in the rutile phase due to the higher surface area of the rutile phase compared to other TiO_2 phases with different morphologies and crystalinities.[34] There are contradictory findings reported on the mechanisms of O_3 transformation on ≡OH. For example, great discrepancy has been observed on the relationship between charge status of ≡OH and O_3 decomposition in the HCO process. The ≡OH sites may be neutrally charged, protonated and positively charged (i.e., $\equiv OH_2^+$) or deprotonated and negatively charged (i.e., $\equiv O^-$) when the pH is equal, below or over the point of zero charge (pH_{pzc}), respectively. Psaltou *et al.*[35] investigated 18 catalysts and found that the catalysts with pH_{pzc} close or slightly over the solution pH were the most effective to oxidize *para*–chlorobenzoic acid (*p*–CBA). Similar results were reported when ceramic honeycomb [36] and Cu–loaded cordierite [37] were employed as the catalysts with the organic oxidation maximized at the solution pH where neutral ≡OH concentration was the highest. This was in agreement with the work by Qi *et al.* which reported that the uncharged ≡OH on γ–AlOOH was most effective in inducing O_3 decay and $^{\bullet}OH$ generation with the catalytic performance decreasing with the decrease in the concentration of ≡OH after thermal treatment.[38] In addition, modification of pumice by Fe improved the concentration of ≡OH thereby resulting in effective transformation of O_3 into $^{\bullet}OH$ at the neutral ≡OH sites.[39] Inhibition of *p*–nitrobenzene oxidation in the presence of phosphate, a strong Lewis acid which competes with O_3 for ≡OH, also supported the involvement of ≡OH during HCO in the presence of Fe–modified pumice.[39] However, some other studies reported that the positively or negatively charged ≡OH (i.e., $\equiv OH_2^+$ or $\equiv O^-$) were the main active sites in HCO.[35, 40, 41] For example, the increase in pH_{pzc} and positively charged $\equiv OH_2^+$ concentration on ceramic honeycomb by loading metal (Zn, Ni and Fe respectively) onto ceramic honeycomb was reported to be beneficial for the catalytic ozonation process.[40] On the other hand, it was reported that the increase in the negatively charged $\equiv^{\bullet}O^-$ on MCM–48 by optimizing the Ce loading enhanced the decay of O_3 and generation of $^{\bullet}OH$.[41] Furthermore, the negatively charged SiO_2 was reported to be effective in oxidation of *p*–CBA through initiating $^{\bullet}OH$ generation via O_3 decay with this observation supporting the conclusion that negatively charged $\equiv O^-$ were active sites during HCO.[35] Byun *et al.* and co-workers [42] found that Ti oxide coated ceramic membrane showed superior effect to reduce membrane fouling and improve organic removal compared to Fe and Mn oxide coated membranes in the hybrid catalytic ozonation-membrane processes due the charge repulsion and generation of $^{\bullet}OH$ at the negatively-charged Ti sites.

Overall, it appears that ≡OH are important active sites during catalytic ozonation although the mechanism of O_3 decay on ≡OH is contradictory. The activity of ≡OH on the catalyst is dependent on the type of active metal, the surface charge as well as the physio–chemical properties such morphologies and crystal phases of the catalysts. Moreover, the properties of ≡OH can be altered to enhance the performance of HCO.

2.1.2 Lewis acid sites

O_3 interacts with the Lewis acid sites on metal oxides with electron–accepting capacities.[43] The transformation of gaseous O_3 into surface atomic oxygen (O^*) at the strong Lewis acid sites has been commonly observed in the presence of metal oxides.[44, 45] Although, the interaction of O_3 with Lewis acid sites is more complicated in the aqueous phase due to competition between water and O_3 for surface sites, some studies have suggested Lewis acid sites on the catalysts play an important role in O_3 decay.[26, 46, 47] Yan *et al.*[48] systematically compared the behaviour of aqueous O_3 transformation in the presence of different iron oxides and showed that that O_3 interacted with Lewis acid sites to form ROS which enhances ibuprofen oxidation. Yu *et al.* reported that the substitution of Ce in iron–organic frameworks creates more ligand deficient defects and increases the Lewis acid sites where O_3 is decomposed forming surface adsorbed $^{\bullet}OH$.[46] In the presence of PdO/CeO_2, dissolved O_3 was decomposed on PdO sites and generated O^* with this contributing to the oxidation of sorbed oxalate on CeO_2 sites.[26] More interestingly, Bing *et al.* [47] suggested that by introducing different metal oxides into the structure of mesoporous SBA–15 silica, the decomposition of adsorbed O_3 on the catalyst surface can be manipulated with their results showing that Al_2O_3 promoted O^*

generation while Fe_2O_3 favoured surface $^{\bullet}OH$ and superoxide ($O_2^{\bullet-}$) production.[47] Yang and co–workers reported that chemically sorbed water at Lewis acid sites on *β*–FeOOH modified mesoporous Al_2O_3 enhanced O_3 decay and formation of ROS thereby improving pharmaceuticals oxidation.[49] The replacement of sorbed water by phosphate ions deceases the activity of the catalyst with this observation supporting the conclusion that Lewis acid sites are involved in ROS generation.[49]

2.1.3 Oxygen vacancies (OVs)

The oxygen vacancies (OVs) in metal oxides usually result from the presence of surface defects which are rich in localized electrons.[50] CeO_2, due to the structure Ce^{4+}–OVs–Ce^{3+}, has been extensively used in HCO.[50, 51 52] Comparison of variant nanoshapes CeO_2 in HCO indicated that CeO_2 with a high proportion of defect sites (i.e., OVs) can effectively donate electrons to O_3 and generate $^{\bullet}OH$ at the surface basic sites and, as a result, exhibits the best performance with respect to organic oxidation.[51] Esmailpour *et al.* reported that light-treated CeO_2 effectively oxidizes salicylic acid.[50] The OVs in CeO_2 adsorb H_2O forming ≡OH groups which act as active sites for O_3 decay generating oxidants which enhance the oxidation of salicylic acid.[50] The OVs present in lanthanum manganite perovskites (LMO) [52] and Mn-modified FeOOH [53] also promote O_3 decay and generate singlet oxygen ($^1O_2$) and $^{\bullet}OH$ respectively.

2.1.4 Redox cycling of multi-valent metal ions

The redox cycling of multi–valent metals assists in O_3 decomposition and generation of ROS. For example, the decomposition of O_3 and concomitant generation of $^{\bullet}OH$ has been reported in the presence of Ce–MCM–48 [41] and Mn_2O_3 modified LMO [52] as a result of the redox cycling of Ce(III)/Ce(IV) and Mn(III)/Mn(IV) respectively. Nawaz *et al.* measured the performance of six phases of MnO_2 in HCO with their results supporting the conclusion that α–MnO_2 with higher ratio of Mn^{3+}/Mn^{4+} exhibited the best 4–nitrophenol removal compared to other MnO_2.[54] Zhang *et al.* found that Ce(III)/Ce(IV) cycling benefited the oxidation of phenol in the presence of CeO_2.[55] In the hybrid catalytic ozonation-metal oxide coated ceramic membrane processes, CeOx was found to be more effective to remove bisphenol A, benzotriazole and clofibric acid compared to MnOx since more $^{\bullet}OH$ was generated due to the cycling of Ce(III)/Ce(IV).[56] Interestingly, the electron transfer from Ni^{2+} in the structure of $NiFe_2O_4$ to O_3 accelerated the generation of $^{\bullet}OH$ and the reversion of Ni^{3+} back to Ni^{2+} was assisted by the oxidation of lattice oxygen.[57] Moreover, oxidation of a cobalt–oxalate complex generates $^{\bullet}OH$ as a result of Co(II)/Co(III) cycling.[58] The partial electron donation from oxalate to Co(II) increases the reactivity of Co(II) towards O_3 compared to free Co(II). The cycling of Fe(II)/Fe(III) and Cu(I)/Cu(II) was also identified to play a role in organic oxidation by HCO employing Cu–Fe–O nanoparticles as the catalyst.[59]

2.1.5 Active sites on carbon-based materials

The carbon–oxygen functional groups with acidic and basic character in carbon materials play a role in HCO via anchoring O_3 and/or organic compounds.[60-62] The acidic functional groups include carboxyl, hydroxyl and carbonyl groups while the basic functional groups arise from the presence of pyrones, chromenes and graphene layers with delocalized electrons.[62, 63] The electrons at the basic centres in carbon materials react with O_3 and generate $^{\bullet}OH$.[29, 63, 64] Conflicting results have been reported on the role of the acid groups, such as carboxyl groups, as active sites for O_3 decay into $^{\bullet}OH$. Oulton *et al.* reported that carboxyl groups on multiwalled carbon nanotube (MWCNT) enhance $^{\bullet}OH$ exposure formed via O_3 decomposition with this conclusion supported by the observation that the *R*ct value increases with the increase in surface acid group density.[60] Similar results were reported by Qu *et al.*[65] However, the oxidized carbon surface was not effective in enhancing the generation of •OH in other studies.[66, 67] The carbon surface may also scavenge •OH thereby limiting the diffusion of •OH from the surface into the interface and/or bulk solution and, as a result, decreasing the oxidation efficiency of organics.[68] Functionalization of carbon materials using methods such as oxidation,[60, 65, 66] heat treatment,[67] heteroatom doping,[69] and metal oxide modification [70, 71] has been reported to improve the performance of carbon material as catalysts in HCO.

Due to the high density of functional groups, surface area and pore volume, carbon materials have strong affinity to most organics via interaction with oxygen containing groups such as carboxyl groups.[62, 72, 73] Thus, in some catalyst designs, carbon materials are used as centres for organic adsorption to accelerate the mass transfer of organics. This was shown to be the case in the presence of multiwalled catalysts with Fe or Ni oxides impregnated on graphene–coated Al_2O_3.[69, 74] The graphitized layer not only acts as the active centres for O_3 decay but also enhances the adsorption of organics.[69, 74] Note however that adsorption is not necessary to assure the catalytic effects of carbon materials [60] under situations where oxidation of organic proceeds in the interface and/or the bulk solution (see more detailed discussion in section 2.3.2).

2.2 Oxidants generated via catalyt-O_3 interaction

2.2.1 Surface O_3

The adsorption of O_3 has been observed in the presence of various catalysts, such as zeolites, iron silicates, pumice and iron oxides.[39, 75, 76 48, 77-79] Diffusion of O_3 onto the surface generates surface O_3 ($\equiv O_3$) which has been identified as the main oxidant in some HCO processes.[80, 81 25, 82, 83] Earlier studies employing zeolite as the catalyst in HCO showed that direct oxidation of the adsorbed organics by O_3 occurs on the zeolite surface.[80, 81] Though the reactivity of O_3 toward many organic compounds is low, in some cases it is reported that complexation of organics with the metal oxides surface sites [84] increases their reactivity towards O_3 and facilitates their oxidation via a non–radical mediated pathway. Pines and Reckhow [83] showed that natural organic matter (NOM) forms surface complexes with various metal oxides such as cobalt oxide, copper oxide, titanium oxide and nickel oxide with these metal-NOM complexes readily oxidized by molecular O_3. Zhang and co–workers [25, 82] also reported that Cu–carboxylate complexes formed via bidentate bridging in the presence of CuO/CeO_2 showed higher reactivity towards O_3 compared to free carboxylate groups. Ikhlaq *et al.*[79] found that the Bronsted sites on the surface of zeolite4A acted as reactive centres for the adsorption of organics and their concomitant oxidation via a non radical pathway.

2.2.2 Hydroxyl radicals

$^{\bullet}OH$ radicals are reported to be the dominant ROS responsible for the destruction of O_3–refractory organic compounds in catalytic ozonation.[33, 46, 60, 65, 68] The contribution of $^{\bullet}OH$ in catalytic ozonation may be assessed via scavenger tests, probe methods and electron paramagnetic resonance (EPR). *tert*–butanol (TBA) is the most widely used $^{\bullet}OH$ scavenger since it reacts quickly with $^{\bullet}OH$ ($k_{^{\bullet}OH}$ = 5.8 $\times 10^8$ $M^{-1}\cdot s^{-1}$) but slowly with molecular O_3 ($k_{^{\bullet}OH}$ = 3.0 $\times 10^{-3}$ $M^{-1}\cdot s^{-1}$).[50, 85] The contribution of $^{\bullet}OH$ is typically estimated based on the difference in the rate and extent of organic removal in the absence and presence of TBA. For example, TBA inhibited the oxidation of short–chain organic acids in CeO_2–catalyzed ozonation suggesting that $^{\bullet}OH$ play a role.[50] However, TBA may interfere with the radical chain reaction and/or adsorption of organic adsorption [86] which questions the reliability of the scavenger method to determine the contribution of $^{\bullet}OH$ in catalytic ozonation processes. Carbonate is used as $^{\bullet}OH$ scavenger in some studies however conflicting results have been reported.[52, 60] For example, the presence of carbonate promoted the extent of *p*–CBA oxidation by HCO employing MWCNT as the catalyst even though $^{\bullet}OH$ was identified to be the dominant ROS.[60] In contrast, carbonate strongly decreased the organic oxidation in the presence of LMO due to the scavenging of $^{\bullet}OH$.[52] Based on the discussion above, more validation tests should be performed in addition to scavenger tests to ascertain the role of $^{\bullet}OH$ during HCO.

The involvement of $^{\bullet}OH$ can be quaantified by addition of chemical probes which specifically react with $^{\bullet}OH$ generated in the system. For example, coumarin (COU) is used as $^{\bullet}OH$ probe since COU reacts with $^{\bullet}OH$ forming 7–hydroxyl COU (7–HC) which is fluorescent.[29] Another frequently used probe is *p*–CBA due to its high reactivity towards $^{\bullet}OH$ ($k_{^{\bullet}OH}$ = 5.0 ×10^{8} $M^{-1}\cdot s^{-1}$) and low reactivity towards O_3 ($k_{^{\bullet}OH}$ = 0.5 ×10^{-1} $M^{-1}\cdot s^{-1}$).[87] For example, in the iron nanoparticle coated ceramic membrane-ozonation processes, *p*-CBA was more effectively removed due to the generation of $^{\bullet}OH$ via O3-iron oxide interaction.[88] *p*–CBA has been extensively used to determine the *R*ct value which is defined as the ratio of exposure of $^{\bullet}OH$ and O_3 exposure in the target system (eq.2.1).[89, 90] The concentration of *p*–CBA spiked into the system should be low to minimize the influence of *p*–CBA on O_3 decay kinetics.[86, 91] Overall, the chemical probes added into the system should: 1) specifically react with $^{\bullet}OH$, and 2) not alter O_3 decay kinetics and associated $^{\bullet}OH$ generation.

$$\mathrm{Rct} = \frac{\int[\,^{\bullet}\mathrm{OH}]\mathrm{dt}}{\int[\mathrm{O_3}]\mathrm{dt}} = \frac{\ln(\frac{[p-\mathrm{CBA}]_t}{[p-\mathrm{CBA}]_0})}{k_{^{\bullet}\mathrm{OH},p-\mathrm{CBA}}\int[\mathrm{O_3}]\mathrm{dt}}$$

(2.1)

EPR has been used as a useful tool to detect and characterize the radicals in chemical and biological systems (detailed review available in Davies [92]). In catalytic ozonation systems where short–lived radicals are produced, a spin trapping agent assisted EPR is often utilized.[29, 52, 85] Generally, the trapping agent is added to the catalytic ozonation system at high concentration (mM to M) which reacts with any radicals present forming stable adducts.[92] Nitrone traps such as 5,5–dimethylpyrroline–N–oxide (DMPO), 5–*tert*–butoxycarbonyl–5methyl–1–pyrroline–N–oxide (BMPO) are mostly used for the detection of $^{\bullet}OH$ and $O_2^{\bullet-}$ in catalytic ozonation systems.[93] The DMOP–$^{\bullet}OH$ peaks are characterized as an intensity ratio of 1:2:2:1. Adding alcohols such as TBA removes the strong DMOP–$^{\bullet}OH$ peak allowing detection of $O_2^{\bullet-}$ as a result of the formation of DMOP–$^{\bullet}OOH$.[52] However, the addition of alcohols could be questionable since the reaction of alcohols and O_3 may possibly result in the formation of other radicals.[22] It is also recommended to use the high–purity traps to alleviate the impact of impurities due to the high concentration of trap used in the target systems.[92] Stronger EPR peaks in catalytic ozonation systems compared with that in conventional ozonation without catalyst is usually indicative of the effectiveness of the catalyst in activating O_3 decay into radicals. However, surface-related processes need to be taken into consideration when interpreting the results from EPR tests obtained in the presence of catalysts. For example, high affinity of traps for the catalyst surface is vital if the radicals are produced and constrained on the surface (more discussion on surface oxidation is available in section 2.3.1). Moreover, molecular O_3 can oxidize nitrones via electrophilic and/or nucleophilic reactions, generating aldehydes or ketones with these compounds being reactive to O_3 and further driving O_3 decay and formation of radicals.[94] Given that radicals could be generated via interaction of these intermediates with the catalyst, conclusions based solely on EPR results could be erroneous. Unfortunately, such discussion is rarely found in the literature on catalytic ozonation processes.

Note that although $O_2^{\bullet-}$ has been identified in many ozone–based processes,[9, 29, 46, 47, 52, 54, 95-97] we are of the opinion that it acts as a chain carrier to promote O_3 decay into $^{\bullet}OH$ rather than an oxidant for organic oxidation since it is very reactive towards O_3 [98] which is present in a higher concentration than target micropollutants during ozonation and HCO.

2.2.3 Singlet oxygen and Surface atomic oxygen

$^1O_2$ is known to oxidize dissolved organic matter [99] and has been detected in HCO.[52, 95] Wang *et al.* reported that the O^* produced by N–doped nanocarbon materials effectively oxidizes oxalic acid on the surface and/or in the bulk solution.[93] It is interesting to note that the mechanism of catalytic ozonation is also dependent on the nature of target organics. For example, while O^* was identified as the main oxidant for oxalic acid, molecular O_3 and $^1O_2$ were responsible for oxidation of phenolic compounds when Co–embedded N–doped carbon nanotubes were used as the catalyst in HCO.[95] Nawaz *et al.* reported that the removal of 4–nitrophenol was inhibited in the presence of NaN_3 with this observation supporting the conclusion that $^1O_2$ played a role during MnO_2 mediated HCO.[54] However, NaN_3 reacts quickly with O_3 making it an improper probe for $^1O_2$ with inhibition in 4–nitrophenol oxidation possibly due to consumption of O_3.[100]

In summary, (1) the reaction of catalyst and O_3 is strongly dependent on the nature of the catalyst, (2) the mechanism of catalytic O_3 decay is usually complex and generates various ROS, and (3) all methods for ROS measurement have some disadvantagess and caution should be exercised when interpreting the results obtained in the presence ROS probes and scavengers to avoid misleading conclusions.

2.3 The role of organic adsorption in HCO

The adsorption of organic compounds onto the catalyst tends to be dependent on the properties of the compounds as well as the nature of the catalyst surface where electrostatic forces, hydrophobic interactions, dipole-dipole interactions, and van der Waal forces may play a role. For examples, electrostatic attraction facilitates the adsorption of organics with this dependent on the pH_{pzc} of the catalysts, acid dissociation constant of the organics and solution pH.[31] Conflicting results have been reported on the role of organic (including both micropollutants as well as NOM) adsorption in organic oxidation during HCO. Some studies have suggested that adsorption improves the contact efficiency of organic and oxidant on the surface thereby increasing the organic oxidation.[25, 101] On the contrary, some studies have suggested that adsorption of organics occupies the surface sites thereby either inhibiting catalyst–O_3 interaction and concomitant oxidant generation [27] or limiting oxidation of organic oxidation by bulk oxidants due to reduced bulk organic concentration.[73] Investigation of the role of organic adsorption on organic oxidation is critical in determining the mechanism of catalytic ozonation and in identifying the major location(s) where organic oxidation occurs.

2.3.1 Organic oxidation on the catalyst surface

Findings of no influence of bulk radical scavengers on the rate and extent of organic oxidation as well as promotion of organic oxidation with increase in the extent of organic adsorption are typically assumed to suggest that the oxidation of organics is occurring on the surface. For example, activated carbon was suggested to facilitate the surface oxidation of organics based on the observation that the performance of HCO was not affected by bulk radical scavengers.[102] Moreover, formation of organic–metal complexes and/or the concentrating of organic contaminants on the surface facilitated organic removal in the presence of CuO/CeO_2.[25] Salla and co–workers found that although Mn_2O_3 induced more significant O_3 decay and generation of surface ROS, limited access of humic acid (HA) to the surface constrained the oxidation of HA.[101] On the other hand, it was reported that the adsorption of HA was favoured on α–Al_2O_3 due to electrostatic attractive forces and high surface area of α–Al_2O_3 with this increase in HA adsorption resulting in effective HA oxidation compared to that observed in the presence of Mn_2O_3.[101] Interestingly, ROS could be generated via surface oxidation of sorbed organics as suggested by the interaction of ozone-soil surface that the $^{\bullet}OH$ generation via O_3 decay was related to the soil organi matters although the metal oxides on the soil surface seemed to be stronger promoters.[103]

During catalytic ozonation, adsorption of organics is related to the nature of surface sites, surface charge and the nature of the organics. The ≡OH groups present on metal oxide surfaces have ion exchange capacity and can be replaced by the organic anions.[104] The surfaces of metal oxides exhibit positive, neutral and negative charge depending on the pH_{pzc} and the solution pH.[105] Usually the positively charged surface is beneficial for adsorption of negatively charged organics due to electrostatic attraction.[106] Thus, organic oxidation is dependent on pH_{pzc} and solution pH. For example, it was reported that the oxidation of OA in the presence of PdO/CeO_2 can be improved when operating at $pH<pH_{pzc}$ since the adsorption of oxalate increases on positively charged surfaces.[26] Similar results have been found in the presence of Fe_2O_3/Al_2O_3 modified mesoporous SBA–15 with higher oxidation of organic observed when $pH<pH_{pzc}$ compared to that observed at $pH>pH_{pzc}$.[47]

The nature of the functional groups in organic compounds also affects the adsorption of organic compounds to catalyst surfaces. For example, functional groups such as carboxylic, phenolic-OH, or amino groups can substitute the ≡OH on the catalyst surface allowing formation of metal–organic complexes.[32, 104] Zhang *et al.*[25] reported that OA exhibited stronger affinity towards CuO/CeO_2 surface compared to formate due to the formation of bidentate Cu–OA complexes. The CuO–OA complex was oxidized on the surface of CuO/CeO_2 as a result of Cu(I)/Cu(II) redox cycling. Wang *et al.* reported that Co–decorated N–-doped carbon nanotubes facilitated oxalic acid oxidation due to increased oxalic acid adsorption on the catalyst surface.[95]

It should be noted that quantification of organic oxidation and/or complete mineralization during HCO processes is challenging due to the complexity in differentiating adsorptive and oxidative organic removal.

2.3.2 Organic oxidation in the interfacial region and/or the bulk solution

Many previous studies found that the adsorption of organic on the catalyst surface was minimal with this observation suggesting that the oxidation of organic was driven by oxidants present in the interfacial regions and/or the bulk solution.[23, 29, 33, 38, 54, 60, 75] Ernst *et al.*[27] found that the adsorption of organics was not necessary to initiate oxidation of organics. Rather, adsorption of organics blocks the ≡OH sites which are the active sites for O_3 decay and generation of $^{\bullet}OH$. Similar results were reported for a MWCNT–O_3 system in which enhancement in *p*–CBA oxidation was observed in the presence of oxidized MWCNT even though the adsorption of *p*–CBA was inhibited in the presence of oxidized MWCNT.[60] Similar findings were reported for MWCNT–catalysed atrazine oxidation wherein atrazine adsorption to the catalyst surface decreased its oxidation via O_3 and/or ROS present in the bulk solution.[73] Zhang *et al.*[29] characterized the uneven distribution of $^{\bullet}OH$ between the carbon nanotube surface and bulk solution using fluorescence microscopy and found that a high concentration of

$^{\bullet}OH$ is located in the solid-liquid interface. The $^{\bullet}OH$ located in the solid–liquid interface contributed to the oxidation of perfluorooctane which has a weak surface affinity towards carbon nanotubes. Slow adsorption and fast oxidation kinetics of 4–nitrophenol in the presence of MnO_2 confirmed that the oxidation occurred mainly in bulk solution in the presence of MnO_2.[54]

The most straightforward way to evaluate the involvement of bulk oxidant(s) in organic oxidation is by comparing the organic removal in the absence and presence of bulk oxidant scavengers. TBA has been widely used as a bulk $^{\bullet}OH$ scavenger in many studies to probe the role of bulk $^{\bullet}OH$ in organic oxidation.[50, 85] The higher organic removal rate in the absence of TBA compared to that measured in the presence of TBA suggests that the oxidation of organics occurs in the bulk solution. Based on the low surface affinity of perfluorooctane and measurement of $^{\bullet}OH$, it was suggested that the oxidation of perfluorooctane occurred at the interface of carbon nanotubes. However, no influence of TBA addition was observed on the oxidation of perfluorooctane with this observation suggesting that TBA might be not able to scavenge the interfacial $^{\bullet}OH$.[29] Note that the differentiation of organic oxidation in the interfacial regions and the bulk solution is not explicit. If the catalytic performance was impacted by the presence of bulk radical scavengers, we are of the opinion that the oxidation of organics proceeds mainly in the interfacial region wherein oxidants such as $^{\bullet}OH$ are present as a result of diffusion from the catalyst surface if catalytic–mediated O_3 decay is important.[22 29]

Chapter 3 Experimental methods

This chapter describes the reagents and experimental methods used in the thesis. For chapter–specific methods, detailed description is included in the relevant chapters.

3.1 Experimental methods

All the chemicals used in the experiments described in subsequent chapters of this thesis were obtained from Sigma Aldrich with analytical grade or above and used without further purifications. All the glassware was soaked in 5% v/v nitric acid (HNO_3) and cleaned thoroughly with Milli–Q (MQ) water before use. The 5% nitic acid bath for soaking the glasses was prepared freshly each month. All the solutions were prepared in MQ water with 18 MΩ cm^{-1} and pH around 7.0 unless stated otherwise. All solutions were stored at 4 °C prior to use unless specified otherwise.

3.1.1 Dissolved O_3

3.1.1.1 Reagents

O_3 stock solution

O_3 stock solution was prepared by sparging gaseous O_3 into MQ water in a Dreschel bottle at room temperature for 30 min. The equilibrium dissolved O_3 concentration in the stock solution was standardized by measuring its absorbance at 260 nm (molar absorptivity = 3200 $M^{-1}\cdot s^{-1}$);[22] with a UV spectrometer (Ocean Optics Spectrophotometry system). The gaseous O_3 was produced by an O_3 generator (T4200, Oxyzone Oty Ltd, Australia) using pure O_2 at a flow rate of 650 mL.min^{-1} as the feed gas. The UV_{260nm} absorbance of O_3 stock solution was generally around 1.0 – 1.2, yielding a dissolved O_3 concentration of 312.5 – 375.0 μM based on the Beer–Lambert law (eq.3.1).

$$A = \varepsilon bc \tag{3.1}$$

where A is the absorbance of O_3 stock solution at 260 nm; ε is the molar absorptivity of O_3 at 260 nm, c is the molar concentration of O_3, and b is the optical path length (1 cm in this thesis).

Indigo stock solution

The stock solution of indigo was prepared by dissolving potassium indigo trisulfonate into 20.0 mM phosphate buffer. [107] Briefly, 0.6 g of potassium indigo trisulfonate and 2.31 g of 85% H_3PO_4 were dissolved in 1.0 L MQ water. The indigo stock solution was covered with aluminium foil prior to use. The absorbance of the indigo stock solution was checked on a weekly–base and replaced when the absorbance at 600 nm decreased to less than 80% of its initial value.

Phosphate buffer at pH 2.0

The phosphate buffer at pH 2.0 for dissolved O_3 measurement was prepared by dissolving 24.4 g anhydrous NaH_2PO_4 and 35.0 g 85% H_3PO_4 into 1.0 L MQ.

3.1.1.2 Method for dissolved O_3 measurement

Dissolved O_3 concentration was measured using the indigo method developed by Bader and Hoigne.[107] Briefly, 1.0 mL of sample was added to 0.2 – 0.3 mL indigo stock solution and 0.8 mL of pH 2.0 phosphate buffer followed by addition of MQ water to achieve a final volume of 5.0 mL. The sample absorbance at 600 nm was measured immediately using an Ocean Optics Spectrophotometry system. Prior to measurement, calibration was performed by standard addition of the O_3 stock solution into indigo solution over the concentration range of 0.0 – 26.0 μM and the absorbance was measured using the procedure described above. A molar absorption coefficient of

26,890 $M^{-1}\cdot cm^{-1}$ was obtained for indigo which is close to the reported value.[107] Figure 3.1 shows an example of a calibration curve of dissolved O_3 obtained in our work.

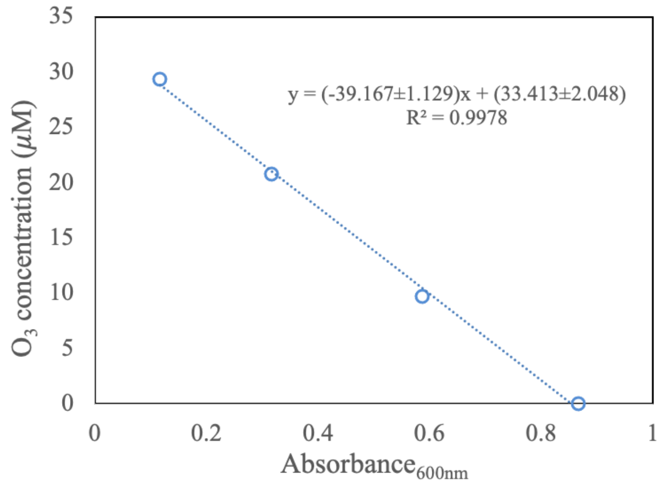

Figure 3.1 Calibration curve of dissolved ozone by indigo method.

Note that for the measurement of O_3 concentration in the presence of catalyst, samples were first added to indigo solution with the mixture filtered immediately using 0.22 µm PVDF syringe filters (Millipore). Control experiments were performed to ensure that the adsorption of indigo on the filter membrane and/or catalyst was negligible during filtration.

3.1.2 *p*–CBA

3.1.2.1 Reagents

p-CBA stock solution

A 80.0 µM stock solution of *p*–CBA was prepared by dissolving 12.53 mg *p*–CBA into 1.0 L MQ water.

p–CBA standard solution

A 1.2 mM standard solution of *p*–CBA was prepared in methanol and used to perform the calibration for *p*–CBA quantification.

Mobile phases for high performance liquid-chromatography (HPLC)

The mobile phases for *p*–CBA detection were 10.0 mM H_3PO_4 and acetonitrile (ACN). The 10.0 mM H_3PO_4 solution was prepared by dilution of 85% H_3PO_4.

3.1.2.2 Method for *p*–CBA measurement

The concentration of *p*–CBA was measured by HPLC (Agilent 1200 Series, USA) employing UV–detection at 234 nm using 45% (v/v) 10.0 mM H_3PO_4 and 55% (v/v) ACN with flow rate of 1.0 mL/min. Calibration was performed prior to *p*–CBA measurement. A calibration curve of *p*–CBA is illustrated in Figure 3.2.

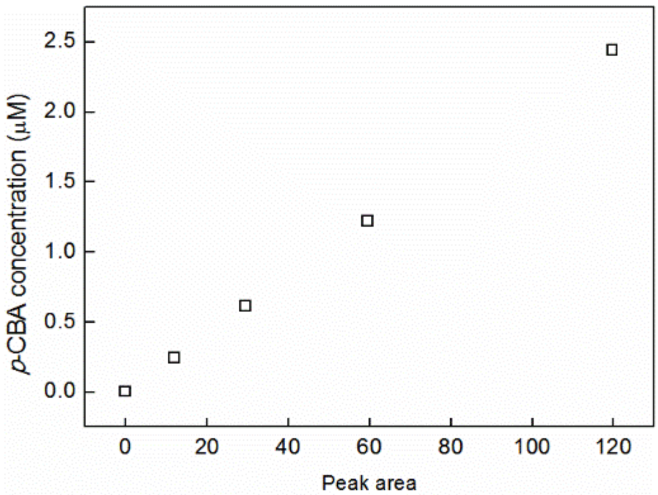

Figure 3.2 Calibration curve of *p*–CBA.

3.1.3 Formate and oxalate

3.1.3.1 Reagents

Radiolabelled formate and oxalate stock solutions

Stock solutions of radiolabelled formate ($HCOO^-$) and oxalate ($C_2O_4^-$) were prepared at concentrations of 90.0 μM and 0.2 mM respectively in MQ water.

Non-radiolabelled formate and oxalate stock solutions

Non–radiolabelled $HCOO^-$ and $C_2O_4^-$ stock solutions were prepared at the desired concentrations by dissolving their sodium salts in MQ water.

3.1.3.2 Method for $H^{14}COO^-$ and $^{14}C_2O_4^-$ measurement

The concentration of $H^{14}COO^-$ and $^{14}C_2O_4^-$ were quantified using a Packard Tri–Carb 2100TR scintillation counter [108] following addition of 0.9 mL of sample into 10.0 mL of liquid scintillation cocktail (Ultima GOLD, PACKARD).

3.2 Experimental set-up

Most experiments for O_3 decay and organic oxidation were performed at pH 3.0, 7.3 or 8.5 unless stated otherwise. The volume of the reactors was 70ml unless otherwise stated. For pH 3.0 studies, a 1.0 mM HNO_3 solution was used as the buffer while a 2.0 mM $NaHCO_3$ air-saturated solution was used for pH 8.5 experiments. For pH 7.3, a 2.0 mM $NaHCO_3$ solution in equilibrium with synthetic air containing 6000 ppm of CO_2 (HiQ certified calibration standards; BOC) was used. To allow equilibration of CO_2 between the solution and the gas phase, solutions were sparged in Dreschel bottles for 2 h prior to experiments. 1.0 M HNO_3 and 1.0 M NaOH stock solutions were used to adjust the pH of the reaction solution when required. While the pH was well controlled in the pH 3.0 and 8.5 experiments (with pH variations of $< \pm 0.1$ units), the pH of the 7.3 system increased by 0.2 – 0.3 units over the course of the ozonation study, most likely as a result of the decrease in the CO_2 partial pressure since sparging with the synthetic CO_2/air mixture was not continued during the experiments.

3.2.1 O_3 decay

Investigation of aqueous O_3 decay was performed in head–space free gas–tight syringe reactors (Figure 3.3). For measurement, aqueous ozone (~120.0 µM) was added to buffer solutions in the absence and presence of catalysts. The aqueous ozone concentration was measured using the indigo method.[107]

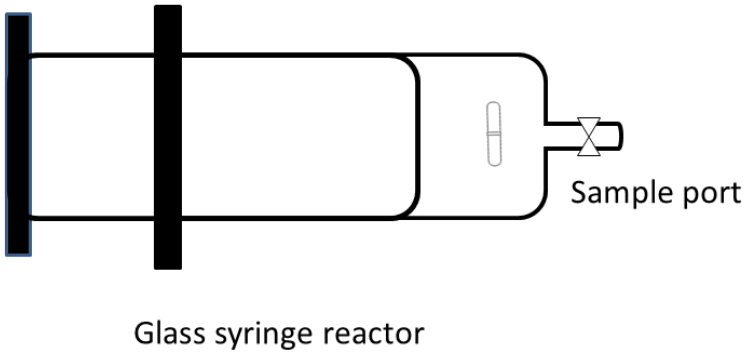

Figure 3.3 Image of head–space free syringe reactors used for measurement of aqueous ozone decay by conventional and catalytic ozonation processes.

3.2.2 $HCOO^-$ and $C_2O_4^-$ oxidation in batch mode

The experimental setup and method used for simultaneous measurement of adsorption and oxidation of $HCOO^-$ and $C_2O_4^{2-}$on ozonation and catalytic ozonation are shown in Figure 3.4. During experiments, the ozone reactor was carefully sealed and gently stirred using a magnetic stirrer. Valves 1, 3 and 4 were closed to reduce the headspace in the reactor. Valve 2 was connected to the sample port and was opened while taking samples. For measurement of formate/oxalate degradation on ozonation, valves 1, 3 and 4 were open and valve 2 was closed and the reactor sparged with N_2 gas to drive out CO_2 formed in the reactor. An appropriate volume of formate/oxalate stock solution was added to 70.0 mL buffer solution in the absence or presence of catalyst to yield a final formate/oxalate concentration of 1.0 µM (consisting of 0.1 µM radiolabelled and 0.9 µM non-radiolabelled formate/oxalate). Subsequently, an appropriate volume of ozone stock solution was spiked into the reactor to initiate the reaction. At desired times, 1.5 mL of sample was withdrawn from the reactor and 1.0 mM non–radiolabelled formate/oxalate was added to cease the reaction by quenching any oxidant(s) present.[108, 109] Subsequently, 10.0 µL concentrated nitric acid (~ 45 mM) was added and the solution was sparged with N_2 to drive out any $^{14}CO_2$ formed from the reactor into the trapping solution (1.0 M NaOH). Note that HCOOH/$HCOO^-$ loss via volatization via N_2 sparging is within 5% under the experimental conditions used in this study (Figure 3.5). The residual $H^{14}COOH/H^{14}COO^-$ concentrations in the reaction vessel and $^{14}CO_2$ concentration in the trapping solution were measured using a Packard Tri–Carb 2100TR scintillation counter (protocol 2, count efficiency 95%) [109] following addition of 0.9 mL of sample (filtered by 0.22 µm PVDF syringe filter) into 10.0 mL of liquid scintillation cocktail (Ultima GOLD, PACKARD).

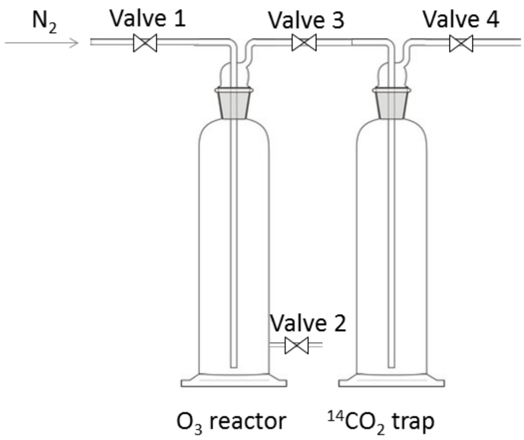

Figure 3.4 Experimental setup used for formate and oxalate removal in batch mode by conventional and catalytic ozonation processes.

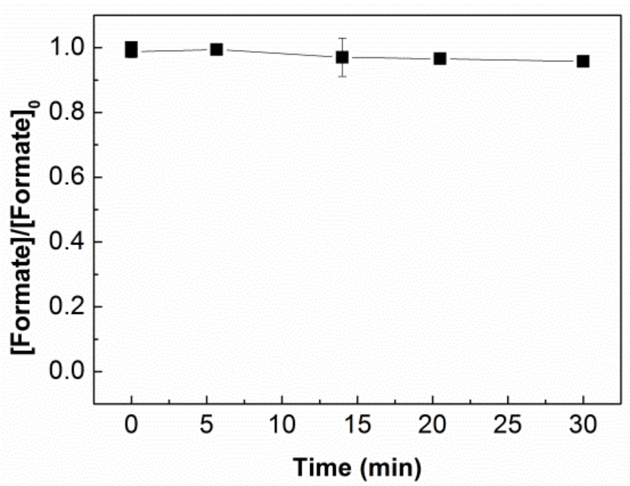

Figure 3.5 Measured formate removal in the reaction vessel during N_2–sparging for 30min. Experimental conditions: $[Formate]_0$ =1.0 µM (0.1 µM as radiolabelled and 0.9 µM as non–radiolabelled formate), pH =3.0.

3.2.3 Organic oxidation in semi-batch system

The setup for oxidation of the selected organic compounds by conventional ozonation and catalytic ozonation in a semi–batch system was shown in Figure 3.6. The volume of the wastewater was fixed at 150 mL. The flow rate of the gas sparged into the wastewater was controlled at 60 mL/min with a gas-phase ozone concentration of 51 mg/L. At predetermined time intervals (i.e., 10, 20, 30, 40 and 60 minutes), 10 mL of sample was withdrawn from the reactor. Following sparging with N_2 gas for 1 min, the samples were filtered (for catalytic ozonation samples only) using 0.22 µm PVDF filters (Millipore) and the chemical oxygen demand (COD) and total organic carbon (TOC) concentrations were measured.

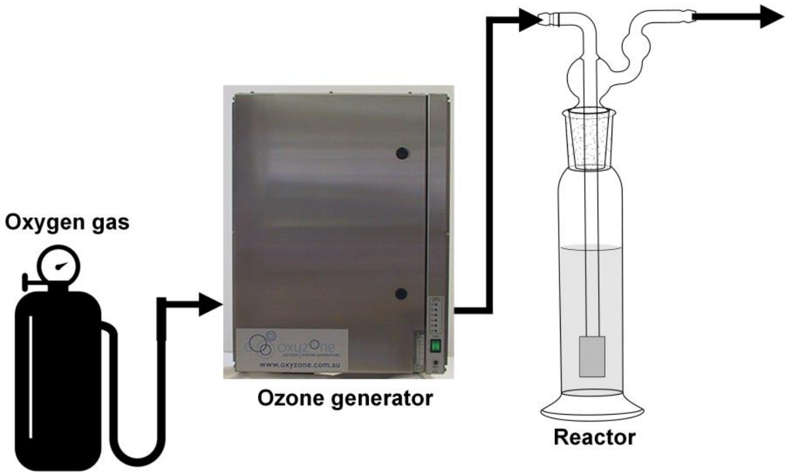

Figure 3.6 Schematic representation of organic oxidation used for TOC/COD removal in semi-batch mode by conventional and catalytic ozonation processes.

3.2.4 $^{\bullet}$OH generation

To evaluate the rate and extent of $^{\bullet}$OH generation on ozone decay, *p*–CBA was used as the $^{\bullet}$OH probe since it has high reactivity towards $^{\bullet}$OH ($k_{^{\bullet}OH,\, p\text{–}CBA} = 5.0 \times 10^9$ $M^{-1}\cdot s^{-1}$) but low reactivity towards ozone ($k_{O_3,\, p\text{–}CBA} = 0.15$ $M^{-1}\cdot s^{-1}$ [87]). For measurement, 1.0 µM *p*–CBA and the desired amount of ozone were added to the sealed reactor (Figure

3.7) to initiate the reaction. The *p*–CBA concentration was measured using HPLC (Agilent 1200 Series, USA) using the method described before.

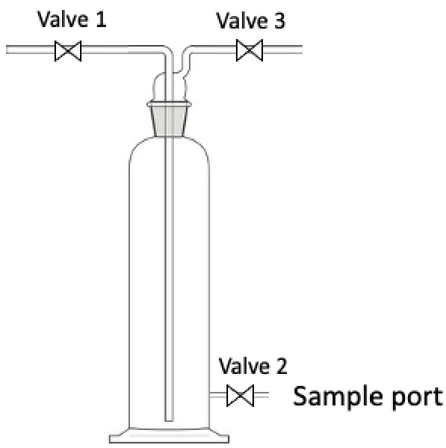

Figure 3.7 Reactor used for measurement of *p*–CBA oxidation by conventional and catalytic ozonation processes.

3.2.4 Kinetic modelling

Statistical analysis was performed using single-tailed student's *t*–test at the 5% significance level. Kinetic modelling of our experimental results was performed using the software package Kintecus.[110] Kintecus is a simulation program that enables prediction of the concentration of reactants and products as a function of time based on numerical integration of the rate equations appropriate to a hypothesized reaction mechanism. The rate constants used for the various reactions used in modelling were either obtained from literature and/or measured experimentally. Agreement (or lack thereof) of the predicted concentrations of reactants and products with measured concentrations for the same entities provides a measure of the veracity of the hypothesized reaction set and/or the rate constants used. An analysis of the sensitivity of species concentrations to perturbations to various rate constants in the model was undertaken by Principal Component Analysis (PCA).[110]

Chapter 4 Mechanistic insights into the catalytic ozonation process using iron oxide-impregnated activated carbon

Some of the material in this Chapter has been drawn from a recent publication, [111] which has been acknowledged and detailed in the 'inclusion of publications statement' for this thesis.

4.1 Introduction

Ozone is a relatively strong oxidant and has been widely used in the treatment of drinking waters and wastewaters. However, conventional ozonation technologies are usually constrained by poor mass transfer of ozone from the gas phase to liquid phase, low ozone utilization efficiency and limited mineralization of organics.[1, 22, 112] The addition of a catalyst has been proposed to overcome some of these problems with the catalyst purportedly enhancing the efficiency of the process as a result of increased generation of oxidants such as $^{\bullet}OH$ on catalyst–ozone interaction.[26, 29, 47, 60, 74, 75, 113, 114] The nature of the oxidant(s) generated in the catalytic ozonation systems appears to depend on the type of catalyst used.[26, 29, 47, 81, 96, 115-119] In addition to formation of reactive oxidants during catalytic ozonation, stabilization of ozone by adsorption onto the catalyst surface and/or adsorption of organics are also reported to enhance the oxidation efficiency in the catalytic ozonation process.[26, 74, 75, 120] However, inconsistent results have been reported on the role of organic adsorption in catalytic ozonation with some studies showing that the adsorption of organics (including parent compound and/or intermediates formed on oxidation) on the catalyst surface increased the overall oxidation capacity during catalytic ozonation [25, 26, 74, 79, 81, 116, 120] while other studies suggesting that the adsorption of organics was not critical [121] and even decreased the performance of catalytic ozonation.[28, 29]

As should be clear from the above brief review, despite extensive studies on catalytic ozonation, the role of the catalyst is not well understood. There is continued controversy regarding the contribution of catalyst to organics adsorption and oxidant generation with the uncertainty in part ascribed to the use of complex organic compounds such as humic substances and aromatic compounds for which oxidation results in formation of a suite of intermediates and by-products.[19, 120, 122] While these organic contaminants may be representative of real wastewaters, the coexistence of the formation of complex oxidized intermediates and their subsequent interaction with the catalyst and ozone makes it very difficult to clearly elucidate the mechanism responsible for contaminant degradation. Moreover, pH is not well controlled in many of the reported studies which makes the comparison of conventional ozonation and catalytic ozonation difficult.[113] To partially address the problems of previous studies, radiolabelled formate and oxalate were chosen as the target compounds in the present chapter since they have well-defined oxidation pathways and, in both cases, result in formation of CO_2 and H_2O as the only products.[123, 124] By quantifying both the loss of formate/oxalate and the generation of CO_2 over time, we are able to explicitly differentiate removal of formate/oxalate by the adsorption and oxidation processes. Additionally, these short chain carboxylic acids are good target contaminants since they are recognized as important end-products on ozonation of aromatic organics such as humic and fulvic acids.[22, 125] Moreover, the pKa of formic and oxalic acid is 3.8 and 4.3(pKa$_2$) respectively which allows variance in dissociated species of the two acids with this possibly influencing the adsorption and oxidative mechanisms. In order to understand the influence of pH on organics removal by ozonation (both conventional and catalytic), we investigated the process performance under varying pH conditions in the pH range 3.0 - 8.5.

A commercially available iron oxide impregnated activated carbon catalyst (provided by Beijing OriginWater (BOW) Technology Co., Ltd, China) was used in all experiments. We chose a carbon–based catalyst for these studies since carbon materials are inexpensive and possess abundant surface sites. Based on our experimental results, a mathematical model has been developed that satisfactorily describes formate oxidation by both ozonation and catalytic ozonation processes.

4.2 Materials and Methods

4.2.1. Reagents

All experiments were performed at pH 3.0, 7.3 or 8.5 using buffer solutions described in chapter 3. Stock solutions of radiolabelled and non–radiolabelled sodium formate, 1.0 mM indigo stock solution, O_3 stock solution and stock solution of *p*–CBA were prepared as described in chapter 3. Since formate exists as both HCOOH and $HCOO^-$ in the pH range investigated here, we use HCOOH/$HCOO^-$ to represent total formate from hereon in this chapter.

4.2.2. Catalyst characterization

A commercial iron oxide impregnated carbon catalyst (termed JBX) and its activated carbon carrier (referred to as carrier from hereon) were supplied by BOW. Upon receipt, the catalyst and the carrier were prewashed with MQ water until the supernatant was clear and then dried at 50°C in air before use. The surface area and the pore size of the catalyst were acquired using N_2 sorption isotherms and analysed by Brunauer–Emmett–Teller (BET) and Barrett–Joyner–Halenda (BJH) models. The samples were degassed at 150 °C for 8 h prior to the test. To further characterize the surface properties and composition of the catalyst and the carrier, scanning electron microscopy with energy dispersive X–ray spectroscopy (SEM–EDX; FEI Nova NanoSEM 230 FE–SEM) was performed on both the surface and core of JBX to investigate the distribution of metals in the catalyst. The catalyst was polished by ion milling (Hitachi Ion Milling System IM4000) and fixed onto a cross–section sample holder by silver glue. Both surface and core of JBX was examined in order to ascertain the distribution of elements through the catalyst. To characterise the surface charge of the catalyst, zeta potential measurements over a pH range of 3.0 to 10.0 were performed using a Malvern Nano ZS ZEN3600 zetasizer. The catalysts used here are in form of pellets with length of ca. 5 mm and 3 mm diameter. Since the catalysts were in the form of relatively large particles, the dosage of catalyst was set at 1.0 or 10.0 g L^{-1} to provide sufficient surface sites for ozone-catalyst and formate/oxalate-catalyst interactions.[118, 126] Note that even though the overall dosage of the catalyst was high, the active metal concentration was very low (< 0.1% of the total weight of the catalyst) and comparable with the catalyst dosages used in various earlier studies.[93, 127-129] We would also like to highlight that we used the activated carbon carrier as the control in all experiments to test the role of the iron oxide (the active site in JBX as discussed later) associated with the carrier rather than using well defined iron oxides since the exact nature of the iron oxide loaded on the carrier cannot be determined (see section 4.3.1 for more details).

4.2.3. Experimental setup

4.2.3.1. Formate degradation

The experimental setup and method used for simultaneous measurement of adsorption and oxidation of $HCOOH/HCOO^{-}$ on ozonation are described in detail in chapter 3.

Briefly, 1.0 μM formate (consisting of 0.1 μM radiolabelled and 0.9 μM non–radiolabelled formate) and ozone (1.0 – 100.0 μM) were added to pH 3.0, 7.3 or 8.5 buffer solution in the absence and presence of 1.0 or 10.0 g L^{-1} catalyst (or carrier). The concentrations of $H^{14}COOH/H^{14}COO^{-}$ remaining and $^{14}CO_2$ formed following oxidation at various time intervals were measured. To investigate the role of $^{\bullet}OH$ in the $HCOOH/HCOO^{-}$ oxidation process, TBA and Cl^{-} (for pH 3.0 only) were used as $^{\bullet}OH$ scavengers.

In order to investigate the importance of formate adsorption on its overall oxidation during catalytic ozonation, pre–adsorption of 1.0 μM formate was performed on 10.0 g L^{-1} JBX at pH 3.0. After 4 h, when nearly 80% of the added formate was adsorbed on JBX, the catalysts were withdrawn and re–dispersed in fresh pH 3.0 buffer solution. Subsequently, 10.0 μM of O_3 was added to initiate the oxidation with the concentrations of $H^{14}COOH/H^{14}COO^{-}$ and $^{14}CO_2$ measured as described in chapter 3.

4.2.3.2 Oxalate degradation

In order to investigate the influence of the nature of the target organic on rate and extent of degradation, the oxidation of oxalate was investigated at pH 7.3. While formate can be oxidized by both O_3 and $^{\bullet}OH$, oxalate has low reactivity towards O_3 (k_{O_3}= 0.04 $M^{-1}\cdot s^{-1}$;[1, 123, 130] with oxidation of oxalate mostly governed by its interaction with $^{\bullet}OH$ ($k_{^{\bullet}OH}$ = 5.6×10^{6} $M^{-1}\cdot s^{-1}$;[123] formed on O_3 decay. The experimental setup and procedure used for oxalate oxidation was identical to that described for formate degradation. Briefly, 1.0 μM oxalate (consisting of 0.1 μM radiolabelled and 0.9 μM non–radiolabelled oxalate) and ozone (10.0 μM) were added to pH 7.3 buffer solution in the absence and presence of 10.0 g L^{-1} JBX with the concentrations of oxalate remaining and $^{14}CO_2$ formed continuously measured using the method described in chapter 3.

4.2.3.3. Ozone decay

Investigation of aqueous ozone decay was performed in head–space free gas–tight syringe reactors (see chapter 3). For measurement, aqueous ozone (~120.0 μM) was added to pH 3.0, 7.3 or 8.5 buffer solution in the absence and presence of 1.0 or 10.0 g L^{-1} JBX (or carrier). We also measured the ozone decay in the presence of formate and H_2O_2 at pH 3.0, 7.3 and 8.5. For measurement of O_3 decay in the presence of H_2O_2, H_2O_2 in the concentration range 10.0 – 100.0 μM was added to pH 3.0 and 8.5 buffer solution with initial ozone concentration of ~120.0 μM. For measurement of ozone decay in the presence of formate, 0.0 – 160.0 μM formate was added to pH 3.0, 7.3 and 8.5 buffer solution and 120.0 μM ozone was spiked into the reactor. The aqueous ozone concentration remaining was measured using the indigo method [107] as described in detail in chapter 3.

We would like to highlight that even though the initial ozone concentration used in formate/oxalate degradation studies and ozone decay studies were different due to the constraints on the detection limit of the method used for ozone measurement, the difference in initial ozone concentration has no impact on the interpretation of our results and conclusions made here since the measured half-lives of ozone were similar for various initial O_3 concentrations ($t_{1/2}$ = 11.7 ± 0.2 and 10.5 ± 0.1 min for initial O_3 concentrations of 10.0 and 120.0 μM respectively at pH 8.5) which is comparable to earlier reported values.[131]

4.2.3.4. Hydroxyl radical measurement

To evaluate the rate and extent of bulk $^{\bullet}OH$ generation on ozone self–decay, *p*–CBA was used as the $^{\bullet}OH$ probe since it has high reactivity towards $^{\bullet}OH$ ($k_{^{\bullet}OH,\, p\text{-}CBA}$ = 5.0 ×

10^9 $M^{-1}s^{-1}$) but low reactivity towards ozone ($k_{O_3,\ p\text{-CBA}}$ = 0.15 $M^{-1}\cdot s^{-1}$;[87]). For measurement, 1.0 µM *p*–CBA and ozone (10.0 – 100.0 µM) were added to pH 3.0, 7.3 and 8.5 buffer solution to initiate the reaction. The *p*–CBA concentration was measured using the method described in detail in chapter 3. Due to the strong adsorption of *p*–CBA on JBX and the carrier, $^{\bullet}$OH measurement experiments were not conducted in the presence of catalyst (or carrier).

4.2.4 Kinetic modelling and statistical analysis

Kinetic modelling of the experimental results was performed using the software package Kintecus [132] as described in chapter 3.

4.3. Results and Discussion

4.3.1. Catalyst characterization

The surface areas of both JBX and its carrier are high with values of 1640 ± 48 and 1499 ± 36 m^2 g^{-1} (BET model) respectively (Figure 4.1). The average pore sizes of JBX and the carrier are 2.8 ± 0.1 and 2.6 ± 0.1 nm (BJH model) respectively. While the detailed synthesis procedure for JBX is commercially confidential, it is purported that metals have been loaded onto the carbon to improve the catalytic activity. In view of the similar surface areas and average pore sizes of JBX and its carrier, we surmise that the metal loading process has little impact on the structural or textural properties of the carrier.

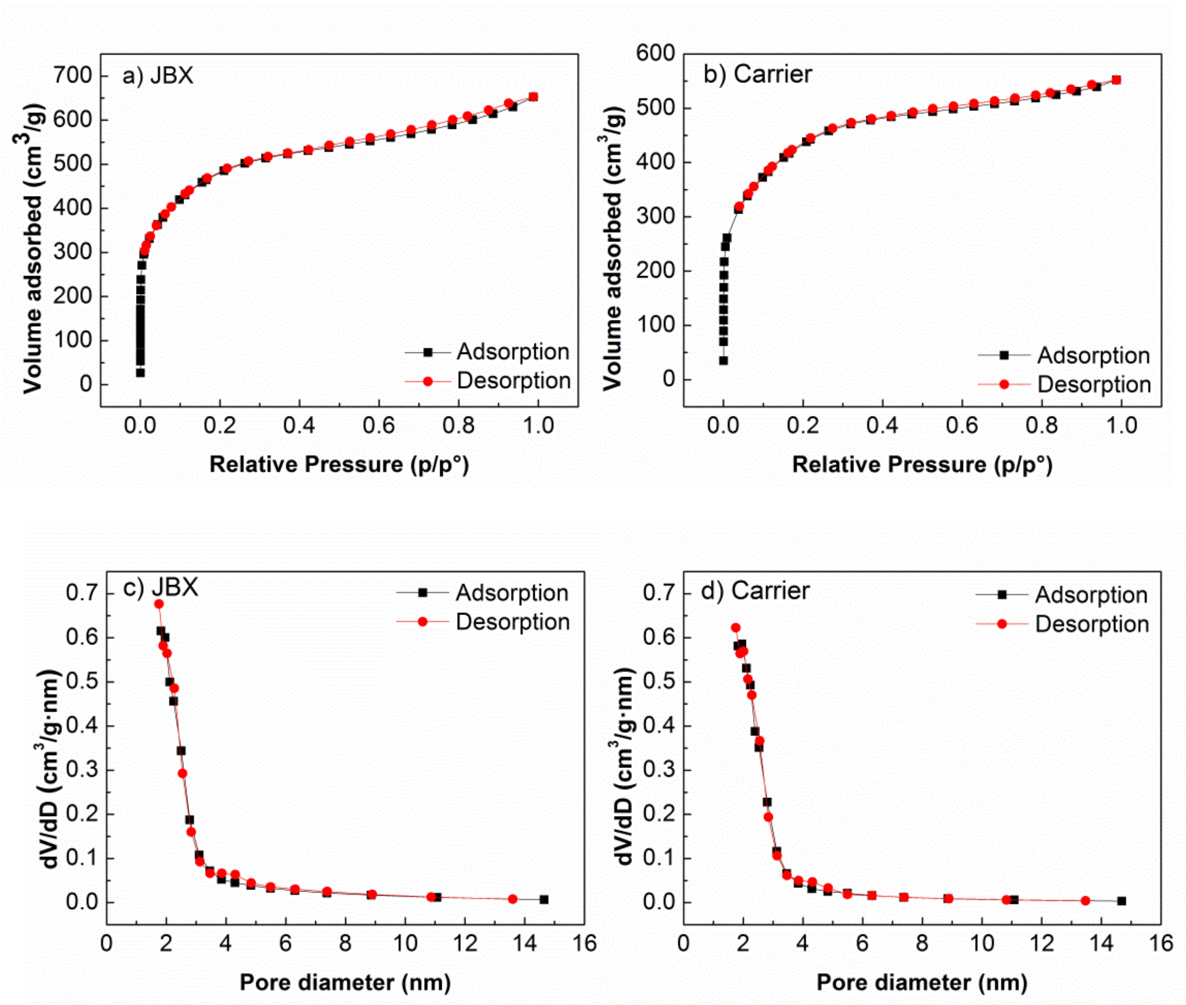

Figure 4.1 N_2 adsorption isotherm of a) JBX (surface area 1640 ± 48 m^2/g), b) carrier (surface area 1499 ± 36 m^2/g). Panel c and d represent the pore size distribution of JBX (average pore size 2.8 ± 0.1 nm) and carrier (average pore size 2.6 ± 0.1 nm) respectively.

SEM–EDX measurements were performed to determine the active metal(s) on the catalyst surface (Figure 4.2). It can be seen that Fe peaks are more evident in the JBX spectrum compared to its carrier. In addition to iron, a variety of elements including sodium, aluminium, calcium, potassium and magnesium were also present in both JBX and the carrier but at comparable abundances. These ubiquitous earth metals are likely associated with the manufacturing process of the carbon carrier rather than addition of these metals for catalytic purposes.[127] As such, we surmise that Fe is the active element loaded onto to the carbon carrier with this element likely present as an iron oxide. The SEM–EDX measurement of the surface layer and the core shows that Fe is present through the entirety of the catalyst (Figure 4.2 and 4.3) indicating that the catalyst is not of a “core–shell” structure. Note that aluminium oxide, present in JBX and the carrier, may also exhibit catalytic activity as described in some earlier studies;[133, 134] however iron oxide is expected to be a more reactive surface than alumina for the reaction with ozone as reported by Mitchell and co–workers [135] and also supported by our experimental results (discussed in detail in later sections) wherein the presence of even a small amount of iron oxide (as in JBX) demonstrates higher catalytic ability than the aluminium containing carrier.

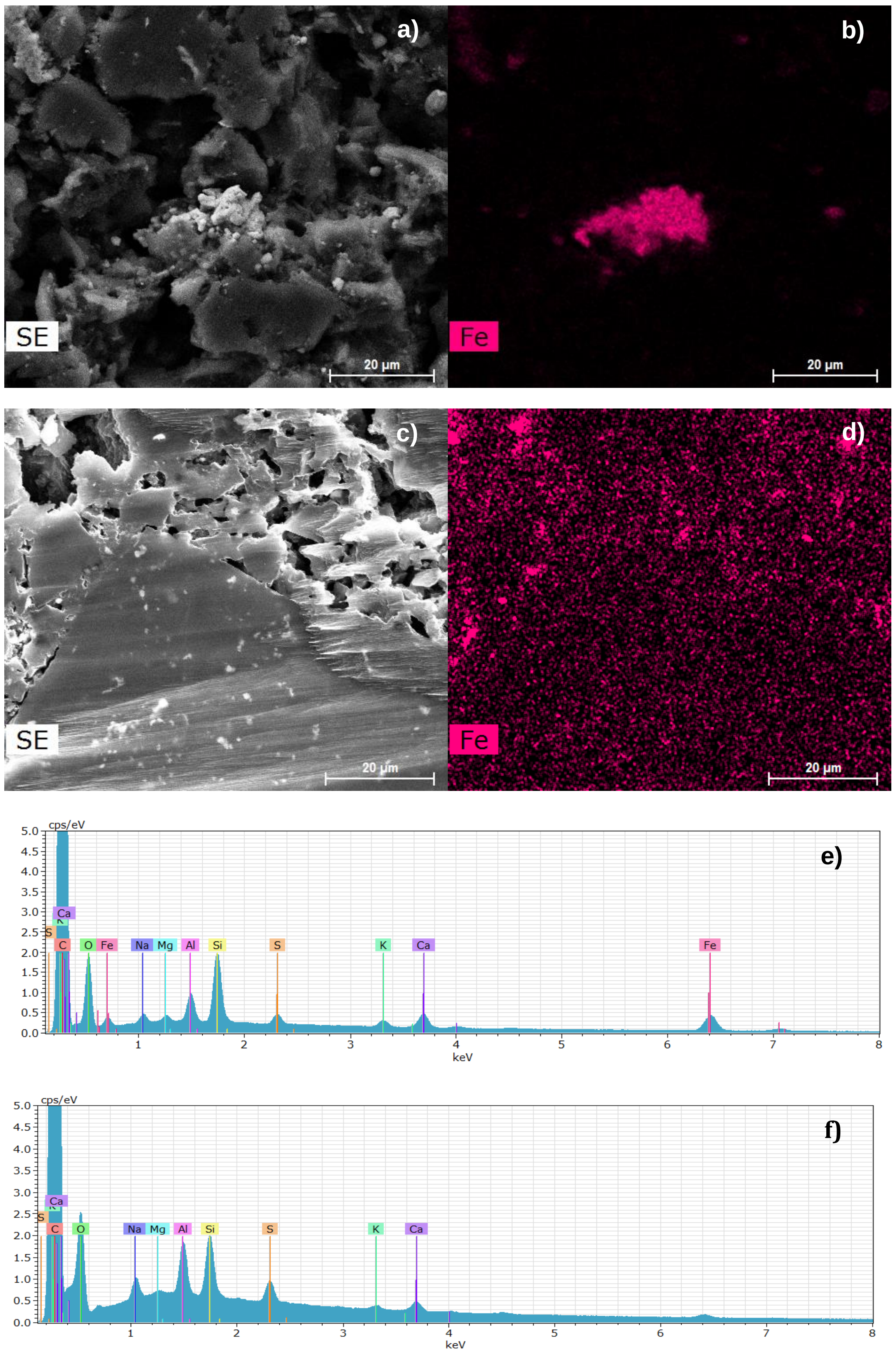

Figure 4.2 SEM–EDX mapping images of JBX (panel a and b) and carrier (panel c and d), and EDX spectra of JBX (panel e) and carrier (panel f).

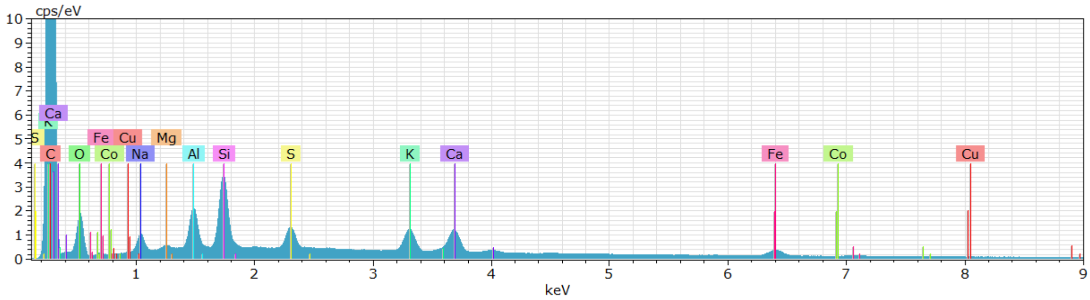

Figure 4.3 SEM–EDX spectrum of the core of JBX

The pH_{pzc} of JBX is 8.3, slightly higher than that of the carrier (7.5, Figure 4.4), suggesting that the presence of Fe may alter the surface properties of the activated carbon. Note that further characterization of the nature of the iron oxides using techniques such as X–ray diffraction (XRD) and X–ray photoelectron spectroscopy (XPS) was not feasible since the loaded Fe concentration was low (< 0.1%).

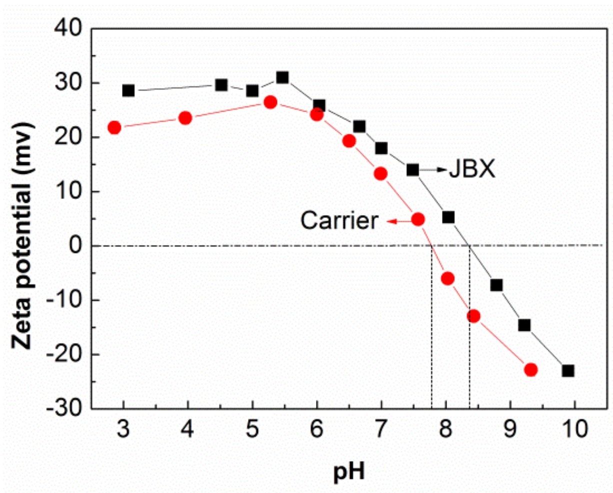

Figure 4.4 Measured zeta potential of JBX and carrier under varying pH conditions. Experimental conditions: [NaCl] = 10.0 mM; [catalyst] = 0.5 g L^{-1}.

4.3.2. Ozone decay in the absence and presence of catalyst

As shown in Figure 4.5, the rate of ozone self–decay (i.e., in the absence of JBX and the carrier) increases with increase in pH with nearly 12%, 40% and 85% ozone consumed within 30 min at pH 3.0, 7.3 and 8.5 respectively. This is in agreement with the mechanism that self–decay of ozone is initiated by hydroxyl ions (OH^-) resulting in the formation of $^{\bullet}OH$ [7, 22, 136, 137] (see eqs 4.1 – 4.7). The formation of $^{\bullet}OH$ on ozone decay is supported by results showing the oxidation of *p*–CBA at pH 3.0, 7.3 and 8.5 (Figure 4.6), which is known to react rapidly with $^{\bullet}OH$ (5×10^{9} $M^{-1}\cdot s^{-1}$) but slowly with O_3 (0.15 $M^{-1}\cdot s^{-1}$).[87] The pH dependence of *p*–CBA oxidation supports the conclusion that O_3 decay to form $^{\bullet}OH$ increases with increase in pH.

$$O_3 + OH^- \rightarrow HO_4^- \tag{4.1}$$

$$HO_4^- \rightleftharpoons HO_2^{\bullet} + O_2^{\bullet-} \tag{4.2}$$

$$HO_2^{\bullet} \rightleftharpoons H^+ + O_2^{\bullet-},\ pK_a = 4.8 \tag{4.3}$$

$$O_2^{\bullet-} + O_3 \rightarrow O_2 + O_3^{\bullet-} \tag{4.4}$$

$$HO_3^{\bullet} \rightleftharpoons H^+ + O_3^{\bullet-},\ pK_a = 8.2 \tag{4.5}$$

$$HO_3^{\bullet} \rightarrow {}^{\bullet}OH + O_2 \tag{4.6}$$

$${}^{\bullet}OH + O_3 \rightarrow HO_2^{\bullet} + O_2 \tag{4.7}$$

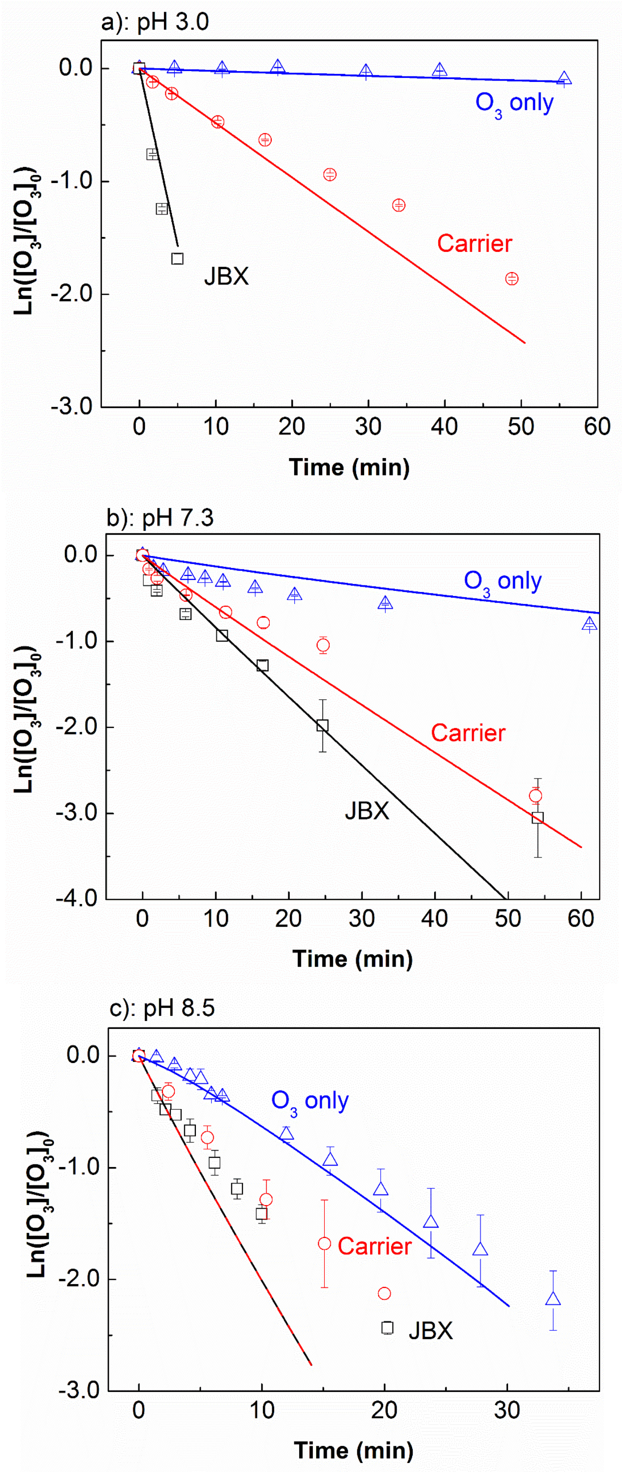

Figure 4.5 O_3 decay in the absence (triangles) and presence of JBA (squares) and carrier (circles) at pH 3.0 (panel a), pH 7.3 (panel b) and pH 8.5 (panel c). Initial conditions: $[O_3]_0 = 120.0$ µM, $[\text{catalyst}]_0 = 10.0$ g L^{-1}. Symbols represent experimental data and lines represent modelled values.

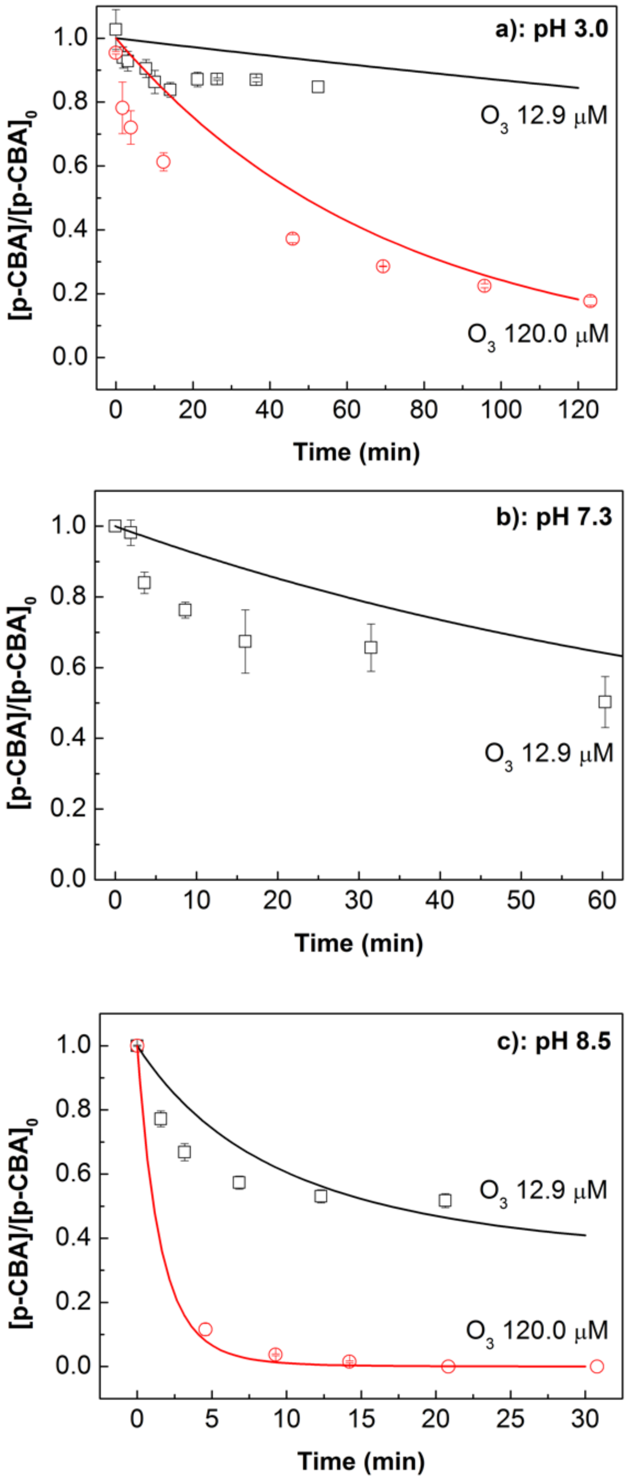

Figure 4.6 Measured decrease in *p*–CBA concentration in the presence of O_3 at (a) pH 3.0, (b) pH 7.3 and (c) 8.5 at ozone concentration of 12.9 μM (solid black square) and 120 μM (solid red dot). Symbols represent experimental data and lines represent modelled values.

The presence of JBX facilitates the decay of aqueous ozone with the impact of JBX much more pronounced at pH 3.0 than at 7.3 and 8.5 (Figure 4.5). Furthermore, our results show that the carrier also enhances the rate of ozone decay at pH 3.0, 7.3 and 8.5. The overall rate of ozone decay measured here can be expressed as:

$$\frac{d[O_3]}{dt} = -(k_{OH^-} + k_{AC} + k_{Fe})[O_3] \tag{4.8}$$

where k_{OH^-}, k_{AC} and k_{Fe} respectively represent the apparent pseudo–first order rate constant of ozone reacting with hydroxyl ions (i.e., self–decay), the activated–carbon surface and iron oxide impregnated catalyst. Based on the measured ozone concentration under various conditions, we calculated the values of k_{OH^-}, k_{AC} and k_{Fe}under varying pH conditions (see Table 4.1). As shown in Table 4.1, the value of k_{OH^-} increases with increase in pH since the self–decay of ozone is initiated by hydroxyl ions. The value of k_{AC} is similar at pH 3.0, 7.3 and 8.5 which suggests that the interaction of ozone with the carbon surface is not dependent on pH. This is in agreement with previous studies in which the catalytic activity of activated carbon was found to be not particularly sensitive to pH change.[63, 138] The value of k_{Fe} decreases with increase in pH from 3.0 to 8.5 which suggests that the protonated positively charged iron oxide surface sites interact with ozone much more rapidly than the negatively charged deprotonated sites. This is in agreement with an earlier report in which only uncharged >Fe–OH^0 and/or positively charged >Fe–OH_2^+ surface groups promote ozone decay when goethite was used as the catalyst.[139] Detailed discussion of model fits is available in section 4.3.5.

Table 4.1 Apparent pseudo–first order rate constant of ozone reaction with hydroxide (k_{OH^-}), iron oxides (k_{Fe})and activated carbon surface (k_{AC}) at pH 3.0, 7.3 and 8.5.

pH	pH 3.0	pH 7.3	pH 8.5
k_{OH^-}	$(4.3 \pm 0.3) \times 10^{-5}$ s^{-1}	$(2.0 \pm 0.4) \times 10^{-4}$ s^{-1}	$(1.1 \pm 0.1) \times 10^{-3}$ s^{-1}
k_{AC}	$(5.6 \pm 0.2) \times 10^{-4}$ s^{-1}	$(5.8 \pm 0.3) \times 10^{-4}$ s^{-1}	$(7.3 \pm 0.2) \times 10^{-4}$ s^{-1}
k_{Fe}	$(5.0 \pm 0.3) \times 10^{-3}$ s^{-1}	$(1.3 \pm 0.2) \times 10^{-4}$ s^{-1}	0.0 ± 0.0 s^{-1}

4.3.3. Formate oxidation by ozonation

As shown in Figure 4.7, the $HCOOH/HCOO^-$ concentration decreases with concomitant formation of CO_2 in the absence of catalyst (Figure 4.8) with this result supporting the conclusion that the oxidation of $HCOOH/HCOO^-$ occurs in the presence of ozone alone. The rate and extent of $HCOOH/HCOO^-$ oxidation increases with increase in pH; for example, nearly 28.8%, 57.7% and 70.5% $HCOOH/HCOO^-$ were oxidized within 30 min at pH 3.0, 7.3 and pH 8.5 respectively (Figure 4.8). Note that the dissociation of formic acid (p*K*a=3.8) is dependent on pH with formic acid and formate dominating at pH 3.0 and 7.3/8.5 respectively. As described in earlier studies,[140] $HCOOH/HCOO^-$ can be oxidized either by direct interaction with O_3 and/or $^{\bullet}OH$ formed on O_3 decay (eqs. 4.9 – 4.12). The direct reaction of O_3 can occur via hydride transfer (eq. 4.9) and/or H abstraction (eq. 4.10) with the latter process resulting in formation of $HO_3^{\cdot}$ which is a precursor for $^{\bullet}OH$ formation.

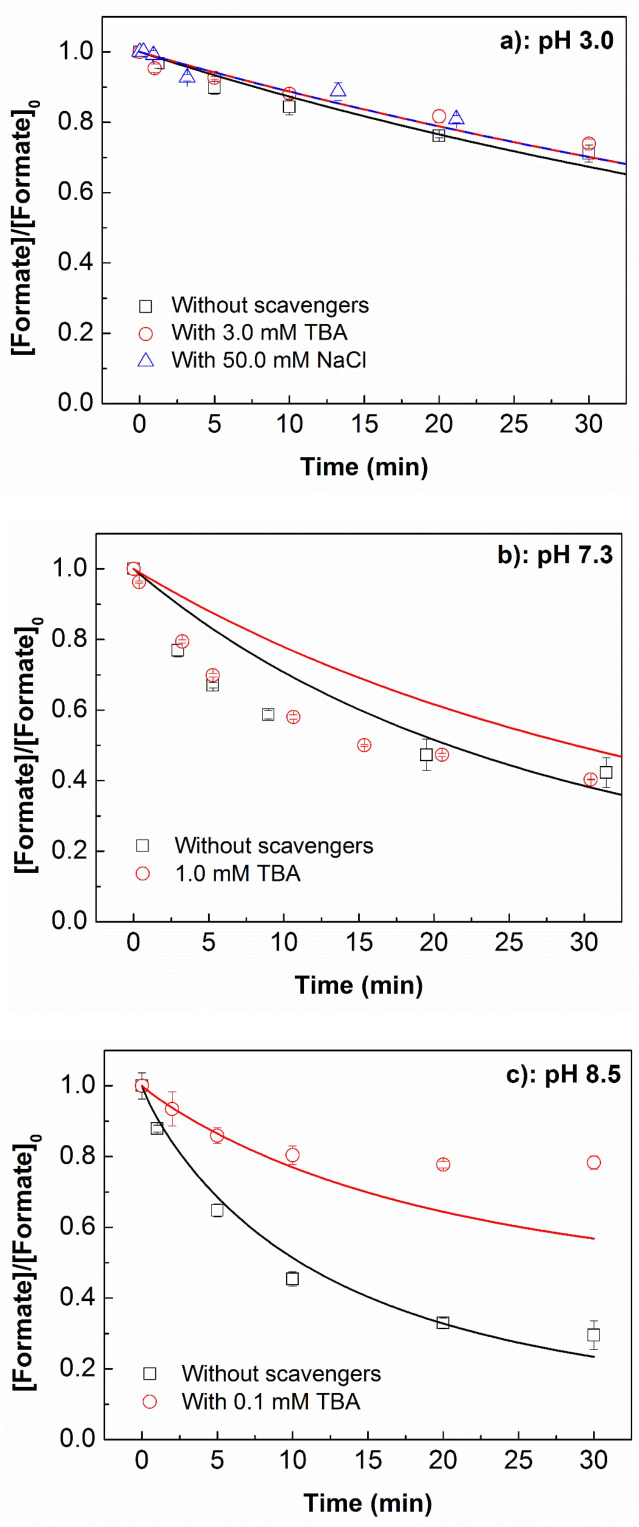

Figure 4.7 Formate removal during ozonation at pH 3.0, pH 7.3 and pH 8.5 in the absence (squares) and presence (circles for TBA and triangles for NaCl) of $^{\bullet}OH$ scavengers. Initial conditions: $[O_3]_0$ = 10.0 µM, $[\text{formate}]_0$ = 1.0 µM, $[\text{TBA}]_0$ = 0.1 mM at pH 8.5, 1.0 mM TBA at pH 7.3 and 3.0 mM at pH 3.0. $[\text{NaCl}]_0$ = 50.0 mM at pH 3.0. Symbols represent measured values and lines represent model results.

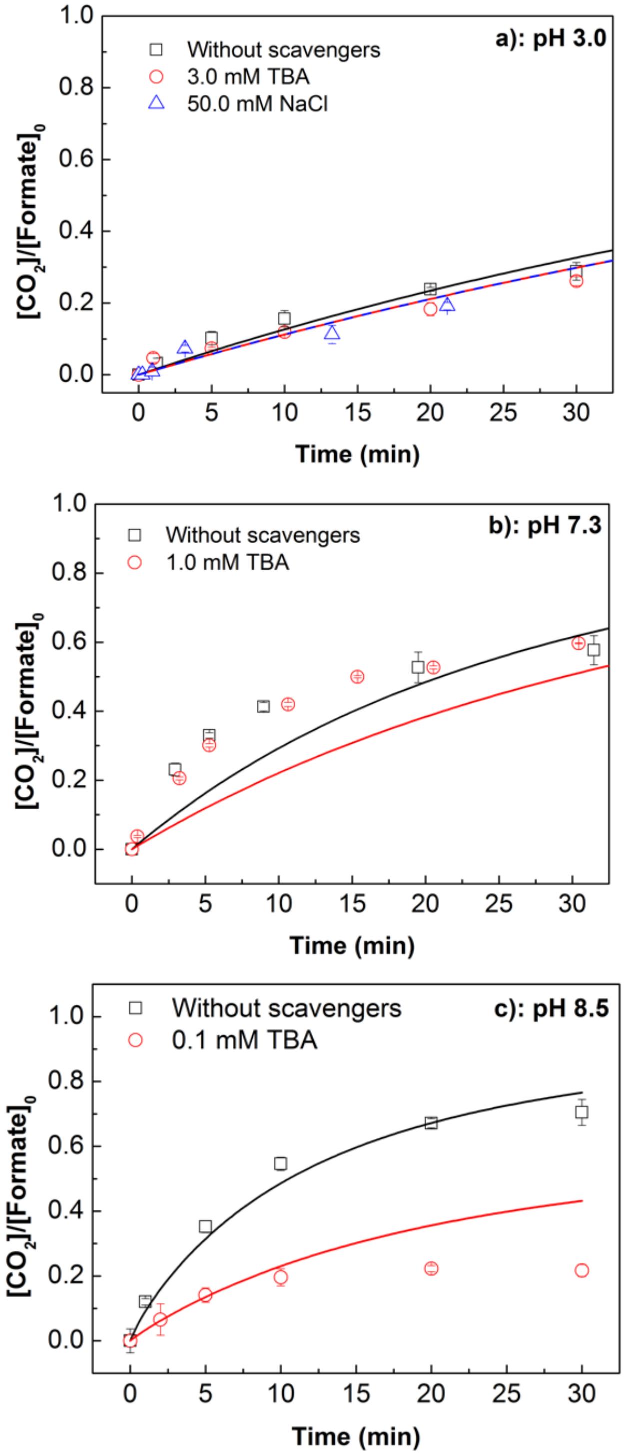

Figure 4.8 CO_2 formation during conventional ozonation at (a) pH 3.0, (b) 7.3 and (c) 8.5 in the presence and absence of TBA or chloride. Initial conditions: $[O_3]_0$ = 10.0 µM, $[\text{formate}]_0$ = 1.0 µM, $[TBA]_0$ = 0.1 mM at pH 8.5, 1.0 mM TBA at pH 7.3 and 3.0 mM at pH 3.0. $[NaCl]_0$ = 50.0 mM at pH 3.0. Symbols represent measured values and lines represent model results.

$$HCOO^- + O_3 \rightarrow CO_2 + HO_3^- \quad (4.9)$$

$$HCOO^- + O_3 \rightarrow CO_2^{\bullet -} + HO_3^{\bullet} \quad (4.10)$$

$$HCOO^- + {}^{\bullet}OH \rightarrow CO_2^{\bullet -} + H_2O \quad (4.11)$$

$$CO_2^{\bullet -} + O_2 \rightarrow CO_2 + O_2^{\bullet -} \quad (4.12)$$

The pH dependence of oxidation of $HCOOH/HCOO^-$ should be related to the pH-dependence of rate of generation (and consumption) of both oxidants. As discussed earlier, O_3 undergoes decay initiated by OH^- resulting in the formation of $^{\bullet}OH$ (eqs 4.1 – 4.7 [7, 22, 136, 137]), leading to the expectation that $^{\bullet}OH$ mediated oxidation should be more important under alkaline conditions. However, as discussed above, $HCOOH/HCOO^-$ may also initiate O_3 decay to form $^{\bullet}OH$ (eqs. 4.10 and 4.5) and, as such, the pH dependence of $^{\bullet}OH$ generation may not be entirely governed by O_3 self–decay. In order to elucidate the contribution of $^{\bullet}OH$ to $HCOOH/HCOO^-$ oxidation in ozonation, we measured the impact of TBA addition ($k_{^{\bullet}OH,\ TBA} = 5.0 \times 10^8$ $M^{-1} \cdot s^{-1}$;[141] on $HCOOH/HCOO^-$ oxidation. It can be seen from Figure 4.7 that addition of TBA significantly inhibited (69.2% in 30 min) $HCOOH/HCOO^-$ oxidation at pH 8.5 however no impact of TBA addition was observed at pH 7.3 and 3.0. Significant inhibition of $HCOOH/HCOO^-$ oxidation at pH 8.5 in the presence of TBA support the conclusion that $HCOOH/HCOO^-$ oxidation is mainly governed by $^{\bullet}OH$ at pH 8.5. In agreement with the impact of TBA addition, we observed no impact of addition of Cl^- (Figure 4.7), a known scavenger of $^{\bullet}OH$ under acidic conditions,[142] on $HCOOH/HCOO^-$ oxidation at pH 3.0. Thus, based on the observed impact of TBA and Cl^-, we conclude that formate oxidation by conventional ozonation occurs via hydride transfer for pH 3. We would like to highlight that the TBA scavenging results may not be conclusive at pH

7.3 as a result of alteration in the oxidation pathway of $HCOOH/HCOO^-$ in the presence of TBA as discussed in detail in chapter 8. As discussed in detail in chapter 8, in the case of compounds such as $HCOO^-$ which promotes O_3 decay and are ozone reactive, the presence of TBA result in the alteration in the pathway of oxidation from $^{\bullet}OH$ mediated $HCOO^-$ oxidation in the absence of TBA to O_3 mediated oxidation in the presence of TBA.

The mechanism of formate oxidation by ozone determined here is in agreement with the mechanism reported by Reisz *et al.*,[140] however differs from that reported in an earlier study.[143] The differences in the experimental conditions (pH, higher formate concentration, etc.) employed in the two studies possibly contributes to the discrepancy in the mechanism which, as shown here, varies considerably with pH as well as formate concentration (discussed in detail in later sections).

We would like to highlight that a significant fraction of the $^{\bullet}OH$ formed on O_3 decay will be scavenged by bicarbonate ions/carbonate ions present in the buffer solution (eq. 4.13). Note that carbonic acid is the dominant specie at pH 3.0 while bicarbonate dominates at pH 7.3 and 8.5 based on the pH-pKa diagram of carbonic acid. While the scavenging of $^{\bullet}OH$ by HCO_3^-/CO_3^{2-} decreases the ozone efficiency in various earlier studies,[144-146] the scavenging of $^{\bullet}OH$ by HCO_3^-/CO_3^{2-} does not influence formate oxidation since carbonate radical ($CO_3^{\bullet-}$) formed from $^{\bullet}OH$ – HCO_3^-/CO_3^{2-} reaction is able to oxidize formate (eq. 4.14) as well.[147] Instead, the scavenging of $^{\bullet}OH$ by HCO_3^-/CO_3^{2-} prevents the futile consumption of ozone via O_3 – $^{\bullet}OH$ interaction (eq. 4.7), thereby stabilizing ozone [145] and increasing the efficiency of the ozonation process.

$$HCO_3^- / CO_3^{2-} + {}^{\bullet}OH \rightarrow CO_3^{\bullet-} + H_2O \qquad (4.13)$$

$$HCOO^- + CO_3^{\bullet-} \rightarrow CO_2^{\bullet-} + HCO_3^- \qquad (4.14)$$

4.3.4. Formate removal by catalytic ozonation

4.3.4.1. Formate oxidation by catalytic ozonation

As can be clearly seen in Figure 4.9, the $HCOOH/HCOO^-$ concentration decreased on ozonation with concomitant formation of CO_2 in the presence of JBX and carrier. The extent of oxidation of $HCOOH/HCOO^-$ by ozonation in the presence of JBX or carrier was slightly lower than that obtained by conventional ozonation at pH 7.3 and 8.5 with this result indicating that the presence of the catalyst and/or carrier does not improve the oxidation efficiency, at least under the circumneutral pH conditions investigated here (see Table 4.2). In contrast, the presence of JBX or carrier enhanced oxidative $HCOOH/HCOO^-$ removal at pH 3.0 (Figure 4.9 and Table 4.2). Note that at all pH conditions investigated here, $HCOOH/HCOO^-$ removal via adsorption during catalytic ozonation was minor (< 20%; Table 4.2). Our results further show that the impact of JBX on $HCOOH/HCOO^-$ oxidation at pH 3.0 was more pronounced than the carrier at pH 3.0. This observation supports the conclusion that the presence of iron oxides at the JBX surface promotes ozone decay (Figure 4.7) and, consequently, oxidant generation and formate oxidation at pH 3.0 (Figure 4.9). Note that no dissolved iron in ozonated pH 3.0 solution containing 10 $g.L^{-1}$ JBX was detected by inductively coupled plasma atomic emission spectroscopy (ICP–OES) suggesting that homogeneous catalytic ozonation as a result of interaction with any leached iron from JBX was negligible. The carrier also improved $HCOOH/HCOO^-$ oxidation at pH 3.0; i.e., the interaction of O_3 with activated carbon alone (at this pH) also results in formation of oxidants capable of oxidizing $HCOOH/HCOO^-$.

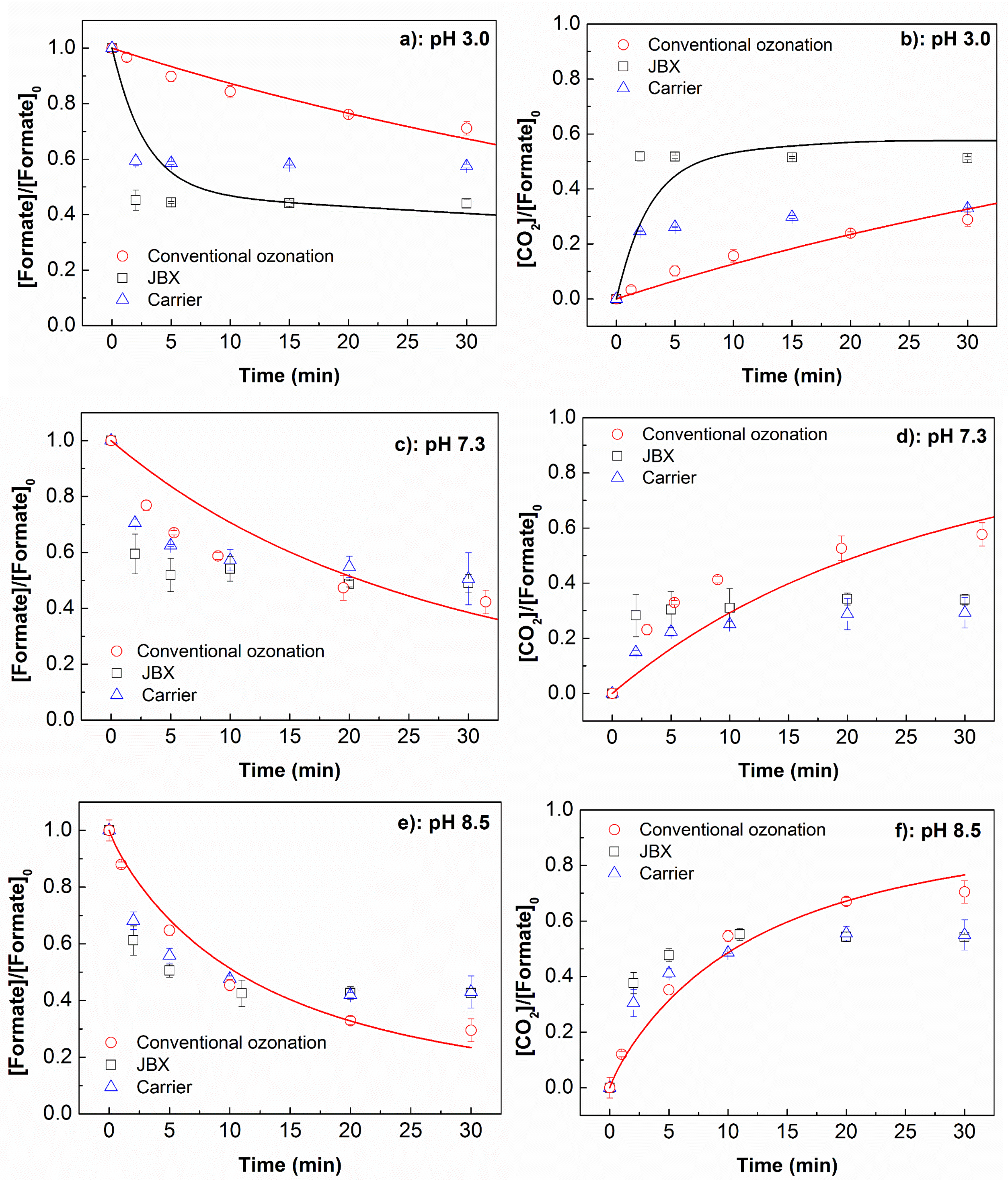

Figure 4.9 Formate removal and concomitant CO_2 formation in conventional O_3 (circles) and catalytic O_3 using JBX (squares) and carrier (triangles) at pH 3.0 (panel a and b respectively), pH 7.3 (panel c and d respectively), and pH 8.5 (panel e and f respectively). Initial conditions: $[O_3]_0$ = 10.0 μM, $[\text{formate}]_0$ = 1.0 μM, $[\text{catalyst}]_0$ = 10.0 g L^{-1}.

Table 4.2 Comparison of oxidative and adsorptive removal of $HCOOH/HCOO^-$ during the catalytic ozonation process at pH 3.0, 7.3 and 8.5.

	HCOOH removal		
pH 3.0			
	% Total removal	% oxidative removal	% adsorptive removal
Adsorption by JBX	28.4±8.5	0.0	28.4±8.5
Adsorption by carrier	2.9±0.4	0.0	2.9±0.4
O_3 only	28.8±2.5	28.8±2.5	0.0
Catalytic O_3 by JBX	60.4±3.9	52.7±4.7	7.7±.4.9
Catalytic O_3 by JBX + TBA	37.0±7.4	27.1±3.0	9.9±10.4
Catalytic O_3 by JBX + Cl^-	37.4±1.8	27.5±1.1	9.9±10.4
Catalytic O_3 by carrier	46.7±4.7	33.9±2.7	12.9±2.1
Catalytic O_3 by carrier + TBA	38.7±0.1	28.9±0.1	10.1±0.3
pH 7.3			
Adsorption by JBX	15.2±1.9	0.0	15.2±1.9
Adsorption by carrier	11.3±0.3	0.0	11.3±0.3
O_3 only	57.7±4.2	57.7±4.2	0.0
Catalytic O_3 by JBX	51.0±3.2	34.0±1.9	17.0±1.9
Catalytic O_3 by carrier	49.5±9.3	29.2±5.5	20.2±3.8
pH 8.5			
Adsorption by JBX	7.4±1.1	0.0	7.4±1.1
O_3 only	70.50±4.01	70.50±4.01	0.0
Catalytic O_3 by JBX	57.4±1.6	54.2±1.7	3.1±0.5
Catalytic O_3 by JBX + TBA	40.8±1.8	33.3±4.2	7.5±2.4
Catalytic O_3 by carrier	57.0±5.7	55.0±5.5	2.0±0.2
Catalytic O_3 by carrier + TBA	43.0±0.7	35.8±0.3	7.2±0.4

Note: % removal shown here were obtained at 30min.

Varying the catalyst dosage from 10.0 to 1.0 g.L^{-1} decreases the rate and extent of ozone decay and formate oxidation at pH 3.0 ; however no significant (p> 0.05 using single tailed student's t–test) influence of varying the catalyst dosage was observed at pH 8.5 (Figure 4.10). This observation further supports the conclusion that JBX is active in initiating ozone decay and oxidant generation under acidic conditions. At pH 8.5, however the catalyst is ineffectual with most of the ozone decay and formate oxidation observed under these conditions occurring via the conventional ozonation process only.

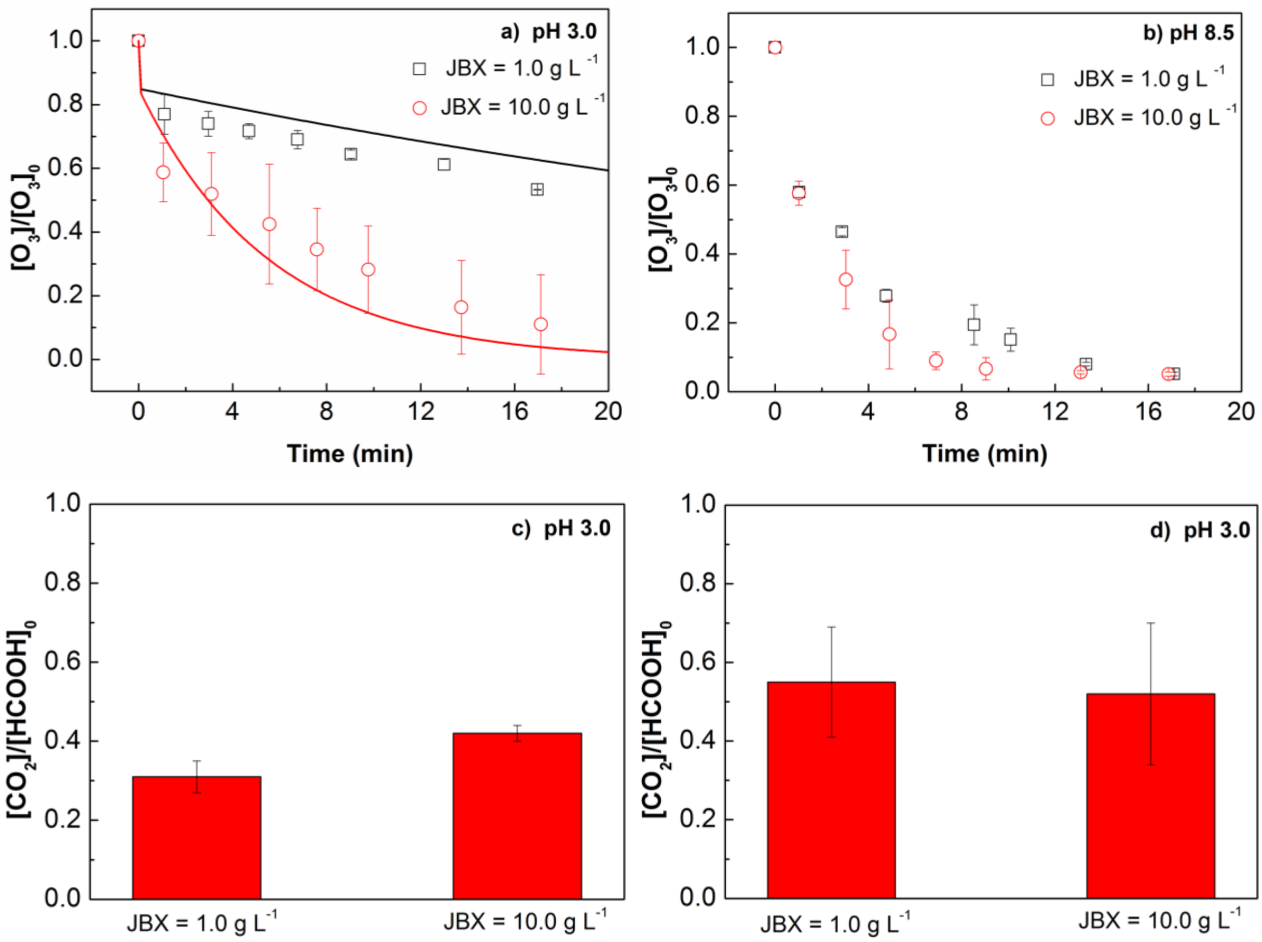

Figure 4.10 Measured ozone decay (panel a and b) in the presence of variant JBX dosage at pH 3.0 and 8.5. Initial condition: $[O_3]_0$ = 100.0 µM, JBX = 1.0 (open squares) or 10.0 g L^{-1} (open circles). Measured formate oxidation after 30 min of reaction time (panel c and d) in the presence of variant JBX dosage at pH 3.0 and 8.5. Initial condition: $[O_3]_0$ = 100.0 µM, JBX = 1.0 or 10.0 g L^{-1}

4.3.4.2. Nature of the oxidant generated during catalytic ozonation at pH 3.0

In order to gain insight into the nature of the oxidant(s) generated during catalytic ozonation at pH 3.0, we measured the impact of TBA and Cl^- addition on the oxidation of $HCOOH/HCOO^-$ in the presence of JBX or carrier at pH 3.0. As shown in Figure 4.11 and Table 4.2, addition of TBA and Cl^- significantly inhibits catalytic oxidation of $HCOOH/HCOO^-$ at pH 3.0 when JBX is used as the catalyst. Specifically, in the presence of 3.0 mM TBA and 50.0 mM Cl^-, the extent of $HCOOH/HCOO^-$ oxidation decreased by 47.1% and 46.1% respectively. This is in contrast with the observed impact of TBA and Cl^- during ozonation only (Figure 4.7) with this result supporting the conclusion that the oxidant involved in $HCOOH/HCOO^-$ oxidation is different for the conventional and catalytic ozonation processes at pH 3.0. Since, TBA and Cl^- are both known to scavenge $^{\bullet}OH$ under acidic conditions,[142, 148] it appears that the oxidant generated during catalytic ozonation using JBX as the catalyst is $^{\bullet}OH$. This hypothesis is in agreement with earlier studies which reported that interaction of O_3 with the iron oxides generates $^{\bullet}OH$.[47, 139, 149] Based on the observed impact of $Cl^-$and TBA, we further envisage that the majority of the oxidation of $HCOOH/HCOO^-$ occurs at the solid–liquid interface and/or in bulk solution.[30, 150] rather than on the surface of the catalyst (Cl^- and TBA is unlikely to scavenge surface oxidant(s)). As the short lifetime of $^{\bullet}OH$ largely excludes the possibility of diffusion into the bulk solution (D = ~10^{-10} $m^2 \cdot s^{-1}$ with the thickness of diffusion boundary layer being 50 – 100 μm,[29] we suggest that oxidation of $HCOOH/HCOO^-$ occurs in the solid–liquid interface with $HCOOH/HCOO^-$ and oxidant concentrations near the surface determining the rate of $HCOOH/HCOO^-$ oxidation. The hypothesis that the majority of the oxidation occurs in the solid-liquid interface rather than on the surface is also in agreement with the exceptionally high oxidation efficiency (i.e., 55% within 5 min as shown in Figure 4.9b) compared to the extent of adsorption observed when no O_3 was added (i.e., 28% after

30 min as shown in Figure 4.12a). Given that the majority of the oxidation likely occurs in the interfacial ozone, it appears that adsorption is not a precursor step for oxidation, at least for the catalyst and the experimental conditions investigated here. This conclusion is further supported by the observation that negligible oxidation of $HCOOH/HCOO^{-}$ was observed when formate was pre–adsorbed onto the catalyst prior to addition of ozone (Figure 4.13).

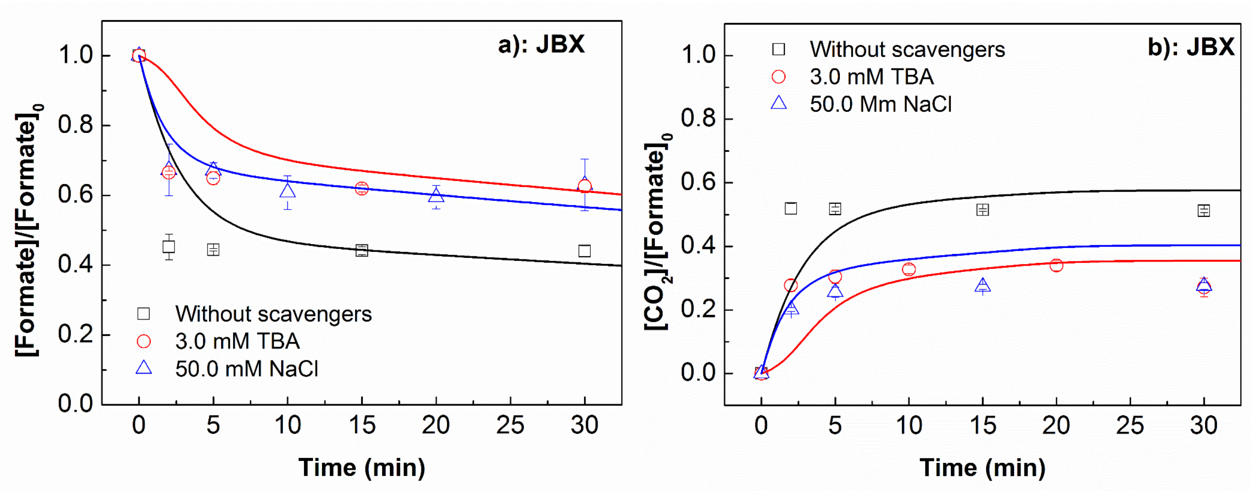

Figure 4.11 Formate removal (panel a) and CO_2 formation (panel b) during catalytic ozonation using JBX at pH 3.0 in the presence of TBA and NaCl. Initial conditions: $[O_3]_0$ = 10.0 µM, $[\text{formate}]_0$ = 1.0 µM, $[\text{TBA}]_0$ = 3.0 mM. $[\text{NaCl}]_0$ = 50.0 mM. Symbols represent measured values and lines represent model results.

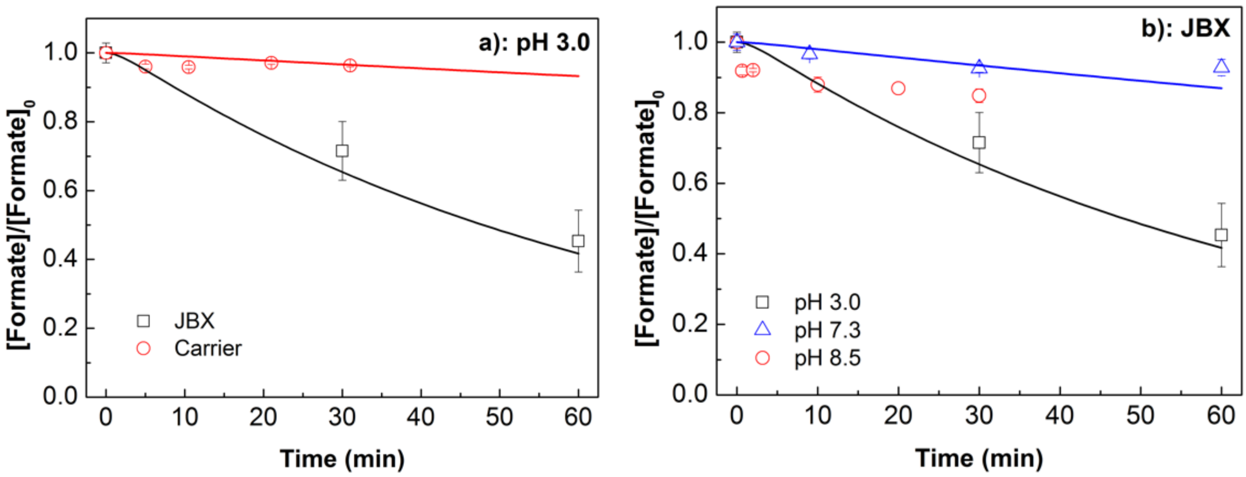

Figure 4.12 (a) Formate adsorption on JBX (squares) and carrier (circles) at pH 3.0 and (b) the influence of pH on formate adsorption in the presence of JBX. Initial conditions: $[\text{formate}]_0$ = 1.0 µM, [catalyst] = 10.0 g L^{-1}, pH 3.0, 7.3 and 8.5.

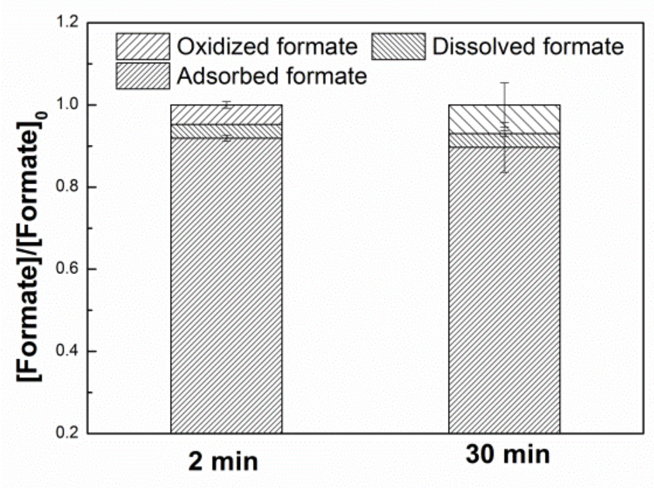

Figure 4.13 Measured change in formate concentration on oxidation of pre–adsorbed formate during catalytic ozonation using JBX at pH 3.0. Initial conditions: $[formate]_0$ = 0.8 μM, [catalyst] = 10.0 g L^{-1}.

The mechanism of $HCOOH/HCOO^-$ oxidation by catalytic ozonation in the presence of the activated carbon carrier appears to differ from that occurring in the presence of JBX since no impact of TBA and Cl^- addition on $HCOOH/HCOO^-$ oxidation was observed at pH 3.0 in the presence of the carrier (Figure 4.14). The exact mechanism and the nature of the oxidant generated on activated carbon–O_3 interaction is not clear based on our results but may possibly include carbon-based radicals that are not readily scavenged by TBA and Cl^-. Note that surface-mediated $HCOOH/HCOO^-$ oxidation is expected to be unimportant in the presence of the carrier since formate was found to adsorb minimally to the carrier at pH 3.0 (Figure 4.12).

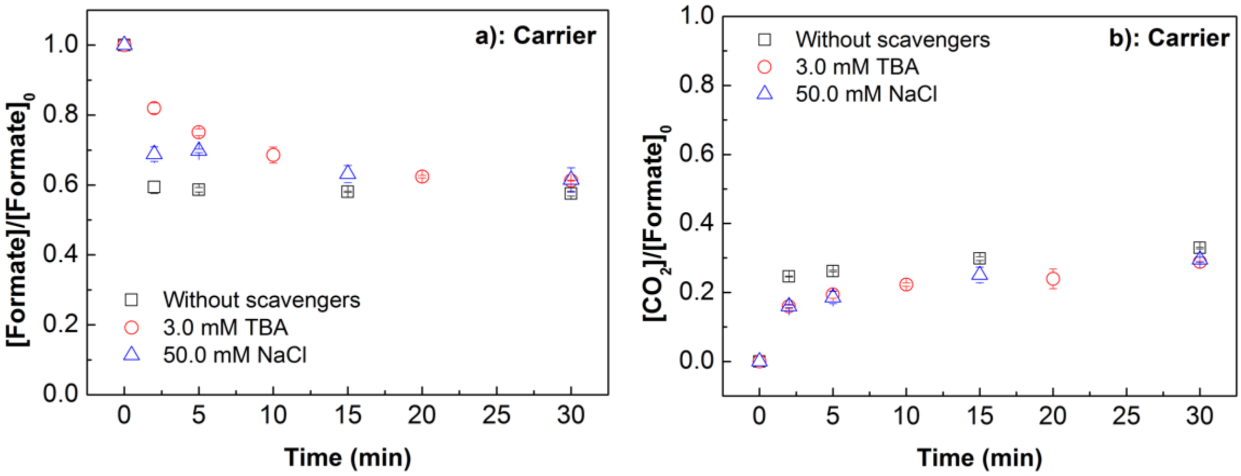

Figure 4.14 (a) Formate oxidation and (b) CO_2 formation during catalytic ozonation using carrier at pH 3.0 in the presence of TBA and NaCl. Initial conditions: $[O_3]_0$ = 10.0 μM, $[\text{formate}]_0$ = 1.0 μM, $[\text{TBA}]_0$ = 3.0 mM. $[\text{NaCl}]_0$ = 50.0 mM. Symbols represent measured values and lines represent model results.

4.3.5. Impact of nature of the organics on catalytic ozonation

As discussed above, the catalyst used here is not effective in promoting oxidation of $HCOOH/HCOO^-$ under circumneutral pH conditions. The ineffectiveness of the catalyst at alkaline pH is possibly related to (i) the inability of the catalyst to promote oxidant generation under circumneutral pH conditions and/or (ii) rapid O_3–formate interaction with formate oxidation not limited by $^{\bullet}OH$ (or other strong oxidant(s)) formation at these pH conditions. As discussed previously, formate can be effectively oxidized by ozone. However, for ozone resistant organic compounds, $^{\bullet}OH$ formation (via O_3 self–decay and/or catalyst–O_3 interaction) will be imperative to induce their oxidation. To probe this issue further, we measured the oxidation of oxalate (an ozone resistant organic compound;[123] during catalytic ozonation using JBX as the catalyst at pH 7.3. As shown in Figure 4.15, no significant increase in oxalate oxidation was observed in the presence of JBX supporting the conclusion that the inefficiency of the catalyst is not related to the nature of the organic compound but, rather, is due to its inability to generate oxidants under circumneutral pH conditions.

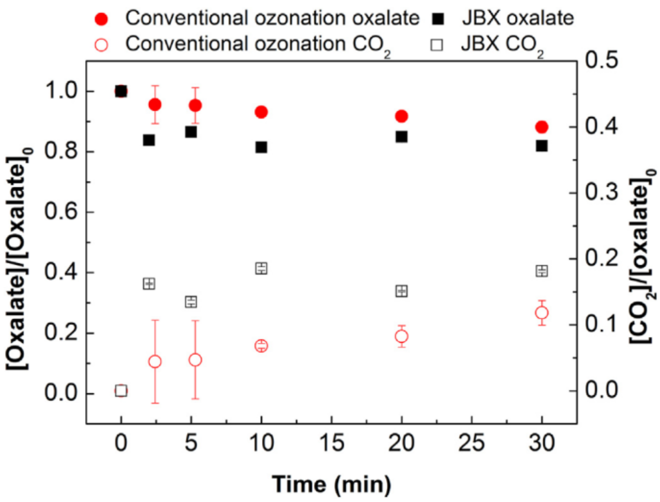

Figure 4.15 Oxalate removal (solid points) and concomitant CO_2 formation (open points) in conventional O_3 (circles) and catalytic O_3 (squares) process at pH 7.3. Initial conditions: $[O_3]_0$ = 10.0 µM, $[oxalate]_0$ = 1.0 µM, $[catalyst]_0$ = 10.0 g L^{-1}.

4.3.6. Mechanism of catalytic ozonation and kinetic modelling

Based on the results presented, we draw the following conclusions regarding the mechanism underpinning $HCOOH/HCOO^-$ oxidation during conventional and catalytic ozonation:

(i) The mechanism and rate of formate oxidation by ozonation are pH dependent. Direct oxidation of $HCOOH/HCOO^-$ by O_3 via hydride transfer is important at pH 3.0 while both O_3 and $^\bullet OH$ are involved in $HCOOH/HCOO^-$ oxidation under alkaline conditions.

(ii) For JBX, iron oxide surface sites present on the activated carbon carrier are the main adsorption sites for $HCOO^-$ with positively charged surface iron sites playing a key role in $HCOO^-$ uptake.

(iii) The activated carbon carrier interacts with O_3 resulting in formation of surface oxidants capable of oxidizing $HCOOH/HCOO^-$ near the carbon surface under acidic conditions.

(iv) Iron oxides on the activated carbon surface enhance ozone decay with resultant formation of oxidants (most likely $^{\bullet}OH$) under acidic conditions only.

(v) The rate and extent of oxidant generation increases with increase in the catalyst dosage under acidic conditions.

(vi) Impact of TBA and Cl^- oxidation during catalytic ozonation at pH 3.0 supports the hypothesis that oxidation of $HCOOH/HCOO^-$ occurs in the solid-liquid interfacial region and/or bulk solution and hence is not limited by the extent of adsorption of the organics.

A schematic of the various reactions potentially involved in the catalytic ozonation–mediated oxidation of $HCOOH/HCOO^-$ is provided in Figure 4.16. Based on the reaction mechanism shown in Figure 4.16, we have developed a reaction set and associated kinetic model to account for ozone decay and formate removal by conventional and catalytic ozonation (Table 4.3). The reactions used to explain self-decay of ozone (reactions 1 – 6, Table 4.3) and formate oxidation (reactions 11 – 15, Table 4.3) by ozonation alone are obtained from the literature with reported rate constants for these reactions used in almost all cases. Furthermore, as discussed earlier we have also included the scavenging of $^{\bullet}OH$ by bicarbonate/carbonate ions and/or H_2O_2 present (reactions 7 – 10, Table 4.3) in the experimental matrix since these reactions also have significant influence on ozone self–decay kinetics as well as $^{\bullet}OH$ availability for formate oxidation.

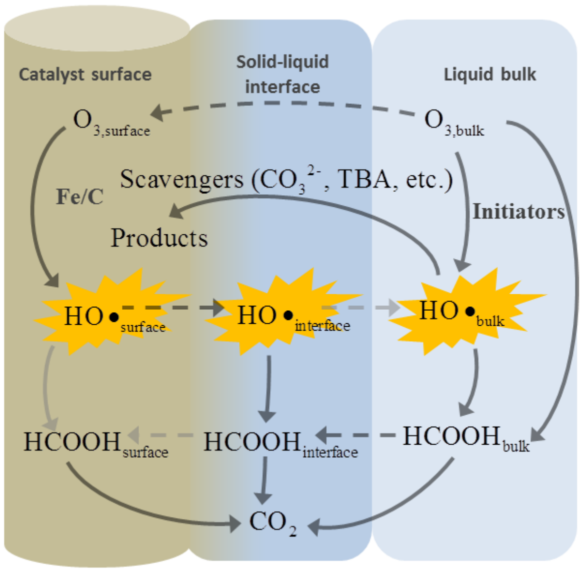

Figure 4.16 Reaction schematic depicting the mechanism of formate oxidation during catalytic ozonation.

Table 4.3 Kinetic model describing ozone decay and $HCOOH/HCOO^-$ removal during conventional ozonation and catalytic ozonation.

No	Reaction	Rate constant ($M^{-1}\cdot s^{-1}$)	Published value ($M^{-1}\cdot s^{-1}$)	Ref.
	Ozone self decay reactions in bulk solution			
1	$O_3 + OH^- \rightarrow HO_2^\bullet + O_2^{\bullet-}$	70.0	70.0	151
2	$O_3 + H_2O_2/HO_2^- \rightarrow HO_3^\bullet + O_2^{\bullet-}$	$\alpha_0 k_{H_2O_2} + \alpha_1 k_{HO_2^-}$ ^{a}	$k_{H_2O_2} = 6.5\times10^{-3}$; $k_{HO_2^-} = 2.8\times10^{6}$	152
3	$O_3 + O_2^{\bullet-} \rightarrow HO_3^\bullet + O_2$	$\alpha_1 k_{O_2^{\bullet-}}$ ^{b}	$k_{O_2^{\bullet-}} = 1.5\times10^{9}$	98
4	$HO_3^\bullet/O_3^{\bullet-} \rightarrow {}^\bullet OH + O_2$	$\alpha_0 k_{HO_3^\bullet} + \alpha_1 k_{O_3^{\bullet-}}$ ^{c}	$k_{HO_3^\bullet} = 1.4\times10^{5}\ s^{-1}$; $k_{O_3^{\bullet-}} = 2.1\times10^{3}\ s^{-1}$	151
5	${}^\bullet OH + O_3 \rightarrow O_2^{\bullet-} + O_2$	1.0×10^{8}	1.0×10^{8}	151
6	$O_3^\bullet + CO_3^{\bullet-} \rightarrow H_2CO_3 + O_2$	1.0×10^{5}	1.0×10^{5}	153
	Scavenging reactions in bulk solution			
7	${}^\bullet OH + H_2O_2/HO_2^- \rightarrow H_2O + O_2^{\bullet-}$	$\alpha_0 k_{H_2O_2} + \alpha_1 k_{HO_2^-}$ ^{a}	$k_{H_2O_2} = 2.7\times10^{7}$; $k_{HO_2^-} = 7.5\times10^{9}$	98
8	${}^\bullet OH + H_2CO_3/\ HCO_3^-/CO_3^{2-} \rightarrow OH^- + CO_3^{\bullet-}$	$\alpha_0 k_{H_2CO_3} + \alpha_1 k_{HCO_3^-} + \alpha_2 k_{CO_3^{2-}}$ ^{d}	$k_{H_2CO_3} = 1.0\times10^{6}$; $k_{HCO_3^-} = 8.5\times10^{6}$;	141

			$k_{CO_3^{2-}}=3.9\times10^8$	
9	$CO_3^{\bullet-} + H_2O_2/HO_2^- \rightarrow O_2^{\bullet-} + H_2CO_3$	$\alpha_0 k_{H_2O_2} + \alpha_1 k_{HO_2^-}$ [a]	$k_{H_2O_2}=4.3\times10^5$; $k_{HO_2^-}=3.7\times10^7$	154
10	$CO_3^{\bullet-} + CO_3^{\bullet-} \rightarrow CO_2^{4-} + H_2CO_3$	2.0×10^7	2.0×10^7	155
	Formate oxidation by O_3 in bulk solution			
11	$HCOOH/HCOO^- + O_3 \xrightarrow{H_2O} HCO_3^- + HO_3^-$	70		140
12	$HCOOH/HCOO^- + O_3 \rightarrow CO_2^{\bullet-} + HO_3^{\bullet}$	30[e]	0.1-100 [a]	3, 143
13	$HCOOH/HCOO^- + CO_3^{\bullet-} \rightarrow CO_2^{\bullet-} + H_2CO_3$	1.5×10^5	1.5×10^5	147
14	$HCOOH/HCOO^- + {}^{\bullet}OH \rightarrow CO_2^{\bullet-} + H_2O$	3.2×10^9	3.2×10^9	141
15	$CO_2^{\bullet-} + O_2 \rightarrow O_2^{\bullet-} + H_2CO_3$	4.2×10^9	4.2×10^9	124
	Ozone decay in the presence of JBX at pH 3.0			
16	$O_3 \rightarrow O_{3,\ interface}$	$\geq 0.01\ s^{-1}$	-	In this chapter
17	$O_{3,\ interface} + \equiv Fe \rightarrow \equiv O_3$	$7\times10^{-3}\ s^{-1}$ [f]	-	In this chapter
18	$\equiv O_3 \rightarrow NRP$	$5\ s^{-1}$	-	In this chapter
19	$\equiv O_3 + \equiv Fe \rightarrow \equiv {}^{\bullet}OH$	$k_{19}/k_{18}= 3\times10^{-5}\ M^{-1}$	-	In this chapter
20	$\equiv {}^{\bullet}OH \rightarrow {}^{\bullet}OH_{\ interface}$	$1\ s^{-1}$	-	In this chapter
	Formate removal in the presence of JBX at pH 3.0			
21	$HCOOH/HCOO^- \rightarrow HCOOH/HCOO^-_{interface}$	$\geq 0.01\ s^{-1}$	-	In this chapter
22	$HCOOH/HCOO^-_{interface} + \equiv Fe \rightarrow \equiv HCOOH/HCOO^-$	2×10^{-4} [g]	-	In this chapter
23	$\equiv HCOOH/HCOO^- + \equiv {}^{\bullet}OH \rightarrow H_2CO_3$	3.2×10^9	3.2×10^9	141
24	$HCOOH/HCOO^-_{interface} + {}^{\bullet}OH_{\ interface} \rightarrow CO_2^{\bullet-}{}_{,\ interface}$	3.2×10^9	3.2×10^9	115, 141
25	$CO_2^{\bullet-}{}_{,\ interface} + O_2 \rightarrow H_2CO_3 + O_2^{\bullet-}{}_{,\ interface}$	4.2×10^9	4.2×10^9	124
26	$O_2^{\bullet-}{}_{,\ interface} + O_{3,\ interface} \rightarrow HO_3^{\bullet}{}_{,\ interface}$	$\alpha_1 k_{O_2^{\bullet-}}$ [b]	$k_{O_2^{\bullet-}}= 1.5\times10^9$	98
27	$HO_3^{\bullet}{}_{,\ interface}/O_3^{\bullet-}{}_{,\ interface} \rightarrow {}^{\bullet}OH + O_2$	$\alpha_0 k_{HO_3^{\bullet}} + \alpha_1 k_{O_3^{\bullet-}}$ [c]	$k_{HO_3^{\bullet}}=1.4\times10^5\ s^{-1}$; $k_{O_3^{\bullet-}}=2.1\times10^3\ s^{-1}$	151

[a] α_0, α_1 are the mole fractions of H_2O_2 and HO_2^- respectively calculated using pK_a value shown in reaction 2, Table 4.4; reported values of $k_{H_2O_2}$ and $k_{HO_2^-}$ were used.

[b] α_1 is the mole fraction of $O_2^{\bullet-}$ respectively calculated using pK_a value shown in reaction 1, Table 4.4; reported value of $k_{O_2^{\bullet-}}$ were used.

[c] α_0, α_1 are the mole fractions of $HO_3^{\bullet}$ and $O_3^{\bullet-}$ respectively calculated using pK_a value shown in reaction 3, Table 4.4; reported values of $k_{HO_3^{\bullet}}$ and $k_{O_3^{\bullet-}}$ were used.

[d] α_0, α_1, α_2 are the mole fractions of H_2CO_3, HCO_3^- and CO_3^{2-} respectively calculated using pK_a values shown in reaction 5 and 6, Table 4.4; reported values of $k_{H_2CO_3}$, $k_{HCO_3^-}$ and $k_{CO_3^{2-}}$ were used.

e the rate constant for reaction 12 at pH 3.0 was 0.1 M^{-1} s^{-1} probably due to different reactivity of protonated and deprotonated HCOOH.

[f] α_0, α_1 are the mole fractions of HCOOH and $HCOO^-$ respectively calculated using pK_a value shown in reaction 4, Table 4.4; $k_{HCOOH} = 0.1$; $k_{HCOO^-} = 10$ were used.

[g] rate constant determined assuming [≡Fe] =1 M

[h] at pH 3.0 in the presence of JBX

Table 4.4 Acid–base equilibria of related species during conventional ozonation and catalytic ozonation.

No	Reaction	pKa	Published pKa	Reference
		Acid-base equilibria		
1	$HO_2^{\bullet} \rightleftharpoons H^+ + O_2^{\bullet-}$	pK_a $=10^{-4.8}$	pK_a $=10^{-4.8}$	98
2	$H2O_2 \rightleftharpoons H^+ + HO_2^-$	pK_a $=10^{-11.5}$	pK_a $=10^{-11.5}$	156
3	$HO_3^{\bullet} \rightleftharpoons H^+ + O_3^{\bullet-}$	pK_a $=10^{-8.2}$	pK_a $=10^{-8.2}$	151
4	$HCOOH \rightleftharpoons H^+ + HCOO^-$	pK_a $=10^{-3.8}$	pK_a $=10^{-3.8}$	143
5	$H_2CO_3 \rightleftharpoons H^+ + HCO_3^-$	pK_a $=10^{-6.3}$	pK_a $=10^{-6.3}$	157
6	$HCO_3^- \rightleftharpoons H^+ + CO_3^{2-}$	pK_a $=10^{-10.3}$	pK_a $=10^{-10.3}$	158

To explain the ozone decay and formate oxidation by catalytic ozonation, we have developed the kinetic model based on the following key processes (shown in reactions 16 – 27, Table 4.3):

(i) Ozone present in the bulk solution diffuses rapidly into the solid-liquid interfacial region, a portion of which subsequently attaches to the iron oxide surface. A portion of the surface ozone results in formation of $^{\bullet}OH$ on interaction with the catalyst which diffuses to the solid–liquid interface (reactions 16 – 20, Table 4.3).

(ii) Formate present in the bulk solution rapidly diffuses to the solid–liquid interface (reaction 21, Table 4.3), a portion of which subsequently attaches to the iron oxide surface (reaction 22, Table 4.3).

(iii) Rapid oxidation of formate present at the solid-liquid interface and on the surface of the catalyst occurs via interaction with $^{\bullet}OH$ present in these zones (reactions 23 and 24, Table 4.3).

The reactions controlling the self – decay of ozone and the rate constants for these reactions (Reactions 1 – 10) were obtained from various earlier studies.[98, 141, 151-155] Please refer to these earlier studies for detailed description of these reactions. Note that some of the radical scavenging reactions are not included here since these were not important due to the low concentration of the radical species involved. Below, we provide brief description of the key reactions accounting for $HCOOH/HCOO^-$ oxidation by ozonation (Reactions 11 – 15, Table 4.3) and catalytic ozonation (Reactions 16 – 27, Table 4.3) as well as the justification of the rate constants used.

(i) Oxidation of $HCOOH/HCOO^-$ by O_3

Reaction 11 (Table 4.3) represents the direct oxidation of $HCOOH/HCOO^-$ by O_3 via hydride transfer as reported to occur in earlier studies.[140] The rate constant for this reaction was determined based on best-fit to the measured oxidation of $HCOOH/HCOO^-$ by O_3 only (Figure 4.7) and decrease in ozone concentration measured in the presence of $HCOOH/HCOO^-$ (Figure 4.17). The rate constant for this reaction was assumed to be constant with pH. Reaction 12 (Table 4.3) represents the direct oxidation of $HCOOH/HCOO^-$ by O_3 via H abstraction as reported to occur in earlier studies.[3, 143] The rate constant for reaction 12 varies with pH with a value of 0.1 $M^{-1}s^{-1}$ and 30 $M^{-1}\cdot s^{-1}$ determined for pH 3.0 and 7.3/8.5 respectively.

The overall rate constant for formate–O_3 reaction determined here lies within the range 1.5 – 100 $M^{-1} \cdot s^{-1}$ of reported values [3, 143] of the rate constants for this reaction.

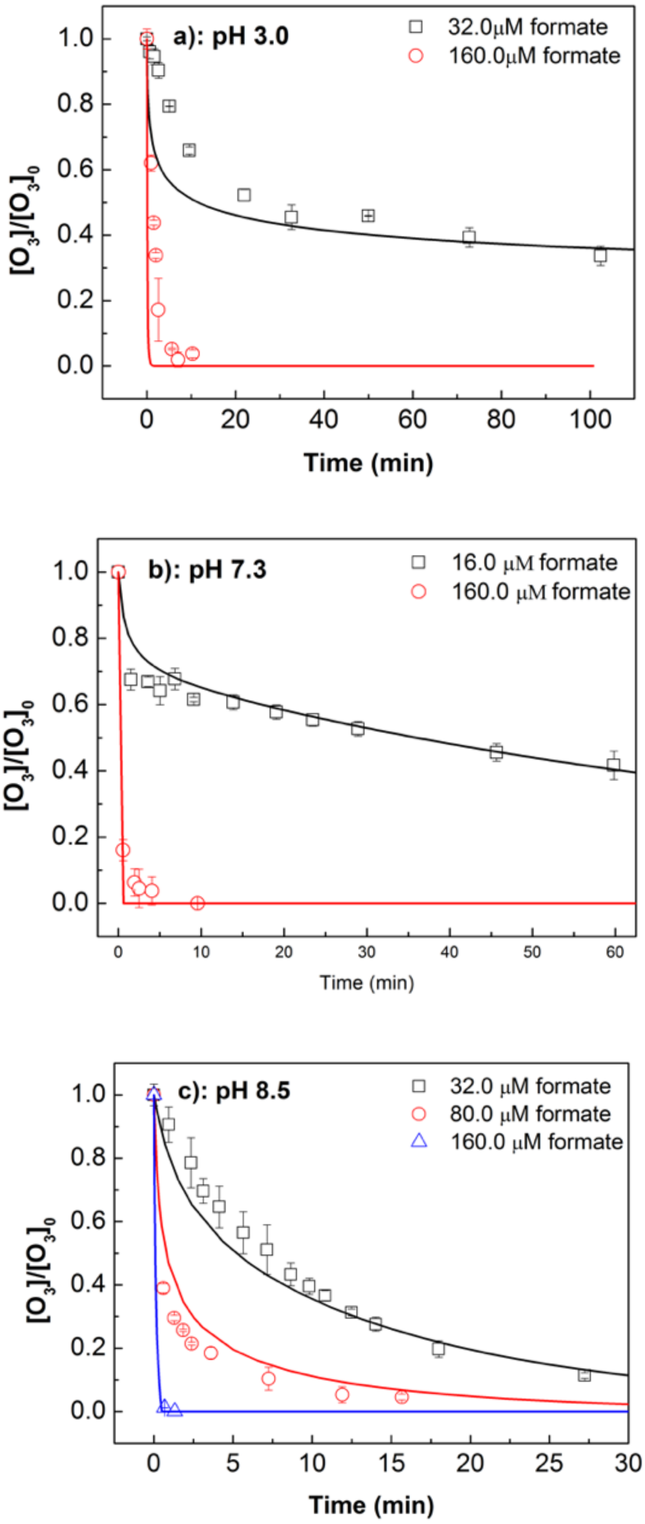

Figure 4.17 Measured decrease in ozone concentration when ~120 μM ozone is added to (a) pH 3.0, (b) pH 7.3 and (c) 8.5 solutions containing formate. Symbols represent measured values, lines represent model results.

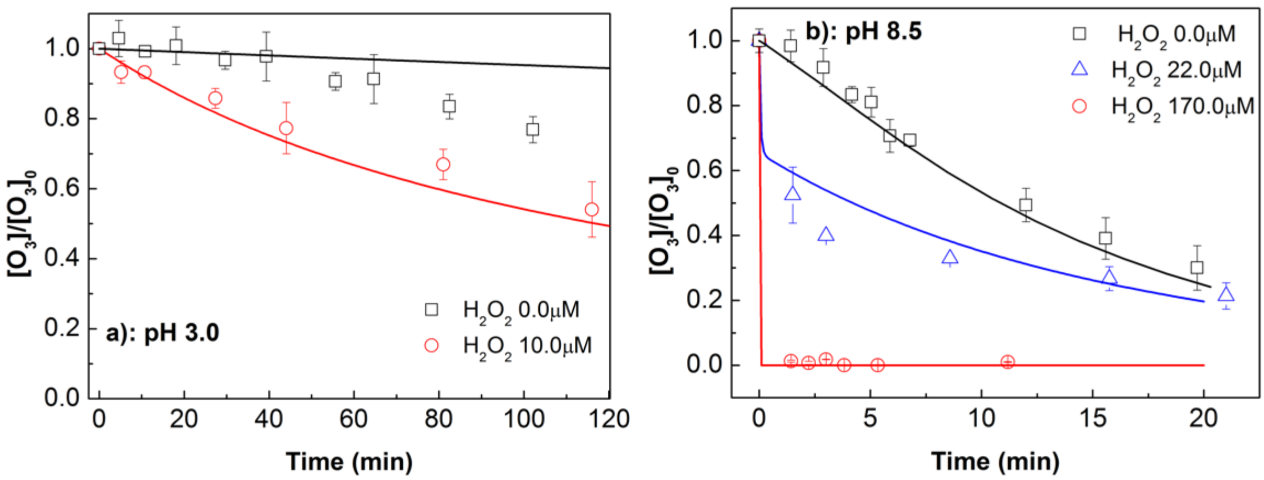

Figure 4.18 Measured decrease in ozone concentration when ~120.0 μM ozone is added to (a) pH 3.0 and (b) pH 8.5 solutions containing H_2O_2. Symbols represent measured values, lines represent model results.

(ii) Oxidation of HCOOH/ $HCOO^-$ by carbonate radicals and hydroxyl radicals

Reactions 13 – 14 (Table 4.3) represent the oxidation of HCOOH/$HCOO^-$ by $CO_3^{\bullet-}$ and $^{\bullet}OH$ respectively as reported to occur in earlier studies.[141, 147] We used the reported values of the rate constants for these reactions in the kinetic model proposed here.

Reaction 15 (Table 4.3) represents the oxidation of $CO_2^{\bullet-}$ which is formed on oxidation of HCOOH/$HCOO^-$ in reactions 13 and 14, resulting in formation of CO_2 and $O_2^{\bullet-}$. We have used the reported values of the rate constant for this reaction in the model. Note that this is an important reaction since the $O_2^{\bullet-}$ produced in this reaction plays an important role in controlling the O_3 decay rate .

(iii) Catalytic ozone decay

Reaction 16 (Table 4.3) represents the diffusion of bulk ozone to the solid–liquid interface. The rate constant for this reaction was assumed to be rapid. Reaction 17 (Table 4.3) represents the interaction of ozone with the catalyst resulting in formation of surface ozone, a small portion of which is transformed to surface $^{\bullet}OH$ (reaction 19,

Table 4.3) while the rest of the surface ozone decays to form non–reactive product (NRP; reaction 18, Table 4.3). The surface $^{\bullet}OH$ formed in reaction 19 diffuses to the solid-liquid interface (reaction 20, Table 4.3). The rate constant for reaction 17 was determined based on the best-fit to the measured ozone decay rate in the presence of catalyst (Figure 4.5). The yield of $^{\bullet}OH$ on ozone-catalyst interaction is determined to very low based on our experimental results.

Reactions 18 and 19 control the yield of $^{\bullet}OH$ available for $HCOOH/HCOO^{-}$ oxidation during catalytic ozonation. While the individual rate constants for these reactions are not constrained by our experimental results, the ratio k_{18} /k_{19} is determined based on best–fit to the measured HCOOH/ $HCOO^{-}$ oxidation during catalytic ozonation (Figure 4.7).

We would like to highlight that while we have assumed $^{\bullet}OH$ is formed on the surface via catalyst–O_3 interaction, an alternate pathway wherein superoxide is formed on the surface which subsequently diffuses into the bulk solution and results in formation $^{\bullet}OH$ upon reaction with ozone as reported earlier is also a possibility.[115] While there is no direct experimental evidence to reject this mechanism of $^{\bullet}OH$ generation during the catalytic ozonation process, we were not able to explain the rate and extent of formate oxidation observed in our experiments based on this mechanism and hence is not discussed further here. Furthermore, the scavenging of $^{\bullet}OH$ generated by the catalyst surface was assumed to be unimportant in the kinetic model developed here given that increasing the catalyst dosage increased $^{\bullet}OH$ generation (Figure 4.10.).

(iv) Adsorption of formate on the catalyst surface

Reactions 21 and 22 (Table 4.3) represent the two-step process to explain the observed adsorption of $HCOOH/HCOO^{-}$ on the catalyst surface (Figure 4.12). Reaction 21 represents the diffusion of $HCOOH/HCOO^-$ from the bulk solution to the solid–liquid interface and was assumed to occur rapidly.

Reaction 22 represents the attachment of $HCOOH/HCOO^-$ to the solid surface. The rate constant for this reaction was determined based on best–fit to the measured $HCOOH/HCOO^-$ adsorption to the catalyst surface (Figure 4.12) at pH 3.0.

(v) Oxidation of surface $\mathbf{HCOOH/HCOO^-}$

Reactions 23 and 24 (Table 4.3) represent the oxidation of adsorbed $HCOOH/HCOO^-$ and $HCOOH/HCOO^-$ present at the solid–liquid interface by surface $^{\bullet}OH$ and $^{\bullet}OH$ present at the solid–liquid interface respectively. The oxidation of adsorbed $HCOOH/HCOO^-$ to CO_2 with surface $^{\bullet}OH$ is expected to proceed via formation of $CO_2^{\bullet-}$ which is further oxidized by surface O_2 to yield CO_2 and $O_2^{\bullet-}$ (eqs 4.15-4.16); i.e.,

$$HCOOH/HCOO^-_{interface} + {}^{\bullet}OH_{\ interface} \rightarrow CO_2^{\bullet-}{}_{,\ interface} \tag{4.15}$$

$$CO_2^{\bullet-}{}_{,\ surface} + O_2 \rightarrow H_2CO_3 + O_2^{\bullet-}{}_{,\ surface} \tag{4.16}$$

The $O_2^{\bullet-}$ so formed may be consumed by the catalyst surface or surface ozone and/or may diffuse into the bulk solution and accelarate aqueous O_3 decay forming $^{\bullet}OH$. Given that diffusion of $O_2^{\bullet-}$ to bulk solution is unlikely due to the short–lifetime of this species, especially under acidic conditons, we have assumed that surface $O_2^{\bullet-}$ formed on $CO_2^{\bullet-}$ oxidation at the surface is not involved in any reaction. To simplify, we have represented the oxidation of adsorbed $HCOOH/HCOO^-$ to CO_2 to occur in a single step. Another possibility is the diffusion of $O_2^{\bullet-}$ to the solid–liquid interface. Due to the slow kinetics of formate adsorption on the catalyst, the concentration of $O_2^{\bullet-}$ derived from the oxidation of surface formate and ozone was low and contributes insignificantly to the model results. For the oxidation of $HCOOH/HCOO^-$ by $^{\bullet}OH$ in the interface, we have assumed that $CO_2^{\bullet-}$ is formed on oxidation of $HCOOH/HCOO^-$ which initiated decay of ozone and generation of $^{\bullet}OH$ at the interface (Reaction 25 – 27, Table 4.3). The rate constant for oxidation of $HCOOH/HCOO^-$ by surface $^{\bullet}OH$ and interfacial $^{\bullet}OH$ were assumed to be the same as that reported for $^{\bullet}OH$ mediated oxidation of $HCOOH/HCOO^-$ in the bulk solution.

Note that for the catalytic ozonation process, modelling of formate oxidation was only performed at pH 3.0 since the catalyst was determined to be active under this pH condition only. It should be noted that the model predictions are not based on empirical fitting; rather, the model output is calculated by solving the rate equations obtained for a comprehensive reaction set that accounts for all key processes operating in the system of interest. As shown in Figures 4.5 – 4.12 and 4.17 – 4.18, the kinetic model developed here provides good description of experimental results obtained at pH 3.0, 7.3 and 8.5. The sensitivity analysis of the model (Table 4.5) using PCA shows that the model output (i.e., formate and ozone concentration) is not sensitive to perturbations in the rate constant for reactions 3, 4, 9, 14 and 19 (Table 4.3) with this result suggesting that these reactions are not critical to ozone degradation or formate oxidation. While the rate constants used to account for formate oxidation by ozone only are well–constrained based on the literature evidence, the deduced rate constants for the dominant catalytic ozonation reactions (i.e., reactions controlling O_3–catalyst interaction (reaction 17) and $^{\bullet}OH$ yield at the solid-liquid interface (reactions 18,19 and 20, Table 4.3) are also well constrained, as evidenced by the relatively deep and narrow minima observed in the plot of the relative residual values against a range of possible rate constant values (Figure 4.19).

Table 4.5 Principal Component Analysis of model reactions controlling O_3 decay and formate oxidation during ozonation and catalytic ozonation.

Eigen value	Dominant reactions in principal components (relative contribution of the component to system response is shown in parentheses
pH 3.0	
1.91×10^{1}	11 (0.92), 13 (0.27), 8 (-0.24),
9.08×10^{-2}	8 (-0.61), 15 (0.52), 13 (0.44), 11 (-0.35)
8.67×10^{-3}	6 (0.73), 13 (-0.47), 2 (0.37), 8 (-0.26)
pH 7.3	
1.77×10^{2}	15 (0.64), 11 (0.63), 13 (0.34), 8 (-0.23)
2.20	1 (0.65), 8 (-0.58), 6 (0.32), 11 (-0.26), 13 (0.25)
3.00×10^{-1}	1 (0.60), 13 (-0.57), 8 (0.38), 11 (0.29), 7 (0.20)
1.74×10^{-2}	2 (0.94), 6 (0.21)
8.01×10^{-3}	6 (-0.67), 1 (0.44), 13 (0.34), 8 (0.32), 15 (-0.30), 2 (0.22)
pH 8.5	
1.77×10^{2}	13 (0.67), 8 (-0.55), 15 (0.26), 11 (0.26), 12 (0.23), 5 (-0.22)
2.20	1 (0.98)
2.98×10^{-1}	12 (0.78), 5 (-0.50), 8 (0.23), 13 (-0.22)
1.52×10^{-2}	6 (-0.72), 8 (0.51), 5 (0.28), 13 (0.22), 11 (0.21)
5.81×10^{-3}	5 (-0.53), 11 (0.49), 10 (0.43), 12 (-0.35), 15 (0.28), 8 (0.24)
JBX at pH 3.0	
1.46×10^{4}	21 (0.91), 16 (-0.41)
1.46×10^{4}	16 (0.91), 21 (0.41)
1.28×10^{2}	17 (0.98), 19 (0.13)
35.1	19 (-0.50), 22 (0.48), 18 (0.41), 26 (-0.39), 20 (-0.29), 23 (0.28), 17 (0.19)
18.5	19 (0.74), 22 (0.67)
2.65	22 (0.56), 19 (-0.43), 18 (-0.40), 26 (0.39), 20 (0.30), 23 (-0.29)

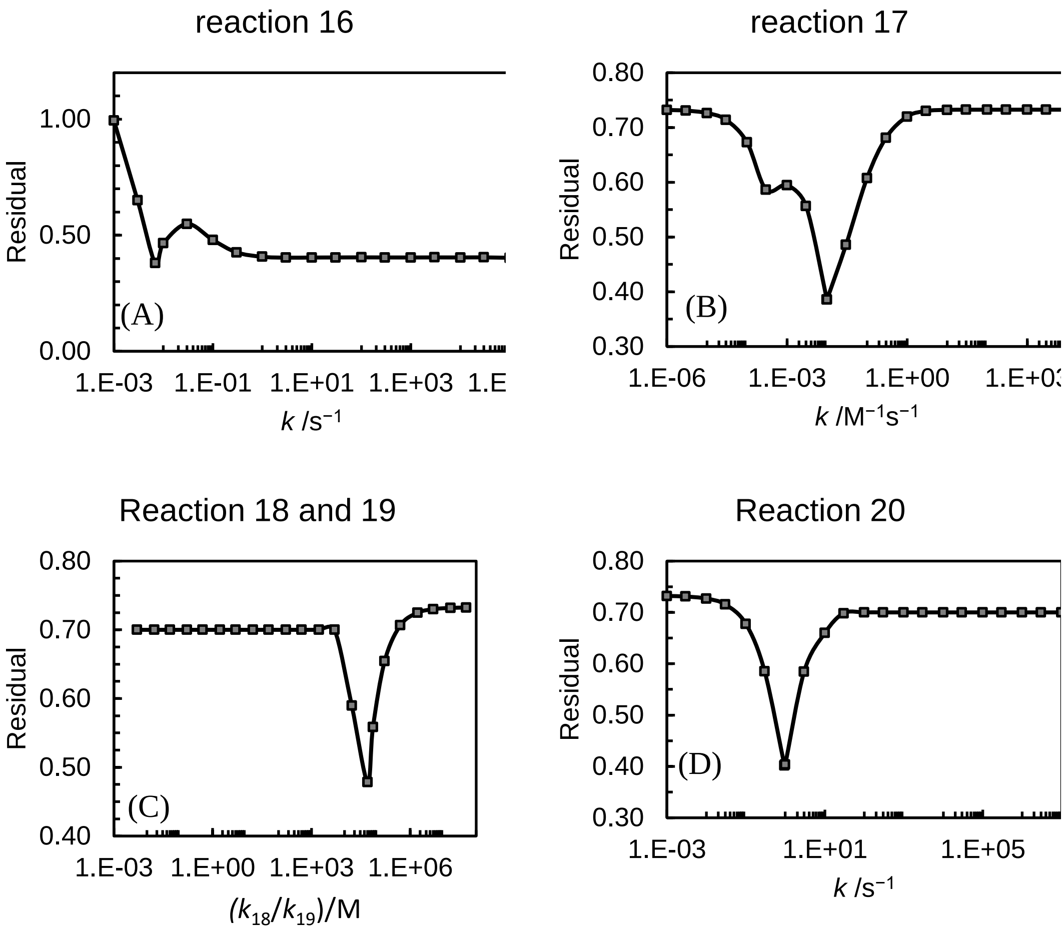

Figure 4.19 Relative residual calculation of the fitted reaction rate constants for reactions 16 , 17, 18, 19 and 20.

We have used the kinetic model to determine the efficiency of ozone usage in ozonation as function of initial organic concentration and pH. As shown in Figure 4.20a, at low organic concentrations, the ozone utilization efficiency is relatively low under alkaline pH conditions due to rapid self-decay of ozone and low selectivity of any $^{\bullet}OH$ formed. However, at higher organic concentrations (a condition more representative of wastewaters), the ozone utilization efficiency is nearly constant with pH since most of the ozone is consumed due to its interaction with the organics rather than self–decay. Overall, these results show that the impact of pH on the rate and extent of oxidation should be taken into consideration, especially for wastewaters containing low organic concentrations, when designing the premixing stage (either as an integrated unit in catalytic ozonation or in a multi-stage ozonation reactor) in order to maximize ozone utilization during this treatment step. Since, the ozone utilization efficiency increases with increase in organic concentration at all pHs, concentrating the organics in wastewaters prior to ozonation will significantly enhance the process efficiency.

As discussed earlier, $HCOOH/HCOO^{-}$ oxidation may occur via direct O_3 interaction and/or via reaction with $^{\bullet}OH$. Note that the $HCOOH/HCOO^{-}$ oxidation by $^{\bullet}OH$ also includes the contribution from $CO_3^{\bullet -}$ which is formed on $^{\bullet}OH$ scavenging by bicarbonate/carbonate ions. We have used the kinetic model developed here to predict the contribution of O_3 and $^{\bullet}OH$ over a range of organic concentrations and pHs. This will be useful in predicting the influence of the matrix on the performance of the ozonation process. For example, if the oxidation is driven by O_3 only, the influence of inorganic and organic entities capable of scavenging $^{\bullet}OH$ (and resulting in formation of non-reactive product) will not be important. In contrast, entities impacting the stability of O_3 (such as carbonate as discussed earlier) will be important for O_3–driven oxidation of organic compounds. As shown in Figure 4.20b, the extent of oxidation of formate occurring via a non-radical pathway varies considerably as function of pH and organic concentration. As shown, while increase in the formate concentration increases the contribution of the non-radical pathway in formate oxidation, the impact of pH on the contribution of the O_3-mediated oxidation pathway is not straightforward. At low pH (i.e., $\leq$3.0), most of the oxidation occurs via a non-radical pathway while at high pH (i.e., $\geq$ 10.0), oxidation of formate occurs via interaction with $^{\bullet}OH$ and $CO_3^{\bullet -}$ but, in the intermediate pH range, the trend is variable. The contribution of O_3, $^{\bullet}OH$ and $CO_3^{\bullet -}$ to formate oxidation in the pH range 4.0 – 10.0 varies as result of the complex influence of carbonate concentration (which varies with pH) on O_3 self–decay and $^{\bullet}OH$ and $CO_3^{\bullet -}$

generation as well as due to variation in the rate constant for O_3–formate reaction with variation in pH. Overall, this result highlights that the mechanism of formate (and possibly other organics) oxidation by ozone varies markedly with pH and organic concentration.

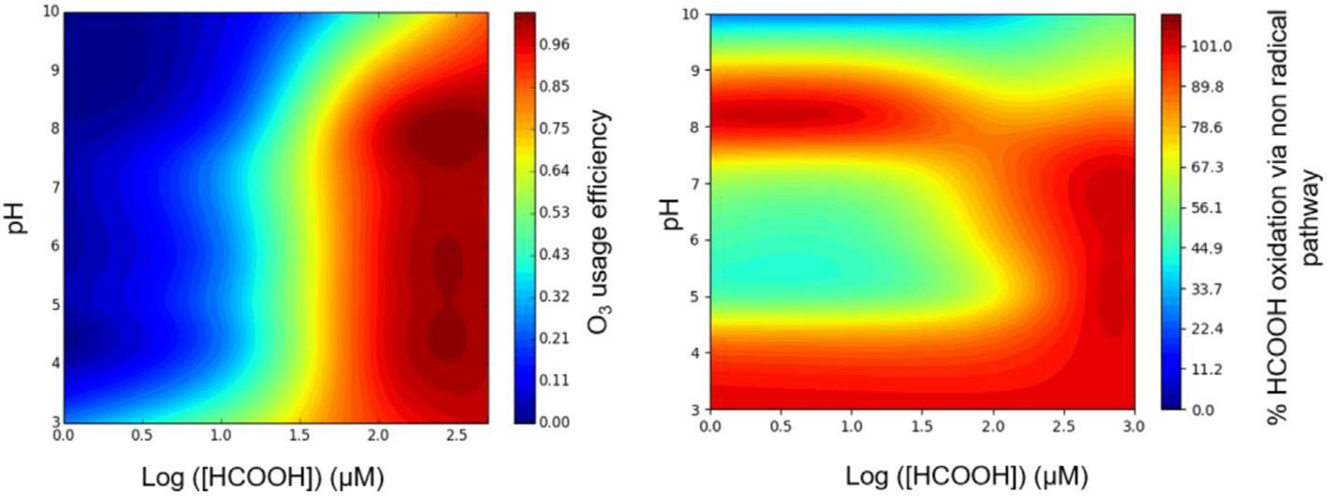

Figure 4.20 (a) Model predicted ozone usage efficiency (i.e., moles of formate oxidized for each mole of O_3 consumed) as function of pH and formate concentration. (b) Model predicted contribution of non–radical mediated pathway (i.e., direct oxidation by O_3) to formate oxidation as function of pH and formate concentration. Note that an initial O_3 concentration of 100.0 µM was used for these predictions.

4.4. Conclusions

In this chapter, $HCOOH/HCOO^-$ was used as a probe compound in order to gain mechanistic insight into the catalytic ozonation process using a commercially available carbon–based catalyst. We simultaneously analysed the adsorptive and oxidative removal of $HCOOH/HCOO^-$ with results indicating that adsorption is not an important precursor step for the subsequent oxidation of this simple target compound. Experimentation and modelling results show that catalytic oxidation proceeds via both homogeneous oxidation in the bulk solution and heterogeneous oxidation at the solid–liquid interface. The solution pH also influences the catalytic ozonation performance as a result of changes in catalyst surface properties and surface iron oxide speciation that determines the extent of generation of surface oxidants. The influence of JBX on ozonation performance determined in the present chapter is in contrast to the results obtained in various previous studies employing iron oxide and manganese oxide-based catalysts.[42, 88, 103, 135, 159-164] The discrepancy in the role of iron oxides as catalyst in the present chapter and various earlier work is possibly related to:

i. **Difference in the nature of the organics used.** Most of the previous studies use complex organic target species [88, 103, 161, 162] which results in formation of a suite of intermediate products however only removal of the parent compound is typically measured in these studies. The nature and influence of intermediate by-products on ozone decay and $^{\bullet}OH$ formation is not investigated in these earlier studies.[88, 103, 161, 162] Furthermore, the overall removal of parent compound is measured with no differentiation made regarding the removal of parent compound by adsorption and oxidation in most of these earlier studies.[88, 103, 161, 162] In comparison, here we use simple target compounds which do not form any intermediate products (in both cases with direct oxidation to CO_2) with quantification of the proportions of the target compounds removed (separately) by adsorption and oxidation in the presence of ozone. It is also possible that the difference in the adsorptive behaviour of formate and oxalate compared to the organics used in various earlier studies [82, 165, 166] contributes to the discrepancy in the results obtained regarding the influence of the catalyst.

ii. **Difference in the nature of iron oxide.** It is possible that the nature and reactivity of the iron oxide used here differs to that of the iron oxides employed in various earlier studies.[88, 103, 135] Since the procedure used for JBX preparation is not available, we are not able to determine the major factors influencing the difference in the nature of iron oxide though we would like to highlight that employing ferrihydrite and an Fe–silicate composite shows similar results to those measured in the presence of JBX in the present chapter.

iii. **Difference in pH and various other solution conditions.** In some of the earlier studies [51, 161, 167-169] in which the ozonation and catalytic ozonation processes were compared, pH was not well controlled and not the same for the ozonation and catalytic ozonation processes under investigation. Comparison of the performance of the ozonation and catalytic ozonation processes at different pH is likely to produce false results since the ozonation performance is strongly dependent on pH as depicted clearly in this chapter and various earlier studies.[1, 22] Furthermore, either no buffer or phosphate buffer was used in some earlier studies [75, 160] rather than the carbonate buffer used in this chapter The presence of a high phosphate concentration in the buffer solution enhances ozone decay,[131] thereby decreasing the efficiency of the ozone-only process. In contrast, as mentioned here the presence of carbonate ions stabilizes ozone [170] thereby increasing the efficiency of the ozone–only process. Hence, in this chapter, the catalyst did not enhance $^{\bullet}OH$ generation beyond what was observed in the absence of catalyst (which is already very rapid in bicarbonate buffered solution).

Our results showed that effective formate oxidation occurs by ozonation alone with this result suggesting that conventional ozonation technologies may be effective for organic abatement in alkaline wastewaters. Conventional ozonation technologies are often limited by the mass transfer of gaseous ozone into the liquid phase and, as such, optimization of reactor design, including the ozone injection system and reactor geometry, should be the focus of future studies. The kinetic model for formate oxidation developed here could be coupled with fluid dynamics models to predict the spatial concentration of organic compounds and oxidants which would assist in optimizing reactor design.

It is also worth noting that iron oxide impregnated activated carbon significantly enhanced formate oxidation at pH 3.0 suggesting that catalytic ozonation could be a potential solution for treatment of acidic wastewaters. For treatment of acidic wastewaters, Fenton processes are often used however catalytic ozonation using iron oxide coated or impregnated activated carbon might be a "cleaner" option since no sludge would be produced. However, the cost of treatment for the two technologies needs to be compared under various scenarios prior to application of catalytic ozonation for treatment of acidic wastewaters. Furthermore, even though leaching of Fe from the catalyst was shown to be minimal at time scales investigated here, it may become important during long–term operation. Dissolved iron leached from the catalyst may contribute to homogeneous catalytic ozonation, but this also inevitably deteriorates the longevity and efficiency of the catalyst. Thus, testing the long–term performance of catalyst in acidic conditions is imperative prior to its application for treatment of acidic wastewaters.

We would like to highlight that even though the current study presents results for a commercial carbon–based catalyst which is not effective under pH conditions similar to most wastewaters, the results of the present chapter provide important insights with regard to the influence of pH on formate oxidation by the conventional ozonation process. Furthermore, this work provides an approach to test the effectiveness of other catalysts (commercial and/or laboratory synthesized). As shown here, systematic measurement of ozone decay, removal of the parent compound as well as formation of the oxidized product(s) under well controlled conditions are required for clearly elucidating the mechanism of catalytic ozonation. pH has a significant influence on both the mechanism and rate of conventional ozonation and hence pH needs to be properly controlled when comparing the effectiveness of any catalytic ozonation process with ozonation only. For example, comparing the performance of a catalytic ozonation process at ~ pH 8.5 with an ozone-only process operating at pH 7.3 for formate removal (see Figure 4.9) would produce erroneous conclusions regarding the effectiveness of the catalyst.

Overall, this work provides important insight into the formate removal mechanism during conventional and catalytic ozonation using iron oxide impregnated carbon catalysts under varying pH conditions.

Chapter 5 Kinetic modelling-assisted mechanistic understanding of the catalytic ozonation process using Cu-Al layered double hydroxides and copper oxide catalysts

Some of the material in this Chapter has been drawn from a recent publication,[171] which has been acknowledged and detailed in the 'inclusion of publications statement' for this thesis.

5.1. Introduction

In this chapter, we examine the performance of laboratory synthesized Cu–Al layered double hydroxides (Cu–Al LDHs) in HCO. LDHs are widely used as adsorbents for contaminant removal [172-174] and hence are expected to facilitate adsorption and, potentially, concomitant oxidation of organics in the presence of O_3. For comparison, we also tested the performance of a Cu oxide (CuO) to determine the influence of the layered structure of Cu–Al LDHs (if any) on the adsorption and oxidation of organics by HCO. We use Cu as the active metal in LDHs since Cu is known to effectively complex carboxylic and phenolic moieties forming reactive surface complexes [25, 175] which may readily be oxidized by oxidants generated during catalytic ozonation. The performance of the Cu catalysts synthesized here was tested using low molecular weight organic acids, formate and oxalate, as the target contaminants. We use formate and oxalate as the target compounds since these are identified as the important end–products on ozonation of aromatic compounds and exhibit substantially different reactivities towards O_3 and $^{\bullet}OH$.[22, 82, 122, 125] Additionally, these short chain carboxylic acids exhibit well defined oxidation pathways and, in both cases, form CO_2 and H_2O as the only products.[123, 124] Based on our experimental results, we provide important insights into the role of the catalyst in oxidation of these organics. We have also developed a mechanistically based mathematical model as an aid to identifying key chemical processes involved in the oxidation of oxalate and formate in the presence of these Cu–based catalysts under circumneutral pH conditions.

5.2. Materials and Methods

5.2.1. Reagents

Most experiments were performed at pH 7.3 using a 2.0 mM $NaHCO_3$ solution as described in chapter 3. Additional kinetic isotope effect (KIE) experiments in deuterated water (D_2O) and aqueous solution were also performed at pH 8.5 (pD 8.8) in air–saturated 2.0 mM $NaHCO_3$ solution. The KIE studies were performed at pH 8.5 (pD 8.8) and not at pH 7.3 since it was difficult to maintain pD at 7.6 in D_2O solution, possibly due to slow dissolution of CO_2 in D_2O. Stock solutions of radiolabelled and non-radiolabelled sodium formate, radiolabelled and non–radiolabelled sodium oxalate, indigo, *p*–CBA and O_3 were prepared as described in chapter 3. A 1.3 mM stock solution of COU was prepared in MQ water.

Since formate and oxalate mostly exist as $HCOO^-$ and $C_2O_4^{2-}$ at the pH value investigated here, we use $HCOO^-$ and $C_2O_4^{2-}$ to represent total formate and total oxalate from hereon in this chapter.

5.2.2. Catalyst synthesis and characterization

We synthesized CuO and Cu–Al LDHs by slightly modifying the previously reported method.[176-178] Briefly, for Cu–Al LDHs synthesis, a 200.0 mL mixture of 25.0 mM of $Cu(NO_3)_2$ and $Al(NO_3)_3$ (100.0 mL of each, denoted as solution A) and 200.0 mL of

50.0 mM Na_2CO_3 (denoted as solution B) were prepared. Subsequently, solution A was added dropwise into solution B while keeping the solution pH constant at pH 10.0 by adding 0.2 M NaOH. The as–formed gel was aged at 80 °C for 24 h and the mixture was washed with MQ water and centrifuged successively three times. The slurry was then dried at 40 °C overnight in air and ground using pestle and mortar. The ground catalyst was kept in a desiccator prior to use. The preparation procedure of CuO and the reference Al hydroxide (confirmed by XRD in Figure 5.1) was exactly the same as that used for Cu–Al LDHs but did not include $Al(NO_3)_3$ or $Cu(NO_3)_2$ addition respectively.

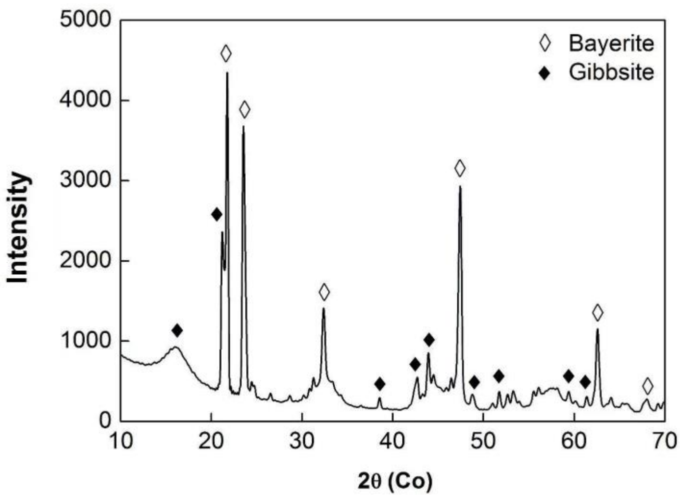

Figure 5.1 XRD pattern of reference Al hydroxide.

The catalysts were characterized using XRD and SEM–EDX. The surface area of the catalyst was quantified using N_2 sorption isotherms and analysed by BET model. The catalysts were degassed at 60 °C for 8 h prior to the analysis. The pH_{pzc} and density of surface hydroxyl groups of CuO and Cu–Al LDHs were measured using acid–base titration and saturated–protonation respectively.[166, 179, 180] Briefly, for pH_{pzc} measurement, two suspensions of 0.3 g catalysts in 30.0 mL $NaNO_3$ were prepared. After 10 min (to attain pH equilibrium), titrations were carried over the pH range 5.0 – 11.0 to avoid any dissolution of catalyst under acidic or alkaline conditions. One suspension was titrated with NaOH while the other one was titrated with HNO_3. During titration, N_2 was bubbled into the suspension to avoid the influence of atmospheric CO_2 on pH. For surface hydroxyl groups measurement, 0.3 g catalyst was mixed with 50.0 mL of 0.01-0.1M NaOH and the suspension was filtered using 0.22 μm PVDF filters after 24 h of shaking. The filtrates were titrated with 0.1 M HNO_3 to determine the residual NaOH. The concentration of acidic surface hydroxyl groups was equal to the concentration of NaOH consumed and the total surface hydroxyl groups was equal to twice the amount of acidic hydroxyl groups based on charge balance. ICP–OES was used to measure the leaching of Cu from the catalyst when exposed to O_3.

5.2.3. Experimental setup

5.2.3.1. Formate and oxalate degradation

The experimental setup and method used for simultaneous measurement of adsorption and oxidation of $HCOO^-$ and $C_2O_4^{2-}$on ozonation are the same as those presented in chapter 3 with formate and oxalate concentration measured in the filtered and unfiltered samples. The $HCOO^-/C_2O_4^{2-}$ concentration measured for filtered samples represents the $HCOO^-/C_2O_4^{2-}$ concentration remaining in solution, noted as $[HCOO^-/C_2O_4^{2-}]_{solution}$. The $HCOO^-/C_2O_4^{2-}$ concentration measured for unfiltered samples represents the sum of $HCOO^-/C_2O_4^{2-}$ concentration remaining in solution and on the surface, if any. The difference of $HCOO^-/C_2O_4^{2-}$ concentration between the filtered and unfiltered samples depicted the fraction of $HCOO^-/C_2O_4^{2-}$ removed by adsorption during the HCO process. The sum of the total residual $H^{14}COO^-/^{14}C_2O_4^{2-}$ concentration (*i.e* $H^{14}COO^-/^{14}C_2O_4^{2-}$ for unfiltered samples) and $^{14}CO_2$ concentration formed is close to the initial $H^{14}COO^-/^{14}C_2O_4^{2-}$ concentration confirming that any $H^{14}COO^-/^{14}C_2O_4^{2-}$ oxidized is transformed to $^{14}CO_2$. The $[^{14}CO_2]$ at various times was quantified using the difference of initial $H^{14}COO^{-}/^{14}C_2O_4^{2-}$ concentration and total residual $H^{14}COO^{-}/^{14}C_2O_4^{2-}$ concentration.

TBA was used as a bulk $^{\bullet}OH$ scavenger in the $HCOO^{-}$ and $C_2O_4^{2-}$ oxidation experiments. The influence of phosphate (a strong Lewis base which inhibits sorption and interaction of organics with surface groups [139]) addition on $HCOO^{-}$ oxidation was also investigated. Measurement of oxidation of $HCOO^{-}$ and $C_2O_4^{2-}$ was also performed in D_2O and H_2O solutions at pH 8.5 (pD 8.8) in order to determine the KIE on both conventional and catalytic ozonation processes using the same procedure as described above. Fourier Transform Infrared Spectroscopy measurements (FTIR, Perkin Elmer Frontier IR spectrometer) were conducted in the presence or absence of ozone to characterize the surface adsorption and concomitant degradation of $C_2O_4^{2-}$ on the catalyst surface. To measure $C_2O_4^{2-}$ adsorption, 1.0 - 10.0 mM $C_2O_4^{2-}$ was added to pH 7.3 solution containing 0.6 g L^{-1} catalysts. To measure the $C_2O_4^{2-}$ oxidation, the $C_2O_4^{2-}$ and catalyst suspension was continuously sparged with gaseous ozone (concentration 51.0 mg L^{-1}, flow rate 100.0 mL min^{-1}) for over 10 min. The obtained suspensions following adsorption and oxidation experiments were centrifuged and washed with MQ three times to remove any $C_2O_4^{2-}$ in the solution. An aliquot of catalyst paste was placed on the 3 mm diamond/ZeSe crystal and blow dried using a gentle N_2 stream (0.4 $Lmin^{-1}$) prior to the measurement of FTIR spectra. Spectra were collected at a resolution of 4 cm^{-1} using 4 scans accumulations over the range of 650 to 4000 cm^{-1}.

The adsorption isotherms of $HCOO^{-}$ and $C_2O_4^{2-}$ on Cu-Al LDHs and CuO was measured at Cu–Al LDHs and CuO dosage of 0.6 g L^{-1} (in term of CuO mass) since the adsorption of $HCOO^{-}$/ $C_2O_4^{2-}$ is discernible to measure. For measurement, 1.0 – 1000.0 μM $HCOO^{-}$/ $C_2O_4^{2-}$ (containing 100 nM $H^{14}COO^{-}/^{14}C_2O_4^{2-}$) and 0.6 g L^{-1}

catalyst was mixed in pH 7.3 buffer solution and 1.5 mL sample were taken from the reactor after 2 h. The samples were filtered using 0.22 μm PVDF filters and the residual $H^{14}COO^{-}/^{14}C_2O_4^{2-}$ in the filtered samples was quantified as described above. The adsorption capacity was calculated using eq. 5.1.

$$q_e = \frac{(C_0 - C_e)V}{m} \tag{5.1}$$

where q_e is the amount of $HCOO^{-}/C_2O_4^{2-}$ removed per gram of catalyst (mg.g^{-1}), m is the mass of the catalyst (g), V is the volume of $HCOO^{-}/C_2O_4^{2-}$ solution (mL), C_0 and C_e are the initial and equilibrium concentration of $HCOO^{-}/C_2O_4^{2-}$ (mg/L). The adsorption data was fitted using Langmuir isotherm employing OriginPro 8.5.

5.2.3.2. Ozone decay

Measurement of aqueous O_3 decay in the absence and presence of catalyst at pH 7.3 was performed in gas-tight reactors as described in chapter 3. Measurement of ozone decay was also performed in D_2O and H_2O solutions at pH 8.5 (pD 8.8) in order to determine the KIE on ozone self–decay and catalyst-mediated ozone decay. For measurement of ozone decay, an appropriate volume of the ozone stock solution was added to pH 7.3 buffer solution in the absence and presence of catalyst and organics ($C_2O_4^{2-}$) resulting in an initial ozone concentration of ~ 120.0 μM. At pre–determined time intervals, 1.0 mL sample was withdrawn from the reactor and was filtered using 0.22 μm PVDF filters. The concentration of ozone in the filtrate was measured using the indigo method as described earlier in chapter 3.[107] For KIE, measurement of O_3 decay in the absence and presence of catalyst was performed in D_2O and aqueous solution at pH 8.5 (pD 8.8) using the same procedure as described above.

To investigate the influence of adsorbed organics on catalyst-O_3 reaction, $C_2O_4^{2-}$ was pre-sorbed on Cu–Al LDHs and CuO surface by adding appropriate amount of catalyst (0.6 g L^{-1} for Cu-Al LDHs and 0.12 g L^{-1} for CuO) to pH 7.3 solution containing $C_2O_4^{2-}$ (10.0 – 100.0 μM). After 2 h, the catalyst was separated by centrifugation the catalyst and was re–dispersed into fresh pH 7.3 buffer. Subsequently, 120.0 μM O_3 was added to initiate the experiment and the measurement of O_3 decay was performed as described above. Note to account for any loss of catalyst that may occur during centrifugation, the results of catalyst–mediated O_3 decay with sorbed $C_2O_4^{2-}$ was compared with the results from the control experiments performed exactly in the same manner except that the catalyst was added to pH 7.3 solution with no $C_2O_4^{2-}$ during the pre-sorption step.

5.2.3.3. Hydroxyl radical generation

We measured the oxidation rate of *p*–CBA, which is a widely used •OH probe,[87, 181, 182] in order to evaluate the rate and extent of •OH generation on O_3 decay during catalytic ozonation. Note that since *p*–CBA adsorption on the catalyst surface was negligible (Figure 5.2) only the extent of bulk •OH generation was measured using *p*–CBA oxidation experiments. Detailed description of the experimental setup used for measurement of *p*–CBA oxidation is provided in chapter 3.

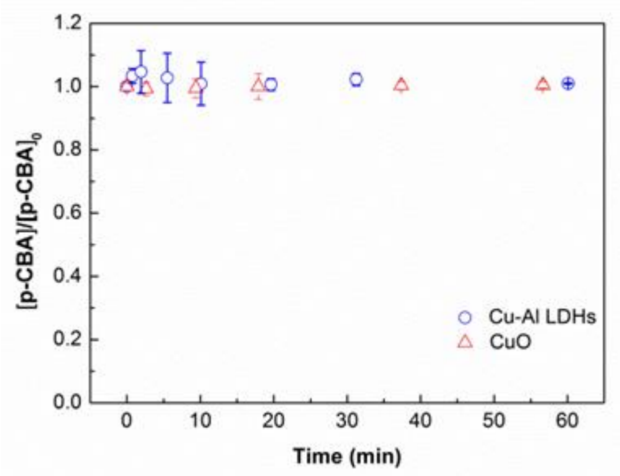

Figure 5.2 Fraction of *p*–CBA remaining in the solution in the presence of Cu–Al LDHs (circles) and CuO (triangles) at pH 7.3. Experimental conditions: [*p*–CBA]$_0$ = 1.0 μM, [catalyst]$_0$ = 0.06 g L^{-1} (in terms of CuO mass).

To measure the generation of surface associated $^{\bullet}OH$ during HCO, we used fluorescence microscopy image analysis using coumarin (COU) as the probe. As described in earlier studies, COU interacts with $^{\bullet}OH$ via hydroxylation forming 7-hydroxyl coumarin (7–HC), a strongly fluorescent compound under UV excitation.[29, 80, 183] An inverted fluorescence microscope (OLYMPUS CKX53) coupled with a mercury lamp (to tune excitation wavelength into UV region) was used to capture the fluorescent images corresponding to 7–HC on the catalyst surface. For fluorescence measurement of 7–HC, 100.0 μM O_3 was added to 0.06 g L^{-1} catalyst suspension containing 10.0 μM COU. After 1 h, 10.0 mL of sample was withdrawn for capturing the fluorescence images. The same experiment was repeated in the presence of 1.0 mM TBA to exclude the contribution from the 7–HC which is formed via COU and $^{\bullet}OH$ in the bulk solution and subsequently adsorbs to the catalyst surface. Control experiments were also performed in order to determine whether 7–HC formation occurred on homogeneous ozonation of coumarin. For these measurements, 100.0 μM O_3 and 10.0 μM coumarin were added to pH 7.3 buffer solution to initiate the reaction of COU with O_3 and/or $^{\bullet}OH$ formed on O_3 self–decay. To eliminate the contribution of $^{\bullet}OH$ in 7–HC formation in the bulk, ozonation of COU was also performed in the presence of 1.0 mM TBA to scavenge any bulk $^{\bullet}OH$ formed. Due to the low sensitivity of the technique for measurement of bulk 7–HC, additional measurements were performed wherein 0.06 g.L^{-1} of Cu–Al LDHs was added to 1 h ozonated solution to adsorb any 7–HC formed in the solution with samples for microscopic images analysis taken after 1 h. For capturing the fluorescence images, 10 mL of each sample was pipetted into a Corning cell culture flask and the image was taken.

5.2.4 Kinetic modelling

Kinetic modelling of our experimental results was performed using the software package Kintecus as described in chapter 3. [110]

5.3. Results and Discussion

5.3.1. Catalyst characterization

Figure 5.3 illustrates the morphologies and the element mapping results of Cu–Al LDHs and CuO. As shown, Cu–Al LDHs are mostly present as nano-sized fine flakes which are the typical morphology of layered double hydroxides.[184-187] In contrast, CuO is mostly present as spherical particles of diameter <4 μm. The element mapping results (Figure 5.3) reveal that Cu and O are evenly distributed on the surface of the Cu–Al LDHs and CuO. The XRD spectra of Cu–Al LDHs and CuO also confirm that Cu–Al LDHs and CuO have been successively fabricated with the main mineral phases identified to be Cu–Al carbonate hydroxide hydrate (ICDD 00–037–0630) and tenorite (ICDD 00–048–1548) respectively (Figure 5.3b and g). The density of surface hydroxyl groups on the Cu–Al LDHs and CuO catalysts was determined to be 36.7 and 150.6 μM g^{-1} respectively. The higher surface hydroxyl content of CuO compared Cu–Al LDHs is possibly due to the higher surface area of CuO (71.4 m^2 g^{-1}) compared to that of Cu–Al LDHs (38.7 m^2 g^{-1}) which facilitates exposure of more surface sites to aqueous solution with concomitant hydroxylation of these sites. The pH_{pzc} values of Cu–Al LDHs and CuO are 8.0 and 7.7 respectively (Figure 5.4) indicating that both catalysts carried positive charge at pH 7.3 (the investigated condition in this study). As such, it is expected that the adsorption of negatively charged organics onto the catalyst's surface will be facilitated by electrostatic attraction.[106] No dissolved Cu was detected by ICP-OES with the detection limit of 0.1 mg $L^{-1}$when the catalyst suspension was continuously sparged with O_3 gas for 1 h at pH 7.3 suggesting that the Cu catalysts synthesized here are stable in the presence of O_3.

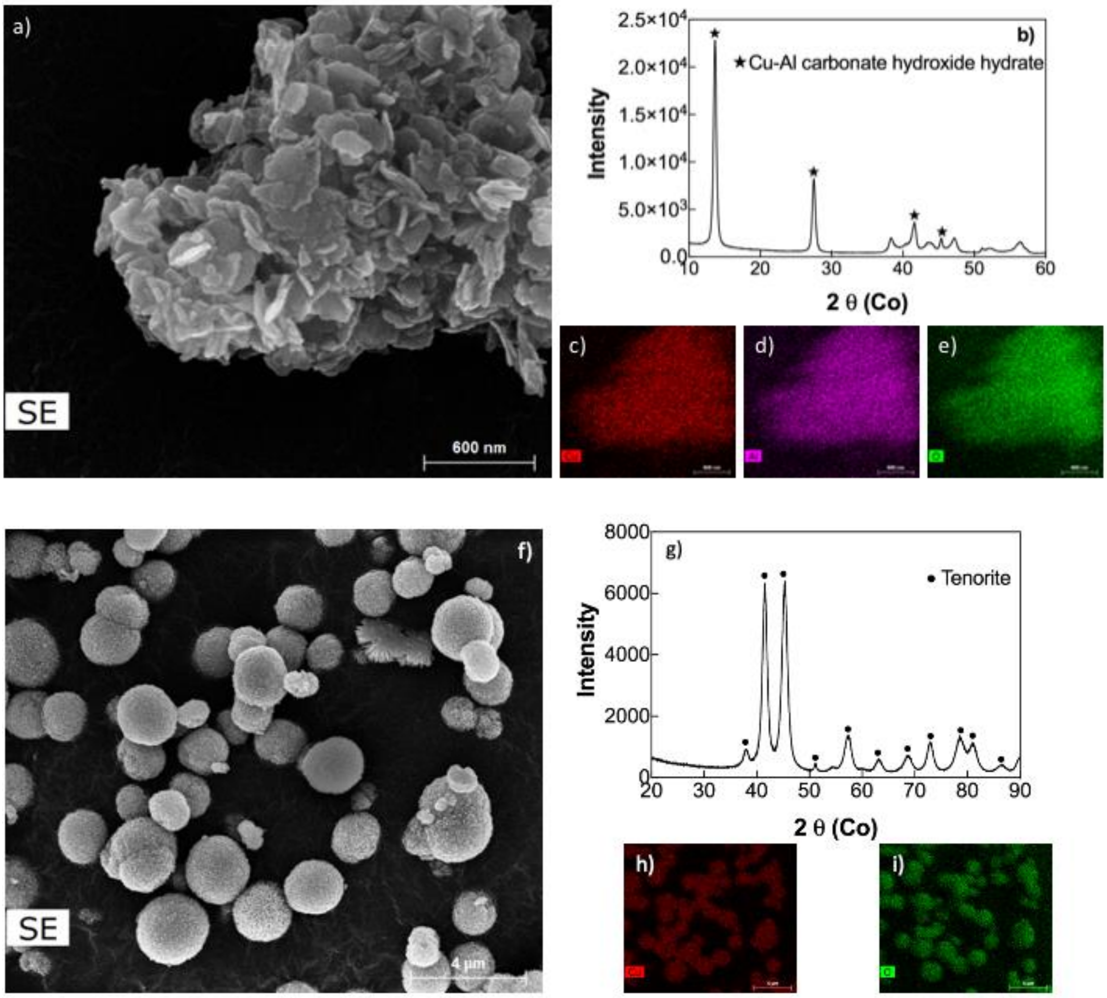

Figure 5.3 SEM images and XRD patterns of Cu-Al LDHs and CuO. Panel a shows the secondary electron image while panel b shows the XRD patterns of Cu–Al LDHs with panels c, d, and e showing the element maps of Al, Cu and O respectively. Panel f shows the secondary electron image while panel g shows the XRD patterns of CuO with panels h and I showing the element maps of O and Cu respectively.

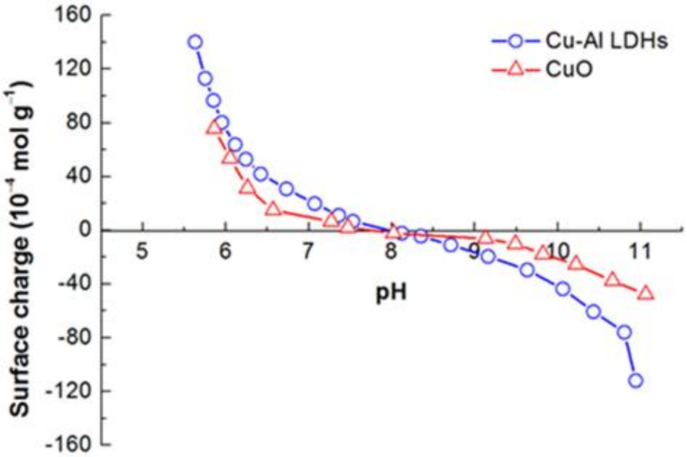

Figure 5.4 Measurement of pH_{pzc} of Cu–Al LDHs and CuO. Experimental conditions: $[catalyst]_0$ = 10.0 g L^{-1} in 0.1 M $NaNO_3$.

5.3.2. Oxidation of oxalate by HCO using Cu-Al LDHs and CuO as the catalysts

As shown in Figure 5.5a, the presence of Cu–Al LDHs as well as CuO increased the rate and extent of $C_2O_4^{2-}$ oxidation considerably compared to that observed by the conventional ozonation process. Nearly 20%, 88% and 89% of 10.0 µM $C_2O_4^{2-}$ was oxidized within 30 min in the absence and presence of Cu–Al LDHs and CuO respectively (Figure 5.5a). Note that $C_2O_4^{2-}$ removed here was mostly via oxidation as confirmed by the concentration profile of CO_2 formed on $C_2O_4^{2-}$ oxidation (see Figures 5.5b). At an initial O_3 concentration of 10.0 µM and catalyst concentration of 0.06 g L^{-1}, increasing the $C_2O_4^{2-}$ concentration decreased the extent of $C_2O_4^{2-}$ oxidation due to ozone limitation (Figures 5.5a & 5.6); however, the overall O_3 usage efficiency (i.e., moles of $C_2O_4^{2-}$ oxidized per mole of O_3 consumed) increases with an increase in $C_2O_4^{2-}$ concentration. Employing the data shown in Figures 5.5 and 5.6, we calculate that O_3 usage efficiency is ~0.1, 0.8 and 0.9 at an initial $C_2O_4^{2-}$ concentration of 1.0, 10.0 µM and 100.0 µM respectively for both Cu–Al LDHs and CuO suggesting that stoichiometric constraints (close to 1:1) have been achieved at higher $C_2O_4^{2-}$ concentrations. The similarity in O_3 usage efficiency for Cu–Al LDHs and CuO confirms that the stoichiometry of the O_3–$C_2O_4^{2-}$ reaction is the same for both catalysts. Note that control experiments using $Al(OH)_3$ as the catalyst showed that oxidative removal of $C_2O_4^{2-}$ in the presence of $Al(OH)_3$ is similar to that observed during the conventional ozonation process (Figure 5.7) with this result confirming that $Al(OH)_3$ is not an effective catalyst for $C_2O_4^{2-}$ oxidation.

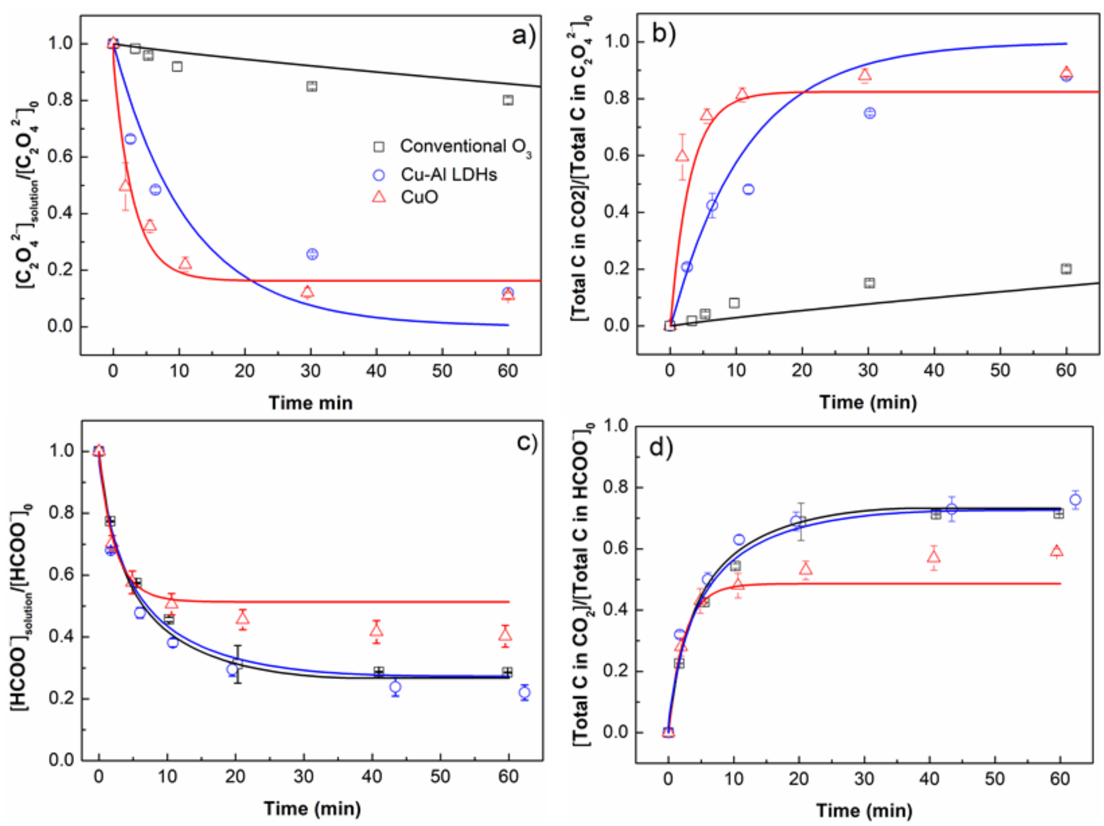

Figure 5.5 Removal of dissolved $C_2O_4^{2-}$ (panel a) and concomitant CO_2 (panel b) formation in the absence (squares) and presence of Cu–Al LDHs (circles) and CuO (triangles) at pH 7.3. Removal of dissolved $HCOO^-$ (panel c) and concomitant CO_2 (panel d) formation in the absence (squares) and presence of Cu–Al LDHs (circles) and CuO (triangles) at pH 7.3. Experimental conditions: $[catalyst]_0 = 0.06$ g L^{-1} (in terms of CuO mass), $[O_3]_0 = 10.0$ μM, $[C_2O_4^{2-}]_0/[HCOO^-]_0 = 10.0$ μM, pH 7.3 using 2.0 mM $NaHCO_3$. Note CO_2 production during conventional O_3 shown here represents the difference between initial $C_2O_4^{2-}/HCOO^-$ concentration and $C_2O_4^{2-}/$ $HCOO^-$ concentration remaining at various times shown in Figure 5.5a. CO_2 production during catalytic ozonation here represents the difference of initial $C_2O_4^{2-}/$ $HCOO^-$ concentration and $C_2O_4^{2-}/$ $HCOO^-$ concentration remaining at various times measured in unfiltered samples following the dissolution of the catalysts. Symbols represent experimental data and the lines represent model values.

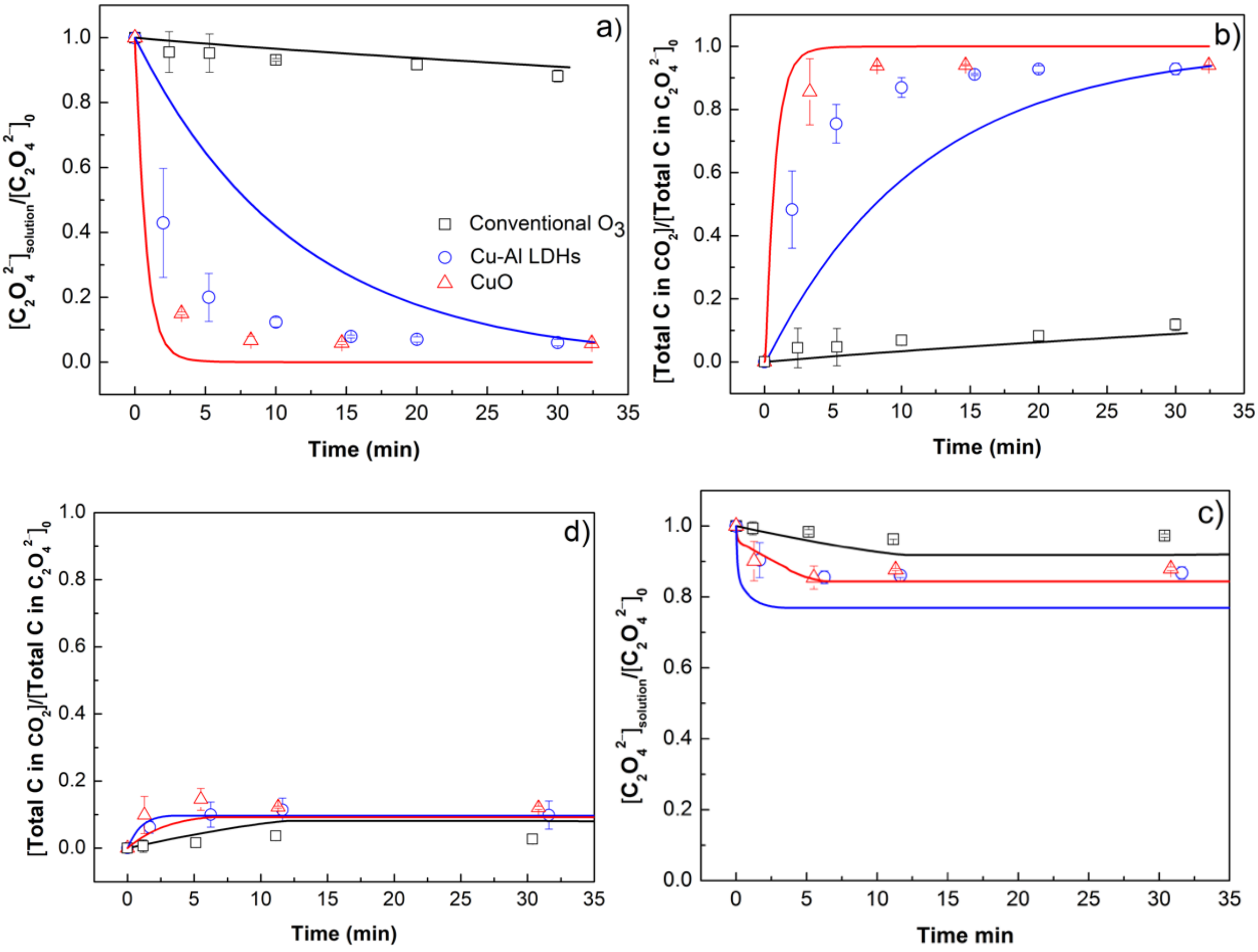

Figure 5.6 Fraction of $C_2O_4^{2-}$ removed (panels a and c) and oxidized (panel b and d) in the absence (squares) and presence of Cu–Al LDHs (circles) and CuO (triangles) at pH 7.3 at an initial $[C_2O_4^{2-}]$ of 1.0 µM (panels a and b) and 100.0 µM (panels c and d). Experimental conditions: $[\text{catalyst}]_0 = 0.06$ g L^{-1} (in terms of CuO mass), $[O_3]_0 = 10.0$ µM, $[C_2O_4^{2-}]_0 = 1.0 – 100.0$ µM, pH 7.3 using 2.0 mM $NaHCO_3$. Note CO_2 production during conventional O_3 shown here represents the difference between initial $C_2O_4^{2}$ concentration and $C_2O_4^{2}$ concentration remaining at various times. CO_2 production during catalytic ozonation here represents the difference of initial $C_2O_4^{2-}$ concentration and $C_2O_4^{2-}$concentration remaining at various times measured in unfiltered samples. Symbols represent experimental data and the lines represent model values.

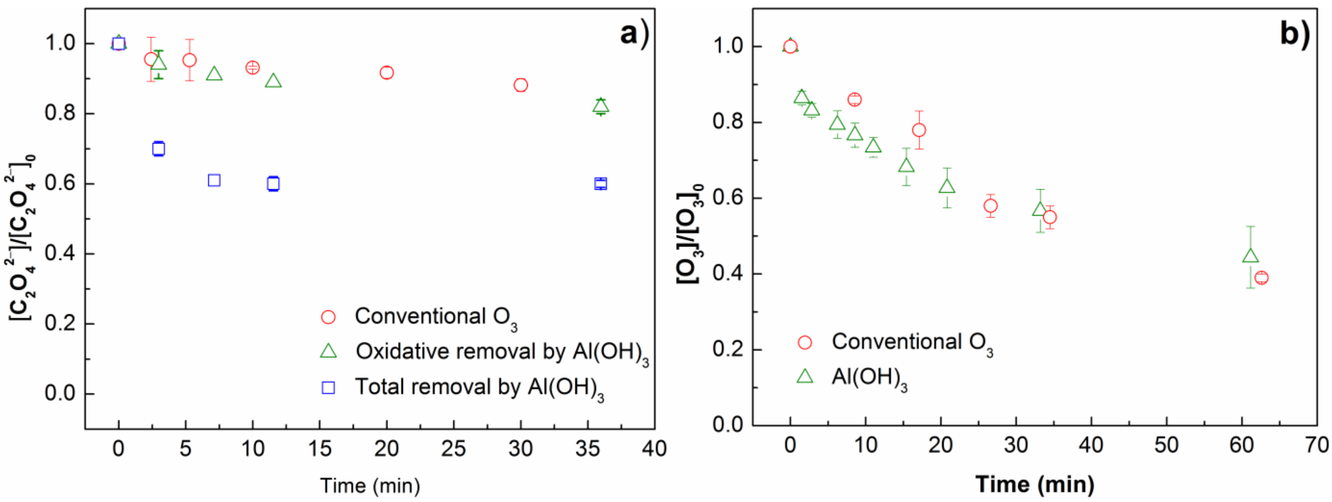

Figure 5.7 (a) Fraction of $C_2O_4^{2-}$ oxidized and removed in the absence (circles) and presence of $Al(OH)_3$ (oxidative removal: triangles; total removal: squares). Experimental conditions: $[\text{catalyst}]_0$ = 0.1 g L^{-1} (in terms of $Al(OH)_3$ mass), $[C_2O_4^{2-}]_0$ = 1.0 µM, $[O_3]_0$ = 10.0 µM, pH 7.3 using 2.0 mM $NaHCO_3$. (b) Measured O_3 decay in the absence (circles) and presence (triangles) of $Al(OH)_3$. Experimental conditions: $[O_3]_0$ = 120.0 µM, $[\text{catalyst}]_0$ = 0.1g L^{-1} (in terms of $Al(OH)_3$ mass), pH 7.3 using 2.0 mM $NaHCO_3$.

5.3.2.1. Influence of catalyst dosage

As shown in Figures 5.8a and 5.9a, minimal influence of the catalyst dosage was observed on $C_2O_4^{2-}$ oxidation by HCO in the presence of Cu–Al LDHs and CuO. Note that at an initial $C_2O_4^{2-}$ concentration of 10.0 µM, a slightly lower (8.2% and 21.7% for Cu–Al LDHs and CuO respectively) removal efficiency was observed at a lower catalyst dosage, though no significant (p > 0.05 using single tailed student's t–test) influence of increasing the catalyst dosage above 0.02 g.L^{-1} was observed. This might also suggested that excessive active sites might exist when catalyst dosage exceeded 0.02 g.L^{-1}. The minimal influence of catalyst dosage on $C_2O_4^{2-}$ oxidation suggests that the futile consumption of oxidant (i.e., O_3 and/or species formed on O_3 decay) by the catalyst was minor, at least in the presence of $C_2O_4^{2-}$. Furthermore, it appears that the generation of oxidant(s) is possibly limited by the O_3 concentration and not influenced by the catalyst dosage, except at low catalyst dosage (≤ 0.02 g L^{-1}).

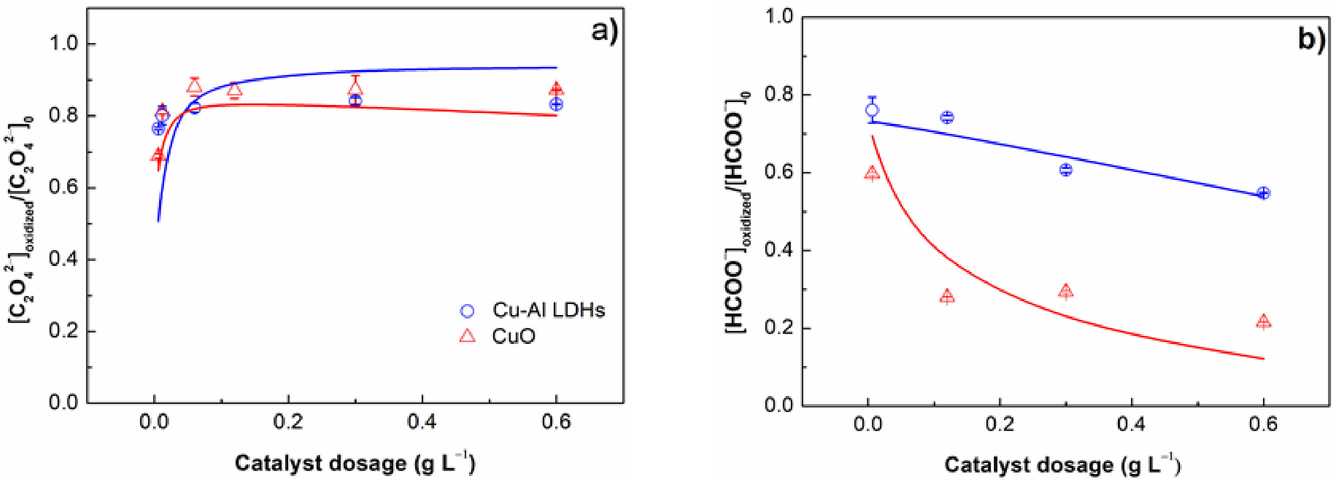

Figure 5.8 Fraction of $C_2O_4^{2-}$ and $HCOO^-$ oxidized in the presence of Cu–Al LDHs (circles) and CuO (triangles) at varying catalyst dosages. Experimental conditions: $[\text{catalyst}]_0$ = 0.006 – 0.6 g L^{-1} (in terms of CuO mass), $[C_2O_4^{2-}]_0$ = 10.0 (panel a) and $[HCOO^-]$ = 10.0 μM (panel b), $[O_3]_0$ = 10.0 μM, pH 7.3 using 2.0 mM $NaHCO_3$, reaction time 2 h. Symbols represent experimental data and the lines represent model values.

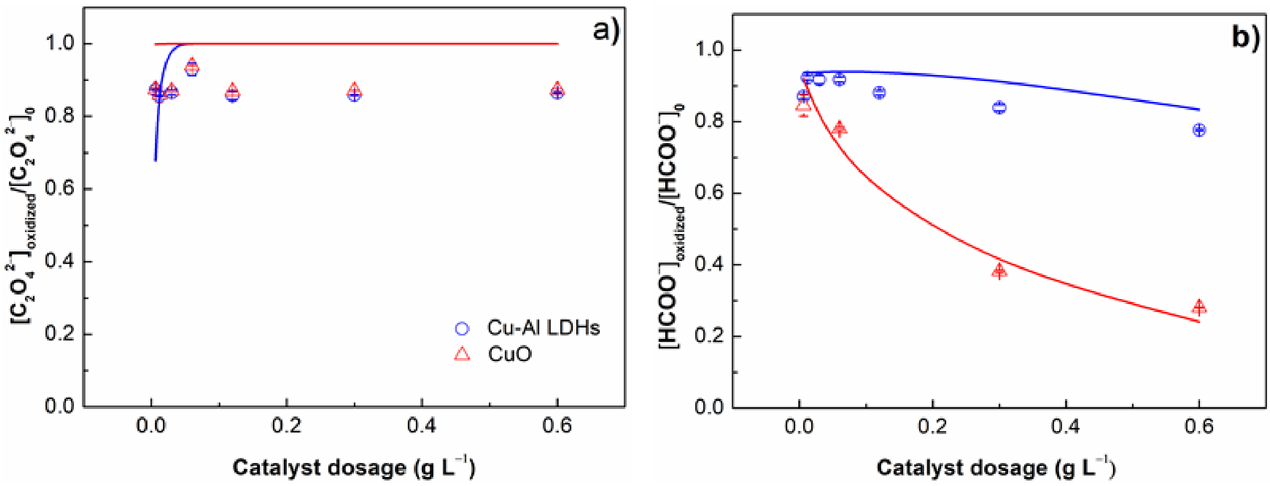

Figure 5.9 Fraction of $C_2O_4^{2-}$ and $HCOO^-$ oxidized in the presence of Cu–Al LDHs (circles) and CuO (triangles) at varying catalyst dosage. Experimental conditions: $[\text{catalyst}]_0$ = 0.006 – 0.6 g L^{-1} (in terms of CuO mass), $[C_2O_4^{2-}]_0$ = 1.0 μM (panel a) and $[HCOO^-]_0$ = 1.0 μM (panel b), $[O_3]_0$ = 10.0 μM, pH 7.3 using 2.0 mM $NaHCO_3$, reaction time 2 h. Symbols represent experimental data and the lines represent model values.

5.3.2.2. Role of hydroxyl radicals

As shown in Figure 5.10, addition of TBA (a bulk $^{\bullet}OH$ scavenger [87]) has no influence on $C_2O_4^{2-}$ oxidation by HCO (for both Cu–Al LDHs and CuO) suggesting that $^{\bullet}OH$ in bulk solution are not involved in $C_2O_4^{2-}$ oxidation.

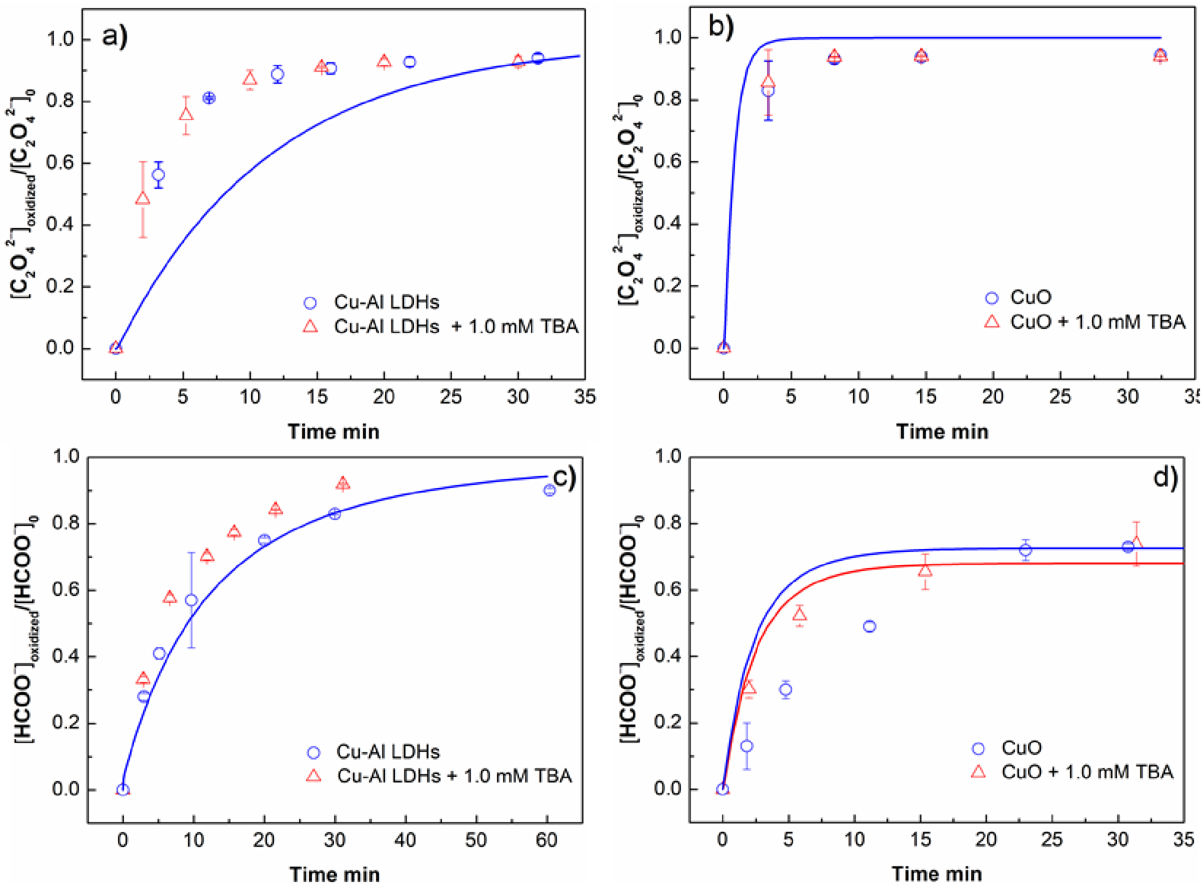

Figure 5.10 Measured influence of 1.0 mM TBA addition on $C_2O_4^{2-}$oxidation (panels a & b) and $HCOO^-$ oxidation (panels c & d) by HCO in the presence of Cu–Al LDHs (panel a & c) and CuO (panel b &d) at pH 7.3. Experimental conditions: $[C_2O_4^{2-}]_0$/ $[HCOO^-]_0$ = 1.0 μM, $[catalyst]_0$ = 0.06 g.L^{-1} (in terms of CuO mass), $[O_3]_0$ = 10.0 μM, $[TBA]_0$ = 1.0 mM. Symbols represent experimental data, lines represent model values. The model results in the absence and presence of TBA are same for $C_2O_4^{2-}$oxidation. Model results for $HCOO^-$ oxidation in the absence and presence of TBA are same for Cu-Al LDHs.

5.3.3. Oxidation of formate by HCO using Cu-Al LDHs and CuO as the catalyst

As shown in Figure 5.5c, the presence of Cu–Al LDHs has no effect on the rate and extent of $HCOO^-$ oxidation compared to that observed by the conventional ozonation process while CuO has minimal effect on $HCOO^{-}$ oxidation rate at early times but reduces the extent of oxidation at later times. Nearly 74%, 76% and 60% of 10.0 µM $HCOO^{-}$ was oxidized in 60 min in the absence and presence of Cu–Al LDHs and CuO respectively. As found to be the case for $C_2O_4^{2-}$, the removal of $HCOO^{-}$ was also mostly via oxidation as confirmed by the CO_2 concentration formed on $HCOO^{-}$ oxidation after 60 min (see Figure 5.6d). The difference in the influence of catalyst on the oxidation rates of $HCOO^{-}$ and $C_2O_4^{2-}$ suggests that the nature of the organic compound impacts the efficiency of HCO. Since $C_2O_4^{2-}$ is an ozone resistant compound ($k_{O_3/C_2O_4^{2-}}$ = 0.04 $M^{-1}\cdot s^{-1}$ [123]), it is not readily oxidized by the conventional ozonation process. In comparison, $HCOO^{-}$ is an ozone reactive compound ($k_{O_3/HCOO^{-}}$ = 1.5 – 100.0 $M^{-1}\cdot s^{-1}$ [3, 140]) and undergoes rapid oxidation by ozone alone. Hence, no significant enhancement in $HCOO^{-}$ oxidation by HCO compared to the ozone only process is observed.

5.3.3.1. Influence of catalyst dosage

Increasing the Cu–Al LDHs concentration caused a slight decrease in the extent of 1.0 and 10.0 µM $HCOO^{-}$ oxidation however increasing the CuO concentration had a more pronounced impact on $HCOO^{-}$ oxidation (Figure 5.8b and 5.9b). This observation suggests that significant futile consumption of the oxidant involved in $HCOO^{-}$ oxidation occurs via interaction with CuO. In contrast, the consumption of the oxidant(s) by Cu–Al LDHs is minor, at least at the conditions investigated here. This is an important observation and suggests that Cu–Al LDHs results in more efficient O_3 usage compared to CuO, at least for organic compounds such as $HCOO^{-}$.

5.3.3.2. Role of hydroxyl radicals

As shown in Figure 5.10, no significant ($p > 0.05$ using single tailed student's t–test) influence of addition of TBA was observed on $HCOO^-$ oxidation in the presence of Cu–Al LDHs and CuO though note that the involvement of bulk $^\bullet OH$ cannot be rejected based on this observation. In the case of compounds such as $HCOO^-$ which promotes O_3 decay and are ozone reactive, the presence of TBA may result in the alteration in the pathway of oxidation from $^\bullet OH$ mediated $HCOO^-$ oxidation in the absence of TBA to O_3 mediated oxidation in the presence of TBA as explained in detail in chapter 8.

5.3.4. Mechanistic aspects of oxalate and formate oxidation by HCO

5.3.4.1. Catalyst - ozone interaction

In order to understand the mechanism of $C_2O_4^{2-}$ and $HCOO^-$ oxidation by HCO, we first investigated the mechanisms of O_3 and catalyst interaction. As shown in Figure 5.11a, in the presence of Cu–Al LDHs, the rate of O_3 decay is slightly higher than that observed in the absence of catalyst which suggests that Cu–Al LDHs catalyse O_3 decay, albeit slowly. Furthermore, the strong fluorescence signals corresponding to 7–HC on the surface of Cu–Al LDHs particles (Figure 5.11b) confirms the generation of $\equiv^\bullet OH$ via O_3 and Cu–Al LDHs interaction.[29, 80, 183] Note that no influence of TBA addition (Figure 5.11c) was observed on the formation of surface 7–HC confirming that (i) 7–HC formation occurs via COU and $^\bullet OH$ interaction on the surface rather than the sorption of 7–HC formed in bulk solution and (ii) scavenging of $\equiv^\bullet OH$ by TBA is unimportant. No 7-HC formation occurred during conventional ozonation (Figure 5.12) with this result confirming that 7–HC formation via interaction with O_3 and/or bulk $^\bullet OH$ is unimportant which agrees with the results reported earlier.[29] The futile consumption of the surface oxidants (i.e., O_3 and $^\bullet OH$) via interaction with the catalyst surface is minimal, at least in the presence of $C_2O_4^{2-}$, since the extent of $C_2O_4^{2-}$

oxidation was nearly constant over a wide range of Cu–Al LDHs dosages (Figure 5.8a and 5.9a) and the ozone usage efficiency in the presence of $C_2O_4^{2-}$ was ~1.0. However, some decrease in the extent of $HCOO^-$ oxidation with increase in Cu–Al LDHs dosage was observed (Figure 5.8b and 5.9b), suggesting that a small portion of oxidants is consumed via interaction with the surface sites with this process particularly important at a higher catalyst dosage and in the absence of organics such as $C_2O_4^{2-}$.

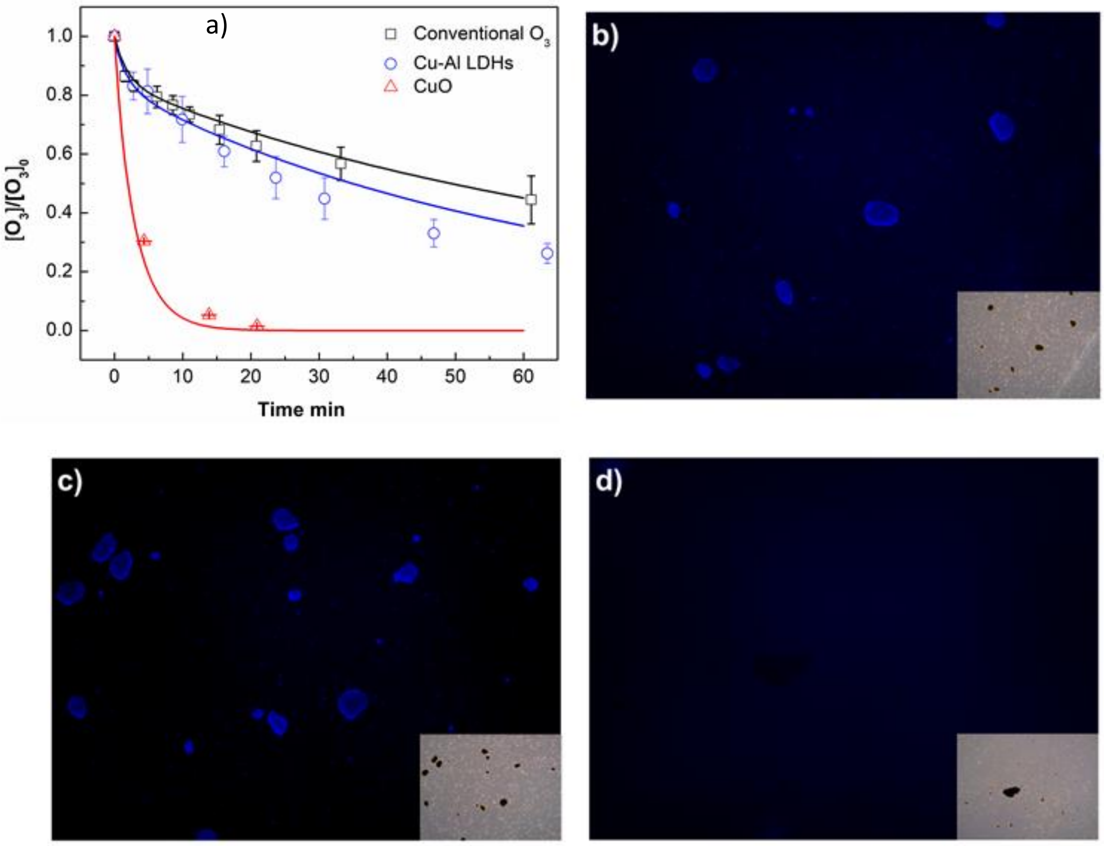

Figure 5.11 (a) O_3 decay in the absence (squares) and presence of Cu–Al LDHs (circles) and CuO (triangles) at pH 7.3. Panels b and c show fluorescence images of Cu–Al LDHs in the absence and presence of TBA respectively following 1 h reaction with O_3 at pH 7.3 while panel d shows fluorescence image for CuO samples following 1 h reaction with O_3 at pH 7.3. Experimental conditions for O_3 decay: $[O_3]_0$ = 120.0 µM, $[catalyst]_0$ = 0.06g L^{-1} (in terms of CuO mass). Experimental conditions for fluorescence images: $[O_3]_0$ = 100.0 µM, $[catalyst]_0$ = 0.06 g L^{-1} (in terms of CuO mass), $[COU]_0$ =10.0 µM, $[TBA]_0$ = 1.0 mM.

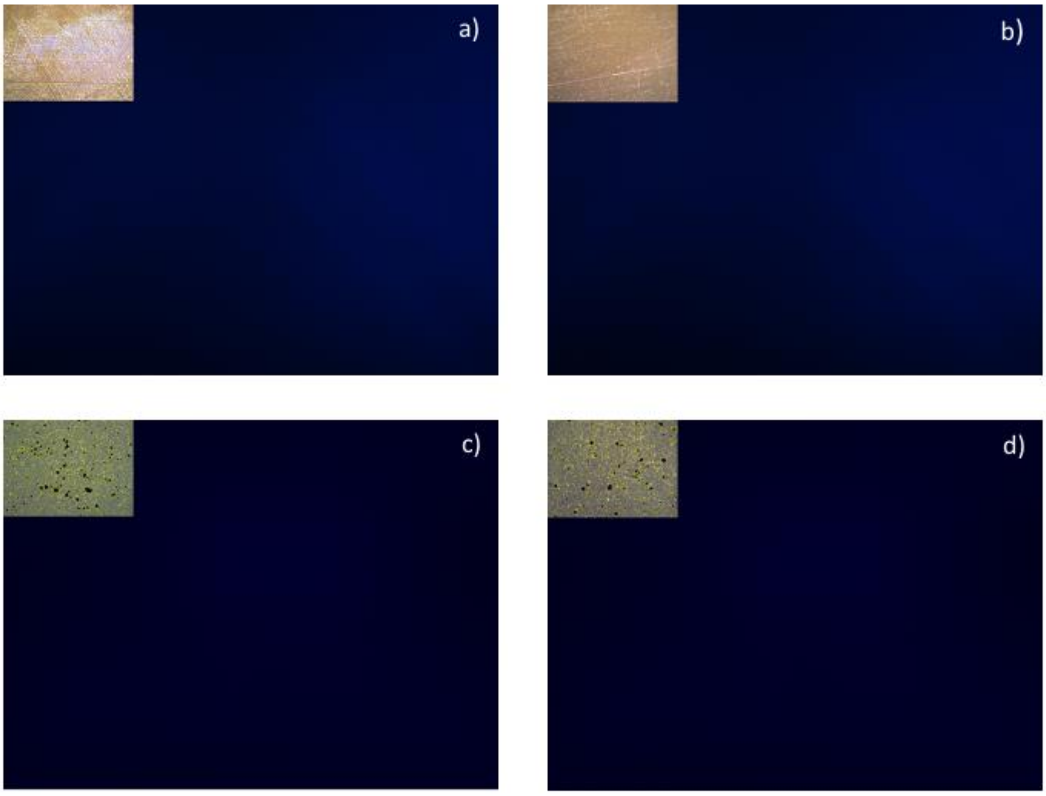

Figure 5.12 Panels a & b: Fluorescence microscopy images of samples prepared by conventional ozonation in the absence (a) and presence (b) of TBA after 1 h exposure to O_3 at pH 7.3. Experimental conditions: $[O_3]_0$ = 100.0 µM, $[TBA]_0$ = 1.0 mM, $[COU]_0$ =10.0 µM. Panels c & d: Fluorescence microscopy image of samples prepared by conventional ozonation of coumarin in the absence (a) and presence of 1.0 mM TBA (b) for 1 h and then sorbed onto Cu–Al LDHs surface for 1 h. Experimental conditions: $[O_3]_0$ = 100.0 µM, $[COU]_0$ = 10.0 µM, pH 7.3 using 2.0 mM $NaHCO_3$. [Cu–Al LDHs]$_0$ = 0.06 g L^{-1} during the sorption step.

In contrast to Cu–Al LDHs, the presence of CuO increases the O_3 decay rate considerably compared to that observed in the absence of catalyst (Figure 5.11a). This observation suggests that in the presence of CuO, O_3 undergoes rapid decay forming reactive oxidants and/or non-reactive products (such as O_2). No fluorescence signal for 7–HC was observed in the presence of CuO (Figure 5.11d), possibly be due to the rapid scavenging of $\equiv^{\bullet}OH$ by CuO outcompeting the $\equiv^{\bullet}OH$−COU reaction. While a similar extent of COU sorption was observed in the presence of CuO and Cu–Al LDHs (Figure 5.13), more rapid scavenging of $\equiv^{\bullet}OH$ by CuO compared to that in case of Cu–Al LDHs (which is supported by the observation that $HCOO^-$ oxidation decreases with increasing catalyst dosage; Figure 5.8b) possibly inhibits 7–HC formation in the case of CuO.

Though no 7–HC formation was observed, even at a higher COU dosage (Figure 5.14), the possibility of formation of ≡•OH still cannot be rejected since increasing COU concentration may facilitate COU–O_3 bulk reaction, thereby decreasing CuO–mediated O_3 decay and concomitant generation of ≡•OH. Overall, it appears that the CuO–O_3 interaction results in formation of surface-located oxidants (such as ≡•OH,[37, 188] surface atomic oxygen or species formed via electron-transfer between Cu(I)/Cu(II) and O_3[25, 189-192]) as well as non-reactive products (such as O_2). As explained in the case of Cu-Al LDHs, the formation of non-reactive products is expected to be minimal, at least in the presence of $C_2O_4^{2-}$, since the extent of $C_2O_4^{2-}$ oxidation was nearly constant at varying CuO dosage and the O_3 usage efficiency was ~1.0 (Figure 5.8a and 5.9a). However, a major portion of O_3 is transformed to non-reactive product(s) in the absence of $C_2O_4^{2-}$ at higher CuO dosage with this conclusion supported by the influence of CuO dosage on $HCOO^-$ oxidation (Figure 5.8b and 5.9b).

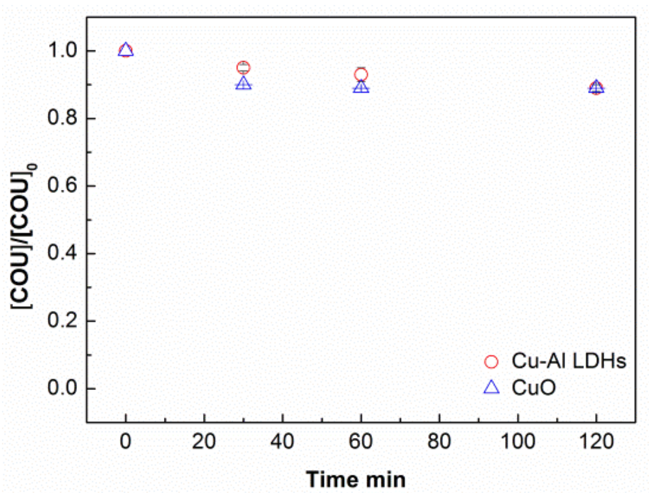

Figure 5.13 Fraction of COU remaining in solution in the presence of Cu–Al LDHs and CuO at pH 7.3. Experimental conditions: $[COU]_0$ = 10.0 µM, $[catalyst]_0$ = 0.06 g L^{-1} (in terms of CuO mass).

Figure 5.14 Fluorescence images of CuO samples after 1 h exposure for O_3 at pH 7.3. Experimental conditions: $[O_3]_0$ = 100.0 μM, $[\text{catalyst}]_0$ = 0.06 g L^{-1} (in terms of CuO mass), $[\text{COU}]_0$ =130.0 μM.

Note that diffusion of the surface oxidant formed on ozone decay in the presence of Cu–Al LDHs and/or CuO to the interfacial zone and/or bulk solution can be rejected based on the measured oxidation rates of *p*–CBA. As shown in Figure 5.15, the rate and extent of oxidation of *p*–CBA in the presence of Cu–Al LDHs and CuO is lower than that observed during use of ozone alone suggesting that $^{\bullet}$OH/other oxidants generated on the catalyst surface do not diffuse into the interfacial zone and/or bulk solution. Note that CuO and Cu–Al LDHs significantly inhibited *p*–CBA oxidation (which mainly occurs in the bulk solution) due to the futile consumption of O_3 and/or bulk $^{\bullet}$OH generated on O_3 self-decay.

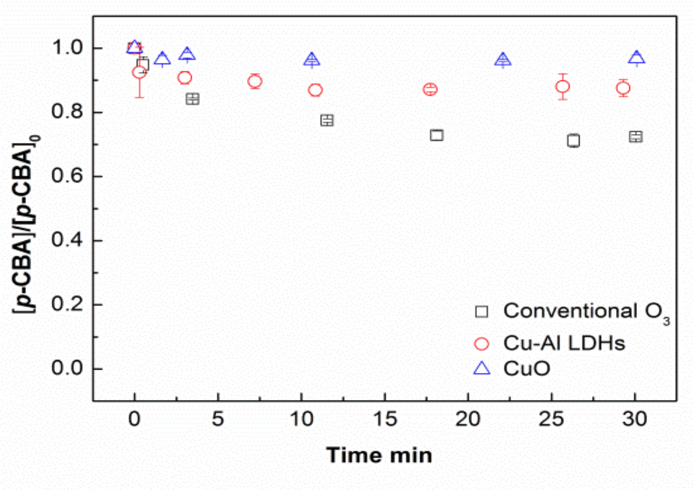

Figure 5.15 Measured *p*–CBA oxidation in the absence (squares) and presence of 0.06 g L^{-1} Cu–Al LDHs (circles) and CuO (triangles) at pH 7.3. Experimental conditions: $[O_3]_0$ = 100.0 μM, $[p\text{–CBA}]_0$ = 1.0 μM, $[\text{catalyst}]_0$ = 0.06 g L^{-1} (in terms of CuO mass).

To sum up, the decomposition mechanism of O_3 on CuO and Cu–Al LDHs is similar. Briefly, O_3 interacts with the surface hydroxyl groups in CuO and Cu–Al LDHs resulting in formation of an unkonwn surface oxidant and surface •OH, respectively. The involvement of surface hydroxyl groups in catalyst–mediated O_3 decay agrees with the observation that O_3 decay in the presence of catalyst is inhibited in the presence of phosphate related species (strong Lewis bases that adsorbs on the surface of catalysts and inhibits O_3 sorption and decay;[193] Figure 5.16) and also with the mechanism of catalytic ozonation employing metal oxides reported in various earlier studies.[40, 48, 49, 166, 194-197] These surface oxidants/•OH entities are consumed via interaction with adsorbed organics and/or surface sites with this conclusion supported by effective catalyst–mediated $C_2O_4^{2-}$/ $HCOO^-$ oxidation (Figure 5.5 and 5.6) and the decrease in $HCOO^-$ oxidation (Figure 5.8b and 5.9b) at higher catalyst dosage respectively. The faster O_3 decay in the presence of CuO compared to Cu–Al LDHs is due to the difference in the nature and concentration of the hydroxyl groups on the surface of the two catalysts. A higher concentration of surface hydroxyl groups is present on the surface of CuO (150.6 μM/g) compared to that on the surface of Cu–Al LDHs (36.7

μM/g) and, hence, the rate of catalyst-mediated O_3 decay is faster in the presence of CuO compared to that measured in the presence of Cu–Al LDHs. Furthermore, the surface hydroxyl groups in CuO are expected to exhibit a stronger acidic character compared to those in Cu–Al LDHs due to the replacement of Cu^{2+} by Al^{3+} and steric shielding of metal cations by carbonate ions.[198] Additionally, in Cu–Al LDHs, the Cu atoms are distributed among Al atoms in the brucite layers and hence O_3 and/or oxidants generated on O_3 decay possibly migrate to and are stabilized by the Al sites (note that no increase in O_3 decay was observed in the presence of $Al(OH)_3$; Figure 5.7b) with interaction between sorbed organics and oxidants occurring at Al sites. A similar mechanism was reported for PdO/CeO_2 wherein O_3 was transformed into ROS on the PdO sites while sorption of $C_2O_4^{2-}$ and concomitant oxidation occurred on the CeO_2 sites.[26] In the case of CuO, the oxidants can only migrate to the ambient Cu centre and are scavenged by Cu due to its strong acidic character.

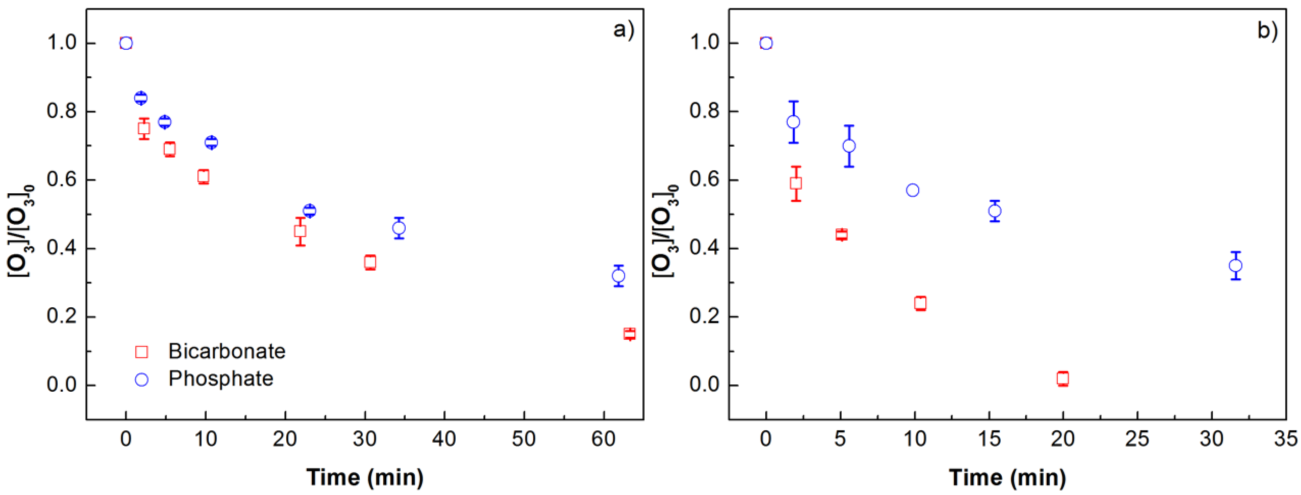

Figure 5.16 Measured O_3 decay in the bicarbonate (squares) and phosphate (circles) buffered solution in the presence of Cu–Al LDHs/CuO at pH 7.3 (panel a Cu–Al LDHs and panel b CuO). Experimental conditions: $[Cu\text{-}Al\ LDHs]_0 = 0.6$ g L^{-1}, $[CuO]_0 = 0.06$ g L^{-1} (in term of CuO mass), $[O_3]_0 = 100.0$ μM, $[phosphate]_0/[HCO_3]_0 = 1.33$ mM.

We would also like to highlight that the sorption of organics on the Cu–Al LDHs and CuO surfaces had minimal influence on the catalyst–O_3 interaction, at least under the conditions investigated here. As shown in Figure 5.17, the O_3 decay rate in the presence of Cu–Al LDHs with pre-sorbed $C_2O_4^{2-}$ is slightly higher than that measured in the presence of catalyst with no sorbed $C_2O_4^{2-}$ with this small difference most likely due to rapid reaction of sorbed $C_2O_4^{2-}$ with surficial O_3 rather than due to the influence of sorbed $C_2O_4^{2-}$ on the catalyst-O_3 interaction. In the case of CuO, similar (p>0.05 using single tailed student's t–test) O_3 decay rates were observed in the absence and presence of sorbed $C_2O_4^{2-}$. Minimal influence of sorption of organics on the CuO–O_3 interaction is consistent with the minor extent of sorption of organics on the CuO surface observed under the conditions investigated in this study (Figure 5.18).

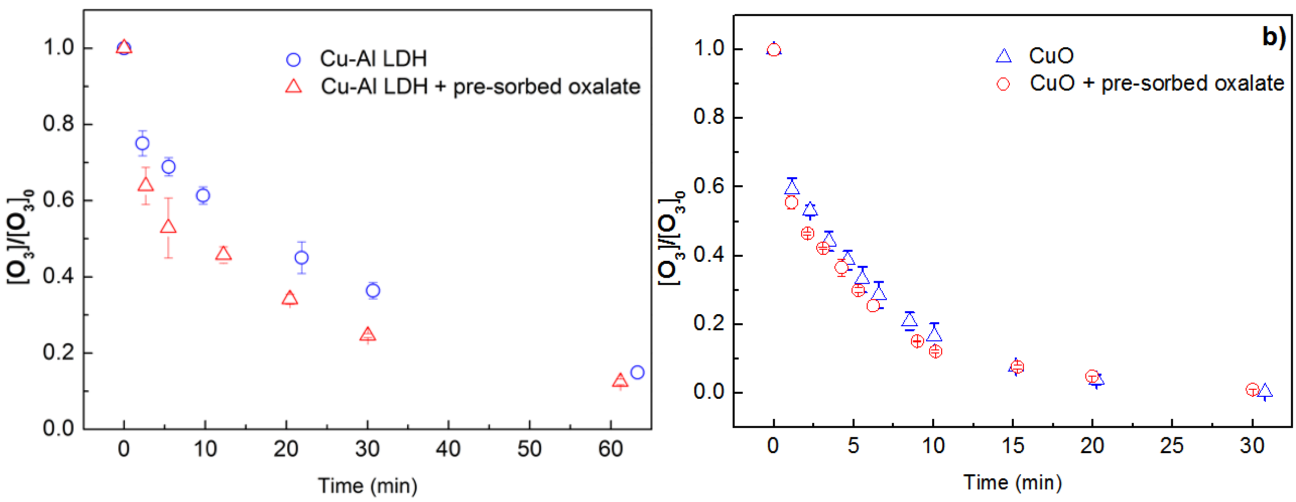

Figure 5.17 Measured O_3 decay in the presence of Cu–Al LDHs (panel a) and CuO (panel b) in the absence and presence of pre-sorbed oxalate on the catalyst surface at pH 7.3. Experimental conditions: $[\text{Cu-Al LDHs}]_0 = 0.6$ g L^{-1} (in terms of CuO), [CuO]= 0.12 g L^{-1} (in terms of CuO), $[O_3]_0 = 100.0$ μM, $[C_2O_4^{2-}]_0 = 20.0$ μM (for CuO) and 100.0 μM for Cu–Al LDHs, pH 7.3 using 2.0 mM $NaHCO_3$.

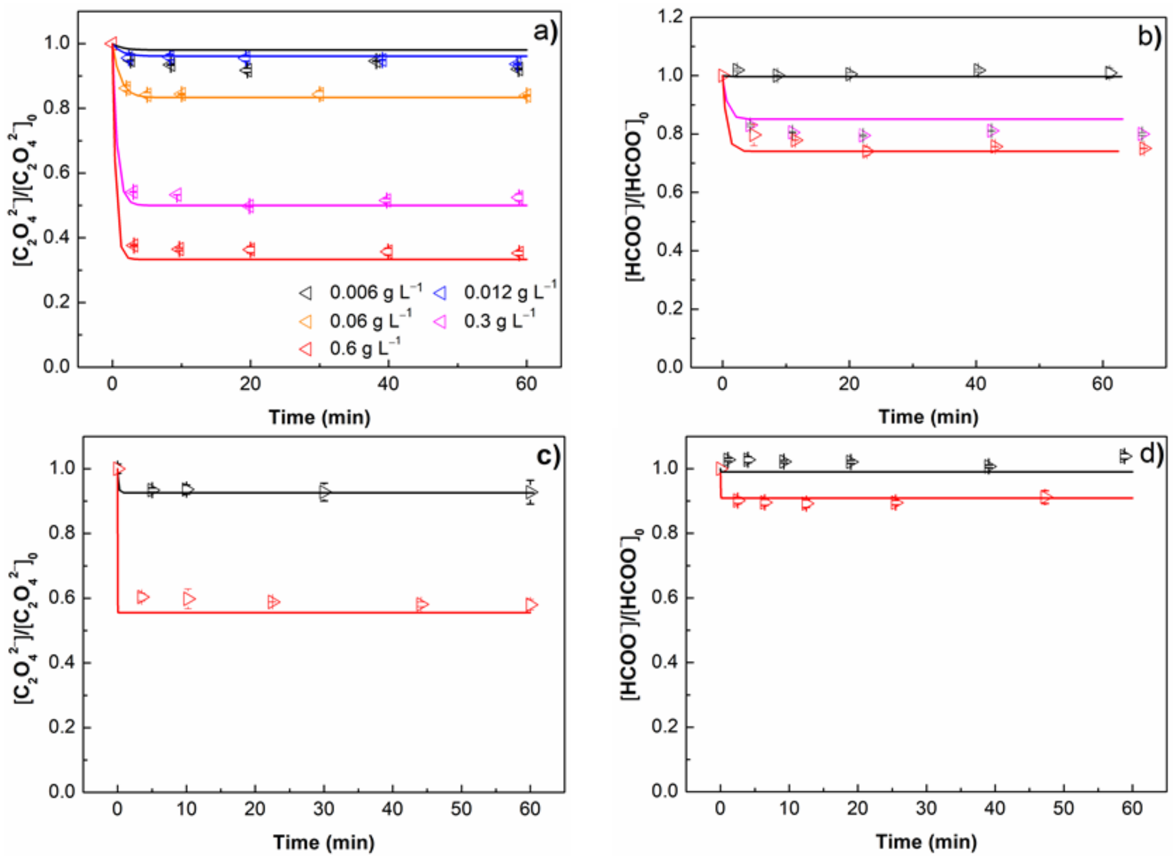

Figure 5.18 Fraction of $C_2O_4^{2-}$ (panels a & c) and $HCOO^-$ (panels b & d) remaining in the presence of varying Cu–Al LDHs (panels a & b) and CuO (panels c & d) dosage at pH 7.3. Experimental conditions: $[C_2O_4^{2-}]_0$ = 1.0 µM, $[HCOO^-]_0$ =1.0 µM, $[catalyst]_0$ = 0.006 – 0.6 g L^{-1} (in terms of CuO mass). Symbols represent experimental data, lines represent model values.

5.3.4.2 Catalyst-organic interaction in the absence of ozone

As shown in Figure 5.18, a small but significant fraction of $C_2O_4^{2-}$ is rapidly adsorbed onto the Cu–Al LDHs/CuO surface and reaches steady–state within 5 min with the surface $C_2O_4^{2-}$ concentration increasing with the increase in Cu–Al LDHs/CuO dosage. The adsorption of $C_2O_4^{2-}$ in the presence of Cu–Al LDHs/CuO was also confirmed by FTIR analysis (Figure 5.19) with a peak corresponding to $C_2O_4^{2-}$ evident at 1650 – 1700 cm^{-1}.[199] The adsorption of $C_2O_4^{2-}$ possibly occurs via binding of $C_2O_4^{2-}$ to the surface Cu sites. The formation of surface Cu-oxalate complexes has been reported in earlier studies with the surface Cu-oxalate complex reported to be potentially more reactive than free $C_2O_4^{2-}$.[25, 82] The extent of adsorption of $HCOO^-$ on the Cu–Al

LDHs/CuO surface was lower than that observed for $C_2O_4^{2-}$(Figure 5.18), possibly due to the higher binding capacity of $C_2O_4^{2-}$ as a result of the presence of two carboxylic binding sites compared to one carboxylic group in $HCOO^-$.[82]

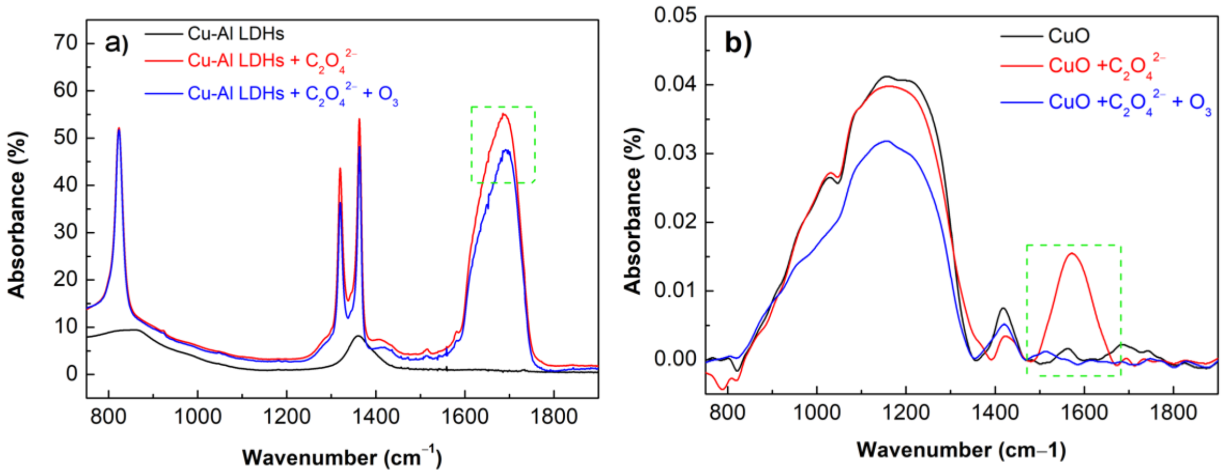

Figure 5.19 FTIR spectra of Cu–Al LDHs (panel a) and CuO (panel b) in the absence and presence of $C_2O_4^{2-}$ and O_3. Experimental conditions: $[C_2O_4^{2-}]_0$ = 1.0 – 10.0 mM, $[catalyst]_0$ = 0.06 g L^{-1} (in terms of CuO mass), $[O_3]_{0,gas}$ =51.0 g m^{-3}, flow rate 0.65 mL min^{-1}, t = 10.0 min.

The adsorption of $C_2O_4^{2-}$/ $HCOO^-$ on Cu–Al LDHs and CuO can be well described by Langmuir isotherms with the maximum adsorption capacities of Cu–Al LDHs and CuO for $C_2O_4^{2-}$ calculated to be 3.44±0.16 mg g^{-1} (K_L=1.72±0.48) and 1.42±0.05 mg g^{-1} (K_L=0.28 ± 0.04) respectively (Figure 5.20a). Similarly, the maximum adsorption capacities for $HCOO^-$ were 0.49±0.03 mg g^{-1} (K_L=0.0106±0.0002) and 0.20±0.02 mg g^{-1}(K_L=0.0026±0.0006) for Cu–Al LDHs and CuO respectively (Figure 5.20b). The higher adsorption capacity of Cu–Al LDHs compared to CuO is likely due to the Al content in the layered structure of Cu–Al LDHs with this hypothesis supported by the observation that significant sorption of $C_2O_4^{2-}$ occurs on $Al(OH)_3$ surfaces (Figure 5.7a).

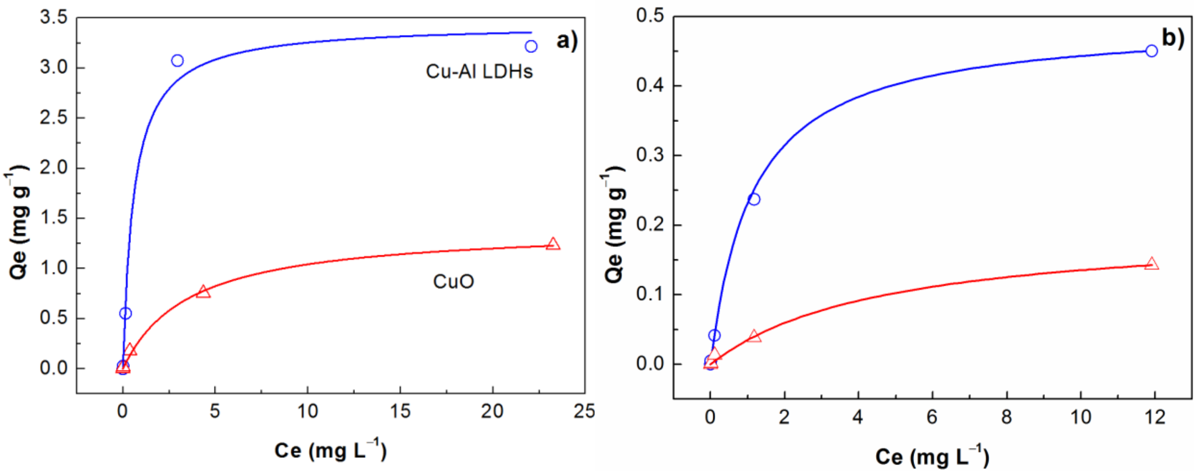

Figure 5.20 Adsorption isotherms of Cu–Al LDHs and CuO for (a) $C_2O_4^{2-}$ and (b) $HCOO^{-}$. Experimental conditions: $[Catalysts]_0$ = 0.6 g L^{-1} (in terms of CuO mass), $[C_2O_4^{2-}]_0$ /$[HCOO^{-}]_0$ = 1.0 – 1000.0 μM, sorption time 2 h, pH = 7.3 buffered by 2.0 mM $NaHCO_3$.

5.3.4.3 Oxidation of organics by HCO

The oxidation of $C_2O_4^{2-}$ in the presence of both Cu–Al LDHs and CuO occurs on the surface of these catalysts since bulk/interfacial $^{\bullet}OH$ are not involved (no influence of TBA addition; Figure 5.10) and the reaction of aqueous O_3 and $C_2O_4^{2-}$ is very slow, at least at the O_3 and $C_2O_4^{2-}$concentrations examined here (Figure 5.5). The decrease in the peak corresponding to adsorbed $C_2O_4^{2-}$ at 1650 -1700 cm^{-1} in the presence of O_3 (Figure 5.19) also supports the conclusion regarding surface oxidation of $C_2O_4^{2-}$. Hence, in the case of Cu–Al LDHs, surface-located O_3 and $^{\bullet}OH$ are expected to play a role however the role of surface-located O_3 is expected to be more prominent than that of $^{\bullet}OH$ since the oxidation rate of $C_2O_4^{2-}$ is much higher than the rate of ozone decay (and associated rate of $^{\bullet}OH$ formation). The oxidation of surface oxalate complexes by O_3 has been reported previously.[25, 82]

In the case of CuO, surficial O_3 and/or other oxidant(s) generated on O_3 decay are expected to play a role in surface oxalate complex oxidation. The high O_3 usage efficiency (~0.8 for 10.0 μM $C_2O_4^{2-}$; Figure 5.5) for $C_2O_4^{2-}$ oxidation in the presence of both CuO and Cu-Al LDHs compared to usage efficiency for aqueous O_3 (~ 0.2 for 10.0 µM $C_2O_4^{2-}$; Figure 5.5) further suggests that the presence of the readily oxidizable surface oxalate complex minimizes O_3 loss in the bulk solution and achieve high O_3 usage efficiency.

In the presence of Cu–Al LDHs, a significant concentration of O_3 is present in the bulk solution which can drive $HCOO^-$ oxidation in the bulk solution in addition to surface-mediated oxidation of sorbed $HCOO^-$. However, limited O_3 is present in the bulk solution in the case of CuO confirming that the oxidation of $HCOO^-$ predominantly occurs on the surface. The oxidation of $HCOO^-$ on the surface of CuO is in agreement with the observed decrease in $HCOO^-$ oxidation in the presence of phosphate ions (Figure 5.21b), a strong Lewis base [139] that adsorbs on the surface of catalysts and inhibits organic sorption. In contrast, no influence of phosphate ions (mainly dihydrogen phosphate and hydrogen phosphate under the conditions in this thesis) was observed on $HCOO^-$ oxidation in the case of Cu–Al LDHs (Figure 5.21a) confirming that the oxidation of $HCOO^-$ occurs in the bulk solution for Cu–Al LDHs.

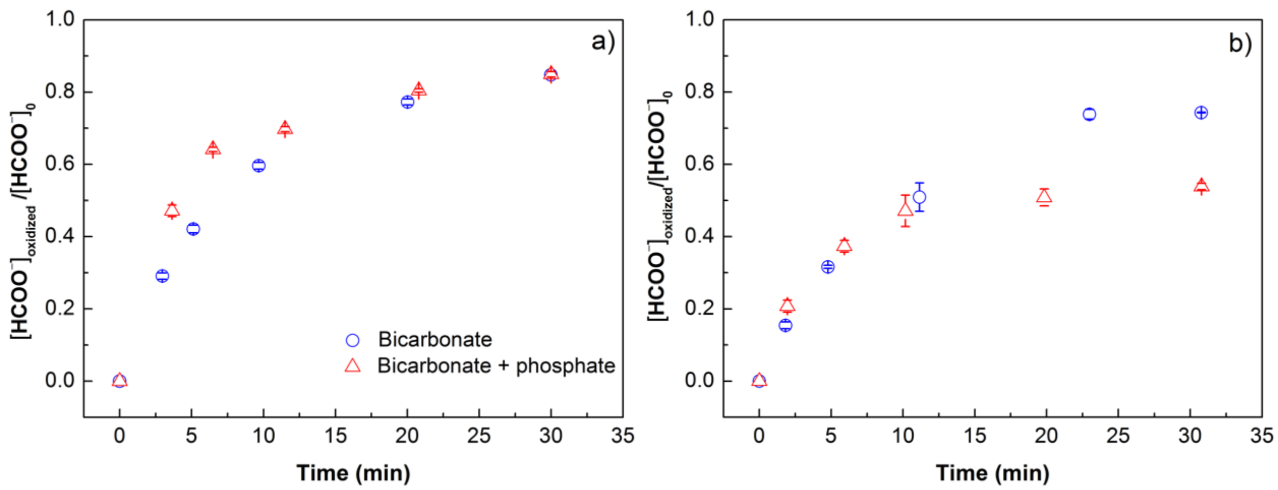

Figure 5.21 Fraction of $HCOO^-$ oxidized in the absence and presence of 1.33 mM phosphate by HCO using Cu–Al LDHs (panel a) and CuO (panel b) as the catalyst at pH 7.3. Experimental conditions: $[HCOO^-]_0$ = 1.0 µM, $[catalyst]_0$ = 0.06 g L^{-1} (in terms of CuO mass), $[O_3]_0$ = 10.0 µM, pH 7.3 using 2.0 mM $NaHCO_3$, $[phosphate]_0$ = 1.33 mM.

To provide further insight on the mechanism of catalytic ozonation, the effect of using D_2O on ozone decay and organic oxidation in the presence of catalyst was also evaluated. No significant KIE was observed in the absence of catalyst with this result in accord with findings of the study by Sein and co–workers.[200] For catalytic ozonation processes (using Cu–Al LDHs or CuO), no KIE was observed on catalyst-mediated O_3 decay and/or $HCOO^-$ oxidation (Figure 5.21a – d). However, the rate of $C_2O_4^{2-}$ oxidation was significantly lower in D_2O solution compared to that observed H_2O in the presence of both Cu-Al LDHs and CuO. The decreased $C_2O_4^{2-}$ oxidation in D_2O solution could be due to weaker ≡OD-O_3 and/or ≡OD–oxalate interaction compared to ≡$^\bullet$OH–O_3 and/or ≡$^\bullet$OH–oxalate interaction respectively. Since similar catalyst–mediated O_3 decay was observed in D_2O and H_2O solutions (Figure 5.21), it appears that the ≡OD-oxalate interaction is weaker than that of the ≡$^\bullet$OH–oxalate interaction. This hypothesis is supported by the observation that decreased $C_2O_4^{2-}$ adsorption was observed in D_2O solution compared to that observed in H_2O solution (Figure 5.21). The decreased sorption of $C_2O_4^{2-}$ on the catalyst surface in D_2O solution supports the hypothesis that surface hydroxyl groups are the active sites for $C_2O_4^{2-}$ adsorption and subsequent oxidation.

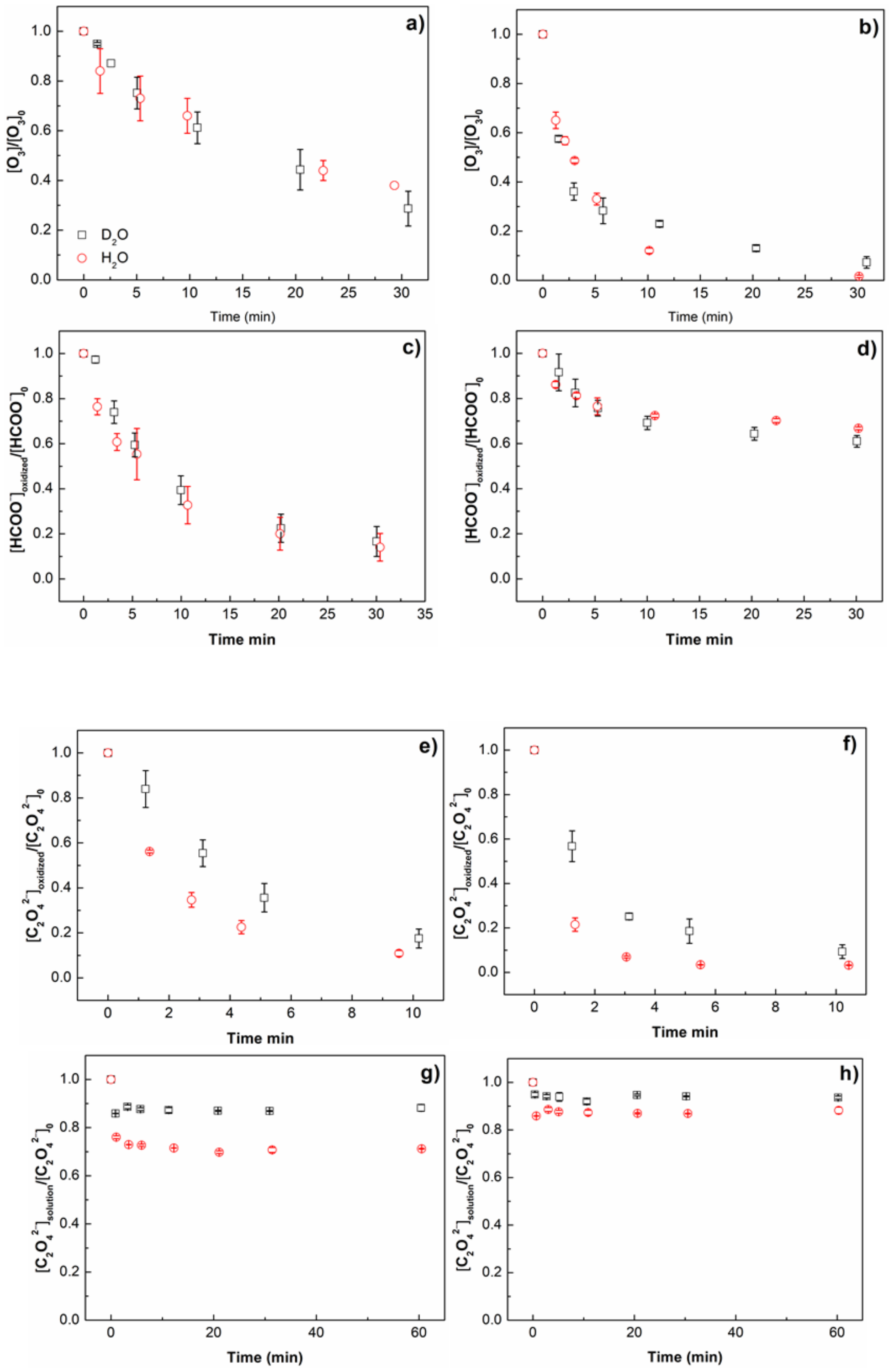

Figure 5.22 Measured O_3 decay (a &b), $HCOO^{-}$ oxidation (c&d), $C_2O_4^{2-}$(e &f) oxidation on HCO in the presence of Cu–Al LDHs (panel a, c and e) and CuO (panel b, d and f) in H_2O and D_2O solution at pH 8.5 (pD 8.8). Panels g & h represents $C_2O_4^{2-}$ adsorption by Cu–Al LDHs and CuO respectively in H_2O and D_2O solution at pH 8.5 (pD 8.8). Experimental conditions: $[\text{Catalysts}]_0$ = 0.06 g L^{-1} (in terms of CuO mass), pH 8.5 (pD 8.8) buffered by 2.0mM $NaHCO_3$. Panel a and b: $[O_3]_0$ = 100.0 μM; panel c and d: $[HCOO^{-}]_0$ = 1.0 μM, $[O_3]_0$ = 10.0 μM; panel e and f: $[C_2O_4^{2-}]_0$ = 1.0 μM, $[O_3]_0$ = 10.0 μM; panel g and h: $[C_2O_4^{2-}]_0$ = 1.0 μM.

Overall, based on the discussion presented above, we draw the following main conclusions regarding the mechanism of the catalytic ozonation process employing Cu based catalysts:

(1) Catalyst and O_3 interaction results in the formation of surface oxidants which are consumed via interaction with adsorbed organics and/or surface sites. In the case of Cu–Al LDHs, the surface oxidant was identified to be surface-located $^{\bullet}OH$.

(2) The diffusion of the surface oxidant(s) generated on O_3-catalyst interaction into the interface and/or bulk solution is negligible.

(3) Rapid binding of $C_2O_4^{2-}$ and $HCOO^-$ by the surface hydroxyl sites occurs in the presence of the catalysts however the extent of $HCOO^-$ binding is less than that observed for $C_2O_4^{2-}$.

(4) Oxidation of $C_2O_4^{2-}$ occurs on the surface of the catalysts with the Cu-oxalate surface complex readily oxidized by O_3 and $^{\bullet}OH$ (in case of Cu–Al LDHs) and O_3 and/or surface oxidants (in case of CuO).

(5) Oxidation of $HCOO^-$ mainly occurs on the surface of CuO, however, in the case of Cu–Al LDHs, oxidation of $HCOO^-$ mainly occurs in the bulk solution.

(6) Surface hydroxyl groups are the main sites for O_3 decay, organic sorption and organic oxidation. The differences in the concentration and nature of the surface hydroxyl groups between Cu–Al LDHs and CuO correlate well with the differences in the O_3 decay and organic oxidation rates observed in the presence of Cu–Al LDHs and CuO.

5.3.4.4 Kinetic modelling

Based on the reaction mechanisms proposed here, we have developed a mathematical kinetic model to describe the $HCOO^-$ and $C_2O_4^{2-}$ oxidation rates in the presence of catalysts. Table 5.1 describes the reactions for self-decay of O_3 and oxidation of $HCOO^-$ and $C_2O_4^{2-}$ by conventional ozonation. The reactions describing the self-decay of O_3 (reactions 1 – 10, Table 5.1) and $HCOO^-$ oxidation by conventional ozonation (reactions 11 – 15, Table 5.1) are same as that determined in chapter 4. The reactions controlling the oxidation of $C_2O_4^{2-}$ by conventional ozonation (reactions 16 – 20, Table 5.1) were determined based on the best fit to our experimental results on $C_2O_4^{2-}$ oxidation by conventional ozonation (Figure 5.5 and 5.6) and O_3 decay in the presence of $C_2O_4^{2-}$ (Figure 5.23). Table 5.2 describes the reactions controlling oxidation of $HCOO^-$ and $C_2O_4^{2-}$ by HCO in the presence of Cu–Al LDHs and CuO. Detailed description of these reactions is provided below.

Table 5.1 Kinetic model for ozone self-decay, formate and oxalate oxidation by conventional ozonation.

No	Reaction	Rate constant ($M^{-1}\cdot s^{-1}$)	Published value ($M^{-1}\cdot s^{-1}$)	Reference
	Ozone self decay reactions in bulk solution			
1	$O_3 + OH^- \rightarrow HO_2^\bullet + O_2^{\bullet-}$	1.0×10^2	7.0×10	151
2	$O_3 + H_2O_2/H_2O^- \rightarrow HO_3^\bullet + O_2^{\bullet-}$	1.7×10^{2a}	1.7×10^2	152
3	$O_3 + O_2^{\bullet-} \rightarrow HO_3^\bullet + O_2$	1.5×10^9	1.5×10^9	98
4	$HO_3^\bullet/O_3^{\bullet-} \rightarrow {}^\bullet OH + O_2$	1.4×10^{5b}	1.4×10^5	151
5	${}^\bullet OH + O_3 \rightarrow O_2^{\bullet-} + O_2$	1.0×10^8	1.0×10^8	151
6	$O_3 + CO_3^{\bullet-} \rightarrow H_2CO_3 + O_2$	1.0×10^5	1.0×10^5	153
	Scavenging reactions in bulk solution			
7	${}^\bullet OH + H_2O_2/H_2O^- \rightarrow H_2O + O_2^{\bullet-}$	2.7×10^{7a}	2.7×10^7	98
8	${}^\bullet OH + H_2CO_3/HCO_3^-/CO_3^{2-} \rightarrow OH^- + CO_3^{\bullet-}$	8.2×10^{6c}	8.2×10^6	141
9	$CO_3^{\bullet-} + H_2O_2/H_2O^- \rightarrow O_2^{\bullet-} + H_2CO_3$	4.3×10^{5a}	4.3×10^5	154
10	$CO_3^{\bullet-} + CO_3^{\bullet-} \rightarrow CO_4^{2-} + H_2CO_3$	2.0×10^7	2.0×10^7	155
	Formate oxidation by conventional O_3			
11	$HCOO^- + O_3 \xrightarrow{H_2O} HCO_3^- + HO_3^-$	7.0×10		140
12	$HCOO^- + O_3 \rightarrow CO_2^{\bullet-} + HO_3^\bullet$	3.0×10	$1.5\text{-}1.0\times10^{2a}$	3, 143

13	$HCOO^- + CO_3^{\bullet-} \rightarrow CO_2^{\bullet-} + HCO_3^-$	1.5×10^5	1.5×10^5	[147]
14	$HCOO^- + {}^\bullet OH \rightarrow CO_2^{\bullet-} + H_2O$	3.2×10^9	3.2×10^9	[141]
15	$CO_2^{\bullet-} + O_2 \rightarrow O_2^{\bullet-} + HCO_3^-$	4.2×10^9	4.2×10^9	[124]
	$C_2O_4^{2-}$ oxidation by conventional O_3			
16	$C_2O_4^{2-} + CO_3^{\bullet-} \rightarrow C_2O_4^{\bullet-} + HCO_3^-$	6.0×10^4	-	
17	$C_2O_4^{2-} + {}^\bullet OH \rightarrow C_2O_4^{\bullet-} + H_2O$	7.7×10^6	7.0×10^6	[141, 201]
18	$C_2O_4^{\bullet-} \rightarrow CO_2^{\bullet-} + HCO_3^-$	1.0×10^9	Rapid	

[a] calculated value at pH 7.3 using the reported rate constant for H_2O_2/HO_2^- and the mole fraction of H_2O_2/ HO_2^- at pH 7.3.

[b] calculated value at pH 7.3 using the reported rate constant for $HO_3^{\bullet-}$ / $O_3^{\bullet-}$ and the mole fraction of $HO_3^{\bullet-}$ / $O_3^{\bullet-}$ at pH 7.3.

[c] Calculated value at pH 7.3 using the reported rate constant for $H_2CO_3/HCO_3^-/CO_3^{2-}$ and the mole fraction of for $H_2CO_3/HCO_3^-/CO_3^{2-}$ at pH 7.3.

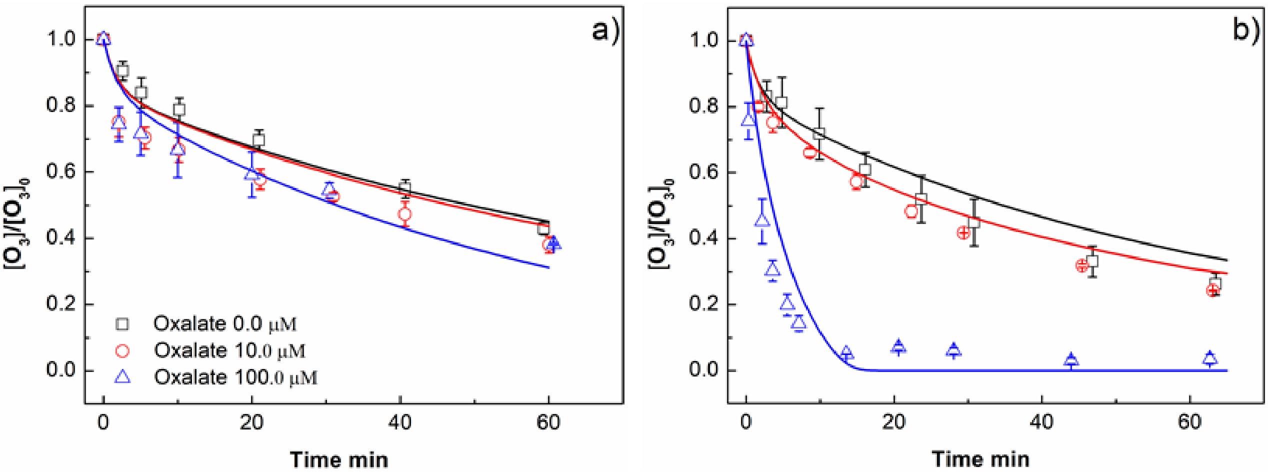

Figure 5.23 Measured O_3 decay in the presence of $C_2O_4^{2-}$ in the absence (panel a) and presence of Cu–Al LDHs (panel b) at pH 7.3. Experimental conditions: $[O_3]_0$ = 120.0 μM, $[C_2O_4^{2-}]_0$ = 0.0 – 100.0 μM, [Cu-Al LDHs]$_0$ = 0.06 g L^{-1} (in terms of CuO mass). Symbols represent experimental data, lines represent model values.

(i) O_3 adsorption by Cu–Al LDHs/CuO

Reactions 1 (Table 5.2) represent the adsorption-desorption of O_3 onto/from the Cu–Al LDHs/CuO surface. The actual values of the forward sorption of O_3 and the backward desorption of O_3 rate constants do not affect the model prediction as long as the rate of reaction 1 exceeds the self-decay rate of O_3 and the ratio of the rate constants for reactions 1 and 2 is 150 for Cu-Al LDHs and 4000 for CuO.

(ii) O_3 transformation on the Cu–Al LDHs/CuO surface

Reaction 2 (Table 5.2) represents the decay of adsorbed ozone forming surface $^{\bullet}OH$ (for Cu–AL LDHs) and another surface oxidant (for CuO). The rate constants for reaction 2 was determined based on best-fit to the measured O_3 decay in the presence of Cu–Al LDHs/CuO (Figures 5.11 and 5.23). Reaction 3 (Table 5.2) represents the decay of adsorbed O_3 via interaction with surface sites resulting in non-reactive products (NRP). Reaction 4 (Table 5.2) represents the decay of surface $^{\bullet}OH$/oxidant via interaction with the surface sites resulting in formation of NRP. The rate constant for reaction 3 and 4 was determined based on best-fit to the influence of Cu–Al LDHs/ CuO dosage on the measured oxidation of adsorbed $HCOO^{-}$ and $C_2O_4^{2-}$ (Figures 5.8 and 5.9).

(iii) Adsorption of $C_2O_4^{2-}$/ $HCOO^{-}$ on the Cu–Al LDHs/CuO surface

Reactions 5 and 6 (Table 5.2) represent the adsorption and desorption of $HCOO^{-}$ and $C_2O_4^{2-}$ on the Cu–Al LDHs/CuO surface respectively. Note that the individual values of the forward adsorption and backward desorption rate constants for reactions 5 and 6 do not affect the model prediction as long as their ratio is the same. The ratio of the rate constants for forward adsorption of organics and desorption of organics (i.e., the adsorption equilibrium constants; *K*) was determined based on best-fit to the measured adsorption of these organics in the presence of Cu–Al LDHs/CuO (Figures 5.18).

(iv) Oxidation of surface $HCOO^{-}$

Reactions 7 and 8 (Table 5.2) represent the oxidation of adsorbed $HCOO^{-}$ by surface O_3 and surface oxidant respectively. The rate constants for the oxidation of adsorbed $HCOO^{-}$ by surface O_3 and/or surface oxidants (formed on surface O_3 decay) were determined based on best–fit to the experimental results on $HCOO^{-}$ oxidation in the presence of varying organic and catalyst concentrations (Figures 5.5-5.6 and 5.8-

5.9).We have assumed that the oxidation of adsorbed $HCOO^-$ by surface O_3 to CO_2 occurs via hydride transfer with no intermediates formed with the rate constant for surface $HCOO^-$ oxidation similar to that determined for bulk O_3 - $HCOO^-$ reaction. However, we would like to highlight that the rate constant for this reaction is not well constrained by our experimental results due to minor contribution of this reaction in $HCOO^-$ oxidation in case of both Cu–Al LDHs and CuO. The oxidation of adsorbed $HCOO^-$ to CO_2 with surface $^{\bullet}OH$/surface oxidant is assumed to proceed via formation of $CO_2^{\bullet-}$ which is further oxidized by surface O_2 to yield CO_2 and $O_2^{\bullet-}$ (reaction 9, Table 5.2). The $O_2^{\bullet-}$ so formed may be consumed by the catalyst surface and/or may diffuse into the bulk solution and accelarate aqueous O_3 decay forming $^{\bullet}OH$. Since Cu is known to rapidly disproportionate $O_2^{\bullet-}$,[202] we have assumed that surface $O_2^{\bullet-}$ formed on $CO_2^{\bullet-}$ oxidation at the surface is consumed by the catalyst surface and is not involved in any reaction. However, note that a model including interaction of surface $O_2^{\bullet-}$ with surface O_3 and/or diffusion of surface $O_2^{\bullet-}$ and its interaction with aqueous O_3 produces same results.

(v) Oxidation of surface $C_2O_4^{2-}$

Reactions 10 and 11 (Table 5.2) represent the oxidation of adsorbed $C_2O_4^{2-}$ by surface O_3 and surface $^{\bullet}OH$ respectively. The rate constants for the oxidation of adsorbed $C_2O_4^{2-}$ by surface O_3 and/or surface oxidants were determined based on best-fit to the experimental results on $C_2O_4^{2-}$ oxidation in the presence of varying organic and catalyst concentrations (Figures 5.5 – 5.6 and 5.8 – 5.10) and O_3 decay in the presence of organics and catalyst (Figure 5.23).We have assumed that the oxidation of adsorbed $C_2O_4^{2-}$ to CO_2 with surface $^{\bullet}OH/O_3$ proceeds via formation of $C_2O_4^{\bullet-}$ which dissociates to form CO_2 and $CO_2^{\bullet-}$ (Reaction 12, Table 5.2). $CO_2^{\bullet-}$, as described above, is further oxidized by surface O_2 to yield CO_2 and $O_2^{\bullet-}$ (reaction 10, Table 5.2).

Table 5.2 Kinetic model for ozone decay, formate and oxalate oxidation by HCO in the presence of Cu–Al LDHs and CuO.

No	Reaction	Rate constant for Cu–Al LDHs ($M^{-1}\cdot s^{-1}$)	Rate constant for CuO ($M^{-1}\cdot s^{-1}$)
1	$O_3 + \equiv \rightleftharpoons \equiv O_3$	$K = 1.5\times10^{1a,b}$	$K = 4.0\times10^{3a,b}$
2	$\equiv O_3 \rightarrow \equiv {}^{\bullet}OH / \equiv Ox$	5.0×10^{-3}	1.0×10^{-1}
3	$\equiv O_3 + \equiv \rightarrow NRP + \equiv^{c}$	3.0	5.0×10^{2}
4	$\equiv {}^{\bullet}OH / \equiv Ox + \equiv \rightarrow NRP + \equiv^{c}$	1.0×10^{6}	5.0×10^{5}
5	$HCOO^{-} + \equiv \rightleftharpoons \equiv HCOO^{-}$	$K=3.5\times10^{2a,b}$	$K=1.0\times10^{2a,b}$
6	$C_2O_4^{2-} + \equiv \rightleftharpoons \equiv C_2O_4^{2-}$	$K=2.0\times10^{3a,b}$	$K=8.0\times10^{2a,b}$
7	$\equiv HCOO^{-} + \equiv O_3 \rightarrow CO_2 + HO_3^{-} + \equiv$	4.0×10^{1d}	4.0×10^{1}
8	$\equiv HCOO^{-} + \equiv {}^{\bullet}OH / \equiv Ox \rightarrow \equiv CO_2^{\bullet-} + \equiv$	1.0×10^{9d}	1.0×10^{9}
9	$\equiv CO_2^{\bullet-} \xrightarrow{O_2} CO_2 + \equiv O_2^{\bullet-}$	1.0×10^{9d}	1.0×10^{9}
10	$\equiv C_2O_4^{2-} + \equiv O_3 \rightarrow \equiv C_2O_4^{\bullet-} + HO_3^{-} + \equiv$	1.0×10^{6}	1.0×10^{6}
11	$\equiv C_2O_4^{2-} + \equiv {}^{\bullet}OH / \equiv Ox \rightarrow \equiv C_2O_4^{\bullet-} + \equiv$	1.0×10^{9d}	1.0×10^{9}
12	$\equiv C_2O_4^{\bullet-} \xrightarrow{O_2} CO_2 + \equiv CO_2^{\bullet-}$	1.0×10^{9}	1.0×10^{9}

[a] based on surface site concentration of 1.7 mmoles.g^{-1} CuO in Cu–Al LDHs and CuO
[b] *K* represents the ratio of the forward adsorption rate constant and back desorption rate constant
[c] NRP represents non reactive product
[d] rate constants are not well constrained by our experimental results since these reactions are not important

Note that for the oxidation of the surface oxalate complex and surface $HCOO^{-}$ complex by O_3, we have assumed that only surficial O_3 (rather than bulk O_3) is involved. A small but constant concentration of surficial O_3 is maintained via rapid adsorption/desorption of O_3 onto/from the Cu–Al LDHs/CuO surface. An alternate mechanism wherein bulk O_3 also oxidizes the surface oxalate/surface formate complex cannot explain all our experimental observations, particularly in the case of CuO. Similarly, an alternate modelling scheme in which the oxidation of the surface-complexes via interaction with both surficial O_3 and bulk O_3 cannot explain our experimental results. Detailed description of the two other modelling schemes are provided below.

(i) Modelling scheme involving oxidation of surface oxalate and surface formate complex by bulk ozone

In this modelling scheme, we use bulk O_3 as the main oxidant for surface oxalate and surface formate complexes. As shown in Table 5.3, interaction of O_3 with the catalyst results in formation of surface oxidant (reaction 1) as well as non–reactive products (reaction 2). The scavenging of surface oxidant by the catalyst (reaction 3, Table 5.3) also occurs. The rate constant for reactions 1 – 3 were determined based on best-fitting to the measured O_3 decay rates (Figure 5.11) as well as influence of catalyst dosage on the extent of $HCOO^-$ and $C_2O_4^{2-}$ oxidation (Figures 5.8 and 5.9). The adsorption of $HCOO^-$ and $C_2O_4^{2-}$ (reactions 4 and 5, Table 5.3) on the catalyst surface occur as described in the model shown in Table 5.2. However, the oxidation of surface $C_2O_4^{2-}/HCOO^-$ occcurs via interaction with bulk ozone and/or surface oxidants (reactions 6 – 11, Table 5.3). For Cu–Al LDHs, the model with bulk O_3 as the major oxidant of surface oxalate/formate complex provides excellent description of our experimental results. However, this model significantly overestimates the fraction of $HCOO^-$ oxidized in the presence of varying CuO dosage (Figure 5.24). Since in this model, both generation and scavenging of oxidant by CuO increases with CuO dosage, there is no significant influence of CuO dosage on the oxidation of organics. An alternative scheme wherein the generation of surface oxidant occurs via formation of an intermediate on CuO–O_3 interaction, which subsequently decays to form surface oxidant and/or is consumed by the catalyst (Table 5.4), was also used to model our experimental results. In this scheme, the rate of oxidant generation decreases with increase in the catalyst dosage and can explain the decrease in the extent of $HCOO^-$ oxidation with the increase in the catalyst dosage however this also results in the decrease in the $C_2O_4^{2-}$ oxidation which is not in agreement with our observed results

(Figure 5.8). Overall, the kinetic model where bulk O_3 was able to oxidize the surface oxalate and formate complexes was not able to correctly predict the influence of CuO dosage on the extent of $HCOO^{-}$ and $C_2O_4^{2-}$ oxidation (Figure 5.24).

Table 5.3 Kinetic model for ozone decay, formate and oxalate oxidation by HCO in the presence of Cu–Al LDHs and CuO— bulk O_3 as the main oxidant.

No	Reaction	Rate constant for Cu–Al LDHs ($M^{-1}\cdot s^{-1}$)	Rate constant for CuO ($M^{-1}\cdot s^{-1}$)
1	$O_3 + \equiv \rightarrow \equiv {}^{\bullet}OH / \equiv Ox$	0.1[a]	2.5×10^{1}[a]
2	$O_3 + \equiv \rightarrow NRP + \equiv$	0.3[a]	3.0[a]
3	$\equiv {}^{\bullet}OH / \equiv Ox + \equiv \rightarrow NRP + \equiv$	1.0×10^{5}	4.0×10^{3}
4	$HCOO^{-} + \equiv \rightleftharpoons \equiv HCOO^{-}$	$K=3.5\times10^{2}$[a,b]	$K=1.0\times10^{2}$[a,b]
5	$C_2O_4^{2-} + \equiv \rightleftharpoons \equiv C_2O_4^{2-}$	$K=2.0\times10^{3}$[a,b]	$K=8.0\times10^{2}$[a,b]
6	$\equiv HCOO^{-} + \equiv O_3 \rightarrow CO_2 + HO_3^{-} + \equiv$	4.0×10[d]	4.0×10
7	$\equiv HCOO^{-} + \equiv {}^{\bullet}OH / \equiv Ox \rightarrow \equiv CO_2^{\bullet-} + \equiv$	1.0×10^{9}[d]	1.0×10^{9}
8	$\equiv CO_2^{\bullet-} \xrightarrow{O_2} CO_2 + \equiv O_2^{\bullet-}$	1.0×10^{9}[d]	1.0×10^{9}
9	$\equiv C_2O_4^{2-} + \equiv O_3 \rightarrow \equiv C_2O_4^{\bullet-} + HO_3^{-} + \equiv$	4.0×10^{3}	4.0×10^{3}
10	$\equiv C_2O_4^{2-} + \equiv {}^{\bullet}OH / \equiv Ox \rightarrow \equiv C_2O_4^{\bullet-} + \equiv$	1.0×10^{9}	1.0×10^{9}
11	$\equiv C_2O_4^{\bullet-} \xrightarrow{O_2} CO_2 + \equiv CO_2^{\bullet-}$	1.0×10^{9}	1.0×10^{9}

[a] based on surface site concentration of 1.7 mmoles.g^{-1} CuO in Cu–Al LDHs and CuO
[b] *K* represents the ratio of the forward adsorption rate constant and back desorption rate constant
[c] NRP represents non reactive product
[d] rate constants are not well constrained by our experimental results

Table 5.4 Kinetic model for ozone decay, formate and oxalate oxidation by HCO in the presence of CuO assuming bulk O_3 as the main oxidant and O_3 decay on the surface occuring via formation of surface intermediates.

No	Reaction	Rate constant ($M^{-1}\cdot s^{-1}$)
1	$O_3 + \equiv \rightarrow Int$	2.3×10^{1a}
2	$\equiv + Int \rightarrow O_2 + \equiv + \equiv$	8.0×10^{7}
3	$Int \rightarrow \equiv {}^{\bullet}OH / \equiv Ox$	8.0×10^{3}
4	$\equiv Ox + \equiv \rightarrow NRP + \equiv$	4.0×10^{5}
5	$HCOO^{-} + \equiv \rightleftharpoons \equiv HCOO^{-}$	$K=1.0\times10^{2a,b}$
6	$C_2O_4^{2-} + \equiv \rightleftharpoons \equiv C_2O_4^{2-}$	$K=8.0\times10^{2a,b}$
7	$\equiv HCOO^{-} + \equiv O_3 \rightarrow CO_2 + HO_3^{-} + \equiv$	4.0×10
8	$\equiv HCOO^{-} + \equiv {}^{\bullet}OH / \equiv Ox \rightarrow \equiv CO_2^{\bullet-} + \equiv$	1.0×10^{9}
9	$\equiv CO_2^{\bullet-} \xrightarrow{O_2} CO_2 + \equiv O_2^{\bullet-}$	1.0×10^{9}
10	$\equiv C_2O_4^{2-} + \equiv O_3 \rightarrow \equiv C_2O_4^{\bullet-} + HO_3^{-} + \equiv$	4.0×10^{3}
11	$\equiv C_2O_4^{2-} + \equiv {}^{\bullet}OH / \equiv Ox \rightarrow \equiv C_2O_4^{\bullet-} + \equiv$	1.0×10^{9}
12	$\equiv C_2O_4^{\bullet-} \xrightarrow{O_2} CO_2 + \equiv CO_2^{\bullet-}$	1.0×10^{9}

[a] based on surface site concentration of 1.7 mmoles.g^{-1} CuO in Cu–Al LDHs and CuO

[b] *K* represents the ratio of the forward adsorption rate constant and back desorption rate constant

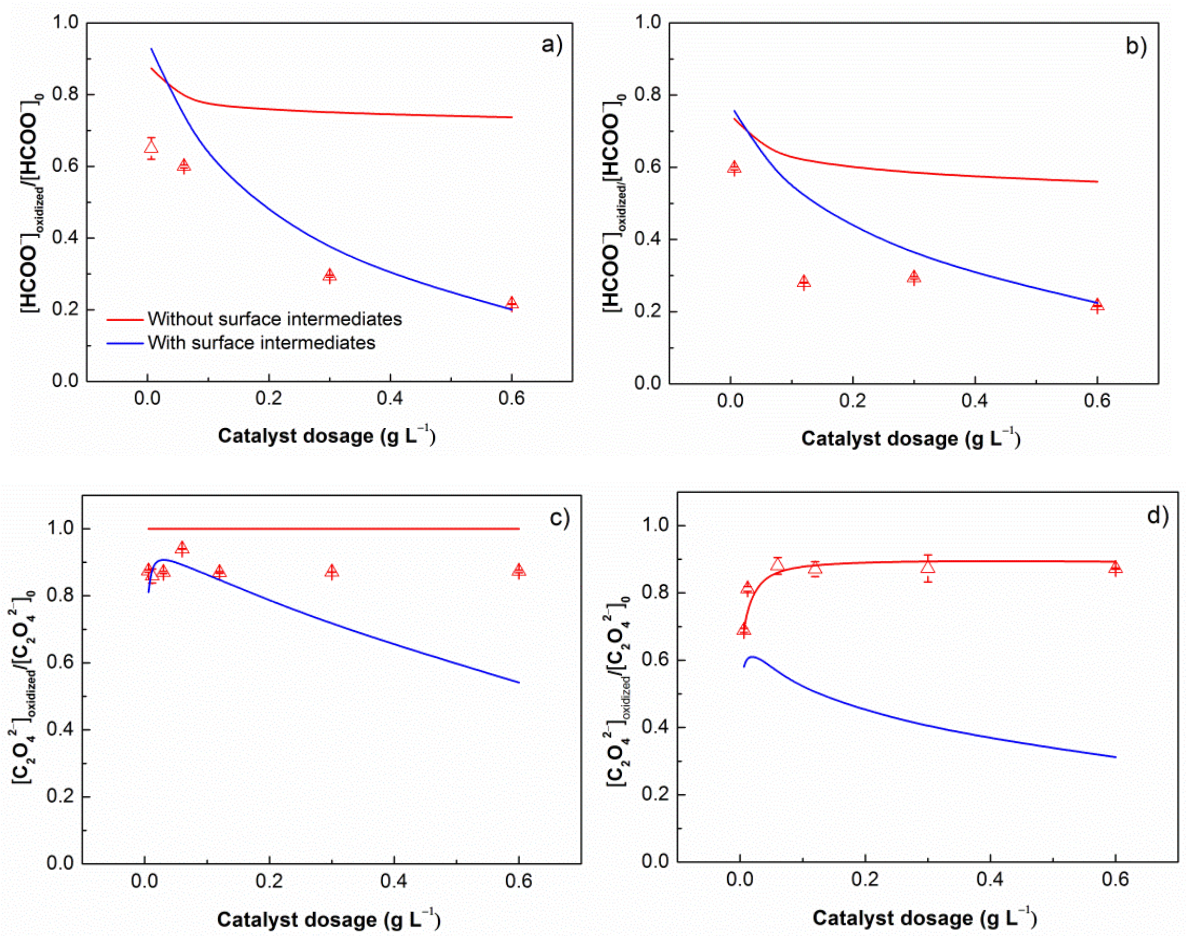

Figure 5.24 Fraction of $HCOO^{-}$ (panel a and b) and $C_2O_4^{2-}$ (panel c and d) oxidized in the presence of CuO (triangles) at varying catalyst dosage. Experimental conditions: $[catalyst]_0$ = 0.006 – 0.6 g L^{-1} (in terms of CuO mass), $[HCOO^{-}]$ = 1.0 (panel a) or 10.0 μM (panel b), $[C_2O_4^{2-}]_0$ = 1.0 (panel c) or 10.0 (panel d) and $[O_3]_0$ = 10.0 μM, pH 7.3 using 2.0 mM $NaHCO_3$, reaction time 2 h. Symbols represent experimental data and the lines represent model values.

(ii) Modelling scheme with no involvement of surficial ozone in oxalate oxidation

In this modelling scheme, the oxidation of surface formate/oxalate complex by surface O_3 (reaction 7 and 10 in Table 5.2) was neglected. From Figure 5.25, the modelled $C_2O_4^{2-}$ without contribution of surface O_3 significantly underestimated $C_2O_4^{2-}$ oxidation in the presence of both Cu–Al LDHs and CuO. The oxidation of surface $C_2O_4^{2-}$ complexes by surface O_3 is needed to explain the experimental results obtained.

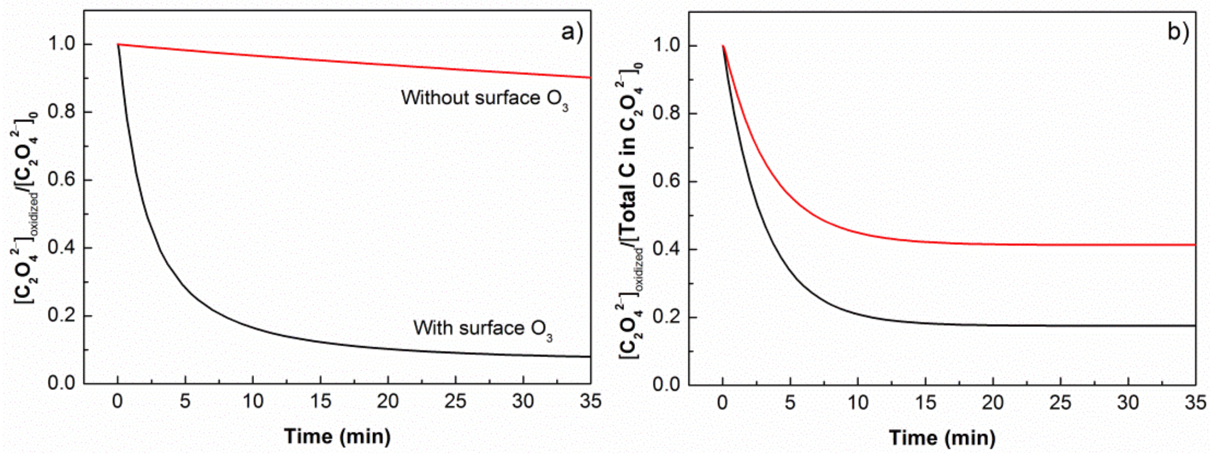

Figure 5.25 Modelled oxidation of $C_2O_4^{2-}$ in the presence of Cu–Al LDHs (panel a) and CuO (panel b). Experimental conditions: $[\text{catalyst}]_0 = 0.06$ g L^{-1} (in terms of CuO mass), $[O_3] = 10.0$ µM $[C_2O_4^{2-}]_0 = 10.0$ µM, pH 7.3 using 2.0 mM $NaHCO_3$.

As shown in Figures 5.5 – 5.6, 5.8 – 5.11 and 5.18, the model presented in Table 5.1 and 5.2 provides reasonable description ($R^2 > 0.9$) of $C_2O_4^{2-}$ and $HCOO^-$ oxidation as well as O_3 decay in the presence of Cu–Al LDHs and CuO. While there is some discrepancy between the experimental results and model-predicted data, the model describes the general trend of the experimental data very well. The sensitivity analysis of the model (Table 5.5) using PCA shows that all the surface reactions shown in Table 5.2 are important for correctly predicting the time varying $C_2O_4^{2-}$, $HCOO^-$ and O_3 concentrations in the presence of CuO. However, in the case of Cu–Al LDHs, reactions controlling surface oxidation of $HCOO^-$ are not important. The model predicted rate constants for oxidation of surface oxalate complexes by surficial O_3 is similar for CuO and Cu–Al LDHs (Table 5.2) suggesting that similar types of complexes were formed in the presence of these catalysts.

Table 5.5 Principal Component Analysis of model reactions controlling O_3 decay and $HCOO^-$/ $C_2O_4^{2-}$ oxidation during HCO using CuO/Cu–Al LDHs at pH 7.3[a].

Oxalate oxidation in the presence of CuO	
Eigenvalue	Dominant reactions in principal components (relative contribution of the component to system response is shown in parentheses)
3.9×10^{10}	1(1.0)
6.3×10^{4}	-6(0.31), 6(-0.28), 3(0.25)
1.7×10^{4}	-6(0.31), 3(0.24)
8.9×10^{2}	-6(0.30), 6(-0.25)
4.8×10^{2}	-6(-0.32), 6(0.24)
2.4×10^{2}	10(-0.62), 2(0.51), 3(-0.39), 6(0.38), -6(0.22), 4(-0.22)
Reactions 6,7 and 19 (Table 5.1) have no impact on the model results.	
Formate oxidation in the presence of CuO	
Eigenvalue	Dominant reactions in principal components (relative contribution of the component to system response is shown in parentheses)
4.1×10^{6}	1(1.0)
1.2×10^{6}	
8.0×10^{3}	3(-0.57), 5(0.48), -5(0.47), 4(-0.43), 8(0.41), 1(-0.37)
3.0×10^{3}	2(1.0), 4(-0.63)
4.4×10^{2}	5(-0.44), -5(-0.42), 8(0.25)
3.3×10^{2}	5(-0.44), -5(-0.43), 7(0.33)
Reactions 6 and 7 (Table 5.1) have no impact on the model results.	
Oxalate oxidation in the presence of Cu–Al LDHs	
Eigenvalue	Dominant reactions in principal components (relative contribution of the component to system response is shown in parentheses)
7.1×10^{4}	10(0.94), -6(-0.75), 6(0.71), 1(-0.66), -1(-0.63)
1.5×10^{3}	1(-0.22), 2(0.21)
6.2×10^{2}	2(-0.81), 1(0.76), -1(0.72), 6(0.43), -6(0.39), 4(0.23), 10(-0.21)
3.5×10^{2}	
2.1×10^{2}	12(0.61), 10(0.50), 11(-0.48), -6(0.44), 6(-0.42), 2(0.42)
1.1×10^{2}	12(-0.23)
Reactions 6 and 7 (Table 5.1) have no impact on the model results.	

[a] Only the highest Eigenvalues are shown here and only the relative contribution of the surface reactions (shown in Table 1 in the main manuscript) are shown here.

[b] Eigenvalues of formate oxidation in the presence the Cu–Al LDHs are not shown here since formate oxidation predominantly occurs in the bulk solution (see detailed discussion in section 5.3.4.3 in the main manuscript).

We have used the model to predict the contribution of bulk as well as surface reactions in the oxidation of $C_2O_4^{2-}$ in the presence of Cu–Al LDHs and CuO (Figure 5.26). As shown in Figure 5.26a and 5.26c, $C_2O_4^{2-}$ oxidation predominantly occurs on the surface of Cu–Al LDHs/CuO with some contribution from bulk oxidation at very low catalyst dosages and higher $C_2O_4^{2-}$ concentrations. Furthermore, as shown in Figure 5.26b, only O_3 is involved in $C_2O_4^{2-}$ oxidation in the case of Cu–Al LDHs. For CuO, the radical-mediated process is important at lower $C_2O_4^{2-}$ and catalyst concentrations (Figure 5.26d). Since most of the oxidation occurs on the CuO surface under these conditions (Figure 5.26c), these results suggest that surface radicals formed on O_3 decay play an important role under these conditions. However, for higher $C_2O_4^{2-}$ and higher catalyst concentrations, surficial O_3 is the dominant oxidant.

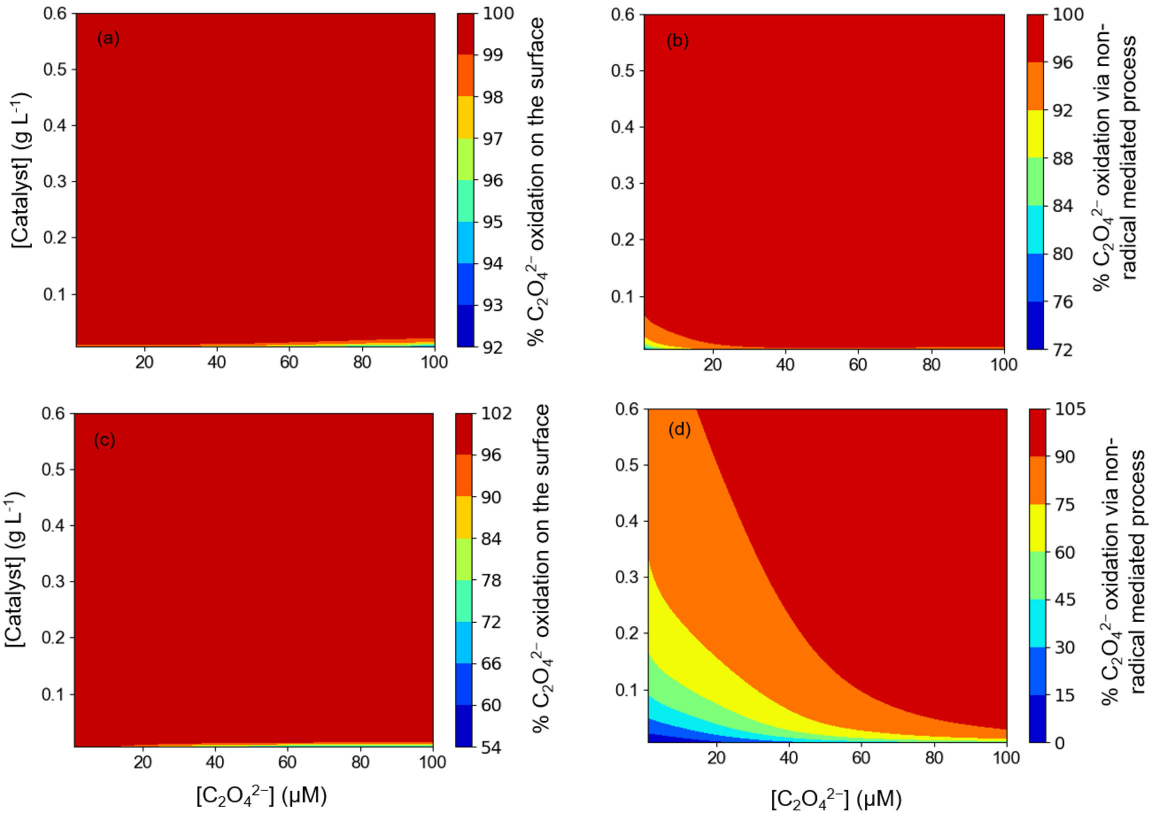

Figure 5.26 Model-predicted % $C_2O_4^{2-}$ oxidation occurring on the surface in the presence of Cu–Al LDHs (a) and CuO (c). Panels (b) and (d) show % $C_2O_4^{2-}$ oxidation occurring via direct reaction with O_3 (including both surface and bulk) in the presence of Cu–Al LDHs and CuO respectively. $[O_3]_0$ = 100.0 µM was used for these predictions.

The contributions of surface reactions as well as the non-radical mediated process in $HCOO^-$ oxidation are shown in Figure 5.27. As shown in Figure 5.27a and 6b, $HCOO^-$ oxidation in the presence of Cu–Al LDHs predominantly occurs in bulk solution via a radical-mediated process, except at low $HCOO^-$ concentration. In the case of CuO, $HCOO^-$ oxidation principally occurs via a radical mediated process in the presence of CuO. At a lower $HCOO^-$ concentration, oxidation occurs principally via interaction with the surface oxidant(s) while at higher $HCOO^-$ concentration, oxidation occurs in the bulk solution via reaction with bulk $^{\bullet}OH$ as well as $CO_3^{\bullet-}$ formed as a result of $^{\bullet}OH$ scavenging by carbonate ions. The variation in the contributions of radical and non-radical mediated processes with the nature and concentration of target organic as well as the catalyst dosage may contribute to the discrepancies in the mechanisms of the

HCO process reported in various earlier studies.[25, 26, 169, 203] The significant variability in controlling processes as a function of reaction conditions is particularly evident for degradation of $HCOO^-$ in the presence of CuO where surface reaction control is evident at higher catalyst loadings and low $HCOO^-$ concentrations while degradation reactions in solution dominate at higher $HCOO^-$ concentrations.

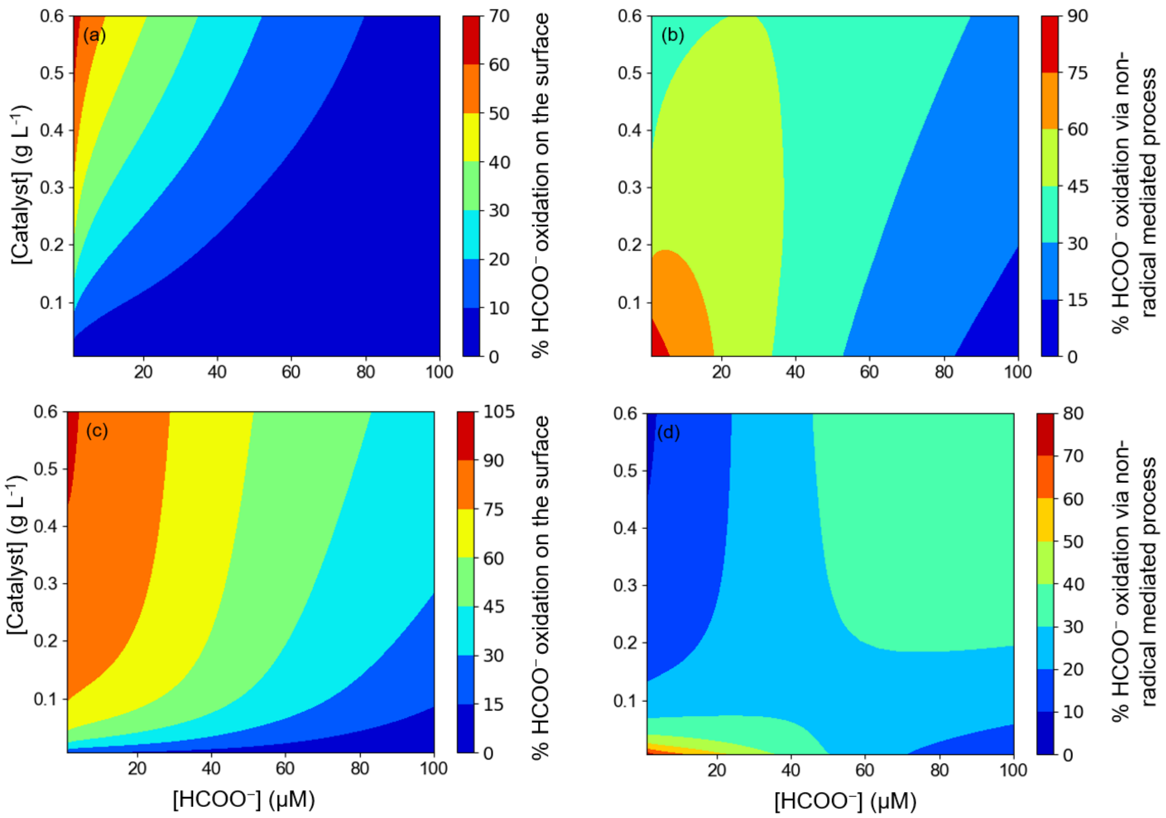

Figure 5.27 Model-predicted % $HCOO^-$ oxidation occurring on the surface in the presence of Cu–Al LDHs (a) and CuO (c). Panels (b) and (d) show % $HCOO^-$ oxidation occurring via direct reaction with O_3 (including both surface and bulk) in the presence of Cu–Al LDHs and CuO respectively. $[O_3]_0 = 100.0$ µM was used for these predictions.

While probe methods employing compounds such as *p*–CBA and TBA can be used to investigate the generation of radicals and the rate and extent of organics oxidation for conventional ozonation,[89, 204-206] quantitative analysis of surface–related reactions with any probe compound is challenging due to the varying surface affinity of probes towards different catalysts and the difficulty in quantifying the extent of oxidation of probe compounds located on the catalyst surface. Hence, for HCO, where surface-mediated processes dominate, we are of the opinion that the kinetic modelling approach used here will be of value in providing mechanistic insight, though more careful validation of these kinetic models is needed prior to their application to complex real wastewater matrices. The kinetic model developed in this study can be easily extended to other catalysts though will require determination of particular rate constants appropriate to the catalyst being used.

5.4. Conclusions

Our results show that Cu based materials function as efficient catalysts for HCO, particularly for ozone resistant compounds such as $C_2O_4^{2-}$. The catalytic activity of Cu-Al LDHs is mostly attributed to the layered structure of the material that facilitates adsorption of organics as well as generation of surface $^{\bullet}OH$ on O_3 decay. As such, it is expected that target organic compounds with high surface affinity will be degraded by this catalyst. While Cu–Al LDHs also result in removal of $HCOO^-$, the enhancement in ozone usage efficiency is not as significant as observed in the case of $C_2O_4^{2-}$ since $HCOO^-$ can be easily oxidized by O_3. Thus, we suggest that the design of the ozonation process should be modified according to the nature of the organic compounds present in the water to be treated. The organic compounds can also be classified based on their reactivity towards O_3. For organic compounds that can be readily oxidized by O_3, a homogeneous ozonation process is expected to be more cost-effective than a catalytic ozonation process. In contrast, a catalytic ozonation process is required for oxidation of organic compounds that are refractory to direct ozone oxidation. In general, a multi–stage ozone process employing a separate homogeneous ozone reactor followed by a catalytic ozone process is recommended for efficient usage of ozone and catalyst for treatment of wastewaters containing complex organic mixtures.

Overall, this chapter provides important insights into HCO employing Cu based catalysts under circumneutral pH conditions. Further work on the influence of the physicochemical properties of Cu–Al LDHs and CuO needs to be performed to correlate the physiochemical properties with the catalyst performance and to optimize the catalyst synthesis. While these catalysts work well for enhancing oxidation of simple carboxylic acids in a simple matrix, the influence of pH as well as various matrix constituents (such as dissolved organic matter and anions) on the efficacy of HCO and the oxidation of a range of other ozone-resistant compounds requires further investigation.

Chapter 6 Comparison of performance of conventional ozonation and heterogeneous catalytic ozonation processes in phosphate and carbonate buffered solutions

Some of the material in this Chapter has been drawn from a recent publication,[207] which has been acknowledged and detailed in the 'inclusion of publications statement' for this thesis.

6.1. Introduction

The degradation of organic compounds during ozonation and heterogenous catalytic ozonation mostly occurs as a result of interaction with O_3 and/or other oxidants (particularly hydroxyl radicals, $^{\bullet}OH$) generated on O_3 decay.[89, 116, 182, 197, 208] The overall process efficiency is highly dependent on pH due to the influence of pH on O_3 self–decay kinetics, surface charge of the catalyst and organic speciation.[8, 26, 34, 36, 37, 47, 87, 209, 210] Research on the ozonation and HCO processes is commonly performed under circumneutral pH conditions (i.e., pH 6.5 – 8.5) with the pH controlled using phosphate and/or carbonate buffered solution.[11, 14, 20, 211-214] While carbonate, the major buffer in natural waters and many wastewaters,[211, 215, 216] is recognised to stabilize O_3 by scavenging $^{\bullet}OH$ and inhibiting radical chain reactions,[170, 217] there are contradictory reports on the influence of phosphate ions on O_3 decay.[131, 218-220] Some studies suggested that the addition of phosphate also decreased the rate of O_3 decay by scavenging $^{\bullet}OH$ and inhibiting radical chain reactions in a manner similar to carbonate [220] while others observed promotion of O_3 decay.[131, 218, 219] Use of phosphate buffers may also have a significant impact on the surface chemistry of catalysts and efficacy of

HCO in organic removal since phosphate is a strong Lewis base that adsorbs on the surface of catalysts thereby inhibiting catalyst–O_3 interaction [121, 139, 221] and/or organic sorption on the catalyst surface.[52, 139, 195, 222-224] Most studies report decrease in organic oxidation during HCO in the presence of phosphate ions due to inhibition of interaction of O_3 and/or organics with the catalyst as a result of phosphate sorption on surface hydroxyl sites,[39, 49, 51, 188, 225-228] some contrasting results are also reported that phosphate did not hamper organic oxidation in HCO.[35, 121] In addition, contradictory results have been reported on the impact of carbonate ions on organic oxidation by HCO with carbonate stabilizing O_3 to promote oxalate oxidation [25] while scavenging bulk $^{\bullet}OH$ to inhibit *p*-nitrophenol removal.[51]

Based on the discussion above, there appears to be contradictory reports on the influence of buffering ions on the performance of the ozonation and HCO processes. Furthermore, due to the difference between the reactivity of buffering ions towards $^{\bullet}OH$ and their affinity towards the catalyst surface, the performance of the ozonation and HCO processes may vary depending on the nature of the buffer employed. While earlier studies have investigated the influence of the solution matrix on the oxidation of organics during HCO,[25, 35, 39, 169] to our knowledge, no systematic evaluation of the influence of choice of buffer on O_3 decay or on the efficacy of degradation of organic target compounds has been performed. Thus, in this chapter, we compare the influence of two buffer solutions, phosphate and carbonate, on O_3 decay (including self–decay and catalyst mediated O_3 decay), $^{\bullet}OH$ generation and associated oxidation of selected organic compounds during the ozonation and HCO processes. The oxidation of three different organics, namely oxalate (OA), formate (FA) and *p*–CBA was measured. We chose OA and FA as the target compounds since these organic compounds have well defined oxidation pathways and result in formation of CO_2 and H_2O as the only products.[123] *p*–CBA was used to probe the extent of bulk $^{\bullet}OH$ generation [87, 182] in phosphate and carbonate buffered solutions. To investigate the influence of buffers on the HCO process, Cu–Al LDHs and CuO were used as the catalysts. The catalytic mechanism of these catalysts in carbonate buffered solution was described in chapter 5. Based on the experimental results obtained here, we provide important mechanistic insights into the role of buffers on O_3 decay and associated oxidation of these organic compounds. We have also developed a mathematical model to accurately predict the O_3 decay and OA/FA removal in phosphate and bicarbonate buffered solutions.

6.2. Material and Methods

6.2.1 Reagents

All experiments were performed at pH 7.3 or 8.5 using carbonate, phosphate and/or borate buffered solution. The concentration of carbonate and phosphate buffers were 1.3 mM and 2.0 mM at pH 7.3 and 8.5, respectively. For borate buffer, a concentration of 5.0 mM was used for pH 7.3 and 8.5 experiments. The initial pH was adjusted using 1.0 M HNO_3 and 1.0 M sodium hydroxide (NaOH) if required. The carbonate buffered solution at pH 7.3 was prepared as described in chapter 3. To avoid atmospheric CO_2 dissolution in phosphate buffer, phosphate buffered solutions were prepared in CO_2–free Milli–Q water by sparging Milli–Q water with N_2 for 2 h prior to addition of phosphate salts. A maximum pH variation of ± 0.2 units was allowed during experiments. Stock solutions of radiolabelled and non–radiolabelled sodium formate/oxalate, indigo, *p*–CBA, TBA and O_3 stock solution were prepared as described in chapter 3. Cu–Al LDHs and CuO were prepared as reported in chapter 5.

6.2.2. Experimental setup for O_3 decay

O_3 decay experiments were conducted in sealed reactors shown in chapter 3. For measurement of O_3 decay, 100.0 µM of dissolved O_3 was added into the phosphate or carbonate buffered solutions containing 0 - 0.6 $g.L^{-1}$ of catalyst (in terms of CuO mass concentration). Subsequently, samples were taken at designated time intervals and the dissolved O_3 concentration was measured using the indigo method.[107] Since the pH of the indigo solution used for O_3 measurement is strongly acidic (pH < 2), it dissolves any catalyst present in the samples. Hence, the concentration of O_3 measured in the presence of catalyst represents the sum of O_3 in the bulk solution and O_3 sorbed on the catalyst surface. We also measured dissolved O_3 concentration wherein samples were filtered using 0.22 µm PVDF filters (Millipore) prior to indigo addition. The measured O_3 concentrations were similar in filtered and non–filtered samples indicating that the concentration of O_3 sorbed onto the catalyst surface was minimal.

6.2.3 Experimental setup for organic oxidation

Measurement of oxidation of FA, OA and *p*–CBA was conducted in a sealed reactor as shown in chapter 3. For catalytic ozonation, the dosage of the catalyst was 0.06 gL^{-1} (in terms of CuO mass concentration). Note that for measurement during catalytic ozonation, since rapid dissolution of the catalysts occurred during acidification of samples, the FA/OA concentration measured represents the total non–oxidized FA/OA concentration including FA/OA concentration remaining in the bulk solution and FA/OA concentration sorbed onto the surface of the catalyst.

p–CBA oxidation experiments were conducted for ozonation only since *p*–CBA does not sorb onto the catalysts surface and hence was not effective in trapping surface associated $^{\bullet}OH$. For measurement, 1.0 µM *p*–CBA and 10.0 µM O_3 were added into the carbonate or phosphate buffered solutions and samples were taken at regular time intervals. Subsequently, samples were sparged with N_2 to remove any residual O_3 present and cease the reaction. The concentration of *p*–CBA remaining was quantified using HPLC as described in chapter 3.

We also measured the R_{ct} value (which is ratio of the $^{\bullet}OH$ exposure to O_3 exposure) during the ozonation process in carbonate and phosphate buffered solutions.[89, 90] To minimize the influence of *p*–CBA on O_3 decay, these measurements were performed at a lower *p*–CBA: O_3 concentration ratio. For R_{ct} measurement, 1.0 µM *p*–CBA and 100.0 µM O_3 were added into the carbonate or phosphate buffered solution and samples were taken over time for measurement of dissolved O_3 concentration and *p*–CBA concentration using the methods described above. As described earlier,[89, 90] the R_{ct} value was calculated using eq. 6.1

$$\mathrm{Rct} = \frac{\int [\,^{\bullet}\mathrm{OH}]\mathrm{dt}}{\int [\mathrm{O_3}]\mathrm{dt}} = \frac{\ln\left(\frac{[p-\mathrm{CBA}]_\mathrm{t}}{[p-\mathrm{CBA}]_0}\right)}{k_{\,^{\bullet}\mathrm{OH},p-\mathrm{CBA}} \int [\mathrm{O_3}]\mathrm{dt}} \tag{6.1}$$

6.2.4 Kinetic modelling

Kinetic modelling of our experimental results was performed using the software package Kintecus [110] as described in detail in chapter 3.

6.3 Results and Discussion

6.3.1 Influence of buffering ions on pure ozonation performance

6.3.1.1. Ozone self-decay and associated $^{\bullet}$OH generation

Figure 6.1 demonstrates that ozone self-decay is substantially more rapid in the phosphate buffered solution at pH 7.3. As reported in various earlier studies [7, 22, 136, 137] and also explained in detail in chapter 4, ozone self–decay kinetics can be described by the reactions shown in eqs. 6.2 – 6.5. In the absence of any $^{\bullet}OH$ scavengers, $^{\bullet}OH$ formed reacts with O_3 forming superoxide ($O_2^{\bullet-}$, eq. 6.4) which further propagates O_3 decay. However, in the presence of $^{\bullet}OH$ scavengers such as carbonate and/or phosphate ions (eqs. 6.6 – 6.7,[141, 145, 218, 229, 230] the generation of $O_2^{\bullet-}$ (the key chain carrier) via O_3–$^{\bullet}OH$ reaction is inhibited, thereby stabilizing O_3. Since O_3 decay is slower in the carbonate buffered system than in the phosphate buffered system, it appears that the rate and extent of scavenging of $^{\bullet}OH$ by HCO_3^-/ CO_3^{2-} is higher than the $^{\bullet}OH$ scavenging by phosphate ions. This agrees with the reported rate constant for $^{\bullet}OH$ reaction with HCO_3^-/CO_3^{2-} (8.5×10^6 and 3.9×10^8 $M^{-1}\cdot s^{-1}$;[137, 141]) and $^{\bullet}OH$ scavenging by phosphate ions ($2\times10^4 – 1.5\times10^5$ $M^{-1}\cdot s^{-1}$; [137, 141]).

$$O_3 + OH^- \rightarrow HO_2^{\bullet} + O_2^{\bullet-} \tag{6.2}$$

$$O_3 + O_2^{\bullet-} \rightarrow HO_3^{\bullet} + O_2 \tag{6.3}$$

$$HO_3^{\bullet} \rightarrow HO^{\bullet} + O_2 \tag{6.4}$$

$$^{\bullet}OH + O_3 \rightarrow O_2^{\bullet-} + O_2 \tag{6.5}$$

$$^{\bullet}OH + HCO_3^- \rightarrow CO_3^{\bullet-} + H_2O \tag{6.6}$$

$$^{\bullet}OH + HPO_4^{2-} \rightarrow PO_4^{\bullet-} + H_2O \tag{6.7}$$

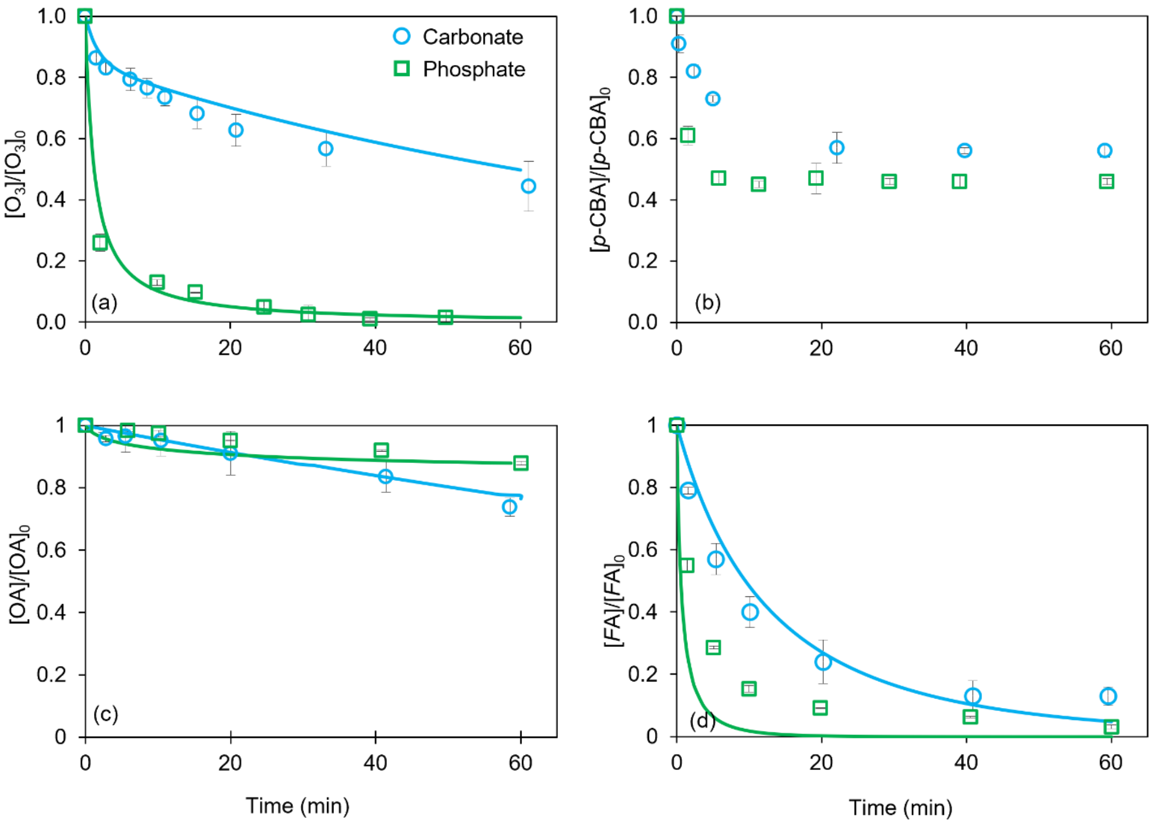

Figure 6.1 (a) Measured O_3 ($[O_3]_0$ = 100.0 µM) self-decay kinetics at pH 7.3 buffered using phosphate (squares) and carbonate (circles) solution. Panels b, c and d represent the measured oxidation of *p*–CBA, OA and FA respectively on ozonation at pH 7.3 with pH buffered using phosphate (squares) and carbonate (circles) solution. Symbols represent measured values; lines represent model results. Experimental conditions for OA/ FA oxidation: $[O_3]_0$ = 10.0 µM; $[OA]_0$ /[$FA]_0$ /[*p*–$CBA]_0$=1.0 µM.

Addition of TBA (a bulk $^{\bullet}OH$ scavenger [29, 231]) had no influence on O_3 decay in carbonate buffered solution confirming that all $^{\bullet}OH$ radicals formed on O_3 self-decay are scavenged by HCO_3^-/CO_3^{2-} (Figure 6.2). In contrast, inhibition of O_3 decay is observed in the presence of TBA in phosphate buffered solution (Figure 6.2), suggesting that a significant fraction of $^{\bullet}OH$ interacts with O_3 in this system, propagating O_3 decay via radical chain reactions (eqs. 6.2 – 6.5). Decrease in the ozone decay rate with increase in the phosphate buffer concentration (Figure 6.3) also supports the conclusion that significant scavenging of $^{\bullet}OH$ by O_3 occurs in the phosphate buffered solution, at least at the lower phosphate concentration employed here. Increase in phosphate concentration increases the scavenging of $^{\bullet}OH$ by phosphate ions, thereby preventing the O_3 – $^{\bullet}OH$ reaction and stabilizing O_3. This is in line with the results reported in various earlier studies which also showed that increase in phosphate concentration inhibited O_3 decay.[220, 232] Note that the O_3 decay rate in phosphate buffered and borate buffered solutions at pH 7.3 is similar (Figure 6.4) confirming that the rate of $^{\bullet}OH$ scavenging by both these buffering ions is comparable, at least under circumneutral pH conditions.

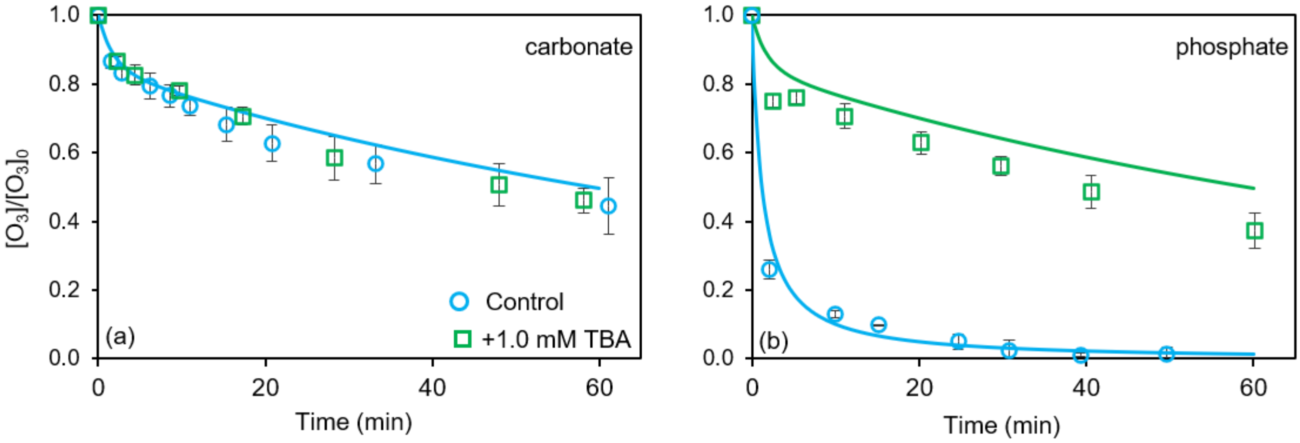

Figure 6.2 Measured O_3 decay rate in the absence (circles) and presence(squares) of 1.0 mM TBA at pH 7.3 buffered using 1.3 mM carbonate (panel a) or 1.3 mM phosphate (panel b) solution.

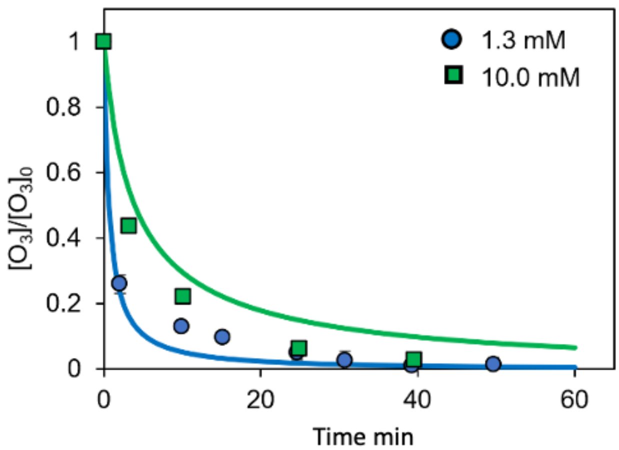

Figure 6.3 Measured O_3 decay rate in pH 7.3 buffered solution using 1.3 mM phosphate (circles) and 10.0 mM (squares) phosphate. Symbols represent average experimental data; lines represent model results.

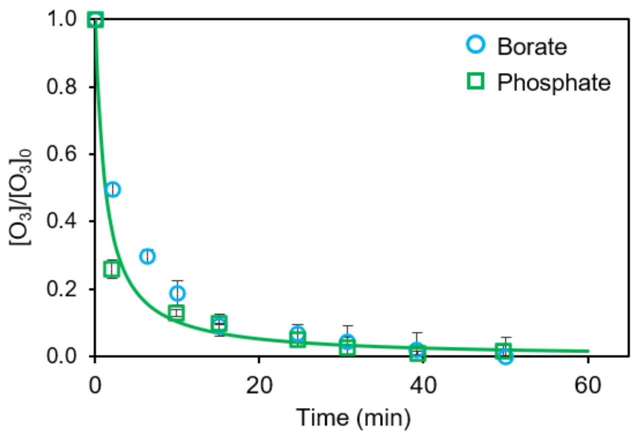

Figure 6.4 Measured O_3 decay rate at pH 7.3 in phosphate and borate buffered solution. Symbols represent average experimental data; lines represent model results.

While the kinetics of O_3 self–decay in the carbonate and phosphate buffer solutions differs, the overall exposure of target organics to $^{\bullet}OH$ appears to be similar in the two buffer systems at pH 7.3 with similar extents of oxidation of *p*–CBA (Figure 6.1b), a widely used $^{\bullet}OH$ probe,[87, 89, 182] in the two cases. The initially higher rate of *p*–CBA oxidation in the phosphate buffered solution than in the carbonate buffered solution is consistent with the higher rate of ozone decay (and concomitant $^{\bullet}OH$ generation) in phosphate buffered solution compared to that observed in the carbonate buffered system (Figure 6.1a). The R_{ct} value was calculated using the measured *p*–CBA oxidation data and O_3 decay rates in phosphate and carbonate buffered solutions (see Figure 6.5). The measured R_{ct} value in carbonate buffered solution is 2.3×10^{-8} however a value $> 10^{-7}$ is obtained for the phosphate buffered solution. Note that *p*–CBA oxidation in the phosphate buffered solution is too fast to quantify accurately with *p*–CBA completely oxidized within 30 s at the *p*–CBA to O_3 molar concentration ratio (1:100) employed here for R_{ct} measurement (results not shown). This observation suggests that while the yield of $^{\bullet}OH$ is higher for phosphate buffered solution in the initial stages due to rapid O_3 decay, the total $^{\bullet}OH$ exposure is the same for the two buffer solutions as confirmed by the similarity in overall *p*–CBA oxidation at higher *p*–CBA to O_3 concentration ratio (molar ratio 1:10, Figure 6.1b).

Overall, it appears that the buffering ions impact O_3 self–decay kinetics however did not show significant influence on the $^{\bullet}OH$ exposure over the full duration of the experiment.

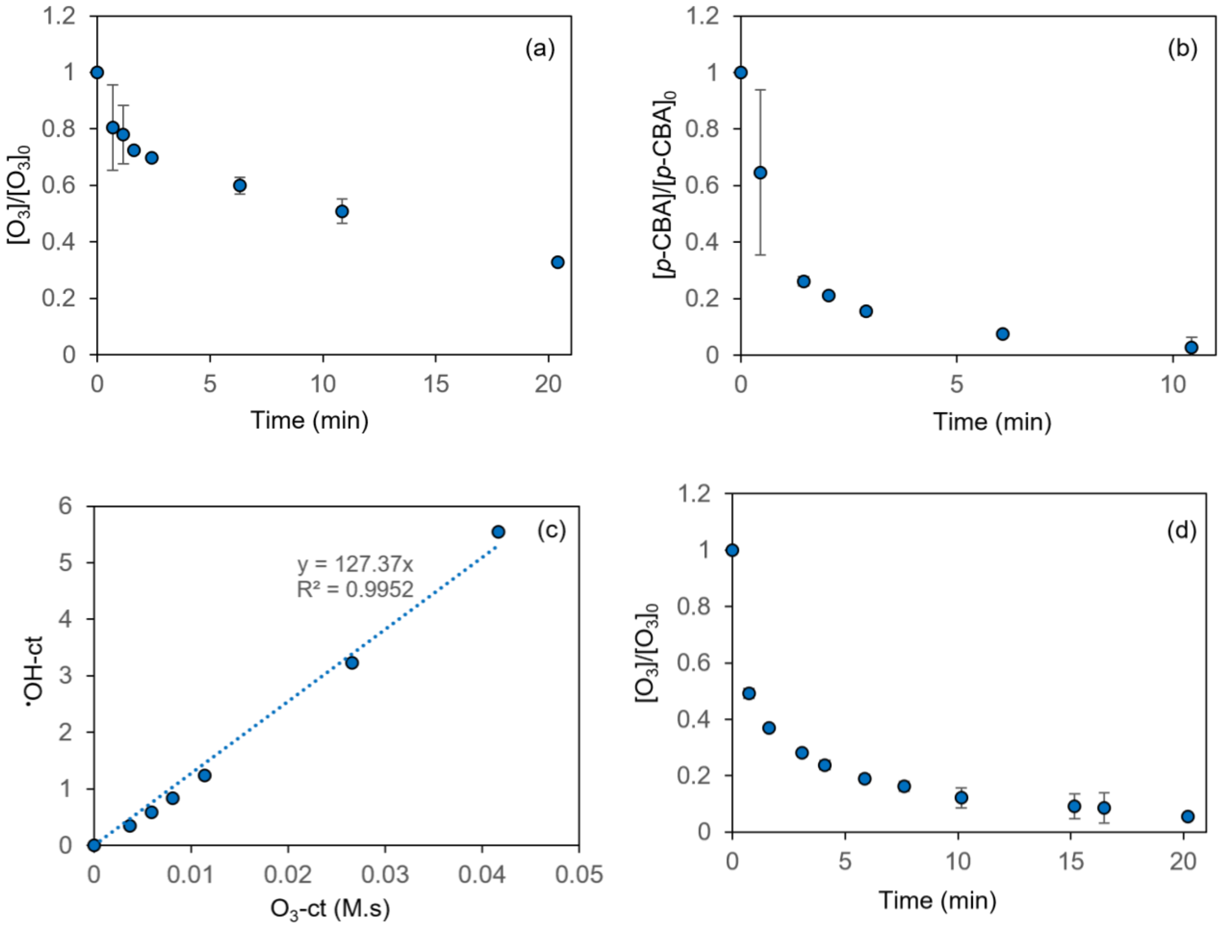

Figure 6.5 Panels a and b show measurement of O_3 decay and *p*–CBA oxidation respectively in carbonate buffer solution at pH 7.3. Panel c shows the plot of $^{\bullet}OH$ exposure vs O_3 exposure in carbonate buffered solution with $^{\bullet}OH$ exposure and O_3 exposure values calculated based on the data shown in panels and b. Panel d shows O_3 decay in phosphate buffered solution at pH 7.3. Experimental conditions: [*p*–CBA]$_0$ = 1.0 µM, $[O_3]_0$ = 100.0 µM, pH =7.3.

6.3.1.2 Oxidation of organics by ozonation

As shown in Figure 6.1c, only a small fraction (< 30%) of OA is oxidized by ozonation at pH 7.3 with a lower extent of OA oxidation observed in the phosphate buffered system (12 ± 2%) compared to that in carbonate buffered solution (26 ± 5%) after 60 min. Since oxidation of OA proceeds mainly via interaction with $^{\bullet}OH$ (eq. 6.8; OA is an ozone resistant compound $k_{C_2O_4^{2-}/O_3}$=0.04 $M^{-1}\cdot s^{-1}$ [123]), it appears that significant scavenging of $^{\bullet}OH$ by HCO_3^-/CO_3^{2-} and phosphate ions (mainly dihydrogen phosphate and hydrogen phosphate under conditions investigated here) occurs, even in the presence of OA, due to the low concentration of OA and its slow rate of reaction with $^{\bullet}OH$ ($k_{C_2O_4^{2-}/^{\bullet}OH}$=7.7×10^6 $M^{-1}\cdot s^{-1}$ [123]). Based on the measured O_3 decay in the two buffer solutions (Figure 6.1a), we had earlier suggested that the scavenging of $^{\bullet}OH$ by HCO_3^-/CO_3^{2-} is much more prominent compared to $^{\bullet}OH$ scavenging by phosphate ions. The faster scavenging of $^{\bullet}OH$ by HCO_3^-/CO_3^{2-} but still slightly higher OA oxidation in the carbonate buffered solution suggests that the carbonate radicals formed on scavenging of $^{\bullet}OH$ by HCO_3^-/CO_3^{2-} (eq. 6.6) also oxidize OA (eq. 6.9), albeit slowly. In contrast, the phosphate radicals formed on $^{\bullet}OH$ – phosphate ions reaction (eq. 6.7) are not able to oxidize OA (at least on the time scale investigated here), thereby resulting in lower OA oxidation rates in phosphate buffered solution. While the oxidation of aromatic compounds by phosphate radicals was reported in some earlier studies,[233] the oxidation of low-molecular weight acids by these radicals appears to be unimportant. We would also like to highlight that while OA oxidation in phosphate buffer solution is lower compared to that observed in carbonate buffered solution at the OA and buffer concentrations used here, it is expected that at higher OA concentrations (i.e., [OA]/[total phosphate] > 0.07 at which OA–$^{\bullet}OH$ reaction outcompetes phosphate ions–$^{\bullet}OH$ reactions), OA oxidation will be faster in phosphate buffered solution compared to carbonate buffered solution due to the higher rate of scavenging of $^{\bullet}OH$ in carbonate buffered solution.

$$C_2O_4^{2-} + {}^{\bullet}OH \rightarrow C_2O_4^{\bullet-} + HO^- \quad (6.8)$$

$$C_2O_4^{2-} + CO_3^{\bullet-} \rightarrow C_2O_4^{\bullet-} + HCO_3^- \quad (6.9)$$

For mildly O_3 reactive compounds such as FA, [140] no significant difference in the extent of FA oxidation is observed in carbonate and phosphate buffered systems, even though the rate of FA oxidation by ozonation is slower in the carbonate buffered system (Figure 6.1d). As described in chapter 4, FA oxidation in carbonate buffered solution occurs via interaction with O_3 with some contribution from $^{\bullet}OH$ under circumneutral pH conditions. In contrast, since rapid O_3 decay is observed in phosphate buffered solution, FA oxidation is expected to mostly occur via reaction with $^{\bullet}OH$ in this system. Hence, the observed difference in the kinetics of FA oxidation in carbonate and phosphate buffered solution is due to the difference in the nature and concentration of the oxidants (i.e., O_3 and $^{\bullet}OH$) as well as the difference in rate constants for the reaction of these oxidants with FA ($k_{O_3\text{-FA}}$ =1.5 – 100 $M^{-1}\cdot s^{-1}$and $k_{^{\bullet}OH\text{-FA}}$ = 1.2×10^9 $M^{-1}\cdot s^{-1}$;[140]). The model results (the lines) provided good description of the experimental data and detailed discussion about the model could be available in section 6.3.2.3.

Overall, we conclude that buffering ions have a significant impact on the kinetics of organic oxidation by the ozonation process. The fast kinetics of organic oxidation in phosphate buffered solution may help in reducing the hydraulic retention time of the ozonation reactors. The extent of organic oxidation may be affected as well due to the scavenging of $^{\bullet}OH$ by buffering ions, though this is dependent on the relative rates of organic oxidation by $^{\bullet}OH$ and scavenging of $^{\bullet}OH$ by buffering ions. Furthermore, the scavenging of $^{\bullet}OH$ by buffering ions may not have any impact on the extent of oxidation of organics that are oxidizable by radical products formed on $^{\bullet}OH$ scavenging however the kinetics of organic oxidation may be impacted since the radicals formed on $^{\bullet}OH$ scavenging are expected to be less reactive than $^{\bullet}OH$.

6.3.2 Influence of buffering ions on HCO performance

6.3.2.1 Catalytic ozone decay

As shown in Figure 6.6a, little difference in the catalyst mediated O_3 decay rate in the presence of Cu–Al LDHs in phosphate and carbonate buffered system is observed at pH 7.3. In comparison, in the presence of CuO, a slower rate of O_3 decomposition is observed in the phosphate buffered system compared to that observed in carbonate buffered solution (Figure 6.6b). As described in chapter 5, while rapid catalyst mediated O_3 decay occurs in the presence of CuO, O_3 decay via interaction with Cu–Al LDHs occurs very slowly with surface hydroxyl groups facilitating O_3 decay in both cases. The inhibition of CuO–catalysed O_3 decay in the phosphate buffered system is possibly due to occupation of surface hydroxyl groups responsible for O_3 decay by phosphate ions, thereby inhibiting surface decomposition of O_3 as has been reported in various earlier studies.[49, 188, 225-228] The influence of occupation of surface sites by phosphate ions on the O_3 decay kinetics, if any, is not apparent in the case of Cu–Al LDHs since surface catalysed O_3 decay is very slow in the presence of Cu–Al LDHs, at least at the Cu–Al LDHs concentration investigated here. Note that measurement of O_3 decay kinetics at 10–fold higher concentration of Cu–Al LDHs (where catalyst mediated O_3 decay becomes important) in phosphate and carbonate buffered solution clearly shows lower O_3 decay kinetics in the phosphate buffered solution compared to carbonate buffered solution (Figure 6.7) confirming the hypothesis that occupation of surface hydroxyl sites by phosphate ions inhibits catalyst mediated O_3 decay in the presence of Cu–Al LDHs as well.

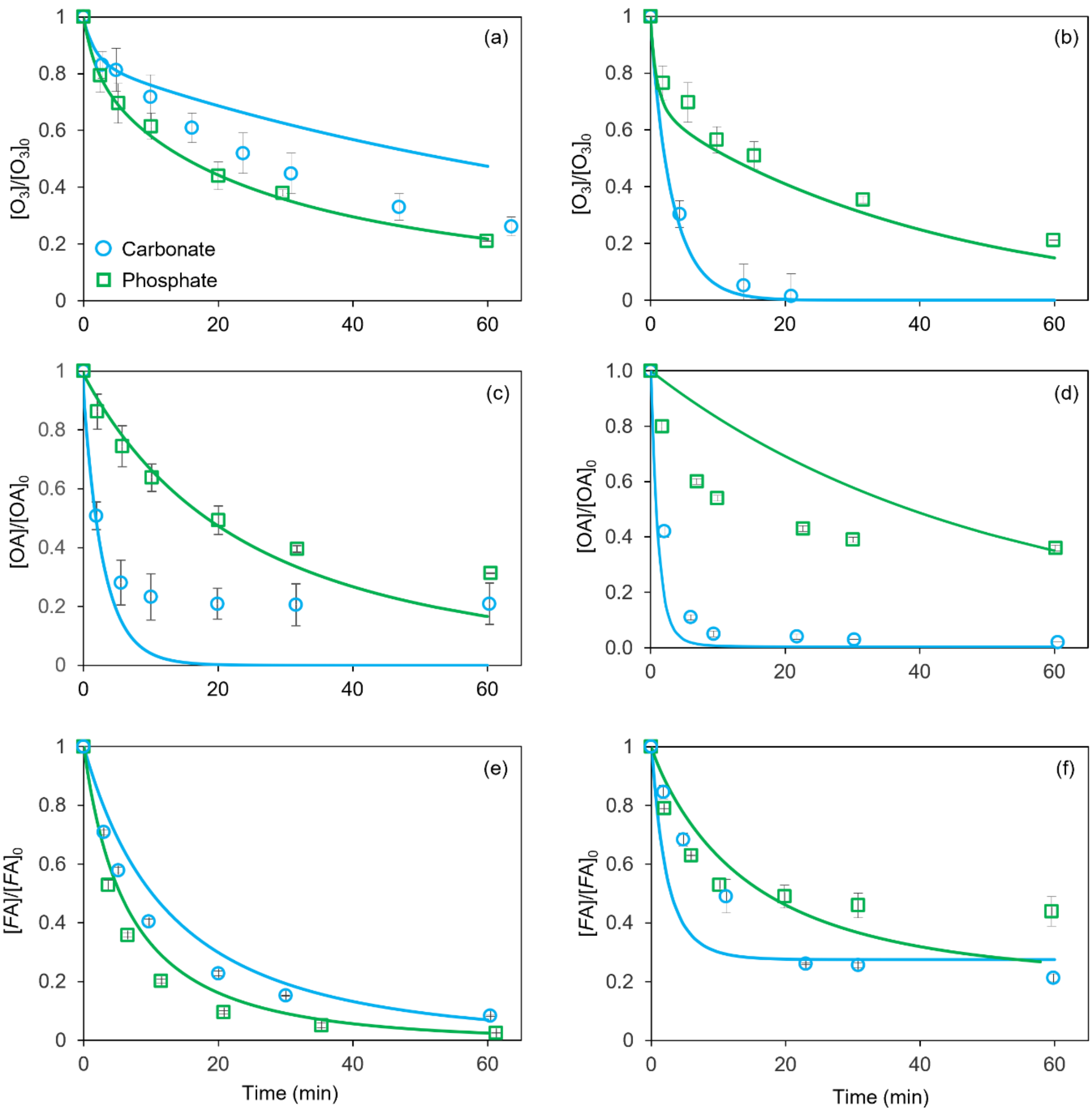

Figure 6.6 Measured O_3 ($[O_3]_0$ = 100.0 μM) decay kinetics in the presence of 0.06 $g.L^{-1}$ Cu–Al LDHs (a, in terms of CuO mass concentration) or CuO (b) at pH 7.3 with pH buffered using phosphate (squares) and carbonate (circles) solution. Panels c and d represent the measured oxidation of OA on HCO using Cu–Al LDHs and CuO respectively at pH 7.3 with pH buffered using phosphate (squares) and carbonate (circles) solution. Panels e and f represent the measured oxidation of FA on HCO using Cu–Al LDHs and CuO respectively at pH 7.3 with pH buffered using phosphate (squares) and carbonate (circles) solution. Initial conditions for OA/FA oxidation by HCO: $[O_3]_0$ = 10.0 μM; $[OA]_0$ /$[FA]_0$ =1.0 μM. Symbols represent measured values; lines represent model results.

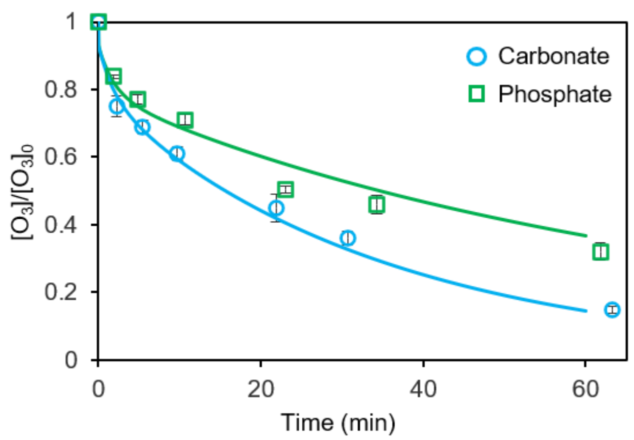

Figure 6.7 Measured O_3 decay rate in the presence of 0.6 $g.L^{-1}$ (in term of CuO mass concentration) Cu–Al LDHs at pH 7.3 buffered using 1.3 mM carbonate (circles) or 1.3 mM phosphate (squares) solution. Symbols represent average experimental data; lines represent model results.

For both CuO/Cu–Al LDHs, the rate of catalyst mediated O_3 decay is slower than the rate of ozone self–decay in the phosphate buffered system (Figure 6.8). As explained above, if the catalyst mediated O_3 decay is completely inhibited in phosphate buffered solution due to the unavailability of surface sites, the measured O_3 decay in phosphate buffered solution is via solution phase reactions even in the presence of catalyst. The significant inhibition of bulk O_3 decay in the presence of catalyst is possibly due to scavenging of bulk $^{\bullet}OH$ by Cu–Al LDHs/CuO with the catalysts outcompeting the scavenging of $^{\bullet}OH$ by phosphate ions (mianly dihydrogen phosphate and hydrogen phosphate, weak $^{\bullet}OH$ scavengers) resulting in slower O_3 decay kinetics in the phosphate buffered system. In the carbonate buffered solution, however, due to rapid scavenging of bulk $^{\bullet}OH$ by HCO_3^-/CO_3^{2-}, the scavenging of bulk $^{\bullet}OH$ by Cu–Al LDHs/CuO is not important.

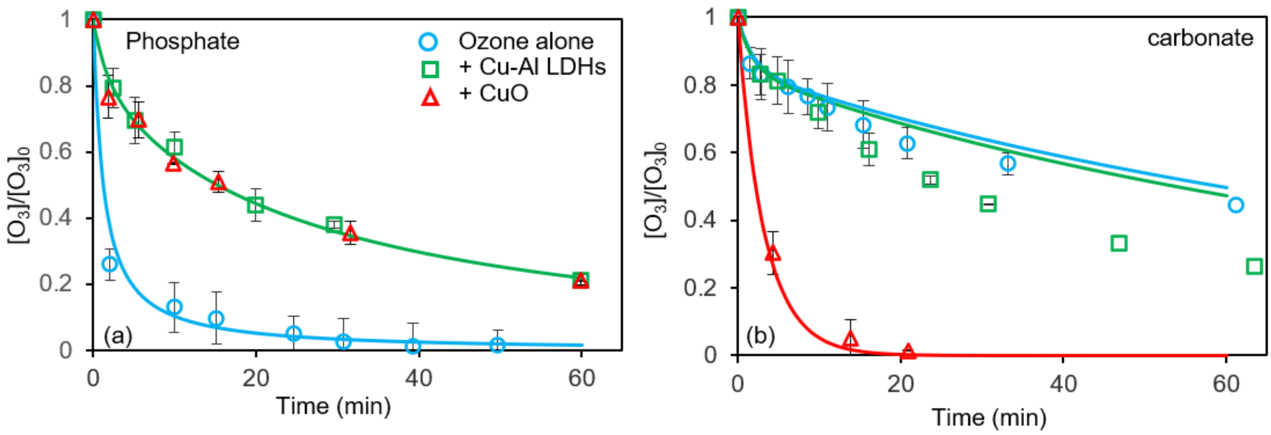

Figure 6.8 Measured O_3 decay rate in the absence (circles) and presence of 0.06 $g.L^{-1}$ (in terms of CuO mass concentration) Cu–Al LDHs (squares) or CuO (triangles) in pH 7.3 solution buffered using 1.3 mM phosphate (panel a) or 1.33mM carbonate (panel b). Symbols represent average experimental data; lines represent model results.

6.3.2.2. Oxidation of organics by HCO

A significantly lower rate of OA oxidation by HCO was observed in phosphate buffered solution compared to that observed in carbonate buffered solution (Figures 6.6c & d) which agrees with the observed influence of buffering ions on catalyst mediated O_3 decay (Figures 6.6a & b). As described in detail in chapter 5, the oxidation of OA in the presence of Cu–Al LDHs and CuO mainly occurs on the catalyst surface via interaction of surface oxalate complexes with surface located O_3 and/or surface oxidants generated on O_3 decay. Significant inhibition of O_3 sorption and catalyst mediated O_3 decay as well as lower adsorption of OA onto Cu–Al LDHs/CuO surface (Figure 6.9) because of blocking of surface sites decreases the rate and extent of OA oxidation in the phosphate buffered solution. Note that the rate of OA oxidation by HCO using Cu–Al LDHs in borate buffer solution (Figure 6.10a), which has the same bulk $^{\bullet}OH$ scavenging capacity as the phosphate buffer (Figure 6.4) but facilitates OA sorption (Figure 6.10b), is similar to that observed in carbonate buffered solution. This observation further supports the conclusion that the inhibition of OA oxidation by HCO in phosphate buffered solution is due to occupation of the surface sites by phosphate ions inhibiting OA adsorption and concomitant oxidation and not due scavenging of bulk $^{\bullet}OH$ by phosphate ions.

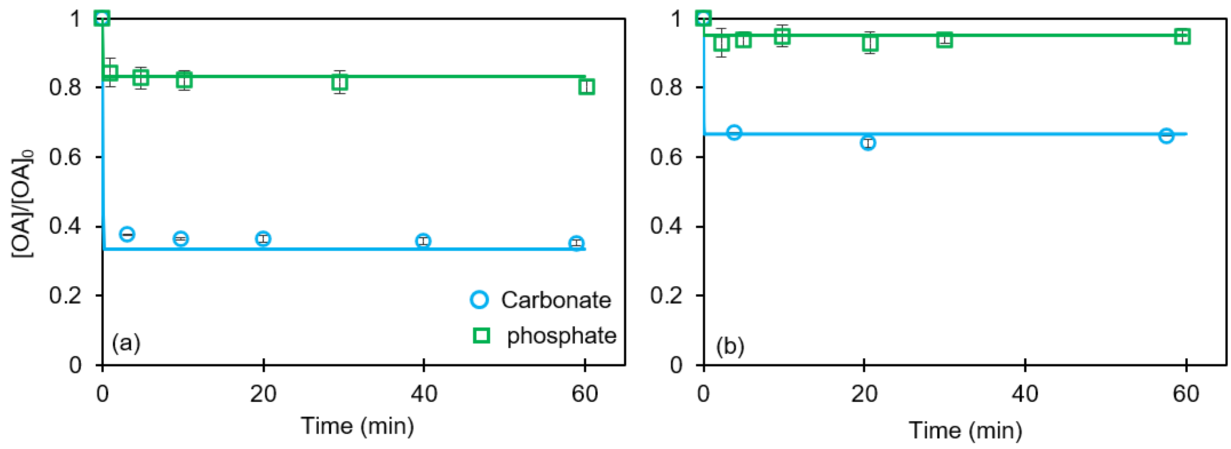

Figure 6.9 Measured OA sorption in the presence of 0.6 g.L^{-1} (in terms of CuO mass concentration) Cu–Al LDHs (a) or CuO (b) at pH 7.3 buffered using 1.3 mM phosphate (squares) and carbonate (circles) solution.

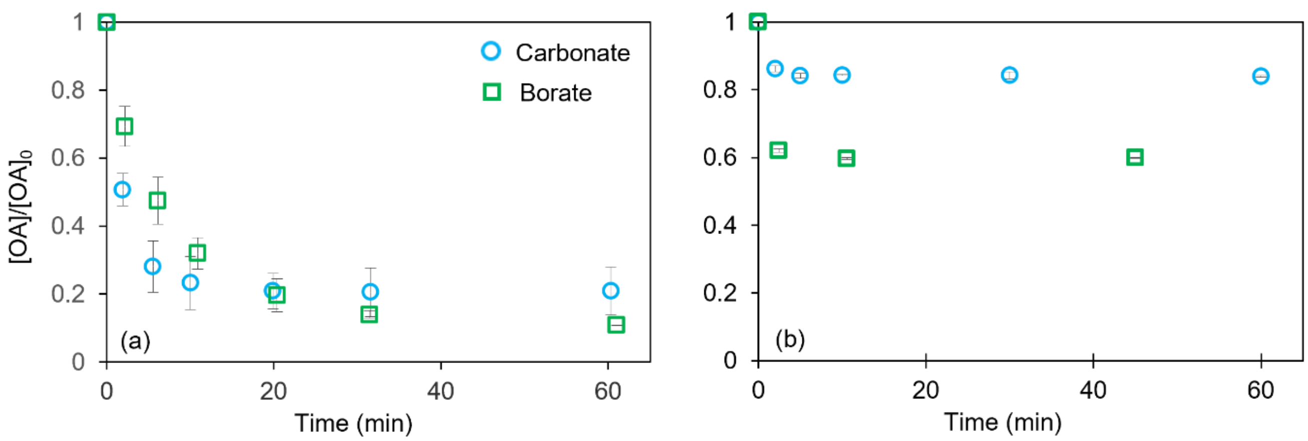

Figure 6.10 Measured OA oxidation (panel a) by HCO in the presence of 0.06 g.L^{-1} (in terms of CuO mass concentration) Cu–Al LDHs at pH 7.3 buffered using 5.0 mM borate (squares) and 1.3 mM carbonate (circles) solution. Measured OA adsorption (panel b) in the presence of 0.06 g.L^{-1} (in terms of CuO mass concentration) Cu–Al LDHs at pH 7.3 buffered using 5.0 mM borate (squares) and 1.3 mM carbonate (circles) solution.

No difference in FA oxidation by HCO using Cu–Al LDHs was observed between carbonate and phosphate buffered solution (Figure 6.6e) which agrees with the mechanism of FA oxidation reported in the presence of Cu–Al LDHs in chapter 5. FA oxidation in the presence of Cu-Al LDHs mainly occurs in bulk solution via interaction with bulk O_3 and $^{\bullet}OH$. Since no difference in the bulk oxidation of FA was observed between phosphate and carbonate buffered solutions (Figure 6.1d), it is not surprising that no influence of buffers was observed in the catalytic system as well. In comparison, significantly lower FA oxidation by HCO using CuO was observed in phosphate buffered solution compared to carbonate buffered solution (Figure 6.6f). Since, in the case of CuO, FA oxidation mostly occurs on the surface of the catalyst via interaction with surface oxidants formed on O_3 decay (see discussion in chapter 5), significant inhibition of catalyst mediated O_3 decay (Figure 6.6b) as well as inhibition of FA sorption (Figure 6.11) accounts for the lower FA oxidation in phosphate buffered solution.

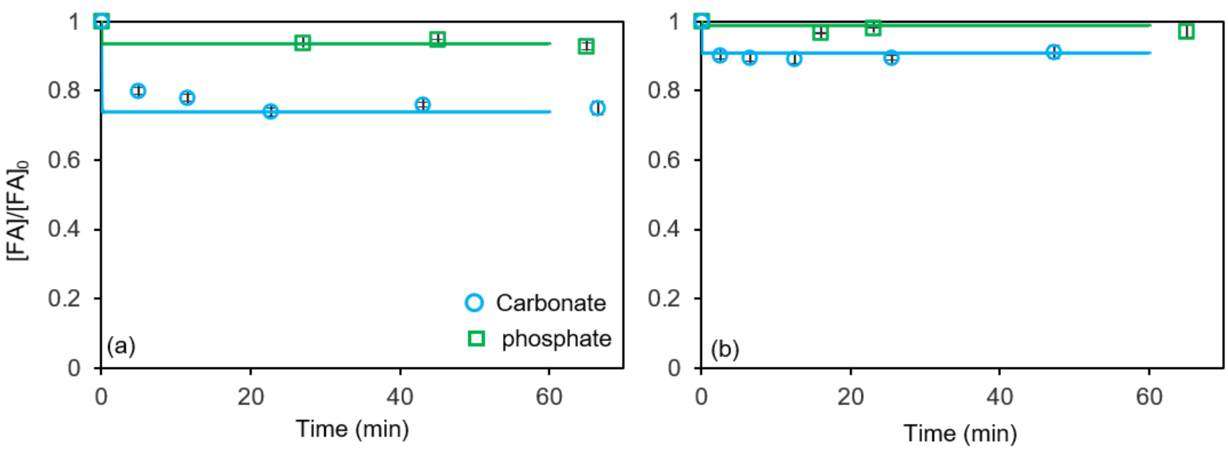

Figure 6.11 Measured FA sorption in the presence of 0.6 g.L^{-1} (in terms of CuO mass concentration) Cu–Al LDHs (a) or CuO (b) at pH 7.3 buffered using 1.3 mM phosphate (squares) and carbonate (circles) solution.

Overall, our results confirm that catalyst mediated ozone decay is inhibited in the presence of phosphate ions with this inhibition expected to have significant influence on the surface associated oxidation of organics. Moreover, the oxidation of organics in bulk solution may also be impacted as a result of the rapid scavenging of bulk $^{\bullet}OH$ by the catalyst with this effect more prominent in phosphate buffered solution compared to carbonate buffered solution, particularly if the catalyst is present in excess and outcompetes organic – $^{\bullet}OH$ interaction. Our results also show that the influence of buffers on HCO efficiency is not only dependent on the nature of the organics but also the mechanism of oxidation of these organics during HCO. For example, the influence of buffers on FA oxidation in the presence of Cu–Al LDHs and CuO differs due to difference in the mechanism of oxidation of FA in the two systems.

6.3.2.3 Kinetic Modelling

We have extended the kinetic model developed in chapter 5 in carbonate buffered solution to predict the FA and OA oxidation in phosphate buffered solution during ozonation and HCO employing Cu–Al LDHs and CuO. Note that the same kinetic model was used to explain O_3 decay and organic oxidation rates in carbonate and phosphate buffered solutions with changes made to the rate constant for certain reactions due to difference in reactivity of carbonate and phosphate ions. Detailed description of the kinetic model and justification of the rate constants used are provided below.

(i) O_3 self–decay

Reactions 1-10 (Table 6.1) describe O_3 self–decay (Figures 6.1a, 6.2 – 6.4) in carbonate and phosphate buffered solution. The rate constants for these reactions are well reported in the literature [98, 141, 151-155] and were used here. Note that the faster $^{\bullet}OH$ scavenging by carbonate/bicarbonate ions (reaction 8, Table 1) compared to phosphate ions explains the difference in O_3 self-decay kinetics in carbonate and phosphate buffered solution.

(ii) Formate oxidation by ozonation

Reactions 11 – 15 (Table 6.1) describes formate oxidation by ozonation as described in chapter 5. The rate constants were determined based on best–fit to the measured formate oxidation rate (Figure 6.1d and 6.12d). Carbonate radicals formed via scavenging of

$^{\bullet}$OH by carbonate/bicarbonate ions also contribute to FA oxidation; however, phosphate radicals formed on $^{\bullet}$OH-phosphate reaction do not play a role in FA oxidation.

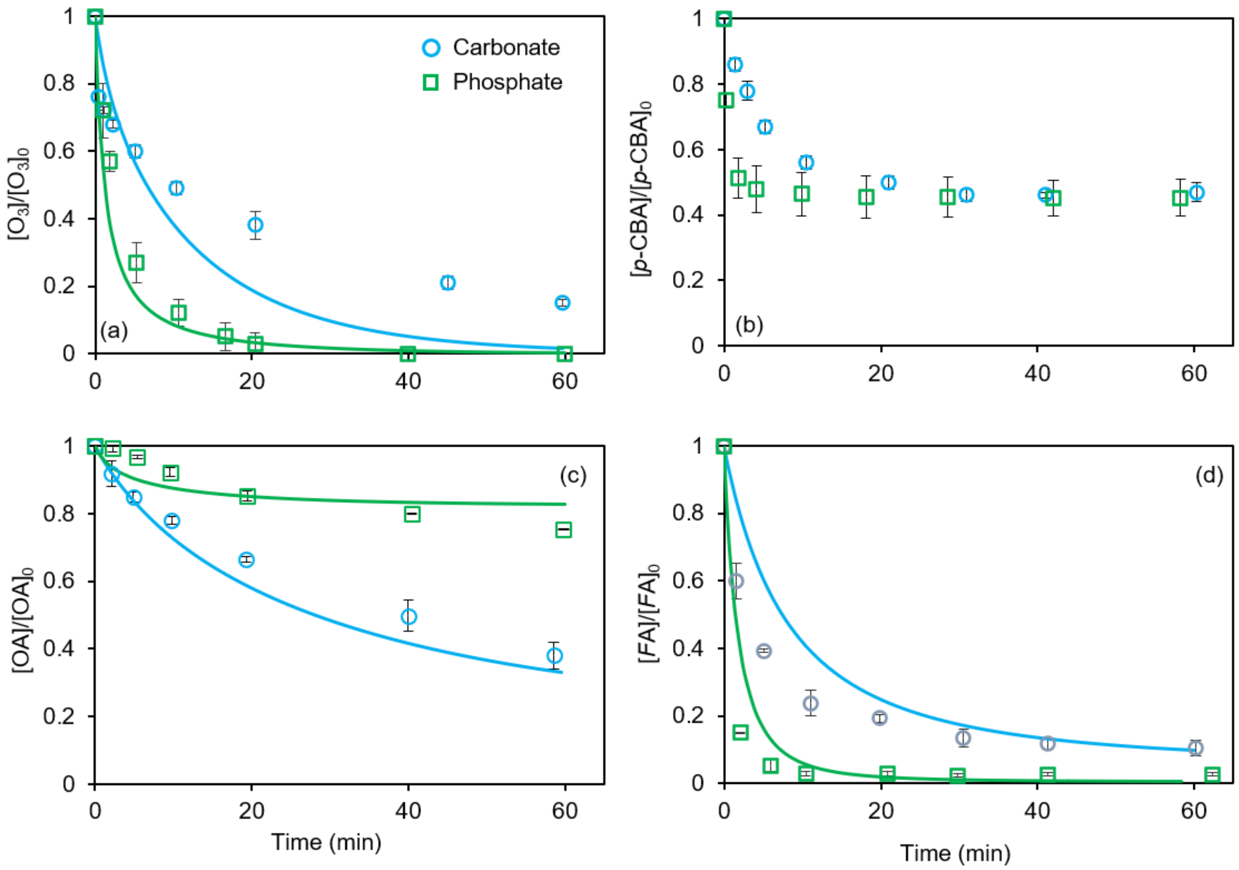

Figure 6.12 (a) Measured O_3 ($[O_3]_0$ = 100.0 µM) self-decay kinetics at pH 8.5 buffered using phosphate (squares) and carbonate (circles) solution. Panels b, c and d represent the measured oxidation of *p*–CBA, OA and FA respectively on ozonation at pH 8.5 with pH buffered using phosphate (squares) and carbonate (circles) solution. Symbols represent measured values; lines represent model results. Experimental conditions for *p*–CBA/FA oxidation: $[O_3]_0$ = 10.0 µM; $[p\text{–CBA}]_0/[\text{FA}]_0$ =1.0 µM. For OA oxidation: $[O_3]_0$ = 100.0 µM; $[\text{OA}]_0$ =1.0 µM, $[\text{phosphate}]_0/[\text{carbonate}]_0$ = 2.0 mM

(iii) Oxalate oxidation by ozonation

Reactions 16 – 20 (Table 6.1) explains the oxalate oxidation by ozonation as described in chapter 5. As in the case of FA, while carbonate radicals oxidize OA, no involvement of phosphate radicals in OA oxidation was observed based on our experimental results.

(iv)Catalyst mediated O_3 decay using Cu-Al LDHs and CuO

The catalyst mediated O_3 decay reactions in the presence of Cu–Al LDHs (reactions 21 – 24, Table 6.1) and CuO (reactions 21A – 24A, Table 6.1) were described in detail in chapter 5. Briefly, O_3 adsorbed onto the surface hydroxyl groups (reaction 21/21A) and was transformed into oxidants (reaction 22/22A; for Cu–Al LDHs surface $^{\bullet}OH$ was produced). The oxidants and/or surface O_3 are consumed by the catalysts (reactions 23 – 24) with the rate constant for scavenging of oxidants by CuO higher compared to that determined for Cu – Al LDHs. The rate constants for catalyst mediated O_3 decay were determined based on best–fit to the measured O_3 decay rates in the presence of catalyst (Figure 6.6a and 6.7-6.8). Due to the occupation of surface hydroxyl sites by phosphate ions, the rate constant for catalyst mediated O_3 decay and scavenging of oxidants by the catalysts in phosphate buffered solution are lower compared to the value used in carbonate buffered solution.

(v) Formate/oxalate adsorption onto Cu-Al LDHs and CuO

Reactions 25 – 26 (Table 6.1) describes FA /OA onto the surface hydroxyl sites of the catalysts with Cu–Al LDHs displaying higher affinity to FA/OA compared to CuO. The adsorption equilibrium constants of FA/OA were determined based on the adsorption data (Figure 6.7 and 6.11). Since phosphate can compete with the organics for the surface hydroxyl sites, the equilibrium constant for adsorption of FA/OA was lower in phosphate buffered solution compared to the value used in carbonate buffered solution.

(vi) Formate oxidation by HCO in the presence of Cu-Al LDHs and CuO

The reactions controlling FA/OA oxidation in the presence of Cu–Al LDHs and CuO were described in detail in chapter 5. As described, FA oxidation by HCO in the presence of CuO occurs via interaction with surface O_3 (reaction 27, Table 6.1) and surface oxidant (reaction 28, Table 6.1). The rate constants for these reactions were determined based on the measured FA oxidation rate in the presence of CuO (Figure 6.6d). The rate constant for oxidation of FA on the CuO surface by surficial O_3/surface oxidant was same in carbonate and phosphate buffered solution. The decrease in the rate and extent of FA oxidation in phosphate buffered solution was mainly due to the slower generation of oxidant and inhibition of FA adsorption in this system.

As described in chapter 5, FA oxidation in the presence of Cu–Al LDHs mainly occur via interaction with bulk O_3 and hydroxyl radicals (reactions 11 – 15, Table 6.1). Note that even though the reactions of surface oxidation of FA by surficial O_3 and surface hydroxyl radicals (reactions 27 – 28, Table 6.1) are included here, these reactions do not play an important in FA oxidation in the presence of Cu–Al LDHs, at least at the conditions investigated here.

(vii) Oxalate oxidation by HCO in the presence of Cu–Al LDHs and CuO

The reactions controlling OA oxidation in the presence of Cu–Al LDHs and CuO was described in chapter 5. As discussed, OA oxidation occurs via surface O_3 (reaction 30, Table 6.1) with some contribution from surface oxidant (reaction 31, Table 6.1). The rate constant for surface oxidation of OA for both CuO and Cu–Al LDHs was similar in carbonate and phosphate buffered solution. The inhibition of OA oxidation in phosphate buffered solution was mainly due to the slower generation of oxidant and oxalate adsorption.

(viii) Scavenging of bulk $^{\bullet}OH$ by Cu–Al LDHs and CuO

Reaction 33 (Table 6.1) represent the scavenging of bulk $^{\bullet}OH$ by catalysts. The rate constant for this reaction is based on the best-fit to measured catalyst mediated O_3 decay in phosphate buffered solution (Figure 6.6b).

Table 6.1 Kinetic model for ozone decay, formate and oxalate oxidation by HCO in the presence of Cu–Al LDHs and CuO in carbonate and phosphate buffer.

No	Reaction	Rate constant in carbonate buffer	Rate constant in phosphate buffer	Ref.
		Ozone self–decay reactions		
1	$O_3 + OH^- \rightarrow HO_2^\bullet + O_2^{\bullet-}$	1.0×10^2	1.0×10^2	[151]
2	$O_3 + H_2O_2/HO_2^- \rightarrow HO_3^\bullet + O_2^{\bullet-}$	$1.7\times10^{2\ a}$	$1.7\times10^{2\ a}$	[152]
3	$O_3 + O_2^{\bullet-} \rightarrow HO_3^\bullet + O_2$	1.5×10^9	1.5×10^9	[98]
4	$HO_3^\bullet/O_3^{\bullet-} \rightarrow {}^\bullet OH + O_2$	$1.4\times10^{5\ b}$	$1.4\times10^{5\ b}$	[151]
5	${}^\bullet OH + O_3 \rightarrow O_2^{\bullet-} + O_2$	1.0×10^8	1.0×10^8	[151]
6	$O_3 + CO_3^{\bullet-} \rightarrow H_2CO_3 + O_2$	1.0×10^5	1.0×10^5	[153]
7	${}^\bullet OH + H_2O_2/HO_2^- \rightarrow H_2O + O_2^{\bullet-}$	$2.7\times10^{7\ a}$	$2.7\times10^{7\ a}$	[98]
8	${}^\bullet OH + HCO_3^-/ HPO_4^{2-} \rightarrow H_2O + CO_3^{\bullet-}/ PO_4^{\bullet-}$	$8.2\times10^{6\ c}$	$5.0\times10^{4\ c}$	[55]
9	$CO_3^{\bullet-} + H_2O_2/HO_2^- \rightarrow O_2^{\bullet-} + H_2CO_3$	$4.3\times10^{5\ a}$	$4.3\times10^{5\ a}$	[154]
10	$CO_3^{\bullet-} + CO_3^{\bullet-} \rightarrow CO_4^{2-} + H_2CO_3$	2.0×10^7	2.0×10^7	[155]
		Formate oxidation by ozonation		
11	$HCOO^- + O_3 \rightarrow HCO_3^- + HO_3^-$	70.0	70.0	[140]
12	$HCOO^- + O_3 \rightarrow CO_2^{\bullet-} + HO_3^\bullet$	30.0	30.0	[3, 143]
13	$HCOO^- + CO_3^{\bullet-} \rightarrow CO_2^{\bullet-} + HCO_3^-$	1.5×10^5	-	[147]
14	$HCOO^- + {}^\bullet OH \rightarrow CO_2^{\bullet-} + H_2O$	3.2×10^9	3.2×10^9	[141]
15	$CO_2^{\bullet-} + O_2 \rightarrow O_2^{\bullet-} + HCO_3^-$	4.2×10^9	4.2×10^9	[124]
		Oxalate oxidation by ozonation		
16	$C_2O_4^{2-} + O_3 \rightarrow C_2O_4^{\bullet-} + HO_3^-$	0.04	0.04	[123]
17	$C_2O_4^{2-} + O_3 \rightarrow C_2O_4^{\bullet-} + HO_3^\bullet$	0.04	0.04	[216]
18	$C_2O_4^{2-} + CO_3^{\bullet-} \rightarrow C_2O_4^{\bullet-} + HCO_3^-$	6.0×10^4	-	
19	$C_2O_4^{2-} + {}^\bullet OH \rightarrow C_2O_4^{\bullet-} + H_2O$	7.7×10^6	7.7×10^6	[141, 201]
20	$C_2O_4^{\bullet-} \rightarrow CO_2^{\bullet-} + HCO_3^-$	1.0×10^9	1.0×10^9	
		Catalytic O_3 decay using Cu–Al LDHs		
21	$O_3 + \equiv \rightleftharpoons \equiv O_3$	$K = 15\times10^{1\ d,e}$	$K = 15\times10^{1\ d,e}$	In chapter 5

22	$\equiv O_3 \rightarrow \equiv {}^{\bullet}OH$	5×10^{-3}	1.5×10^{-3}	In chapter 5
23	$\equiv O_3 + \equiv \rightarrow$ NRP + $\equiv$ [f]	3.0	1.0	In chapter 5
24	$\equiv {}^{\bullet}OH + \equiv \rightarrow$ NRP + $\equiv$ [f]	1.0×10^{6}	3×10^{5}	In chapter 5
		Catalytic O_3 decay using CuO		
21A	$O_3 + \equiv \rightleftharpoons \equiv O_3$	$K = 4.0\times10^{3}$ [d,e]	$K = 4.0\times10^{3}$ [d,e]	In chapter 5
22A	$\equiv O_3 \rightarrow \equiv Ox$	1.0×10^{-1}	1.0×10^{-3}	In chapter 5
23A	$\equiv O_3 + \equiv \rightarrow$ NRP + $\equiv$ [f]	500.0	5.0	In chapter 5
24A	$\equiv Ox + \equiv \rightarrow$ NRP + $\equiv$ [f]	5.0×10^{5}	5.0×10^{5}	In chapter 5
		FA/OA sorption on Cu–Al LDHs surface		
25	$HCOO^{-} + \equiv \rightleftharpoons \equiv HCOO^{-}$	3.5×10^{2} [d,e]	7.0×10^{1} [d,e]	In chapter 5
26	$C_2O_4^{2-} + \equiv \rightleftharpoons \equiv C_2O_4^{2-}$	2.0×10^{3} [d,e]	2.0×10^{2} [d,e]	In chapter 5
		FA/OA sorption on CuO surface		
25A	$HCOO^{-} + \equiv \rightleftharpoons \equiv HCOO^{-}$	1.0×10^{2} [d,e]	1.0×10^{1} [d,e]	In chapter 5
26A	$C_2O_4^{2-} + \equiv \rightleftharpoons \equiv C_2O_4^{2-}$	5.0×10^{2} [d,e]	5.0×10^{1} [d,e]	In chapter 5
		FA oxidation by HCO using Cu-Al LDHs/CuO		
27	$\equiv HCOO^{-} + \equiv O_3 \rightarrow CO_2 + HO_3^{-} + \equiv$	4.0×10^{1} [g]	4.0×10^{1} [g]	In chapter 5
28	$\equiv HCOO^{-} + \equiv {}^{\bullet}OH$ / $\equiv Ox \rightarrow \equiv CO_2^{\bullet-} + \equiv$	1.0×10^{9} [g]	1.0×10^{9} [g]	In chapter 5
29	$\equiv CO_2^{\bullet-} + O_2 \rightarrow CO_2 + \equiv O_2^{\bullet-}$	1.0×10^{9} [g]	1.0×10^{9} [g]	In chapter 5
		OA oxidation by HCO using Cu–Al LDHs/CuO		
30	$\equiv C_2O_4^{2-} + \equiv O_3 \rightarrow \equiv C_2O_4^{\bullet-} + HO_3^{-} + \equiv$	1.0×10^{6}	1.0×10^{6}	In chapter 5
31	$\equiv C_2O_4^{2-} + \equiv {}^{\bullet}OH$ / $\equiv Ox \rightarrow \equiv C_2O_4^{\bullet-} + \equiv$	1.0×10^{9} [g]	1.0×10^{9}	In chapter 5
32	$\equiv C_2O_4^{\bullet-} \rightarrow CO_2 + \equiv CO_2^{\bullet-}$	1.0×10^{9}	1.0×10^{9}	In chapter 5
		Scavenging of bulk ${}^{\bullet}OH$ by catalyst		
33	$\equiv + {}^{\bullet}OH \rightarrow \equiv + H_2O$	1.0×10^{7}, 1.0×10^{9} [h,i]	1.0×10^{7}, 1.0×10^{9} [h]	In chapter 5

[a] calculated value at pH 7.3 using the reported rate constant for H_2O_2/HO_2^{-} and the mole fraction of H_2O_2/HO_2^{-} at pH 7.3.
[b] calculated value at pH 7.3 using the reported rate constant for $HO_3^{\bullet-}/O_3^{\bullet-}$ and the mole fraction of $HO_3^{\bullet-}/O_3^{\bullet-}$ at pH 7.3.
[c] calculated value at pH 7.3 using the reported rate constant for $H_2CO_3/HCO_3^{-}/CO_3^{2-}$ and the mole fraction of for $H_2CO_3/HCO_3^{-}/CO_3^{2-}$ at pH 7.3.
[d] based on surface site concentration of 1.7 mmoles.g^{-1} CuO in Cu–Al LDHs and CuO
[e] *K* represents the ratio of the forward adsorption rate constant and back desorption rate constant
[f] NRP represents non-reactive product
[g] rate constants are not well constrained by our experimental results since these reactions are not important

[h] 1.0×10^7 for Cu-Al LDHs and 1.0×10^9 for CuO.
[i] rate constant is not well-constrained since this reaction is not important in carbonate buffered solution.

As shown in Table 6.1, employing a lower rate constant for scavenging of $^{\bullet}OH$ by phosphate ions (mainly dihydrogen phosphate and hydrogen phosphate) compared to HCO_3^{-}/CO_3^{2-} (reaction 8, Table 6.1) explains the difference in the ozone self-decay kinetics in the phosphate and carbonate buffered systems. The rate constant for scavenging of $^{\bullet}OH$ by phosphate ions and HCO_3^{-}/CO_3^{2-} used here agrees with the values reported in earlier studies.[98, 141, 143] The difference in the rate constants for scavenging of $^{\bullet}OH$ by buffering ions also explains the faster kinetics of FA oxidation in the phosphate buffered solution. Furthermore, our modelling results clearly demonstrate that carbonate radicals formed on scavenging of $^{\bullet}OH$ by HCO_3^{-}/CO_3^{2-} play an important role in FA and OA oxidation (reactions 13 and 18, Table 6.1). For HCO, the lower rate constant for catalyst mediated O_3 decay (reactions 23 and 24, Table 6.1) as well as lower sorption of OA (reaction 25, Table 6.1)/ FA (reaction 26, Table 6.1) on the catalyst surface in the phosphate buffered solution accounts for the difference in the O_3 decay rate as well as OA/FA oxidation rate by catalytic ozonation in the two buffer systems.

As shown in Figures 6.1 – 6.4, 6.6 – 6.9 and 6.11 – 6.13, the kinetic model presented here describes our experimental results in both carbonate and phosphate buffered solution very well. Using the kinetic model presented here, we also predicted the influence of buffering ions on OA oxidation for a wide range of organic and buffer concentrations. To predict the influence of buffers on the efficacy of ozonation and HCO for organics oxidation, we simulate results in a continuous flow reactor with a hydraulic retention time of 60 min in which a constant dissolved O_3 concentration of 100.0 μM is maintained via continuous sparging of gaseous ozone since this setup is more representative of real conditions. Note that we show the results for OA oxidation only since no influence of buffering ions is observed on FA oxidation with complete removal of FA observed under all conditions investigated. As shown in Figure 6.13, the influence of buffers on ozonation efficiency is quite variable with higher OA removal observed in carbonate buffered solution compared to phosphate buffered solution at higher buffer concentration. In contrast, the oxidation of OA is higher in phosphate buffered solution at lower buffer concentration and lower organic concentration. At higher buffer concentration, significant scavenging of $^{\bullet}$OH by buffering ions occur. While the carbonate radicals formed in carbonate buffered solution via $^{\bullet}$OH scavenging contribute to OA oxidation, phosphate radicals formed in phosphate buffered solution cannot oxidize OA and hence lower OA oxidation is observed in phosphate buffered solution. During HCO employing Cu–Al LDHs, OA oxidation is lower in phosphate buffered solution for all OA and buffer concentrations due to inhibition of surface mediated reactions in the presence of phosphate ions.

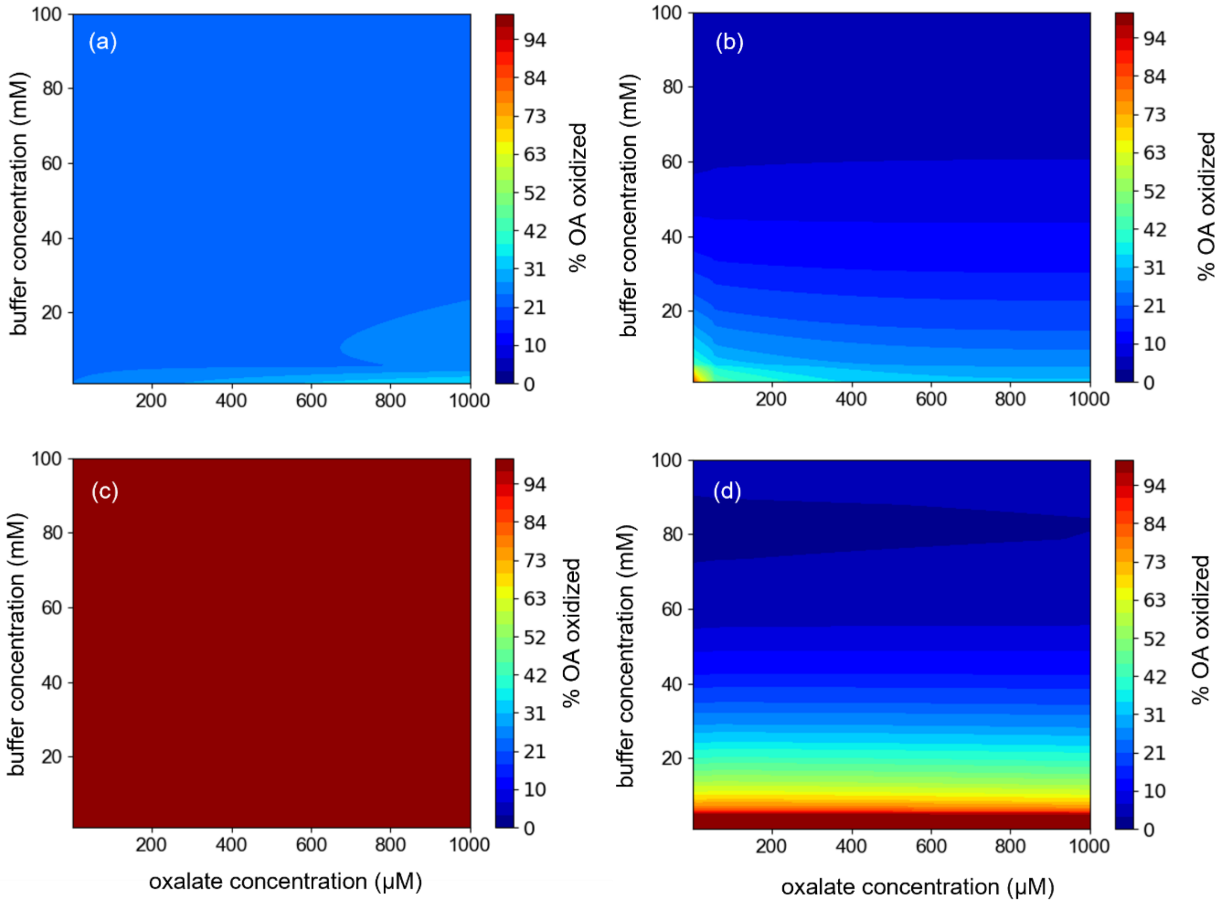

Figure 6.13 Model predicted OA oxidation under varying OA and buffer concentration. Panels a and b show the OA oxidation during ozonation process at pH 7.3 in carbonate and phosphate buffered solution respectively. Panels c and d show the OA oxidation during HCO process using Cu–Al LDHs at pH 7.3 in carbonate and phosphate buffered solution respectively. Note that for these predictions $[O_3]_{ss}$ =100.0 μM was used. The z-axis shows the % OA removal observed in carbonate buffered and phosphate buffered after 60 min of reaction time.

6.4 Conclusions

Our results clearly demonstrate that the nature of the buffering ions present has a significant influence on ozone decay kinetics during ozonation due to the differing $^{\bullet}OH$ scavenging capacity of particular buffering ions. Thus, caution should be exercised in comparing O_3 decay data obtained in different buffering solutions. The difference in the O_3 decay rates significantly affects the kinetics of organic oxidation, however, has no influence on the overall extent of organic oxidation by ozonation unless the relative rate of organic oxidation by bulk $^{\bullet}OH$ is small compared to overall scavenging of $^{\bullet}OH$

by buffering ions. However, in flow systems, where wastewaters have limited residence time in the reactor, the influence of buffering ions on the kinetics of organic oxidation will be key determinant of the efficacy of the oxidation process. Our results further highlight that carbonate radicals are involved in oxidation of low molecular organic acids (i.e., FA and OA) however the oxidation of these organics by phosphate radicals appears to be unimportant. This is an important insight since in most of the earlier studies [51, 234] it is assumed that $^{\bullet}OH$ scavenging by carbonate ions decreases the oxidation efficiency of organics however this may not be the case if the target organics are reactive towards carbonate radicals. The presence of phosphate ions also affects the surface chemistry of the catalyst inhibiting catalyst mediated O_3 decay and organic sorption and hence is likely to have a significant impact on the surface oxidation of organics by HCO. Thus, the catalytic performance of a catalyst may be underestimated if measured in phosphate buffered solution, particularly if surface reactions are prominent. Our results clearly show that the influence of buffering ions on the oxidation efficiency of organics is not only dependent on the nature of the organics but also the mechanism of the catalytic ozonation process. While we have performed detailed investigation of influence of buffers on the ozonation and HCO performance at pH 7.3 here, similar results on O_3 decay and oxidation of organics were observed at pH 8.5 as well (Figure 6.12) with these results supporting the conclusion that the influence of buffering ions determined here is valid for a wide range of pHs in the circumneutral pH range. Overall, the mechanistic insights into the influence of buffering ions on ozone decay and associated sorption and oxidation of organics presented here are critical to proper understanding of the efficacy of the ozonation and HCO processes.

Chapter 7 Influence of salinity on the heterogeneous catalytic ozonation process: Implications to treatment of high salinity wastewater

Some of the material in this Chapter has been drawn from a recent publication,[235] which has been acknowledged and detailed in the 'inclusion of publications statement' for this thesis.

7.1 Introduction

The coal chemical industry (CCI) produces large amounts of wastewater containing highly toxic and refractory organic compounds, including phenolic, heterocyclic and low molecular weight neutral organics.[236-238] The disposal of coal chemical wastewater (CCW) poses a serious challenge around the world. Recently, multi-stage reverse osmosis (RO) has been used for the treatment of CCW with this process capable of producing desalinated effluents that are suitable for internal reuse in production and cooling. However, this practice inevitably results in the accumulation of salts and refractory organic matter in the RO membrane concentrate (ROC). Heterogeneous catalytic ozonation (HCO) has shown promising results for the treatment of ROC from the coal chemical industry.[239-242] However, large amounts of salts (particularly Na^+, Cl^- and SO_4^{2-} salts) in ROC may potentially impact the efficacy of the HCO process as a result of scavenging of O_3 [243] and bulk and/or surface hydroxyl radicals formed on O_3 decay by Cl^- and/or SO_4^{2-} forming less reactive and more selective oxidants ($Cl^•$, $Cl_2^{•-}$, $ClO^•$ and $SO_4^{•-}$).[244, 245] Furthermore, deposition of salts on the catalyst surface has been reported to decrease the specific surface area of catalyst,[246, 247] hindering the performance of HCO. In contrast, in some other studies no influence of Cl^- was observed on organic oxidation in the presence of a variety of catalysts such as MnO_2, MgO, molecular sieve and Fe_3O_4 loaded PAC.[248-251] Based on the discussion above, understanding and quantification of the severity of the "salt effect" on HCO performance is required before application of HCO for treatment of CCW.

In this chapter, we investigate the influence of salts on the performance of both conventional ozonation and catalytic ozonation processes for treatment of ROC obtained from CCI. The pH of a variety of CCI concentrates was determined to be largely circumneutral with Na^+ being the dominant cation and Cl^- and SO_4^{2-} being the dominant anions (see Table 7.1). Furthermore, liquid chromatography–organic carbon detection (LC–OCD) analysis of a variety of CCI concentrate samples showed that humic-like substances and low molecular weight (LMW) neutral compounds (such as alcohols, aldehydes and ketones) were the dominant organic components in all CCI concentrates (see Figure 7.1). Hence, synthetic wastewater prepared using a mixture of humic acid (HA) and TBA (a representative LMW neutral compound) at circumneutral pH was used for investigating the influence of salts on conventional ozonation and HCO performance. We chose to use synthetic wastewaters rather than real CCI concentrate since the salinity of the synthetic wastewaters can be readily varied over the range of concentrations of major interest (i.e., from very low concentrations to concentrations representative of the highest concentrations experienced in real concentrates). In this way, proper controls (with low salt concentration) can be undertaken with results obtained in increasing salt concentration compared. The TOC concentration and Cl^- and SO_4^{2-} of the synthetic wastewater were comparable to that of CCI concentrate obtained from a coal gasification wastewater treatment plant in China (Xintian) as shown in Table 7.1. The method for parameter test in table 7.1 was provided as below. The wastewater was filtered with 0.45μm membrane and the remaining solids after evaporation were measured as the dissolved solids. TOC and soluble COD were quantified in the filtered (0.45μm) wastewater samples. Alkalinity is measured by alkalinity meter. Na^+ is measured by flame atomic adsorption spectrophotometry. Cl^- and SO_4^{2-} were measured by ion chromatography. Ion strength is measured by ion strength meter. LC and GC are performed by Agilent LC and GC systems.

Note that we use TBA as the representative LMW neutral compound in these studies since the COD and TOC removal during ozonation of TBA containing synthetic wastewater and COD/TOC removal for LMW neutrals in real CCI concentrates was comparable.[252] Furthermore, RO membranes used in coal chemical wastewater treatment are expected to exhibit a very high rejection (99%) for LMW alkanes such as TBA, resulting in their accumulation in the concentrate. Thus, the LMW neutral compounds in CCI concentrates are expected to have structure similar to TBA making TBA a reasonable representative of LMW neutral compounds present in CCI concentrates.

Based on our results, we provide important insights into the influence of salts on the conventional ozonation and catalytic ozonation processes. We have also developed a mathematical kinetic model which can predict "salt effect" on the ozone decay and oxidation of oxalate under a range of conditions by both conventional ozonation and catalytic ozonation process.

Table 7.1 Composition of real CCI concentrates and synthetic wastewater employed in this study.

Items	Unit	Real wastewater	Synthetic wastewater
pH		7.8 − 8.0	8.3
Ionic Strength	M	NA	0.21
Dissolved solids	mg/L	8208 ± 1895	12425
TOC	mg/L	41.2±1.0	33
Soluble COD	mg/L	112 ± 30	100
Alkalinity	mg/L as $CaCO_3$	203 ± 11	200
Na^+	mg/L	2138 ± 788	4290
Cl^-	mg/L	1640 ± 338	2427
SO_4^{2-}	mg/L	4455 ± 1190	5679

Note that there are other cations with concentration below 200 mg/L present in the real wastewater such as Mg^{2+}, Ca^{2+} and K^+ which are not listed.

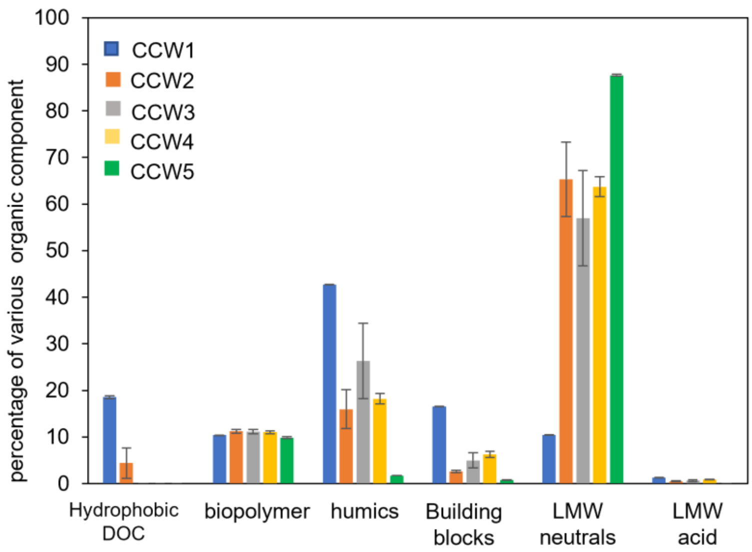

Figure 7.1 LC–OCD analysis of the organic components of various CCI concentrate samples (adapted from Kong *et al.*[252] CCW1 represents coking wastewater samples from the Qian-an treatment plant, CCW2 and CCW3 represents the RO concentrate from a coal gasification wastewater treatment plant (Xintian), CCW4 represents another RO concentrate sample from a treatment facility for coal gasification

wastewater.CCW5 represents a combined stream of concentrates from the ion exchange and RO units used for treatment of methanol synthesis wastewater (Zhongmei Yuanxing), which was further treated using coagulation and ultrafiltration prior to collection.

7.2 Experimental Methods

7.2.1 Reagents

All experiments were performed at a constant pH of 8.3 or 4.0 with a maximum pH variation of ± 0.3 units observed during experiments. In the case of studies at pH 8.3, solutions were maintained at this pH by $NaHCO_3$ buffered solutions as described in chapter 3. For pH 4.0 studies, 0.1 mM HNO_3 solution was used as the buffer solution. We have used Aldrich humic acid as the representative of humic substances present in the CCI concentrates. A 1.0 g/L stock solution of HA sodium salts was prepared in MQ water and filtered using 0.22 µm PVDF filters (Millipore) prior to use. The TOC of the filtered HA stock solution was around 220 mg L^{-1} with pH of 9.0. A 1.1 M stock solution of TBA was prepared in MQ by dilution of 10.5 M TBA solution. A 20.0 mM stock solution of oxalate ($C_2O_4^{2-}$) was prepared in MQ water by dissolution of 268.0 mg sodium oxalate in 100 mL of MQ. A 1.3 mM stock solution of coumarin was prepared in MQ water. Gas phase ozone was produced from an ozone generator (T4000, 5.0 g L^{-1}, Oxyzone Pty Ltd, Australia) with pure oxygen used as the gas source. The preparation of O_3 stock solution and 1.0 mM indigo solution were described in chapter 3. Synthetic wastewater was prepared using a mixture of 20.0 mg C/L HA, 13.0 mg C/L TBA (total TOC = 33 mg/L and total COD = 60 mg/L), 4.0 g/L NaCl and 8.4 g/L sodium sulphate at pH 8.3 in 2.0 mM $NaHCO_3$ solution. To determine the influence of salts on the performance of the ozonation and catalytic ozonation processes, control experiments were performed using solutions containing 20.0 mg C/L HA and 13.0 mg C/L TBA at pH 8.3 in 2.0 mM $NaHCO_3$ solution. Additional experiments were also performed using synthetic wastewaters containing varying concentrations of NaCl or Na_2SO_4 to determine the influence of varying salt concentration on the ozonation and catalytic ozonation processes. To test the influence of cations, synthetic wastewaters containing 20.0 mg C/L HA, 13.0 mg C/L TBA (total TOC = 33 mg/L and total COD = 60 mg/L), 0.5 g/L $MgCl_2$, 3.4 g/L NaCl and 8.4 g/L sodium sulphate at pH 8.3 in 2.0 mM $NaHCO_3$ solution was used. Note that higher $MgCl_2$ concentrations were not investigated here since Mg^{2+} precipitates as $MgCO_3$ precipitates above 0.5 g/L at pH 8.3.

7.2.2 Catalyst Characterization

The Fe–loaded Al_2O_3 catalyst was provided by the Coal Chemical Research Institute (CCRI, China) using a proprietary preparation procedure. Upon receipt, the catalyst was prewashed with MQ water and then dried at 60ºC prior to use. To characterise the surface properties and composition of the catalyst, SEM–EDX (FEI Nova NanoSEM 230 FE–SEM) was performed. Catalysts were also characterized using XRD (Empyrean II XRD Diffractometer, Malvern Panalytical). The pH_{pzc} was measured using acid–base titration.[179]

7.2.3 Organic characterization

The concentration of organics present in synthetic wastewater was quantified using total organic carbon (TOC) and chemical oxygen demand (COD) measurement. TOC and COD were measured using a Shimadzu TOC analyser and Hach COD reactor respectively. Note that the presence of Cl^- and SO_4^{2-} did not interfere with the COD measurement with similar COD calibration curves obtained in the absence and presence of salts (see Figure 7.2) at the salt concentrations used here. LC–OCD (DOC Labor, Dr. Huber, Germany) analysis of the raw and treated wastewaters was performed to identify the dominant organic components in raw/treated wastewater in the absence and presence of salts using pH 6.85 phosphate buffer as the mobile phase. Note that in LC–OCD, the fractionation is based on steric interaction over a wide range of molecular weights.[253] LC–OCD separates DOC into five different fractions that are routinely referred to as biopolymers (MW > 20000 $g \cdot mol^{-1}$), humic substances (MW ≈ 50 to 1000 $g \cdot mol^{-1}$), building blocks (MW ≈ 300−500 $g \cdot mol^{-1}$), low molecular weight (LMW) acids (MW < 350 $g \cdot mol^{-1}$) and LMW neutrals (MW < 350 $g \cdot mol^{-1}$). The sum of these five fractions is termed as chromatographable DOC. The hydrophobic DOC content was also calculated based on the difference between measured DOC and chromatographable DOC. The fractionation of HA into hydrophilic and hydrophobic fractions in the absence and presence of salts was also performed using XAD resin adsorption techniques as reported earlier.[254, 255] Briefly, 0.5 L of 33.0 mg C/L HA solution at pH 2.0 with and without salts was passed sequentially through XAD–7HP and XAD–4 resins. The organics eluted from the resin represents the hydrophilic fraction (HPI). Subsequently, XAD–7HP and XAD–4 resin were back–eluted with 100 mL of 0.1 M NaOH to desorb the retained organics in each column. Organic compounds retained by the XAD–7HP resin represents the hydrophobic fraction (HPO) while those retained by the XAD–4 resin corresponds to transphilic fraction (TPI). Note that while XAD resin adsorption techniques measure various fractions of organics for an acidic humic solution (pH 2), LC-OCD fractionation was performed at the *in-situ* pH of the wastewater samples (*i.e* pH 8.3) and hence quantitative comparison of various organic fractions from the two methods may not be correct. However, both these methods can be used for qualitative comparison of the changes in organic fractionation in the absence and presence of salts.

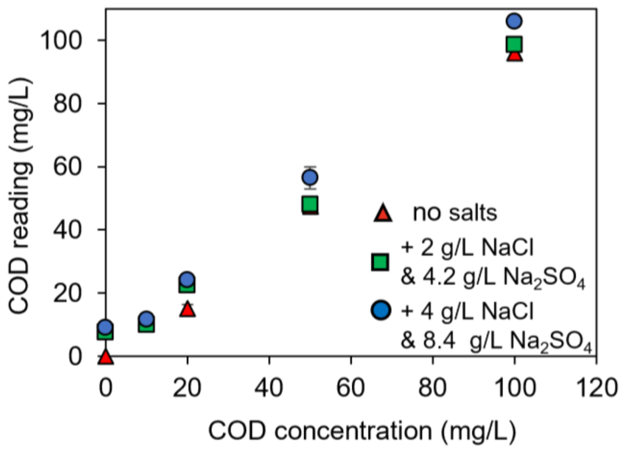

Figure 7.2 COD calibration curve in the absence and presence of salts.

7.2.4 Measurement of oxidation of organics

Oxidation of the organic compounds present in synthetic wastewater by conventional ozonation and catalytic ozonation was carried out in a semi-batch system (as shown in chapter 3). Note that as 10 mL of sample is withdrawn each time, the volume of wastewater in the reactor decreases over time. This decrease in the wastewater volume will have some influence on the kinetics of oxidation of organics, particularly during the later stages of the experiment. However, since all the experiments investigating the influence of salts on TOC/COD removal were conducted under the same conditions with same sampling volume, any difference in the TOC/COD removal observed in the absence and presence of salts is expected to be related to the "salt effect" and not due to the changes in the wastewater volume.

The same experimental setup was used for examination of the oxidation of HA, TBA and $C_2O_4^{2-}$ solutions individually. The removal of HA and TBA was quantified by measuring the TOC and COD of the samples that were periodically removed from the reaction vessel. In the case of TBA, the decrease in TBA concentration and various oxidation products formed after 1 h of reaction were also measured by gas chromatography-mass spectrometry (GC–MS) employing the method described by

Dorubet *et al.*[256] An Agilent mass spectrometer interfaced to a gas chromatograph (GC) and headspace sampler was operated in electron impact GC–MS mode, scanning m/z 34 – 320 at a rate of 4.9 scans/sec for all analyses. The removal of $C_2O_4^{2-}$ was quantified by measuring the $C_2O_4^{2-}$ concentration remaining overtime. The $C_2O_4^{2-}$ concentration was measured using high performance liquid chromatography (HPLC, Agilent 1200 series, USA) employing 10.0 mM H_3PO_4 (20%) and acetonitrile (80%) at a flow rate of 1.0 mL/min as the mobile phase.

7.2.5 Measurement of ozone dissolution

The measurement of O_3 dissolution was performed in the semi-batch system shown in chapter 3. The volume of the synthetic wastewater was fixed at 150 mL (note that the addition of organics was omitted in these experiments to minimize decay of O_3 due to interaction with organics). The flow rate of the gas sparged into the wastewater was controlled at 60.0 ± 0.5 mL/min with a gas-phase ozone concentration of 51 mg/L. At predetermined time intervals (i.e., 10, 20, 30, 40, 60 and 120 min), 1 mL of sample was withdrawn from the reactor and the dissolved O_3 concentration was measured using the indigo method as described in chapter 3.[107]

7.2.6 Measurement of ozone decay

The measurement of O_3 decay was conducted in batch mode as described in detail in chapter 3. Note that the measurement of O_3 decay was performed in batch–mode using a fixed concentration of dissolved O_3 rather than in semi-batch mode to avoid any influence of changes in O_3 dissolution with variation in the solution conditions. For measurement of catalyst-mediated O_3 decay, a known volume of ozone stock solution was spiked into the air-tight reactor containing pH 8.3 or pH 4.0 buffer solution, 20.0 g/L catalyst, 4.0 g/L NaCl and 8.4 g/L Na_2SO_4. For measurement of O_3 self-decay, the experiment was performed in the absence of catalyst. Subsequently, 1.0 mL of sample was withdrawn at regular time intervals and the residual ozone concentrations in the sample was measured using the indigo method.[107] To determine the influence of salts, control experiments (for both catalyst mediated O_3 decay and O_3 self–decay) were performed in pH 8.3 (2.0 mM $NaHCO_3$) or pH 4.0 (0.1 mM HNO_3) solution in the absence of salts.

7.2.7 Fluorescence microscopy image analysis

We used fluorescence microscopy image analysis to measure the generation of surface associated $^{\bullet}OH$ during HCO using coumarin as the probe. The detailed method was described in chapter 5. For measurement, 100.0 µM of dissolved O_3 was added to pH 8.3 buffer solution containing 0.1 g/L of ground catalyst, 4.0 g/L NaCl and 8.4 g/L Na_2SO_4. Note that ground catalyst was used in these experiments to enhance the adsorption of coumarin on the catalyst surface.

7.2.7 Kinetic modelling

Kinetic modelling of ozone decay and oxalate oxidation was performed employing the software package Kintecus [257] by extending the kinetic model for ozone self–decay and oxalate oxidation described in chapter 4 and chapter 5 respectively .

7.3 Results and Discussion

7.3.1 Catalyst characterization

Figure 7.3 shows the morphology and elemental distribution of the catalyst. As shown, the catalyst is mainly composed of Al, Mn and Fe oxides with Al: Mn: Fe mass concentration ratio of ~ 31.3:2.5:17.8. The cross–sectional analysis of the catalyst using SEM–EDX shows that elements are distributed throughout the catalyst structure and the catalyst is not of core-shell structure. The XRD patterns reveal the presence of hematite (01–084–9870), Al_2O_3 (00–046–1131) and MnO_2 (04–009–8106) which correlate well with the elements detected by SEM–EDX. The pH_{pzc} of the catalyst was around 8.4 indicating that the catalyst surface should be slightly positively charged at pH 8.3.

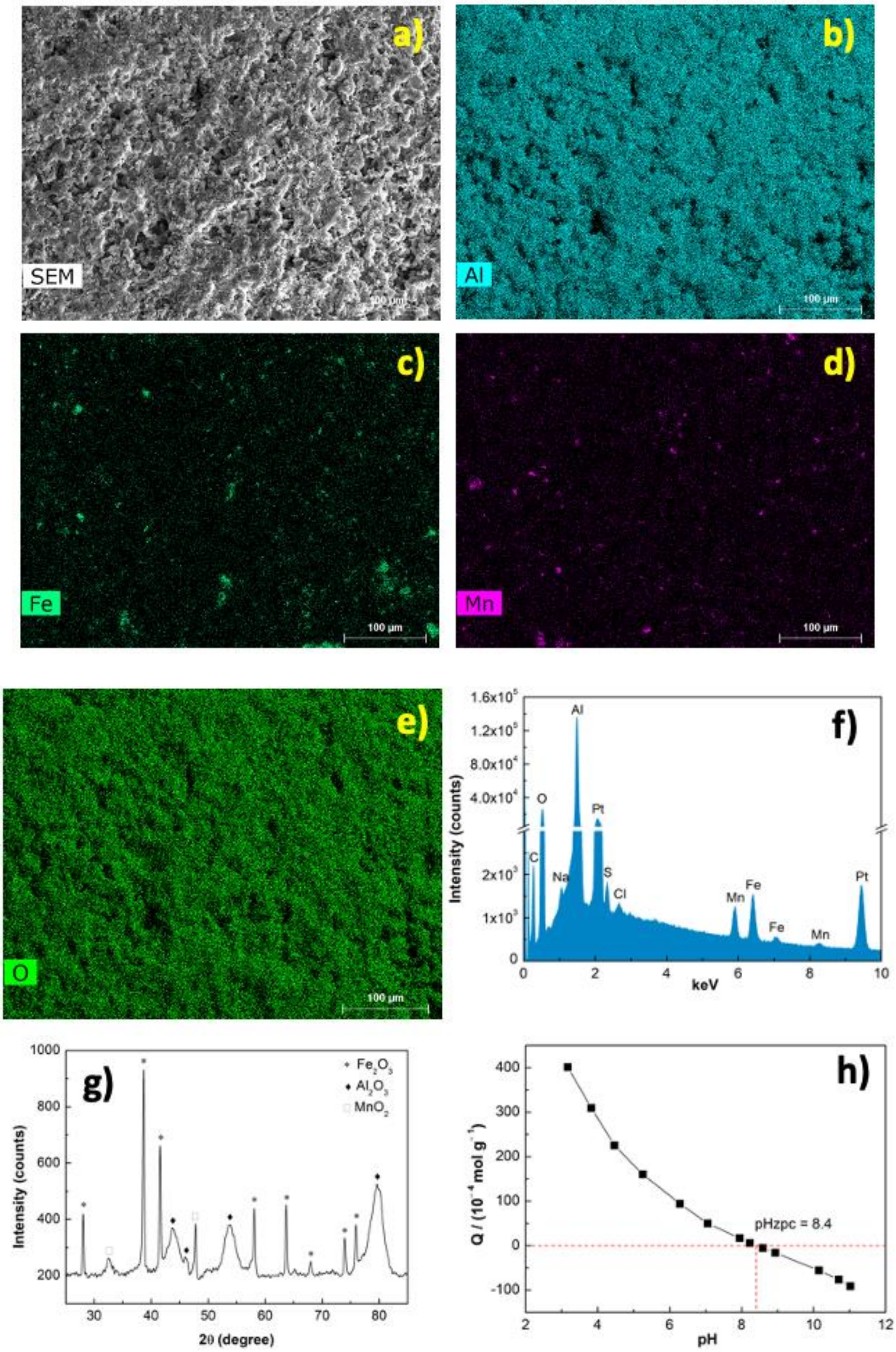

Figure 7.3 Secondary electron image (a), element map of Al, Fe, Mn and O (panels b-e) and EDX spectrum (f) of catalyst using SEM-EDX. Panel g shows the XRD spectrum of the catalyst. Panel h shows surface charge as function of pH. Experimental conditions for surface charge measurement: $[\text{catalyst}]_0 = 10.0$ g L^{-1} in 0.1 M $NaNO_3$.

7.3.2 Mechanism of catalytic ozonation in the absence of salts

In order to gain insights into the effect of salts on the catalytic ozonation process, it is firstly necessary to understand the mechanism of catalytic ozonation process in the absence of salts. Thus, we investigated the mechanism of the catalytic ozonation prior to investigating the influence of salinity on the process. To probe the mechanism of catalytic ozonation in the absence of salts, we measured the oxidation of $C_2O_4^{2-}$, an ozone resistant compounds [258] which has a well-defined oxidation pathway and results in formation of CO_2 and H_2O as the only products. As can be seen in Figure 7.4, the rate and extent of $C_2O_4^{2-}$ oxidation in the presence of the catalyst is higher than that measured in the absence of the catalyst suggesting that the catalyst facilitates generation of oxidants (such as $^{\bullet}OH$) that are capable of oxidizing $C_2O_4^{2-}$. Our results further show that complete inhibition of $C_2O_4^{2-}$ oxidation was observed in the presence of TBA (a bulk $^{\bullet}OH$ scavenger [80] confirming that the oxidation of $C_2O_4^{2-}$ occurs in the bulk solution. Due to short lifetime of $^{\bullet}OH$, it is also possible that the oxidation of $C_2O_4^{2-}$ occurs in the interfacial boundary layer with $^{\bullet}OH$ present in this region as a result of diffusion from the surface. Although TBA has a weak affinity for the catalyst surface,[259, 260] it may scavenge the $^{\bullet}OH$ present in the interfacial region. Overall, it appears that O_3 decays on the catalyst surface forming surface–located $^{\bullet}OH$ which then diffuse away from the surface and interact with organic compounds present in the interfacial boundary layer and/or bulk solution. The strong fluorescence signals corresponding to 7–HC on the surface of catalyst (Figure 7.5) confirms the generation of surface $^{\bullet}OH$ resulting from O_3 and catalyst interaction. However, the contribution of surface associated $^{\bullet}OH$ in oxalate oxidation is minimal due to low surface affinity of oxalate.

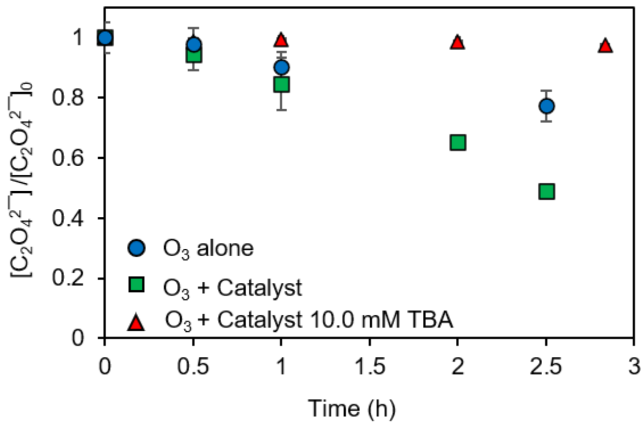

Figure 7.4 Oxidation of $C_2O_4^{2-}$ in the absence (circles) and presence of 10.0 mM TBA (squares) by catalytic ozonation. Symbols represents the average of duplicate measurements; error bars represent the standard deviation of measurement. Experimental conditions: pH = 8.3, O_3 gas flow rate = 60.0 ±0.5 mL/min, reactor volume =150 mL, $[C_2O_4^{2-}]$ = 2.75 mM, $[\text{catalyst}]_0$ = 20.0 g/L.

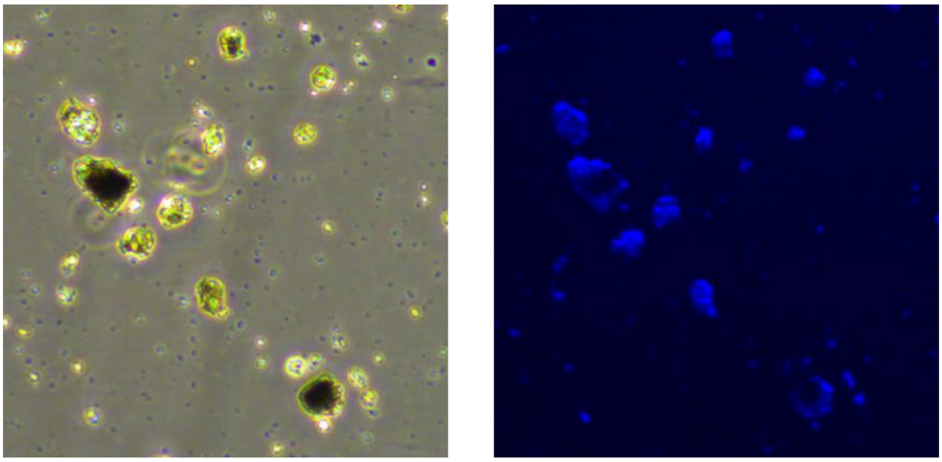

Figure 7.5 Fluorescence images of catalysts following 1 h reaction with O_3 and coumarin at pH 8.3. Experimental conditions: $[O_3]_0$ = 100.0 µM, $[\text{catalyst}]_0$ = 0.1g L^{-1}, $[\text{coumarin}]_0$ =10.0 µM. Note that we used ground catalyst for these measurements.

7.3.3 Influence of salts on the catalytic ozonation process

7.3.3.1 COD and TOC removal on oxidation of synthetic wastewater

As shown in Figure 7.6, 33.1±3.7% and 41.1±5.5% of TOC and COD were removed respectively following 60 mins of conventional ozonation of the synthetic wastewater with no added salts. Furthermore, the presence of salts (Na^+, Cl^- and SO_4^{2-}) had no influence (*p*> 0.05 using single tailed student's *t*-test) on the TOC and COD removal by conventional ozonation (Figure 7.6a and 7.6c). During catalytic ozonation of the synthetic wastewater in the absence of added salts (other than the $NaHCO_3$ buffer), higher COD removal (72.0±6.1%) was achieved (Figure 7.6d) over the same time period compared to that observed during the conventional ozonation process (41.1±5.5%) with these results suggesting that the catalyst is effective in enhancing the oxidation of the organic compounds present (i.e., HA and TBA). However, the presence of salts inhibited COD removal by the catalytic ozonation process with the COD removal in high salinity waters (39.5±5.9%; Figure 7.6d) similar to that measured during the conventional ozonation process. No influence of salts on TOC removal by catalytic ozonation was observed (Figure 7.6b). This lack of influence of salts on TOC removal but significant influence on COD removal suggests that while the total carbon mineralized in the absence and presence of salts is similar, different intermediate oxidation products are formed with these products exhibiting differing susceptibility to attack by the dichromate oxidant used in COD measurement. This hypothesis agrees with the difference in the organic fractions present following oxidation of synthetic wastewaters by the catalytic ozonation process in the absence and presence of salts (Figure 7.7). As shown, while compounds classified as “building blocks” are the main fraction remaining following treatment in the absence of salts, LMW neutral compounds are the dominant organic fraction remaining in the presence of salts with this difference in the nature of the oxidation products responsible for the difference in the COD measurements. We would also like to highlight that at the salt concentration investigated here (i.e., 4g/L NaCl and 8.4 g/L Na_2SO_4), the observed effect of salts on COD removal during catalytic ozonation is due to the presence of chloride ions since (i) the observed COD removal in the presence of chloride ions alone is similar to that observed in the presence of chloride and sulphate ions and (ii) no significant influence of sulphate ions was observed on COD removal (Figure 7.8). However, increasing the sulphate ion concentration to ≥ 20 g/L causes slight inhibition of COD removal following oxidation by catalytic ozonation (Figure 7.9a). In contrast, increasing the chloride ion concentration beyond 2 g/L did not result in further inhibition of COD removal (Figure 7.9b). No influence of higher chloride and/or sulphate concentration was observed on TOC removal. Our results further show that higher adsorption of untreated (HA and TBA) and treated organics on the catalyst surface was observed in the presence of salts (Figure 7.10) with this effect most likely a result of compression of the electric double layer (EDL), thereby facilitating adsorption of organics to the catalyst surface. This observation confirms that the decrease in COD removal in the presence of salts during the catalytic ozonation process is not due to inhibition of sorption of organics on the catalyst surface.

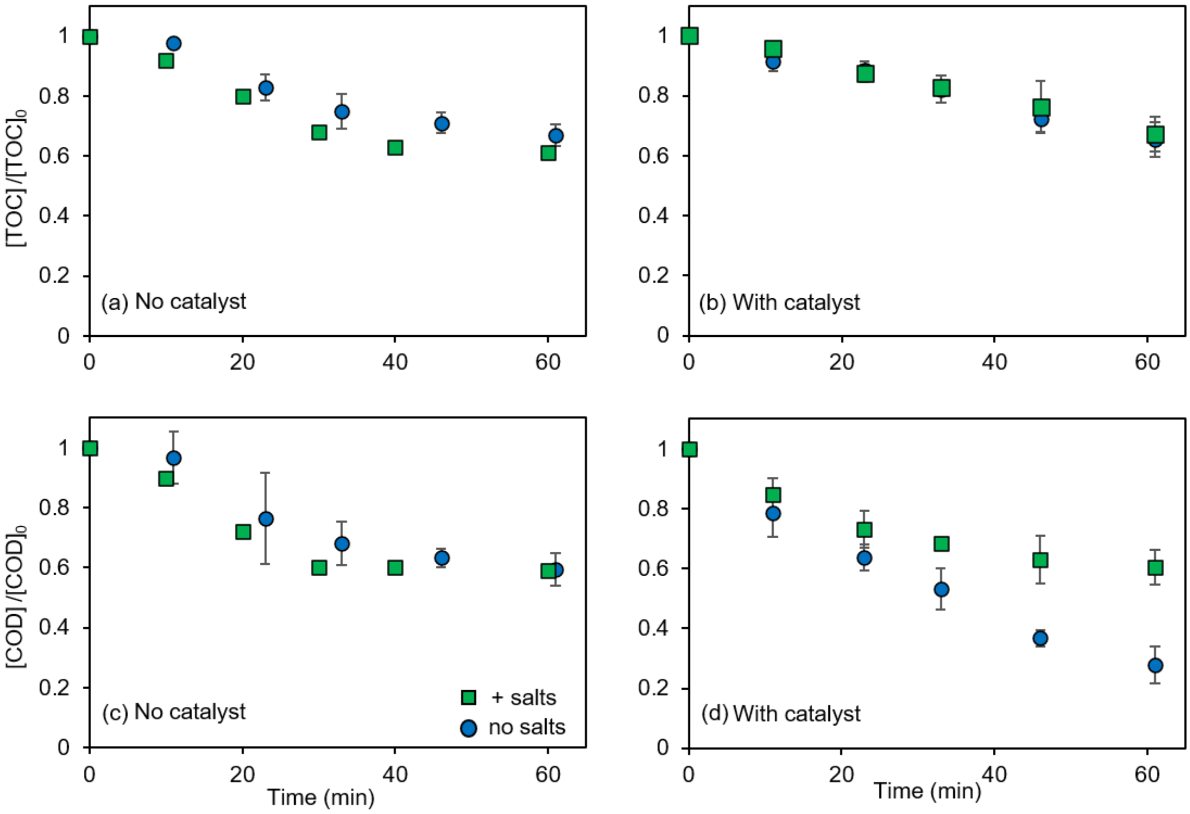

Figure 7.6 Measured decrease in TOC (panels a & b) and COD (panels c & d) during conventional ozonation (panels a & c) and catalytic ozonation (panels b & d) of synthetic wastewater (20.0 mg C/L HA + 13.0 mg C/L TBA) in the absence (circles) and presence of salts (squares). Symbols represents the average of duplicate measurements; error bars represent the standard deviation of measurement. Experimental conditions: pH = 8.3, O_3 gas flow rate = 60.0±0.5 mL/min, flow rate = 51 mg/L, reactor volume = 150 mL, [salt] = 4.0 g/L NaCl + 8.4 g/L Na_2SO_4), [catalyst]$_0$ = 20.0 g/L.

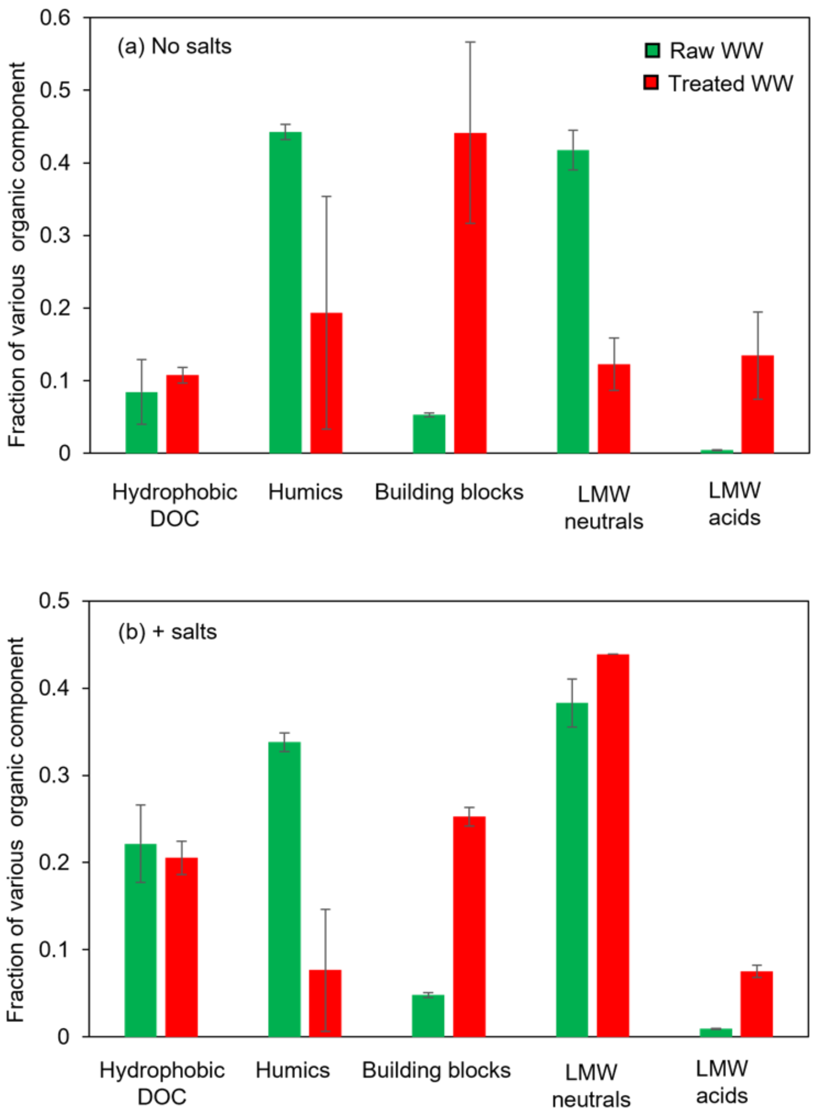

Figure 7.7 Measured organic composition of raw (green bars) and treated synthetic wastewater (red bars) using catalytic ozonation in the absence and presence of salts. Bars represents the average of duplicate measurements; error bars represent the standard deviation of measurement. Experimental conditions: pH = 8.3, O_3 gas flow rate = 60.0±0.5 mL/min, flow rate = 51 mg/L, reactor volume =150 mL; [Catalyst] = 20 g/L; [salt] = 4.0 g/L NaCl + 8.4 g/L Na_2SO_4; reaction time = 60 min.

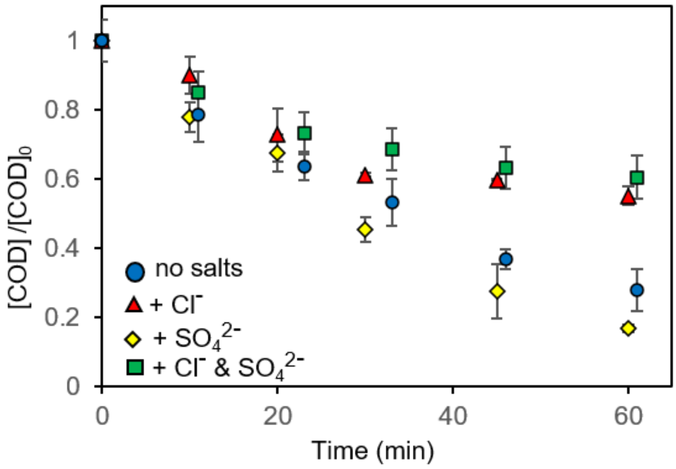

Figure 7.8 Measured decrease in COD during catalytic ozonation of synthetic wastewater (20 mg C/L HA + 13 mg C/L TBA) in the absence (circles) and presence of 4.0 g/L NaCl (triangles), 8.4 g/L Na_2SO_4 (diamonds) and 4 g/L NaCl + 8.4 g/L Na_2SO_4 (squares). Experimental conditions: pH = 8.3, O_3 gas flow rate = 60.0±0.5 mL/min, flow rate = 51 mg/L, reactor volume =150 mL; [catalyst]$_0$ =20.0 g/L.

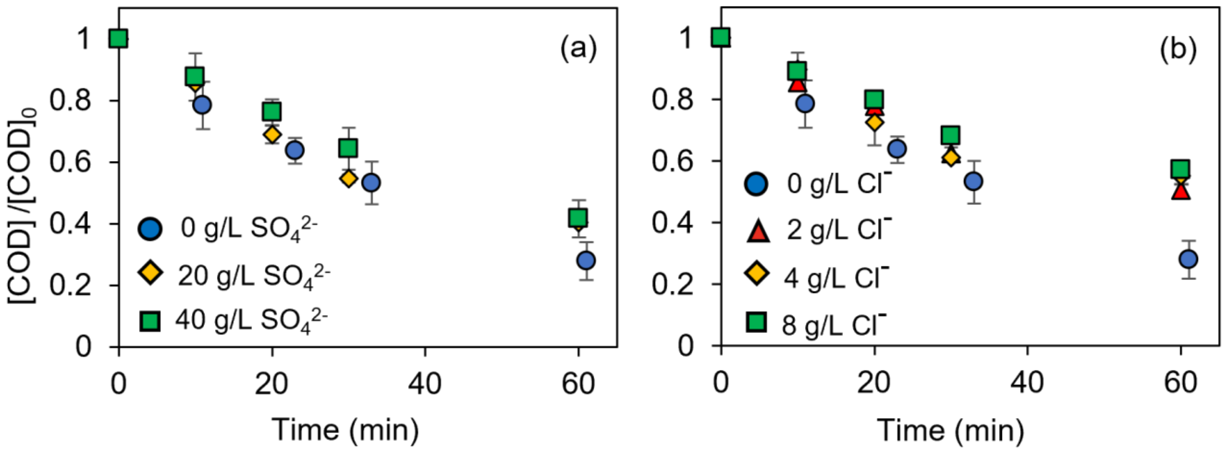

Figure 7.9 Measured decrease in COD during catalytic ozonation of synthetic wastewaters (containing 20.0 mg C/L HA + 13.0 mg C/L TBA) in the presence of varying sulphate concentration (a) and chloride concentration (b). Symbols represents the average of duplicate measurements; error bars represent the standard deviation of measurement. Experimental conditions: pH = 8.3, O_3 gas flow rate = 60.0±0.5 mL/min, flow rate = 51 mg/L, reactor volume =150 mL; [salt] = as specified in legend, [catalyst]$_0$ = 20.0 g/L.

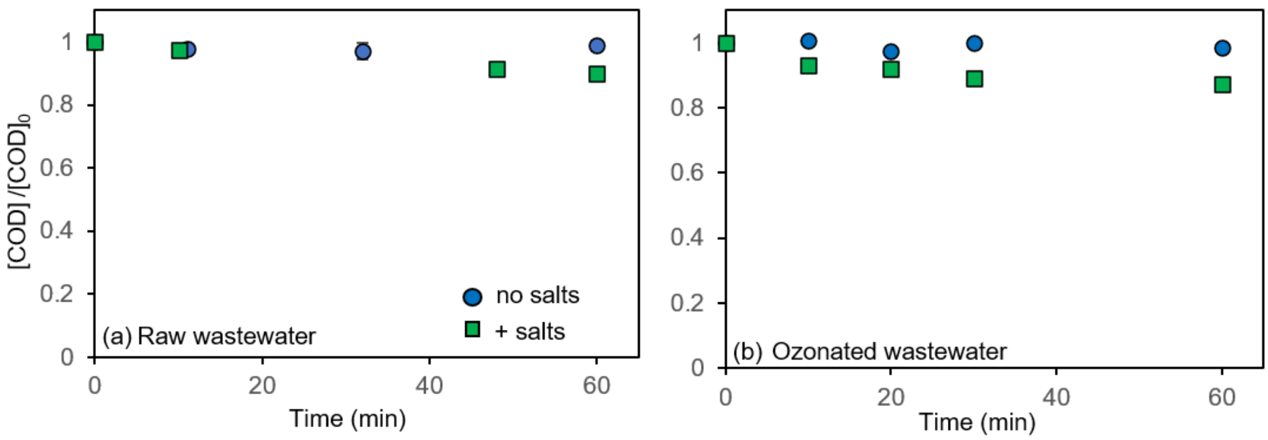

Figure 7.10 Measured removal of organics in raw wastewater (a) and pre-ozonated wastewater (b) as a result of sorption on the catalyst surface. Experimental conditions: pH = 8.3, reactor volume =150 mL; [salt] = 4.0 g/L NaCl + 8.4 g/L Na_2SO_4 ; [catalyst]$_0$ =20.0 g/L.

We also measured the TOC and COD removal of HA and TBA solutions in order to determine the influence of salts on the oxidation of these organic compounds separately. As shown in Figure 7.11, slower COD removal of pure HA solution by both conventional ozonation and catalytic ozonation processes in the presence of salts was observed however no influence of salts on TOC removal was apparent. One important point to note here is that while COD is completely removed following the oxidation of HA for 1 h by the ozonation/catalytic ozonation process, a significant amount of TOC is still present (Figure 7.11) suggesting that some of the oxidation products of HA cannot be oxidized using the COD reagents. The trend of varying chloride and sulphate concentrations on TOC/COD removal of HA solution (Figures 7.12) is the same as that observed in the case of the synthetic wastewaters containing a mixture of HA+TBA (Figure 7.9); however, the effect of salts on oxidation of pure HA solution is more prominent. Slower COD removal of pure TBA solution was observed in the presence of salts during conventional ozonation and catalytic ozonation (Figure 7.13a and 7.13b) confirming that the rate of oxidation of TBA and/or its oxidation products is also influenced by salts. Measurement of TBA concentration after 1 h (Figure 7.13c) shows that there was no influence of salts on TBA oxidation by conventional ozonation, however, significant influence ($p > 0.05$ using single tailed student's t–test; 67.3±4.4% and 52.2±8.8% TBA removal in the absence and presence of salts, respectively) of salts on TBA removal by catalytic ozonation was observed suggesting that the influence of salts on the extent of TBA oxidation is unimportant in the case of conventional ozonation but is significant during the catalytic ozonation process. As shown in Figure 7.14, the same oxidation products (i.e., methanol, acetaldehyde, formaldehyde and acetone) are formed after 1 h of oxidation of TBA by conventional ozonation in the absence and presence of salts with this result in accord with the minimal difference observed in COD removal observed after 1h in the absence and presence of salts. During the catalytic ozonation process, there is a difference in the oxidation products formed with no formation of methanol observed in the absence of salts. Overall, these results show that the conventional ozonation process is also affected by the presence of salts, at least for organic compounds such as humic acids and TBA. Interestingly, while the influence of salts on the conventional ozonation process is not discernible when synthetic wastewater containing a mixture of TBA and HA is used, the effect of salts is quite evident when HA and TBA are treated separately by conventional ozonation.

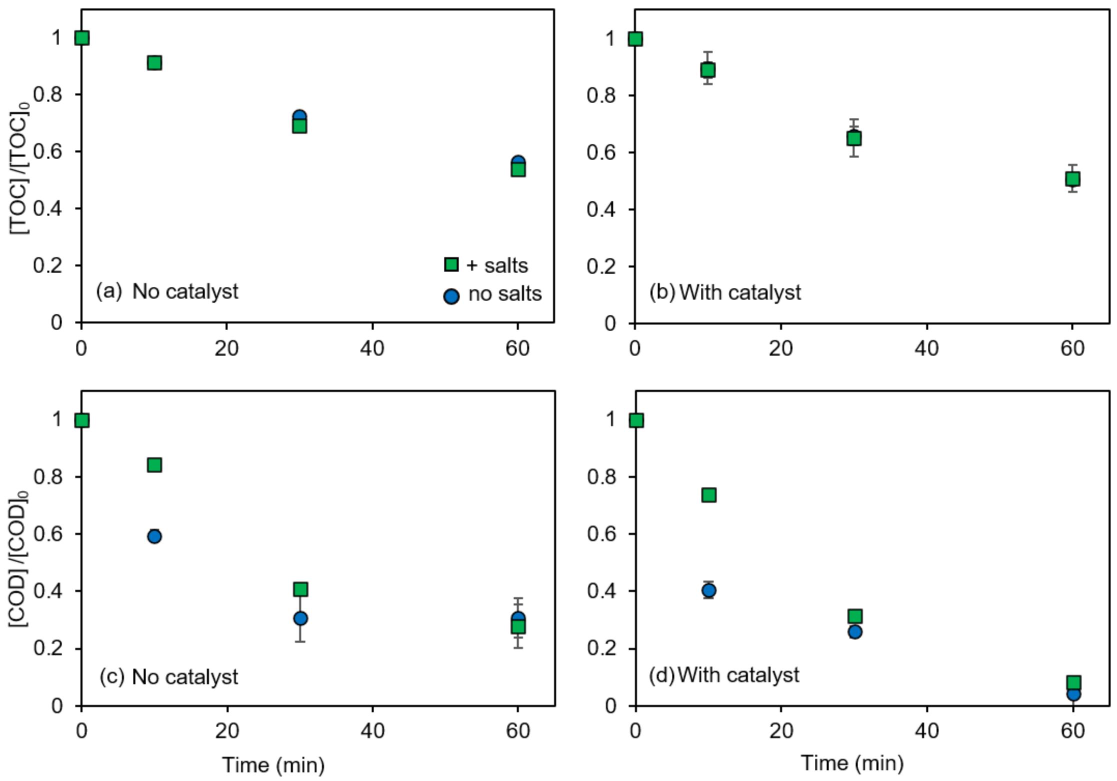

Figure 7.11 Measured decrease in TOC (panels a & b) and COD (panels c & d) during conventional ozonation (panels a & c) and catalytic ozonation (panels b &d) of 33.0 mg C/L HA solution in the absence (circles) and presence of salts (squares). Symbols represents the average of duplicate measurements; error bars represent the standard deviation of measurement. Experimental conditions: pH = 8.3, O_3 gas flow rate = 60.0±0.5 mL/min, flow rate = 51 mg/L, reactor volume = 150 mL, [salt] = 4.0 g/L NaCl + 8.4 g/L Na_2SO_4), $[catalyst]_0$ = 20.0 g/L.

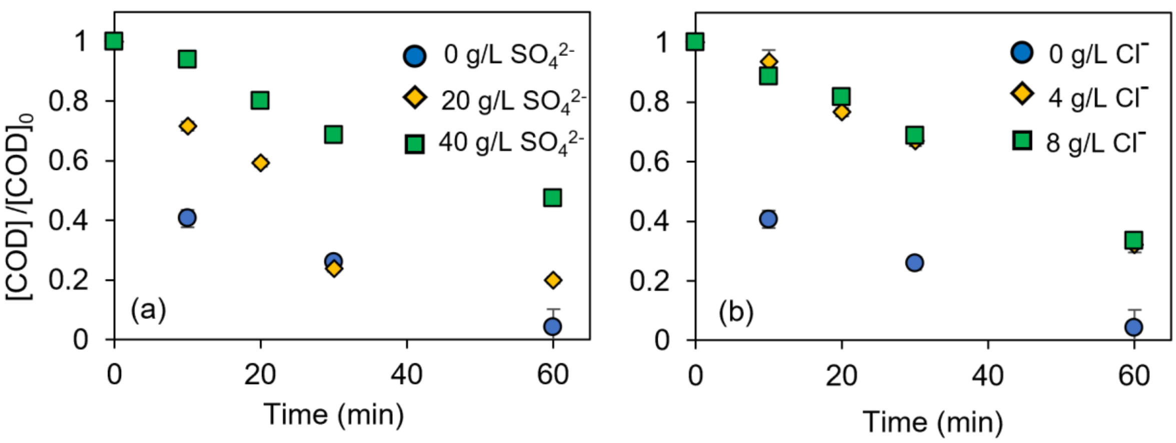

Figure 7.12 Measured decrease in COD during catalytic ozonation of 33 mg C/L HA solution in the presence of varying sulphate concentration (a) and chloride concentration (b). Symbols represents the average of duplicate measurements; error bars represent the standard deviation of measurement. Experimental conditions: pH = 8.3, O_3 gas flow rate = 60.0±0.5 mL/min, flow rate = 51 mg/L, reactor volume =150 mL; [salt] = as specified in legend, $[catalyst]_0$ = 20.0g/L.

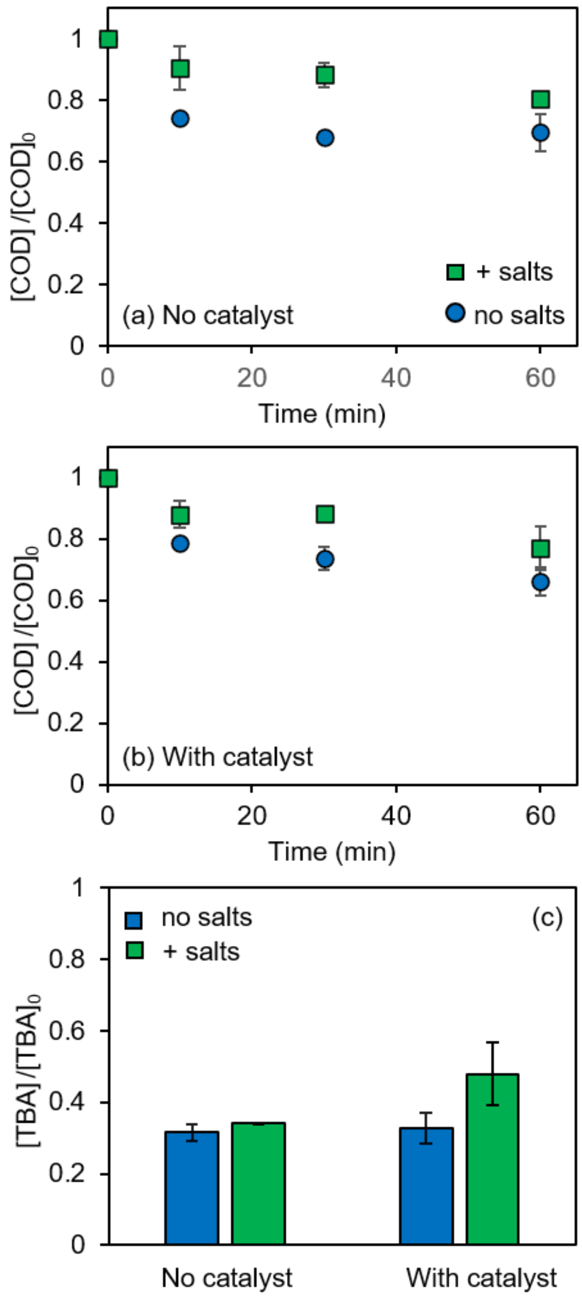

Figure 7.13 Measured decrease in COD during conventional ozonation (a) and catalytic ozonation (b) of 33.0 mg C/L TBA solution in the absence (circles) and presence of salts (squares). Panel c shows the concentration of TBA remaining after 1 h of oxidation by conventional ozonation and catalytic ozonation process. Symbols represents the average of duplicate measurements; error bars represent the standard deviation of measurement. Experimental conditions: pH = 8.3, O_3 gas flow rate = 60.0±0.5 mL/min, flow rate = 51 mg/L, reactor volume = 150 mL, [salt] = 4.0 g/L NaCl + 8.4 g/L Na_2SO_4, [catalyst]$_0$ = 20.0g/L.

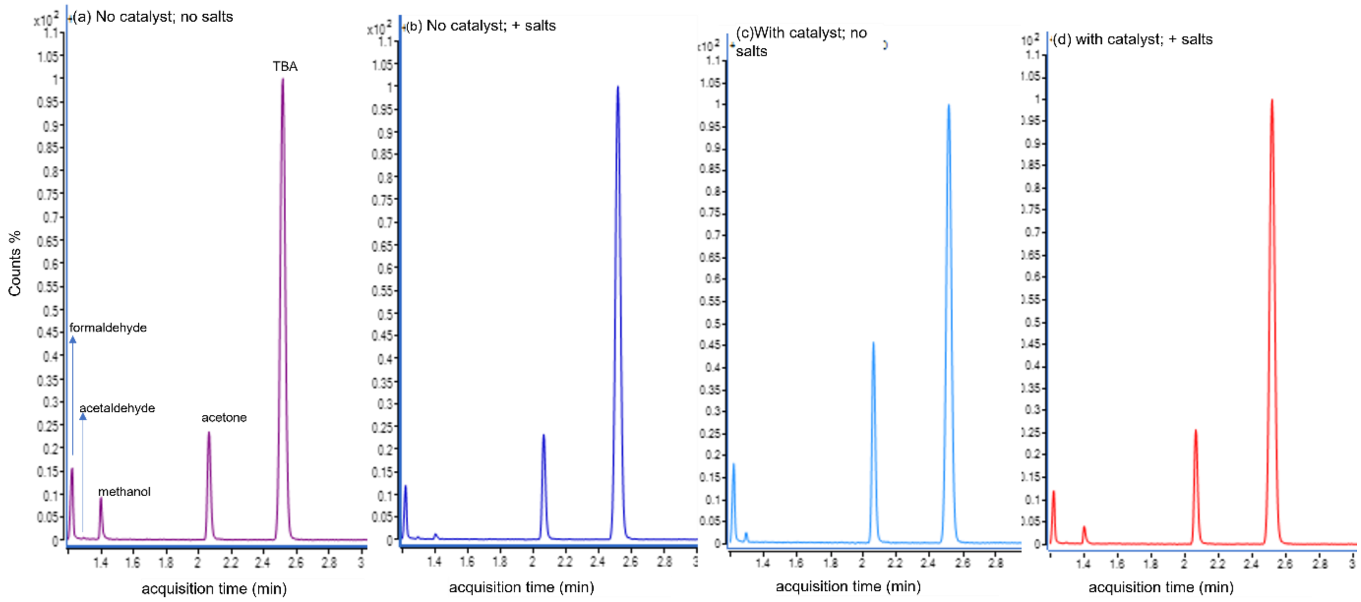

Figure 7.14 GC-MS spectrum of treated 33 mg C/L TBA solution. Experimental conditions: pH = 8.3, O_3 gas flow rate = 60.0±0.5 mL/min, flow rate = 51 mg/L, reactor volume =150 mL; [salt] = 4 g/L NaCl +8.4 g/L Na_2SO_4, $[catalyst]_0$ = 20.0g/L; reaction time = 60 min.

The decreased COD removal in high salinity waters is possibly due to:

(i) Scavenging of bulk oxidants (O_3 and hydroxyl radicals) by salt anions;

(ii) Decrease in the dissolution of O_3(g);

(iii) Inactivation of active sites (for O_3 decay) due to salt sorption;

(iv) Alteration in the nature of the organics as a result of the presence of salts;

(v) Scavenging of surface oxidants (i.e., surficial O_3 and/or oxidants generated on catalyst–O_3 interaction) by salts.

Results from a variety of control experiments that were undertaken to ascertain the reasons for the inhibition of COD removal in the presence of salts are presented in the following sections. The studies undertaken included investigation of the impact of salts on O_3 decay, O_3 dissolution, raw and treated organic characteristics and catalyst structure.

7.3.3.2 Influence of salts on ozone decay

As shown in Figure 7.15a, the rate of ozone self-decay slightly increases in the presence of salts. The slight increase in O_3 decay in the presence of salts is possibly due to reaction of O_3 with chloride ions (eqs. 7.1-7.4 [243]):

$$O_3 + Cl^- \longrightarrow O_2 + OCl^- \tag{7.1}$$

$$O_3 + OCl^- \longrightarrow 2O_2 + Cl^- \tag{7.2}$$

$$O_3 + OCl^- \longrightarrow O_2 + ClO_2^- \tag{7.3}$$

$$O_3 + ClO_2^- \longrightarrow O_2 + ClO_3^- \tag{7.4}$$

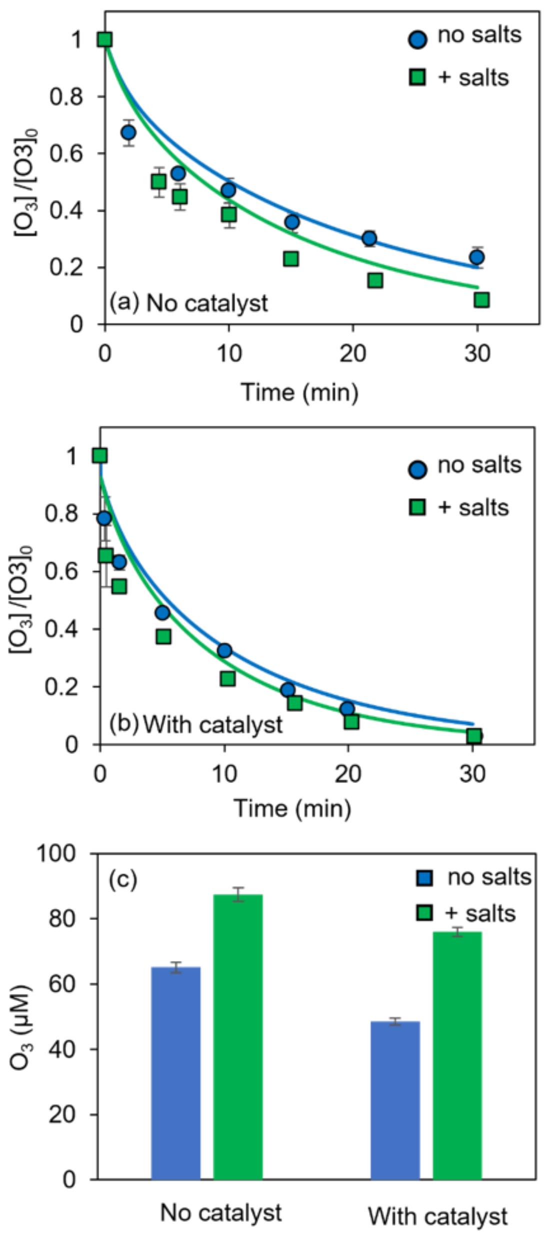

Figure 7.15 Measured O_3 self–decay (a) and catalyst mediated O_3 decay (b) in the absence (circles) and presence (squares) of salts. Experimental conditions: $[O_3]_0$ =100 µM; $[catalyst]_0$ = 20.0 g/L [salt] = 4.0 g/L NaCl and 8.4 g/L Na_2SO_4, pH = 8.3. Panel c shows measured dissolved O_3 concentration at O_3 gas flow rate of 60.0±0.5 mL/min in the absence and presence of salts during conventional ozonation and catalytic ozonation. Symbols represents the average of duplicate measurements; error bars represent the standard deviation of measurement. Lines represents model values. Experimental conditions: pH = 8.3, reactor volume =150 mL, flow rate = 51 mg/L, O_3 gas flow rate = 60.0±0.5 mL/min; [salt] = 4.0 g/L NaCl + 8.43 g/L Na_2SO_4, $[catalyst]_0$ = 20.0g/L.

Combining the kinetic model developed for O_3 self–decay in chapter 4 with the reactions shown in eqs. 7.1 – 7.4, we modelled the effect of salts on ozone self-decay (Table 7.2 and 7.3). As shown in Figure 7.15a, the slightly enhanced O_3 decay in the presence of salts can be explained by the reactions shown in eqs. 7.1 – 7.4. This futile decay of ozone via interaction with the chloride ions may have significant influence on the oxidation of organics during both the conventional ozonation and catalytic ozonation processes. Note that based on the kinetic model presented here, the scavenging of bulk hydroxyl radicals by salt anions is unimportant at pH 8.3 which agrees with the earlier report [261] and suggests that scavenging of bulk hydroxyl radical by salt anions is not responsible for the decrease in the conventional ozonation/catalytic ozonation performance in the presence of salts.

Table 7.2 Reaction set and associated constants for ozone self–decay and catalyst mediated O_3 decay in the absence and presence of salts.

No	Reaction	Rate Constant ($M^{-1}\cdot s^{-1}$) pH 8.3	pH 4.0
1	$O_3 + OH^- \longrightarrow HO_2^\bullet + O_2^{\bullet-}$	70.0	70.0
2	$O_3 + H_2O_2/HO_2^- \longrightarrow HO_3^\bullet + O_2^{\bullet-}$	1.7×10^{3a}	8.9×10^{-2a}
3	$O_3 + O_2^{\bullet-} \longrightarrow HO_3^\bullet + O_2$	1.5×10^{9}	2.1×10^{8}
4	$HO_3^\bullet/O_3^{\bullet-} \longrightarrow {}^\bullet OH + O_2$	6.3×10^{4b}	1.4×10^{5b}
5	${}^\bullet OH + O_3 \longrightarrow O_2^{\bullet-} + O_2$	1.0×10^{8}	1.0×10^{8}
6	$CO_3^{\bullet-} + O_3 \longrightarrow H_2CO_3 + O_2$	1.0×10^{5}	1.0×10^{5}
7	${}^\bullet OH + H_2O_2/HO_2^- \longrightarrow H_2O + O_2^{\bullet-}$	3.2×10^{7a}	2.7×10^{7a}
8	${}^\bullet OH + H_2CO_3/HCO_3^-/CO_3^{2-} \longrightarrow H_2O + CO_3^{\bullet-}$	1.2×10^{7c}	1.1×10^{6c}
9	$CO_3^{\bullet-} + H_2O_2/HO_2^- \longrightarrow H_2CO_3 + O_2^{\bullet-}$	4.3×10^{5a}	4.3×10^{5a}
10	$CO_3^{\bullet-} + CO_3^{\bullet-} \longrightarrow H_2CO_3 + CO_4^{2-}$	2.0×10^{7}	2.0×10^{7}
	O_3 loss via interaction with salts[262]		
11	$O_3 + Cl^- \longrightarrow OCl^- + O_2$	3.0×10^{-3}	3.0×10^{-4}
12	$O_3 + OCl^- \longrightarrow Cl^- + 2O_2$	1.1×10^{2}	1.1×10^{2}
13	$O_3 + OCl^- \longrightarrow ClO_2^- + O_2$	3.0×10^{1}	3.0×10^{1}
14	$O_3 + ClO_2^- \longrightarrow ClO_3^- + O_2$	4.0×10^{6}	4.0×10^{6}
	Bulk scavenging of hydroxyl radicals by salts		
	See Table 7.3[d]		
	O_3 decay in the presence of catalyst		
15	$O_3 + \equiv \leftrightarrow \equiv O_3$	$K=7.5\times10^{1b}$	$K=7.5\times10^{1b}$
16	$\equiv O_3 + \equiv \longrightarrow \equiv {}^\bullet OH$	8.0×10^{-3}	1.6×10^{-3}
17	$\equiv O_3 + \equiv Cl^- \longrightarrow \equiv OCl^- + O_2$	3.0×10^{-3d}	3.0×10^{-4d}
18	$\equiv O_3 + \equiv OCl^- \longrightarrow \equiv Cl^- + 2O_2$	1.1×10^{2}	1.1×10^{2}

19	$\equiv O_3 + \equiv OCl^- \longrightarrow \equiv ClO_2^- + O_2$	3.0×10^{1}	3.0×10^{1}
20	$\equiv O_3 + \equiv ClO_2^- \longrightarrow \equiv ClO_3^- + O_2$	4.0×10^{6}	4.0×10^{6}
	$\equiv HO^{\bullet}$ decay[e]		
21	$\equiv {}^{\bullet}OH + \equiv \longrightarrow NRP$	>0.1	
22	$\equiv {}^{\bullet}OH + \equiv Cl^- \longrightarrow \equiv HOCl^{\bullet -} \xrightarrow{\equiv} NRP$	$k_{21}/0.2$	
23	$\equiv {}^{\bullet}OH \longrightarrow {}^{\bullet}OH + \equiv$	$k_{21}/10.0$	
	Oxalate oxidation in the bulk solution		
24	$C_2O_4^{2-} + {}^{\bullet}OH \longrightarrow C_2O_4^{\bullet -} + H_2O$	7.7×10^{6}	
25	$C_2O_4^{2-} + CO_3^{\bullet -} \longrightarrow C_2O_4^{\bullet -} + H_2CO_3$	6.0×10^{3}	
26	$C_2O_4^{\bullet -} \longrightarrow CO_2^{\bullet -} + H_2CO_3$	1.0×10^{9}	

[a] calculated value at pH 8.3 /4.0 using the reported rate constant for H_2O_2/HO_2^- and the mole fraction of H_2O_2/HO_2^- at pH 8.3/4.0.
[b] calculated value at pH 8.3/4.0 using the reported rate constant for $HO_3^{\bullet -}$ / $O_3^{\bullet -}$ and the mole fraction of $HO_3^{\bullet -}$ / $O_3^{\bullet -}$ at pH 8.3/4.0.
[c] calculated value at pH 8.3/4.0 using the reported rate constant for $H_2CO_3/HCO_3^-/CO_3^{2-}$ and the mole fraction of for $H_2CO_3/HCO_3^-/CO_3^{2-}$ at pH 8.3/4.0.
[d] radical scavenging reactions by Cl^- and SO_4^{2-} are shown in Table 7.3 however these reactions have no influence on the model output.
[e] the surface chloride ions concentration was determined based on best fit to the measured O_3 decay rates. A 10-fold and ~70 fold higher surface chloride ion concentration compared to bulk concentration at pH 8.3 and 4.0 respectively is determined based on best-fit to our results.

Table 7.3 Radical scavenging reactions in the presence of Cl^- and SO_4^{2-}.[263-265]

No	Reaction	Rate constant ($M^{-1}\cdot s^{-1}$)
1	$SO_4^{\bullet -} (+H_2O) \rightarrow {}^{\bullet}OH + H^+ + SO_4^{2-}$	$4.6 \times 10^2\ s^{-1}$
2	$SO_4^{\bullet -} + SO_4^{\bullet -} \rightarrow S_2O_8^{2-}$	6.1×10^8
3	$SO_4^{\bullet -} + H_2O_2 \rightarrow SO_4^{2-} + HO_2^{\bullet}$	1.2×10^7
4	$Cl^{\bullet} + H_2O_2 \rightarrow Cl^- + H^+ + HO_2^{\bullet}$	2.0×10^9
5	$Cl_2^{\bullet -} + H_2O_2 \rightarrow 2\,Cl^- + H^+ + HO_2^{\bullet}$	1.4×10^5
6	${}^{\bullet}OH + S_2O_8^{2-} \rightarrow OH^- + S_2O_8^{\bullet -}$	1.2×10^7
7	$SO_4^{\bullet -} + S_2O_8^{2-} \rightarrow SO_4^{2-} + S_2O_8^{\bullet -}$	5.5×10^4
8	$Cl^{\bullet} + S_2O_8^{2-} \rightarrow Cl^- + S_2O_8^{\bullet -}$	8.8×10^6
9	$Cl_2^{\bullet -} + S_2O_8^{2-} \rightarrow 2\,Cl^- + S_2O_8^{\bullet -}$	1×10^4
10	$SO_4^{\bullet -} + Cl^- \rightarrow SO_4^{2-} + Cl^{\bullet}$	3.2×10^8
11	${}^{\bullet}OH + Cl^- \rightarrow ClOH^{\bullet -}$	4.3×10^9
12	$ClOH^{\bullet -} + Cl^- \rightarrow Cl_2^{\bullet -} + OH^-$	1.0×10^4

13	$ClOH^{\bullet-} \rightarrow Cl^- + {}^{\bullet}OH$	6.1×10^9
14	$ClOH^{\bullet-} + H^+ \rightarrow Cl^{\bullet} + H_2O$	2.1×10^{10}
15	$Cl^{\bullet} + Cl^- \rightarrow Cl_2^{\bullet-}$	6.5×10^9
16	$Cl^{\bullet} + OH^- \rightarrow ClOH^{\bullet-}$	1.8×10^{10}
17	$Cl^{\bullet} + Cl^{\bullet} \rightarrow Cl_2$	1.0×10^8
18	$Cl^{\bullet} (+H_2O) \rightarrow HClOH^{\bullet}$	2.5×10^5 s^{-1}
19	$Cl_2^{\bullet-} \rightarrow Cl^{\bullet} + Cl^-$	1.1×10^5 s^{-1}
20	$Cl_2^{\bullet-} + O_2^{\bullet-} \rightarrow 2\ Cl^- + O_2$	1.0×10^9
21	$Cl_2^{\bullet-} + OH^- \rightarrow ClOH^{\bullet-} + Cl^-$	4.5×10^7
22	$Cl_2^{\bullet-} + Cl_2^{\bullet-} \rightarrow Cl_2 + 2\ Cl^-$	8.3×10^8
23	$Cl_2^{\bullet-} (+H_2O) \rightarrow HClOH^{\bullet} + Cl^-$	1.3×10^3 s^{-1}
24	$Cl_2^{\bullet-} + {}^{\bullet}OH \rightarrow HOCl + Cl^-$	1.0×10^9
25	$HClOH^{\bullet} \rightarrow ClOH^{\bullet-} + H^+$	1.0×10^8 s^{-1}
26	$HClOH^{\bullet} \rightarrow Cl^{\bullet} + H_2O$	1.0×10^2 s^{-1}
27	$HClOH^{\bullet} + Cl^- \rightarrow Cl_2^{\bullet-} + H_2O$	5.0×10^9
28	$Cl_3^- + O_2^{\bullet-} \rightarrow Cl_2^{\bullet-} + Cl^- + O_2$	3.8×10^9
29	$Cl_2 + O_2^{\bullet-} \rightarrow Cl_2^{\bullet-} + O_2$	1.0×10^9
30	$HOCl + {}^{\bullet}OH \rightarrow ClO^{\bullet} + H_2O$	8.0×10^9
31	$HOCl + O_2^{\bullet-} \rightarrow Cl^{\bullet} + OH^- + O_2$	1.7×10^8
32	$Cl^- + Cl_2 \rightarrow Cl_3^-$	2.0×10^4
33	$Cl_3^- \rightarrow Cl_2 + Cl^-$	1.1×10^5
34	$Cl^- + HOCl \rightarrow Cl_2OH^-$	1.5×10^4
35	$Cl_2 (+H_2O) \rightarrow Cl_2OH^- + H^+$	1.5×10^1 s^{-1}
36	$Cl_2OH^- \rightarrow HOCl + Cl^-$	5.5×10^9 s^{-1}
37	$Cl_2OH^- + H^+ \rightarrow Cl_2 + H_2O$	2.0×10^{10}
38	$Cl_2 + H_2O_2 \rightarrow 2\ HCl + O_2$	1.3×10^4
39	$HOCl + H_2O_2 \rightarrow HCl + H_2O + O_2$	1.5×10^5

The catalyst-mediated ozone decay rate was also slightly higher in the presence of salts compared to that observed in the absence of salts (Figure 7.15b). Characterization of the catalyst surface by SEM–EDX did not show any significant extent of salt sorption on the catalyst surface (Figure 7.16), at least during the short-term studies performed here. This result suggests that the small effect of salts on O_3 decay observed in the presence of catalyst is also due to scavenging of bulk O_3 by the salts rather than the inactivation of surface sites. Kinetic modelling of catalyst mediated O_3 decay (Reactions 15 – 20, Table 7.2) in the presence and absence of salts also confirms that the small change (8.8%) in catalyst mediated O_3 decay rate observed in the presence of salts is due to scavenging of O_3 by the salts with no inhibition of catalyst activity apparent in the presence of salts. Note that the reactions used to describe catalyst mediated O_3 decay in the absence of salts is same as that used for other catalysts used in our work and described in detail in earlier chapters (chapters 4 and 5).

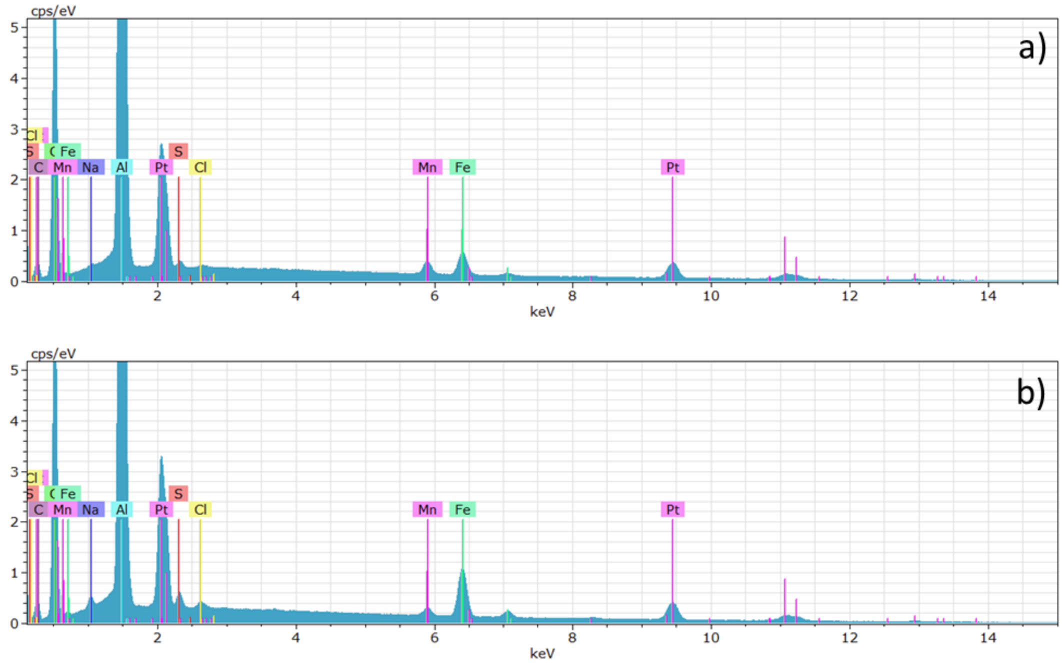

Figure 7.16 EDX spectra of used catalyst following treatment of (a) synthetic wastewater containing no salts or (b) wastewater containing 4 g/L NaCl + 8.4 g/L Na_2SO_4.

7.3.3.3 Influence of salts on ozone dissolution

The difference in Henry's law constant and/or ozone bubble size due to variation in salt concentration may impact gas-phase O_3 dissolution [243, 266-268] and concomitant oxidation of organics. As shown in Figure 7.15c, the measured dissolved O_3 concentration is slightly higher in the absence of catalyst (65.2 ± 1.7 μM) compared to that measured in the presence of catalyst (48.6 ± 1.1 μM) due to the enhanced O_3 decay in the presence of the catalyst (k_{O_3} =0.05 ± 0.03 s^{-1} and $k_{O_3\text{-cat}}$ =0.14 ± 0.04 s^{-1} where k_{O_3} and $k_{O_3\text{-cat}}$ represents the pseudo-first order O_3 decay rate constant in the absence and presence of catalyst calculated using the data shown in Figure 6a and 6b). In both cases (i.e., with and without catalyst), higher dissolved O_3 concentrations are measured in the presence of salts compared to that measured in the absence of salts. Since the measured O_3 decay rate in the presence of salts is slightly higher compared to that measured in the absence of salts (Figure 7.15a and 7.15b), the higher dissolved O_3 concentration in the presence of salts suggests that the dissolution of O_3(g) increases in the presence of salts. The increased dissolution of O_3(g) is in agreement with the results of recent studies [267, 269] and is possibly due to the change in the O_3(g) bubble size in the presence of chloride ions.[267] Moreover, based on an earlier study,[243] the influence of salt on Henry's law constant of O_3(g) at the salt concentration investigated here was considered to be minimal. However, this was contradictory to various earlier studies which suggesting the "salt out" effect on ozone dissolution.[270-273] More controlled experiments are required to draw conclusion on the salting out effect on ozone dissolution.

A higher dissolved O_3 concentration in the presence of salts should result in higher COD removal, however opposite trend is observed here. This observation suggests that the concentration and/or nature of the main oxidant involved in organic oxidation is affected in the presence of salts, thereby resulting in a reduced extent of oxidation of organics, even in the presence of higher O_3 concentration. For example, futile scavenging of O_3 by chloride ions (eqs. 7.1 – 7.4) may decrease the formation of $^{\bullet}OH$ (which is the main oxidant for ozone resistant organics such as TBA present in wastewaters). Furthermore, scavenging of surface $^{\bullet}OH$ by chloride ions may transform surface $^{\bullet}OH$ to chlorine–based radicals [244, 245] which are less reactive than $^{\bullet}OH$, thereby decreasing the rate and extent of oxidation of organics present in wastewaters. Alternatively, it is also possible that the nature of the organics is altered in the presence of salts with this change rendering them less oxidizable. We further discuss these possibilities in detail in the following sections.

7.3.3.4 Transformation of organics in the presence of salts

To determine if there is a difference in the nature of organics in the absence and presence of salts, LC–OCD analysis of HA and TBA solutions was performed. As shown in Figure 7.17, the hydrophobic DOC content of the HA increases in the presence of salts with this effect possibly associated with a change in structure of humics in the wastewater. Measurement of the hydrophobic fraction of HA using the XAD resin fractionating method also showed that the presence of salts slightly increased the hydrophobic fraction (Figure 7.18) in agreement with the LC–OCD results. The changes in the hydrophobic fraction of HA is consistent with the results of an earlier study in which it was reported that humic substances have a branched open structure in low salinity waters but have a more compact structure in high salinity waters [274] with this change in structure associated with the ability of cations (especially divalent species such as Ca^{2+} and Mg^{2+}) to either shield the negatively charged repulsive effects of adjacent functional groups and/or act as bridging cations in inducing intermolecular binding. This hypothesis agrees with the observation that addition of Mg^{2+} had more significant influence on HA oxidation during conventional ozonation/catalytic ozonation compared to that observed in the presence of Na^{+} (Figure 7.19). The increased charge shielding between adjacent functional groups in the presence of Mg^{2+} compared to that observed in the presence of Na^{+},[274] results in increased transformation of HA to more compact and more hydrophobic assemblages.

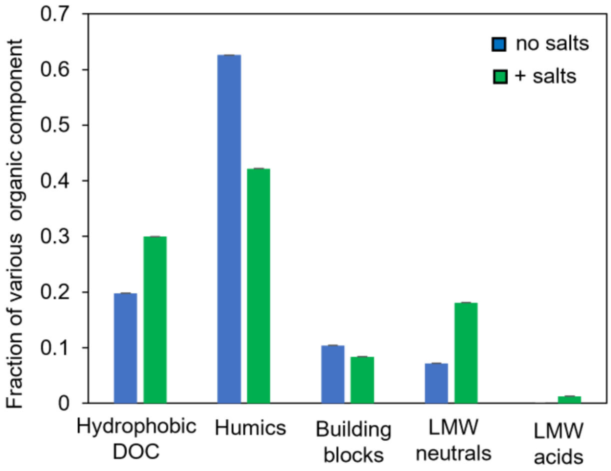

Figure 7.17 Measured organic composition of HA in the absence and presence of salts using LC-OCD. Bars represents the average of duplicate measurements; error bars represent the standard deviation of duplicate measurement.

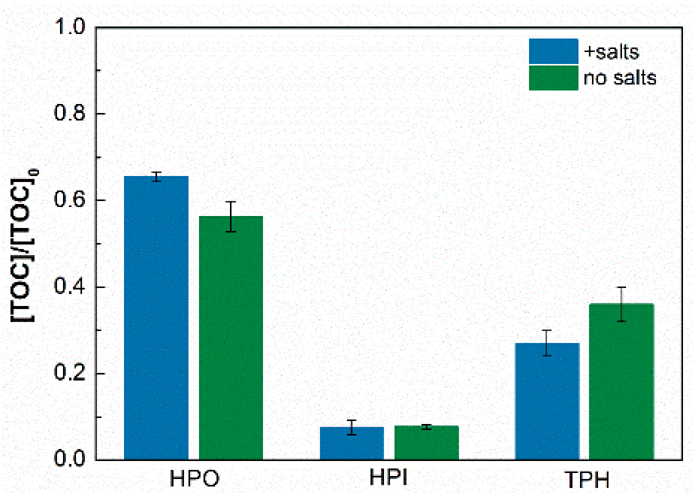

Figure 7.18 Measured hydrophobic (HPO), hydrophilic (HPI) and transphilic (TPH) fractions in HA in the absence (green bars) and presence of salts (blue bars) using XAD resin fractionating method.

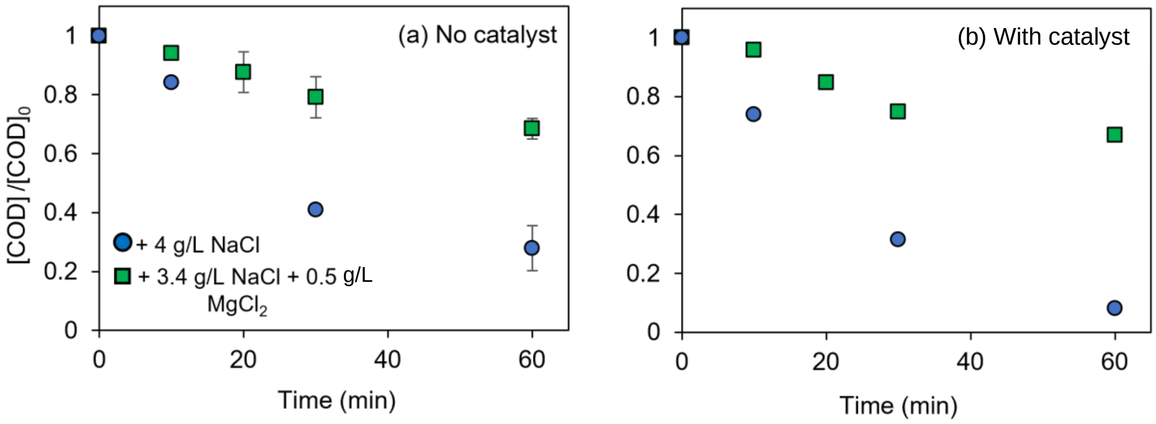

Figure 7.19 Influence of Mg^{2+} on COD removal during conventional ozonation of 33 mg C/L HA solution by conventional ozonation (a) and catalytic ozonation process (b). Experimental conditions: pH = 8.3, O_3 gas flow rate = and 60.0±0.5 mL/min, flow rate = 51 mg/L, reactor volume =150 mL; [salt] as specified in the legend + 8.4 g/L Na_2SO_4;$[TOC]_0$ = 33.0 mg/L ; $[catalyst]_0$ = 20.0 g/L.

The transformation of humics to more compact hydrophobic DOC may inhibit the rate of oxidation of humics with this result potentially explaining the observed decrease in the rate of HA oxidation in the presence of salts in the first 10 – 20 minutes of exposure to O_3 (Figure 7.11). Comparing the LC–OCD fractions of raw and treated HA for both conventional ozonation and catalytic ozonation in the absence and presence of salts, we observe one major difference. As shown in Figure 7.20, humics are transformed to LMW neutral compounds in the presence of salts but building blocks are identified as the main fraction following oxidation in the absence of salts during both the homogeneous ozonation and heterogeneous catalytic ozonation processes. It is possible that the more compact humics in the presence of salts oxidize to LMW neutrals while in the absence of salts, the more branched humics are transformed to other readily oxidizable organic fractions (i.e., building blocks, LMW acids). The formation of LMW neutrals on humics oxidation in saline waters is expected to prevent further breakdown of organics (in accord with the lower extent of removal of TBA – a typical LMW neutral – in the presence of salts; Figure 7.13), thereby resulting in overall lower organic removal.

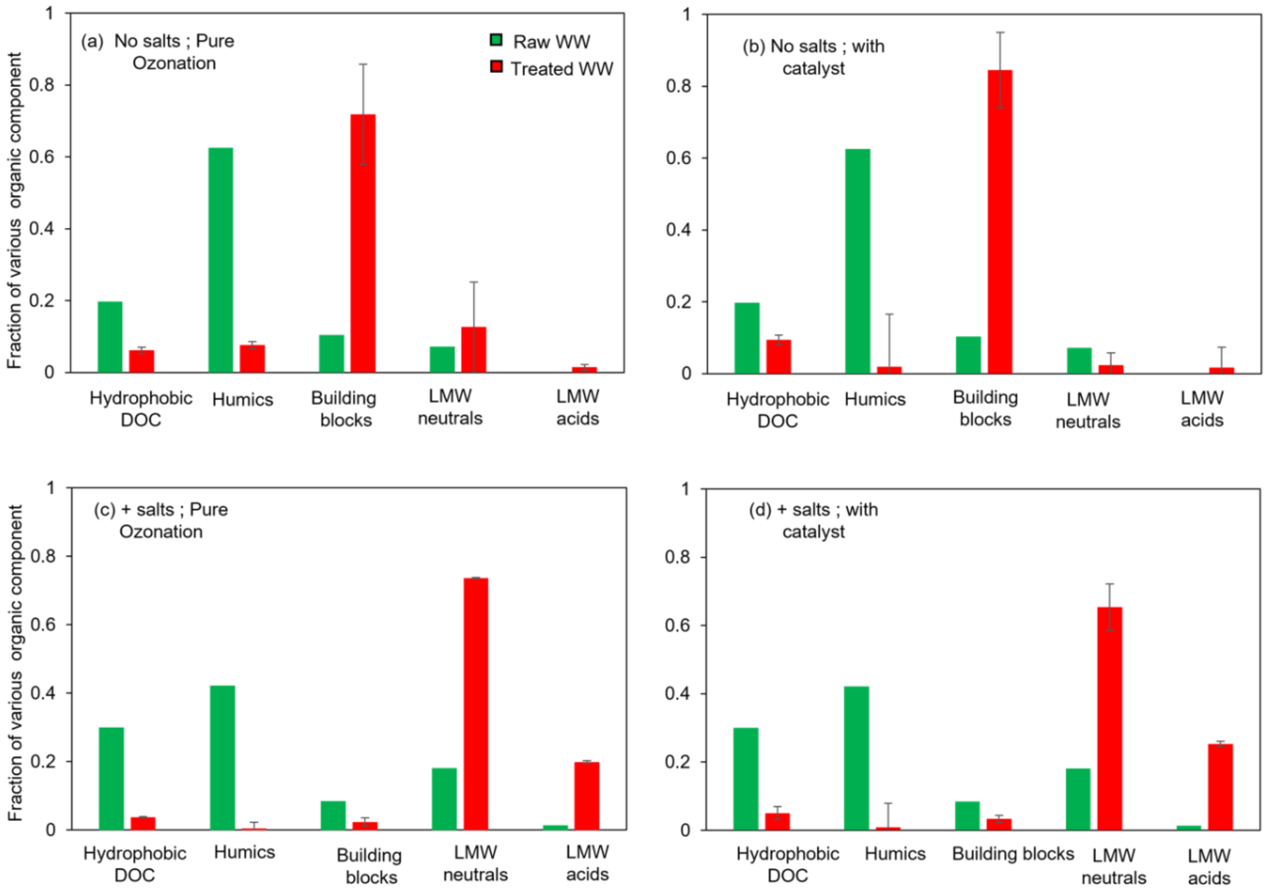

Figure 7.20 Measured organic composition of raw (green bars) and treated HA (red bars) in the absence and presence of salts using LC–OCD. Panels a & c show the results of conventional ozonation in the absence and presence of salts respectively while panels b & d show the results of catalytic ozonation. Bars represents the average of duplicate measurements; error bars represent the standard deviation of measurement. Experimental conditions: pH = 8.3, O_3 gas flow rate = 60.0±0.5 mL/min, flow rate = 51 mg/L, reactor volume = 150 mL, [catalyst]$_0$ = 20.0 g/L, [salt] = 4.0 g/L NaCl + 8.4 g/L Na_2SO_4, reaction time = 60 min.

While a significant influence of salts on the HA structure was observed, no effect of salt is expected on the structure of TBA (as confirmed by LC-OCD analysis) with this result confirming that factors other than transformation of organics in the presence of salts also play a role in inhibiting the oxidation of organics (such as TBA) in high salinity waters.

7.3.3.5 Scavenging of surface O_3 and/or surface hydroxyl radicals by chloride and sulphate ions

In order to determine the influence of salts on the extent of hydroxyl radical generation, we measured the rate and extent of $C_2O_4^{2-}$ oxidation in the absence and presence of salts. As shown in Figure 7.21a, no influence of salts on $C_2O_4^{2-}$ oxidation was observed during conventional ozonation which suggests that the there is no influence of salts on bulk hydroxyl radical generation and consumption, at least at the salt concentration used here. There is a significant decrease in the oxidation of $C_2O_4^{2-}$ during catalytic ozonation in the presence of salts (Figure 7.21b) with 50.9±1.9 % and 34.5 ± 1.7 of $C_2O_4^{2-}$ oxidized after 3 h of catalytic ozonation in the absence and presence of salts respectively.

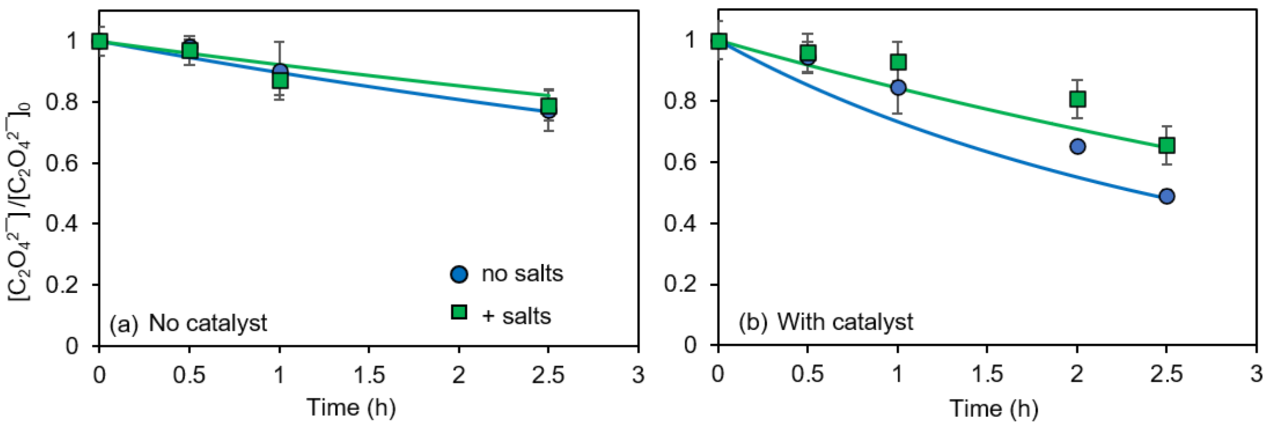

Figure 7.21 Measured oxidation of $C_2O_4^{2-}$ in the absence (circles) and presence of salts (squares) by conventional ozonation (a) and catalytic ozonation (b) at pH 8.3. Symbols represents the average of duplicate measurements; error bars represent the standard deviation of measurement. Lines represent model values. Experimental conditions: pH = 8.3, O_3 gas flow rate = 60.0±0.5 mL/min, flow rate = 51 mg/L, reactor volume = 150 mL, $[C_2O_4^{2-}]$ = 2.75 mM, [salt] = 3.95 g/L NaCl + 8.43 g/L Na_2SO_4, $[\text{catalyst}]_0$ = 20.0g/L.

Given that the oxidation of $C_2O_4^{2-}$ during catalytic ozonation occurs mostly via interaction with hydroxyl radicals in the bulk solution (see Figure 7.4), it appears that the concentration of hydroxyl radicals formed on the catalyst surface and released into the bulk solution decreases in the presence of salts, possibly due to scavenging of surface hydroxyl radicals by chloride ions. It is also possible that the scavenging of ozone by chloride ions at the catalyst surface inhibits catalyst–O_3 interaction, thereby decreasing the rate of hydroxyl radical generation. The concentration of chloride ions within the EDL at the catalyst-solution interface is expected to be higher than the bulk chloride concentration if the catalyst surface sites are positively charged (which will be the case if the solution pH is lower than that of the pH_{pzc}). If this is the case, more extensive scavenging of O_3 and/or surface hydroxyl radicals is expected to occur during catalytic ozonation compared to that observed during conventional ozonation. Employing the kinetic model for O_3 self-decay presented here (Table 7.2), we show that at chloride concentration > 0.2 M, more than 50% of O_3 is scavenged by chloride ions (Figure 7.22). Hence, if the concentration of chloride ions near the catalyst surface increases up to 0.2 M as a result of counter ion attraction, significant scavenging of O_3 may occur by salt ions resulting in futile consumption of O_3 and decrease in the catalyst performance.

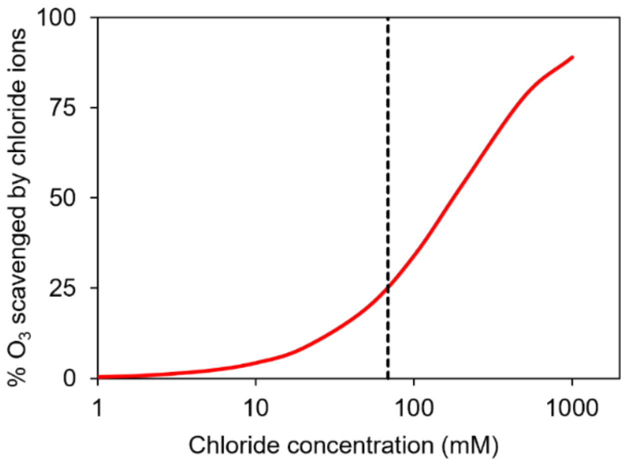

Figure 7.22 Model-predicted scavenging of O_3 by chloride ions at varying chloride concentration. Dashed lines represent the chloride concentration present in the synthetic wastewaters.

The observation that significant inhibition of $C_2O_4^{2-}$ oxidation by conventional ozonation occurs in the presence of 10-fold higher chloride ions concentration (Figure 7.23) also supports the hypothesis that accumulation of chloride ions in the EDL (at > 10–fold higher concentrations in the bulk solution) may result in more significant scavenging of surficial O_3/surficial hydroxyl radicals. As the concentration of chloride ions within the EDL at the catalyst-solution interface would be expected to be higher at solution pH<pH$_{pzc}$, we expect to see a more dramatic salt effect at lower pH. Studies of the salt effect on O_3 decay in the absence and presence of catalyst at pH 4.0 (i.e., pH<pH$_{pzc}$) confirms that the influence of salts on catalyst–mediated O_3 decay is greater at pH 4.0 compared to that at pH 8.3. As shown in Figure 7.24, no influence of salts on O_3 self–decay is observed at pH 4.0; however, catalyst mediated O_3 decay increases in the presence of salts suggesting that scavenging of O_3 by bulk chloride ions is trivial but scavenging of O_3 by chloride ions accumulated in the EDL is important at pH 4.0. In comparison, the salt-effect on O_3 decay rate in the absence and presence of catalyst is similar at pH 8.3 (Figure 7.15a and 7.15b) in accord with expected limited accumulation of chloride ions at the catalyst surface when the solution pH is similar to the pH$_{pzc}$ of the catalyst.

Overall, it appears that scavenging of surficial ozone and hydroxyl radicals by salts results in decreased catalytic ozonation performance.

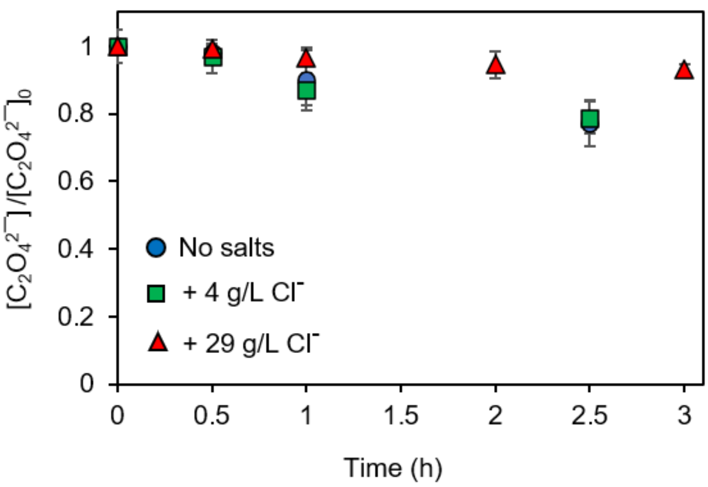

Figure 7.23 Measured oxidation of $C_2O_4^{2-}$ in the absence (circles) and presence of 4.0 g/L (squares) and 29.3 g/L (triangles) chloride ions by conventional ozonation at pH 8.3. Experimental conditions: pH = 8.3, O_3 gas flow rate = 60.0±0.5 mL/min, flow rate = 51 mg/L, reactor volume =150 mL, [catalyst]$_0$ = 20.0g/L.

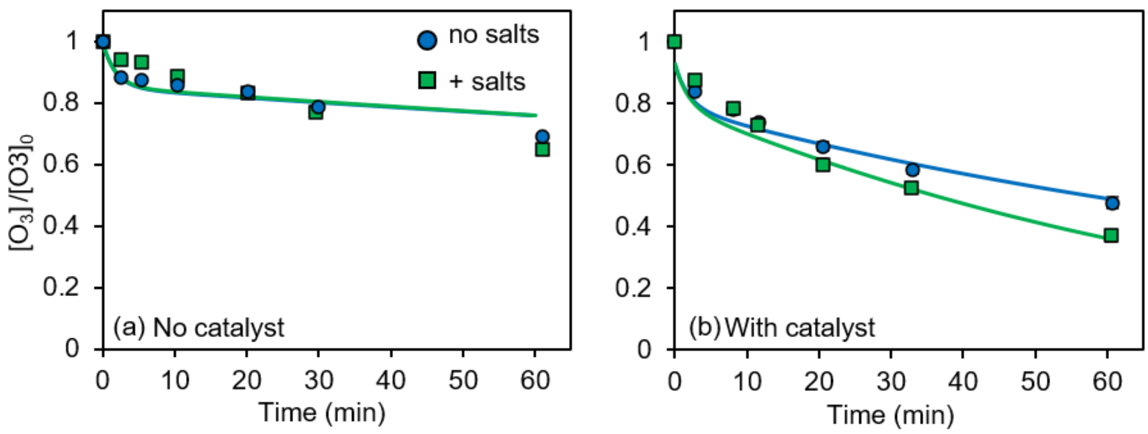

Figure 7.24 Measured O_3 self-decay (a) and catalyst-mediated O_3 decay (b) in the absence (circles) and presence (squares) of salts. Experimental conditions: $[O_3]_0$ =100 μM; $[catalyst]_0$ = 20.0 g/L [salt] = 4.0 g/L NaCl and 8.4 g/L Na_2SO_4, pH =4.0.

7.3.4 Mechanism of inhibitory effect of salt on conventional ozonation and catalytic ozonation processes

Based on the discussion presented above, the inhibitory effect of salt on organic oxidation by the conventional ozonation and catalytic ozonation process is due to:

(i) Scavenging of dissolved ozone by chloride ions present in the bulk solution.

(ii) Transformation of humics to more compact hydrophobic DOC due to charge shielding by cations between adjacent functional groups.

(iii) Scavenging of surface O_3 and surface hydroxyl radicals by chloride ions accumulated in the EDL.

To further verify the mechanism of the inhibitory effect of salts on organic oxidation, we have developed a kinetic model to describe the oxidation of oxalate by both the conventional ozonation and catalytic ozonation processes in the absence and presence of salts. The kinetic model was developed by extending the kinetic model for O_3 decay (Table 7.2, reactions 1-20) that we have previously described in chapter 4. The additional reactions included to explain oxalate oxidation are (i) reactions describing surficial hydroxyl radical decay and its diffusion into the bulk solution (Reactions 21 – 23, Table 7.2) (ii) oxidation of oxalate via interaction with hydroxyl radicals in the bulk solution (Reactions 24 – 26, Table 7.2). Detailed description of the reactions and justification of the rate constants used is provided below:

(i) O_3 self-decay

Reactions 1 – 10 (Table 7.2) describes the reactions controlling the self-decay of ozone. The rate constants for these reactions (Reactions 1 – 10, Table 7.2) were same as that used in chapter 4.

(ii) Bulk O_3 loss via interaction with salts

The reactions describing scavenging of bulk O_3 by chloride ions (reactions 11 – 14, Table 7.2) were obtained from Levanov *et al.*[243]

(iii) Bulk hydroxyl radical scavenging via interaction with salts

Reactions in Table 7.3 describes the scavenging of bulk hydroxyl radicals by salts based on previous studies;[141, 263, 275] however these reactions have no influence on the overall ozone decay or the oxidation of organics by ozonation and catalytic ozonation process.

(iv) Catalyst-mediated O_3 decay

Reactions 15 – 20 in Table 7.2 describes the catalyst mediated O_3 decay. Reaction 15 represents the diffusion of bulk ozone to the catalyst surface. Reaction 16 represents the interaction of ozone with the catalyst resulting in formation of surface $^{\bullet}OH$. To simplify the modelling process, we have assumed that for each mole of O_3 decayed on reaction with the catalyst, one mole of $^{\bullet}OH$ is formed. The rate constant for these reactions were determined based on best–fit to the measured ozone decay in the presence of catalyst (Figure 7.15 and 7.24) with no salts present. Reactions 17-20 (Table 7.2) represents the scavenging of surficial O_3 by chloride ions accumulated in EDL. The rate constant for the scavenging of O_3 by chloride ions and other chloride radicals is assumed to be the same as that reported for bulk O_3. The concentration of chloride ions in the EDL is determined based on fit to the measured ozone decay in the presence of catalyst (Figure 7.15 and 7.24) with salts present.

(v) Decay and diffusion of surface hydroxyl radical into the bulk solution

Reactions 21 – 22 (Table 7.2) represents the decay of surface-generated hydroxyl radical via interaction with catalyst surface and chloride ions accumulated in the EDL, respectively. The reaction of surface-generated hydroxyl radical with the catalyst surface results in the formation of non-reactive product (such as H_2O) while the reaction of chloride ions with hydroxyl radicals results in the formation of $HOCl^{\bullet-}$ which is presumed to decay to form non-reactive product via interaction with the catalyst surface. Reaction 23 (Table 7.2) represents the diffusion of surface hydroxyl radical to the interface/bulk solution. The rate constant for these reactions were determined based on the best-fit to oxalate oxidation by catalytic ozonation process in the absence and presence of salts (Figure 7.17b). Note that the exact values of the rate constants for these reactions cannot be determined based on our experimental results with any value of k_{21}, k_{22} and k_{23} describing the data as long the k_{21}/k_{22} and k_{21}/k_{23} ratio shown in Table 7.2 is met. Note that for simplification, we have assumed that most of surface hydroxyl radical diffuses into the bulk solution and oxidation of oxalate occur in the bulk solution; however, a mathematical model where diffusion of surface hydroxyl radical to the interface occur with concomitant oxidation of oxalate present in the interfacial zone produces the same result as well if the interfacial zone composition is same as the bulk composition. The model can be easily extended to describe interfacial oxidation of oxalate by including same series of reactions that occur in the bulk solution (i.e., reactions 1 – 14 and reactions 24 – 26 in Table 7.2) for the interfacial zone and diffusion of surface hydroxyl radicals (reaction 23, Table 7.2) to the interface.

(vi) Oxalate oxidation in the bulk solution

Reactions 24 – 26 (Table 7.2) describes oxalate oxidation via reaction with bulk hydroxyl radicals as described in chapter 5.

As shown in Figure 7.21, the model provides excellent description of the oxalate oxidation in the absence and presence of salts for both the conventional ozonation and catalytic ozonation processes supporting the mechanism of inhibitory effect of salts proposed here. Employing the kinetic model presented here (Table 7.2), we have also predicted the influence of chloride ions on oxalate oxidation by conventional ozonation and catalytic ozonation under varying chloride and oxalate concentrations. As shown in Figure 7.25a, there is a small (≤8%) influence of chloride ions on oxidation of oxalate by conventional ozonation with the influence of chloride ions more prominent at higher oxalate concentrations. A more significant influence (~15 – 20%) of chloride ions was observed on oxalate oxidation in the presence of catalyst (Figure 7.25b) as a result of scavenging of surface O_3/hydroxyl radicals by salts.

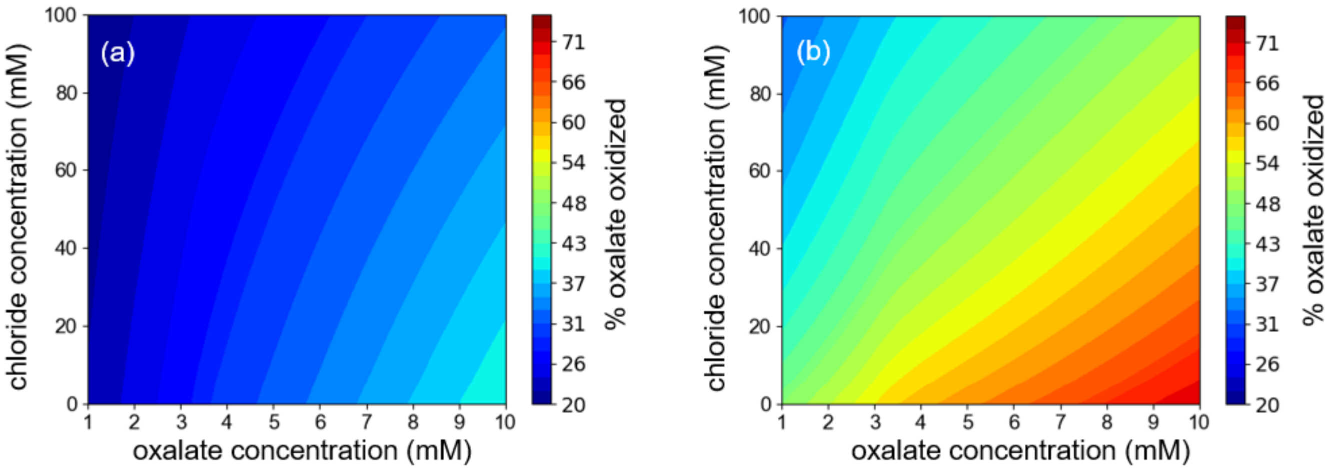

Figure 7.25 Model-predicted oxalate oxidation for varying chloride and oxalate concentration by conventional ozonation (a) and catalytic ozonation(b). For these predictions, a steady state $[O_3]$ was used. Note that since dissolution of ozone increases with increase in chloride concentration, varying $[O_3]_{ss}$ at different chloride concentrations were used. The equation to calculate the steady state $[O_3]$ here is determined based on the measured effect of salt on O_3 dissolution (Figure 7.15c). $[O_3]_{ss}=[O_3]_0+332.3\times[Cl^-]$ and $[O_3]_{ss}=[O_3]_0+409.3\times[Cl^-]$ was used for conventional ozonation and catalytic ozonation, respectively ; $[O_3]_0$ = 60.0 μM, which represents the $[O_3]_{ss}$ in the absence of chloride ions, was used for these simulation.

7.4 Conclusions

Based on the results presented here, it appears that the presence of salts in high salinity wastewaters influences the oxidation of organic contaminants by both conventional ozonation and catalytic ozonation processes. The inhibition effect of salt during conventional ozonation is partly attributed to the transformation of humic-like substances, present in the wastewater, to more compact hydrophobic organic compounds that are more resistant to oxidation. In addition, scavenging of O_3 by Cl^- also contributes to the inhibition of oxidation of organic contaminants during the conventional ozonation process. During catalytic ozonation, in addition to the aforementioned factors, it appears that scavenging of surface O_3 and surface hydroxyl radicals by salts further increases the inhibition effect of salts on the oxidation performance using the Fe oxide- based catalyst for which oxidation mainly proceeds in the solid-liquid interfacial region and /or bulk solution. The scavenging of the surficial ozone/ $^{\bullet}OH$ could possibly be minimized by operating at pHs above the pH_{pzc} of the catalyst since the accumulation of chloride ions in the electrical double layer surrounding the particle (which results in enhanced scavenging of O_3 and $^{\bullet}OH$) will be prevented in this case.

It should be noted that the use of synthetic wastewater containing HA and TBA in this study might have limitations since the composition of real wastewater from coal chemical industry is very complex. More typical contaminants from coal chemical wastewater such as polycyclic poly aromatic hydrocarbons and riverine humic substance should be investigated in the future to extend our understanding of the salt effects on treatment of coal chemical wastewater via ozone-related technologies.

Chapter 8 Caveats in the use of tertiary butyl alcohol (TBA) as a probe for hydroxyl radical involvement in conventional ozonation and catalytic ozonation processes

8.1 Introduction

The oxidation of organic contaminants by ozonation (including both conventional ozonation and/or HCO processes) occurs via radical–mediated and/or direct ozonation processes.[63] In the radical mediated process, ROS, predominantly $^{\bullet}OH$, derived from ozone decay are involved in the oxidation of organic contaminants while in the direct ozonation process, direct oxidation of organics occurs via interaction with O_3. In the past decade, researchers have focussed on the development of catalysts wherein the radical-governed process dominates since ROS formed on ozone decay are more reactive than O_3. The contribution of radical mediated oxidation of organics is usually probed using TBA as a scavenger of $^{\bullet}OH$ [33, 47, 276-280] due to its relatively high reaction rate constant with $^{\bullet}OH$ (5×10^{8} $M^{-1}\cdot s^{-1}$)[141] but low reaction rate constant with O_3 (3×10^{-3} $M^{-1}\cdot s^{-1}$).[4] The observed decrease in the rate and extent of oxidation of organic compounds in the presence of TBA is usually assumed to represent the contribution of $^{\bullet}OH$ mediated organic oxidation during ozonation. However, due to the low surface affinity of TBA[259, 260] and/or its interference with the sorption of organic compounds on the catalyst surface,[149, 281] the results from TBA scavenging experiments during HCO may not correctly predict the contribution of $^{\bullet}OH$ to organic oxidation. Furthermore, researchers have reported that the presence of TBA alters the ozone decay rate [86, 192, 229, 282-284] as a result of inhibition of radical chain reactions [86] and hence has an impact on the rate of $^{\bullet}OH$ generation and associated oxidation of organics via the radical mediated pathway. Researchers also employ TBA as a $^{\bullet}OH$ scavenger to determine the second–order rate constant for organic-ozone reaction by monitoring the decrease in organic and/or ozone concentration;[140, 229] however, variation in the O_3 decay kinetics in the presence of TBA may influence the value of the rate constant determined. The influence of intermediates/products formed on TBA–$^{\bullet}OH$ reaction on ozone decay and oxidation of organics is assumed to be negligible,[4, 140] though no clear evidence is typically provided to support this hypothesis. Given the rapidly increasing research on application of HCO and selection of catalysts based on the purported mechanism of reaction, it is our strong view that clarification regarding the correct use of TBA in gaining mechanistic insight is urgently needed.

In this chapter, we discuss the various caveats associated with the use of TBA to probe the contribution of $^{\bullet}OH$ in catalytic as well as conventional ozonation processes. For HCO, we have used three types of catalysts including a commercially available Fe–loaded activated carbon (Fe–AC) catalyst, laboratory synthesized Cu–Al LDHs and CuO. We used formate $HCOO^-$ and oxalate $C_2O_4^{2-}$ as the target contaminants since both these compounds have well defined oxidation pathway and forms CO_2 and H_2O as the only products.[123] *p*–CBA and coumarin were employed as probe compounds to measure the yield of bulk hydroxyl radical and generation of surface hydroxyl radical, respectively.[29, 89] Based on our experimental results, we highlight that caution needs to be exercised when interpreting the observations made in the presence of TBA. Furthermore, we describe the additional experiments required to conclusively determine the role of $^{\bullet}OH$ depending on the results obtained when using TBA as the probe compound.

8.2 Materials and Methods

8.2.1 Reagents

Experiments were performed at pH 3.0 or 7.3 with a maximum pH variation of ±0.1 with reagents prepared as described in chapter 3. Note that both carbonate and phosphate buffer at pH 7.3 were used to determine if the influence of TBA varies in matrix with different $^{\bullet}OH$ scavenging capacity. While carbonate/bicarbonate ions are known scavenger of $^{\bullet}OH$,[285] the scavenging of $^{\bullet}OH$ by phosphate ions (mainly dihydrogen phosphate and hydrogen phosphate) is relatively small compared to carbonate/bicarbonate ions though dihydrogen phosphate and hydrogen phosphate may act as secondary promoter of ozone decay.[229] Stock solutions of radiolabelled and non–radiolabelled sodium formate, radiolabelled and non-radiolabelled sodium oxalate, *p*–CBA, indigo and O_3 stock solution were prepared as described in chapter 3. Stock solutions of 1.3 mM coumarin and 1.0 M TBA were prepared in MQ water. The procedures used for synthesis of the Cu–Al LDHs and CuO catalysts are described in chapter 5. The Fe–loaded activated carbon catalyst is same as that used in chapter 4 and was provided by BOW using a proprietary preparation procedure.

8.2.2 Ozone measurement

Measurement of O_3 self–decay in the absence and presence of 1.0 mM TBA was performed in pH 7.3 phosphate buffered and/or carbonate buffered solutions in gas–tight reactors as described in chapter 3 with the concentration of O_3 measured using the indigo method.[107] For measurement of ozone decay in the presence of $HCOO^{-}$, O_3 at an initial concentration of 100.0 µM was added to pH 7.3 phosphate/carbonate buffered solutions containing 10.0 – 50.0 µM $HCOO^{-}$ and the concentration of ozone was measured overtime as described above.

8.2.3 Organic adsorption and oxidation

Adsorption of HCOOH on the Fe-AC surface at pH 3.0 was measured in the absence and presence of 0.1 mM TBA. The sorption of $C_2O_4^{2-}$ on the CuO surface in the absence and presence of 0.1 M TBA was measured in pH 7.3 carbonate buffered solution. The oxidation of 1.0 µM $HCOO^-$ /*p*–CBA by ozone alone in the absence and presence of 1.0 mM TBA was performed in pH 7.3 carbonate buffered solution. The experimental setup and method used for measurement of adsorption of $HCOO^-$/ $C_2O_4^{2-}$ and oxidation of $HCOO^-$/*p*–CBA on ozonation is identical to that described in chapter 4. Note that a final TBA concentration of 1.0 mM was used in all experiments investigating the role of $^\bullet$OH in organic oxidation during ozonation since the results of control experiments (i.e., influence of TBA addition on *p*–CBA oxidation, a bulk $^\bullet$OH probe;[182] see Figure 8.1) confirm that a TBA concentration of 1.0 mM is sufficient to scavenge all bulk $^\bullet$OH, at least under the conditions investigated in this study. TBA of a higher concentration (10.0 – 100.0 mM) was employed for some HCO studies to ensure that TBA concentration is not limiting to scavenge surface $^\bullet$OH.

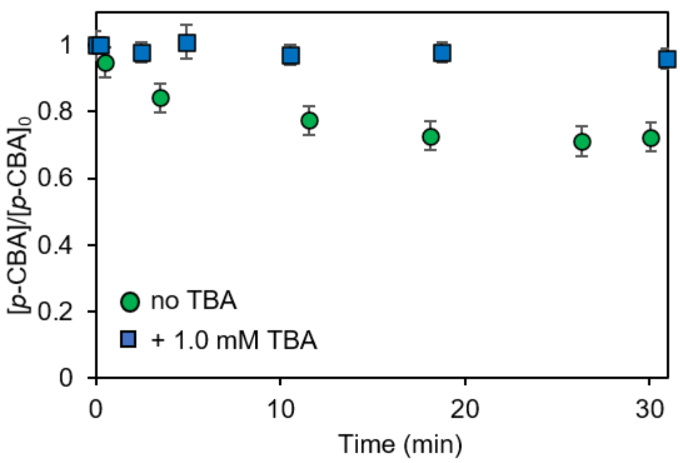

Figure 8.1 Measured *p*–CBA decay on ozonation in the absence (circles) and presence of 1.0 mM (squares) of TBA. Experimental conditions: $[O_3]_0$ =10.0 µM; [*p*–CBA] =1.0 µM; pH =7.3 using 1.33 mM $NaHCO_3$ solution.

8.2.4 Fluorescence microscopy image analysis

We characterized the surface associated •OH originating from HCO using fluorescence microscopy image analysis as described in detail in chapter 5. The fluorescent images in the absence and presence of CuO and Cu–Al LDHs were captured in the absence and presence of 1.0 mM TBA. Control experiments were also performed in order to determine whether 7–HC formation occurred on homogeneous ozonation of coumarin as described in chapter 5.

We would like to highlight that the fluorescence imaging method was employed only to illustrate the presence of surface-associated •OH in the presence and absence of TBA with no attempt made to use this method to quantify the surface •OH generation rate. Inner filter effects due to coumarin absorbance and/or variation in surface affinity [286, 287] are expected to be the same in the presence and absence of TBA and, as such, are not expected to influence the conclusions reached based on the fluorescence imaging results.

8.2.5 Kinetic modelling

Kinetic modelling of ozone self-decay and oxidation of various organics on ozonation was performed using kinetic modelling software Kintecus.[257] The mathematical model describing ozone self–decay kinetics and organic oxidation was described in detail in chapters 4 and 5.

8.3 Results and Discussion

8.3.1 Limitations associated with the use of TBA in ozonation

Inconclusive assessment of •OH involvement for ozone reactive compounds

As shown in Figure 8.2, minimal influence of TBA addition was observed on $HCOO^-$ oxidation during ozonation at pH 7.3 suggesting that $HCOO^-$ oxidation by bulk $^{\bullet}OH$ is not important. However a R_{ct} (i.e., $^{\bullet}OH$ radical exposure/O_3 exposure;[89] see section 2.2.2 in chapter 2 for calculation of R_{ct}) value of 3.5×10^{-8} was calculated for this system (Figure 8.3) which suggest that the contribution of $^{\bullet}OH$ in $HCOO^-$ oxidation ($f_{^{\bullet}OH}$; calculated using eq. 8.1) should be around 29.6% based on the reported rate constant of $HCOO^-$ oxidation by $^{\bullet}OH$ (1.2×10^9 $M^{-1}\cdot s^{-1}$; [141]) and O_3 (100.0 $M^{-1}\cdot s^{-1}$; [4]).

$$f_{^{\bullet}\mathrm{OH}} = \frac{R_{ct} k_{^{\bullet}\mathrm{OH}}}{R_{ct} k_{^{\bullet}\mathrm{OH}} + k_{\mathrm{O_3}}} \tag{8.1}$$

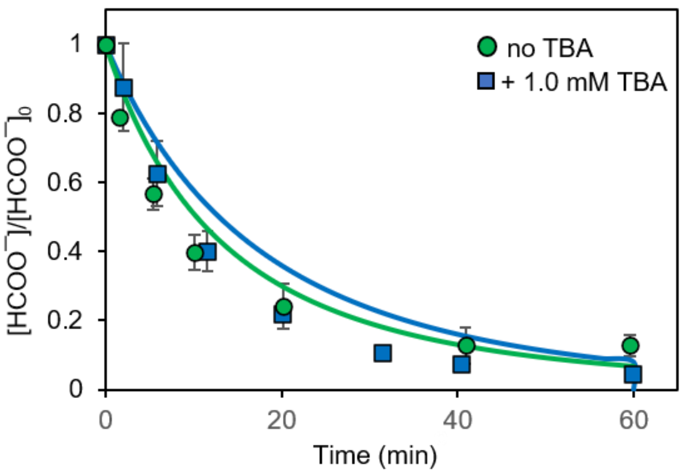

Figure 8.2 Oxidation of $HCOO^-$ by ozonation in the absence (circles) and presence of 1.0 mM TBA (squares) at pH 7.3. Experimental conditions: $[O_3]_0$ = 10.0 µM, $[HCOO^-]_0$ = 1.0 µM, pH 7.3 using 1.33 mM $NaHCO_3$. Symbols represent experimental data, lines represent model-predicted values.

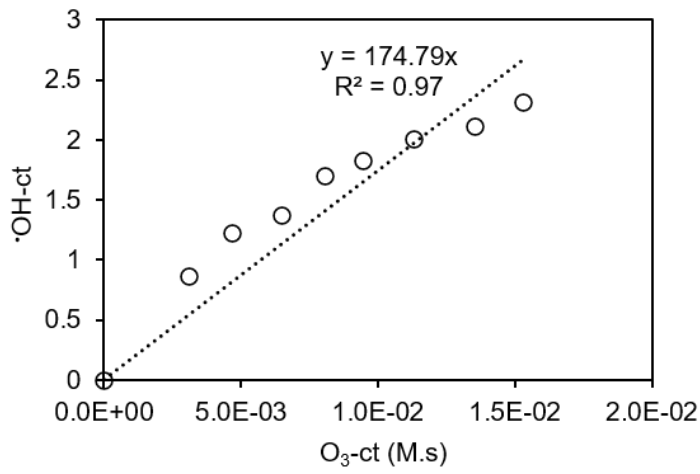

Figure 8.3 Measured $^{\bullet}$OH -exposure ($^{\bullet}$OH–ct) versus the corresponding O_3-exposure (O_3–ct) for ozonation of $HCOO^-$ solution. Experimental conditions: $[p\text{–CBA}]_0$ = 1.0 µM, $[O_3]_0$ =100.0 µM; $[HCOO^-]$ =10.0 µM; pH =7.3 using 1.33 mM $NaHCO_3$ solution.

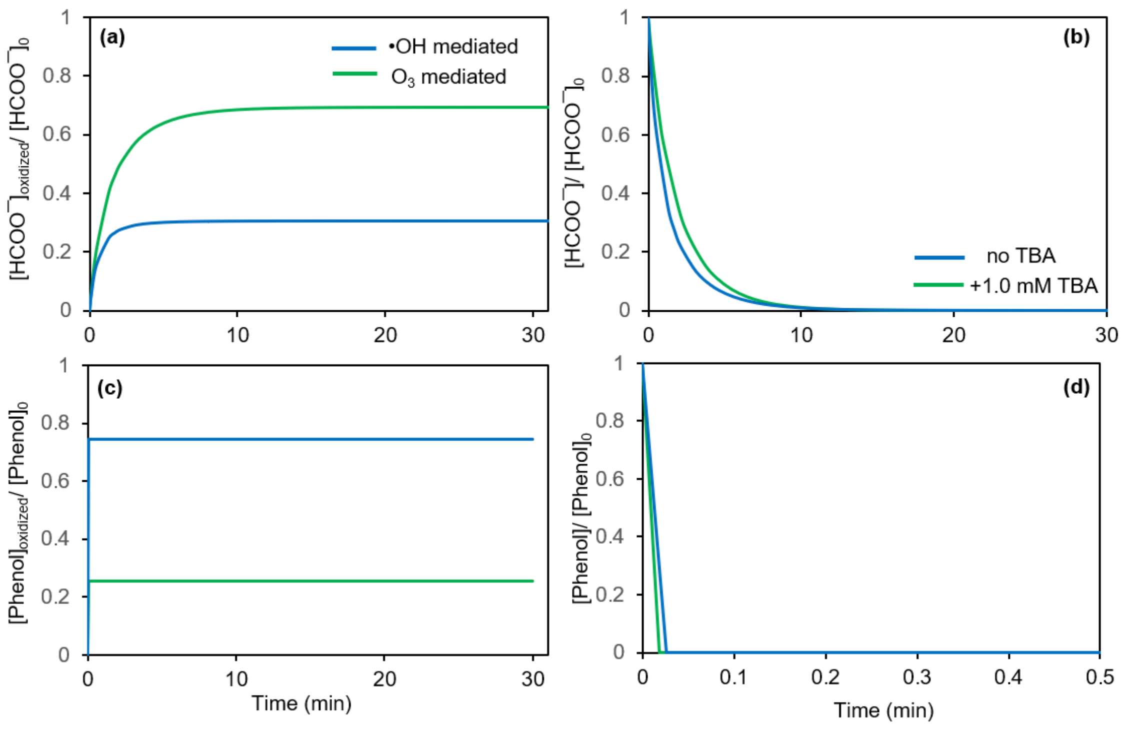

Figure 8.4 Model-predicted fraction of organic oxidized via interaction with ozone and hydroxyl radicals during conventional ozonation process in the absence of TBA at pH 7.3 (panels a and c). Model-predicted influence of 1.0 mM TBA addition on the rate and extent of organic oxidation during conventional ozonation process at pH 7.3 (panel b and d). $[Org]_0$ = 10.0 µM, $[O_3]_0$ =100.0 µM for all predictions.

Table 8.1 Kinetic model for ozone self–decay at pH 7.3 as described in chapter 4.

No	Reaction	Rate constant ($M^{-1}\cdot s^{-1}$)	Published value ($M^{-1}\cdot s^{-1}$)
1	$O_3 + OH^- \rightarrow HO_2^{\bullet} + O_2^{\bullet-}$	100.0	70.0
2	$O_3 + H_2O_2/HO_2^- \rightarrow HO_3^{\bullet} + O_2^{\bullet-}$	1.7×10^{2a}	1.7×10^{2}
3	$O_3 + O_2^{\bullet-} \rightarrow HO_3^{\bullet} + O_2$	1.5×10^{9}	1.5×10^{9}
4	$HO_3^{\bullet}/O_3^{\bullet-} \rightarrow {}^{\bullet}OH + O_2$	1.4×10^{5b}	1.4×10^{5}
5	${}^{\bullet}OH + O_3 \rightarrow O_2^{\bullet-} + O_2$	1.0×10^{8}	1.0×10^{8}
6	$O_3^{\bullet} + CO_3^{\bullet-} \rightarrow H_2CO_3 + O_2$	1.0×10^{5}	1.0×10^{5}
7	${}^{\bullet}OH + H_2O_2/HO_2^- \rightarrow H_2O + O_2^{\bullet-}$	2.7×10^{7a}	2.7×10^{7}
8	${}^{\bullet}OH + H_2CO_3/\ HCO_3^-/CO_3^{2-} \rightarrow OH^- + CO_3^{\bullet-}$	8.2×10^{6c}	8.2×10^{6}
9	$CO_3^{\bullet-} + H_2O_2/HO_2^- \rightarrow O_2^{\bullet-} + H_2CO_3$	4.3×10^{5a}	4.3×10^{5}
10	$CO_3^{\bullet-} + CO_3^{\bullet-} \rightarrow CO_2^{4-} + H_2CO_3$	2.0×10^{7}	2.0×10^{7}

[a] calculated value at pH 7.3 using the reported rate constant for H_2O_2/HO_2^- and the mole fraction of $H_2O_2/\ HO_2^-$ at pH 7.3.
[b] calculated value at pH 7.3 using the reported rate constant for $HO_3^{\bullet-}$ / $O_3^{\bullet-}$ and the mole fraction of $HO_3^{\bullet-}$ / $O_3^{\bullet-}$ at pH 7.3.
[c] calculated value at pH 7.3 using the reported rate constant for $H_2CO_3/HCO_3^-/CO_3^{2-}$ and the mole fraction of for $H_2CO_3/HCO_3^-/CO_3^{2-}$ at pH 7.3.

Table 8.2 Reactions used for modelling of oxidation of formate and phenol during ozonation.

No	Reaction	Rate constant ($M^{-1}\cdot s^{-1}$)	Ref.
	Formate (O_3 decay promoter)		
1	$HCOO^- + O_3 \rightarrow CO_2 + HO_3^-$	70.0	In chapter 4
2	$HCOO^- + O_3 \rightarrow CO_2^{\bullet-} + HO_3^{\bullet}$	30.0	In chapter 4
3	$HCOO^- + {}^{\bullet}OH \rightarrow CO_2^{\bullet-} + H_2O$	1.2×10^{9}	[141]
4	$CO_2^{\bullet-} + O_2 \rightarrow O_2^{\bullet-} + H_2CO_3$	1.0×10^{9}	
5	$HCOO^- + CO_3^{\bullet-} \rightarrow CO_2^{\bullet-} + HCO_3^-$	1.5×10^{5}	
	Phenol (O_3 decay promoter)[288]		
1	$Phe + O_3 \rightarrow Phe^{\bullet} + HO_3^{\bullet}$	1.0×10^{6}	[288]
2	$Phe + {}^{\bullet}OH \rightarrow Phe^{\bullet}$	1.0×10^{10}	[141]
3	$Phe^{\bullet} + O_2 \rightarrow Prod + O_2^{\bullet-}$	$\sim1.0\times10^{9}$	

This discrepancy in the expected role of $^{\bullet}OH$ and the observed influence of TBA on $HCOO^{-}$ oxidation is due to the involvement of both O_3 and $^{\bullet}OH$ in $HCOO^{-}$ oxidation. In the absence of TBA, $^{\bullet}OH$ (formed on O_3 self-decay; eqs. 8.2-8.7) oxidizes $HCOO^{-}$ (eq. 8.8) with the $CO_2^{\bullet-}$ formed on $HCOO^{-}$ oxidation facilitating $O_2^{\bullet-}$ (eq. 8.9) and subsequent $^{\bullet}OH$ generation (eqs. 8.4 – 8.7), which drives further $HCOO^{-}$ oxidation by $^{\bullet}OH$. In the presence of TBA however, $HCOO^{-}$ is instead oxidized by O_3 (eq. 8.13) with the rate and extent of $HCOO^{-}$ oxidation similar and/or slightly lower than that observed in the absence of an $^{\bullet}OH$ scavenger, particularly when $[O_3]>>[HCOO^{-}]$. This behaviour is quantitatively shown in Figures 8.4a and 8.4b using mathematical modelling developed by combining the mathematical model for O_3 self-decay kinetics reported in chapter 4 with the reaction for $HCOO^{-}$ oxidation by O_3 and $^{\bullet}OH$ using the reported rate constants for these reactions (see Table 8.2). As shown, the oxidation of $HCOO^{-}$ is driven by both $^{\bullet}OH$ and O_3 in the absence of TBA however, in the presence of TBA, $HCOO^{-}$ is oxidized by ozone at a comparable rate to that observed in the absence of TBA, thereby resulting in flawed conclusions regarding involvement of $^{\bullet}OH$ in $HCOO^{-}$ oxidation. Note that the modelling approach used here is reasonable, at least for the simple matrix tested here, since the model-predicted $f_{\bullet OH}$ for $HCOO^{-}$ oxidation is the same as that calculated using R_{ct} measurements (29.6%). Additionally, the model describes both the ozone decay in the absence and presence of $HCOO^{-}$ (Figure 8.5) and $HCOO^{-}$ oxidation (Figure 8.2) reasonably well. This alteration in the oxidation pathway in the presence of TBA possibly explains the apparent lack of involvement of $^{\bullet}OH$ in oxidation of phenol, a compound recognized to react rapidly with $^{\bullet}OH$ and to promote subsequent O_3 decay,[289] even under highly alkaline conditions.[290-292] Since the $f_{\bullet OH}$ value for phenol cannot be reliably determined experimentally using the R_{ct} approach due to rapid decay of O_3 and *p*–CBA in the presence of phenol, we used the mathematical modelling approach to predict the $f_{\bullet OH}$ for phenol oxidation (see Table 8.2 for model reactions). As shown in Figures 8.4c and 8.4d, the modelling results show that the oxidation of phenol is driven by both $^{\bullet}OH$ and O_3 in the absence of TBA however, in the presence of TBA, phenol is oxidized by ozone at a comparable rate to that observed in the absence of TBA, thereby resulting in flawed conclusions regarding involvement of $^{\bullet}OH$ in phenol oxidation. We would like to highlight that while earlier work by Elovitz and von Gunten [89] showed that there is no involvement of $^{\bullet}OH$ in the oxidation of organic compounds with $k_{O_3} \geq 10^5$ $M^{-1}\cdot s^{-1}$and $R_{ct} \leq 10^{-6}$; however since phenol promotes O_3 decay, the R_{ct} value in the presence of phenol is expected to be higher than 10^{-6} [289] and hence $^{\bullet}OH$-mediated oxidation of phenol is important even though $k_{O_3} = 10^6$ $M^{-1}\cdot s^{-1}$ for phenol under circumneutral pH conditions. Thus, it appears that for compounds that are (i) reactive with ozone and (ii) promotes O_3 decay (i.e., convert $^{\bullet}OH$ into superoxide ($O_2^{\bullet-}$), TBA scavenging experiments will be inconclusive. Table 8.3 provides a potential list of compounds for which TBA scavenging results may not be conclusive under circumneutral pH conditions in determining the role of $^{\bullet}OH$ in organic oxidation, particularly if O_3 is present in excess. Based on our calculations, it appears that for compounds which promote O_3 decay and have $k_{\bullet OH}/k_{O_3}$ in the range ~10^3–10^6 (for $k_{\bullet OH}$ in a range of $(0.05 - 5.0)\times10^{10}$ $M^{-1}\cdot s^{-1}$), TBA scavenging results cannot be used to correctly determine the contribution of $^{\bullet}OH$.

$$O_3 + OH^- \rightarrow O_2^{\bullet-} + HO_2^{\bullet} \quad (8.2)$$

$$HO_2^{\bullet} \rightleftharpoons O_2^{\bullet-} + H^+ \quad (8.3)$$

$$O_3 + O_2^{\bullet-} \rightarrow O_3^{\bullet-} + O_2 \quad (8.4)$$

$$HO_3^{\bullet} \rightleftharpoons O_3^{\bullet-} + H^+ \tag{8.5}$$

$$HO_3^{\bullet} \rightarrow {}^{\bullet}OH + O_2 \tag{8.6}$$

$$O_3 + {}^{\bullet}OH \rightarrow O_2 + O_2^{\bullet-} \tag{8.7}$$

$$HCOO^- + {}^{\bullet}OH \rightarrow CO_2^{\bullet-} + H_2O \tag{8.8}$$

$$CO_2^{\bullet-} + O_2 \rightarrow O_2^{\bullet-} + H_2CO_3 \tag{8.9}$$

$$HCOO^- + O_3 \rightarrow CO_2 + O_2 + OH^- \tag{8.10}$$

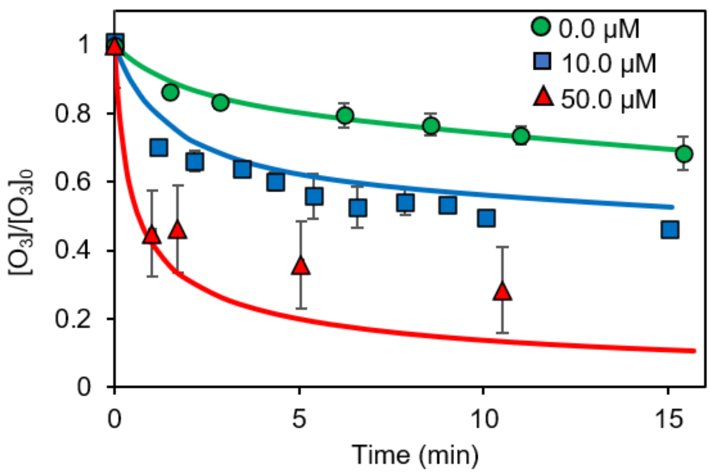

Figure 8.5 Measured O_3 decay in the absence (circles) and presence of 10.0 µM (squares) and 50.0 µM (triangles) of $HCOO^-$ solution. Experimental conditions: $[O_3]_0$ =100.0 µM; $[HCOO^-]$ =0-50.0 µM; pH =7.3 using 1.33 mM $NaHCO_3$ solution. The symbols represent the experimental data and the lines represent the model results.

Table 8.3 List of potential compounds for which TBA scavenging experiments will result in inconclusive assessment.

Compounds	$\boldsymbol{k_{O_3}}$ **($M^{-1}\cdot s^{-1}$)**	
Olefins		Initiates O_3 decay and promotes O_3 decay via H_2O_2 formation[22]
cis-1,2-Dichloroethene	310-540	[22]
trans-1,2-Dichloroethene	6.5×10^3	[22]
Maleic acid	$\sim 6.5\times 10^3$	[22]
Muconic acid	$\sim 7.0\times 10^3$	[22]
Aromatics		Olefins formed on breakage of aromatic ring promotes O_3 decay via H_2O_2 formation[182]
Phenol	1.3×10^3- 1×10^{9a}	[22]
Chloro phenol	1100- 2×10^{8a}	[22]
Dimethyl phenol	$2.0 \times 10^4 – 10\times 10^4$	[22]
Naphthalene	1500-3000	[22]
Xylene	100	[22]
Bezafibrate	590	[22]
Catechol	5.2×10^5	[22]
1,4-Benzoquinone	2.5×10^3	[22]
Salicylic acid	$500 – 3.0\times10^{4a}$	[4]
Aliphatic acids		Promotes O_3 decay [91]
Formic acid	1.5 –100.0	[140, 143]
Glyoxalic acid	20.0	[293]

[a] Lower and upper limits represent the rate constants for the protonated and deprotonated forms respectively.

Table 8.4: Kinetic model describing reactions with TBA.

No	Reaction	Rate constant ($M^{-1}\cdot s^{-1}$)	Ref.
1	$^{\bullet}OH + (CH_3)_3COH \rightarrow H_2O + {}^{\bullet}CH_2C(CH_3)_2OH$	6×10^8	[141]
2	$2^{\bullet}CH_2C(CH_3)_2OH \rightarrow HO(CH_3)_2CH_2CH_2C(CH_3)_2OH$	6.5×10^8	[294]
3	$^{\bullet}CH_2C(CH_3)_2OH + O_2 \rightarrow {}^{\bullet}OOCH_2C(CH_3)_2OH$	1.8×10^9	[295]
4	$2^{\bullet}OOCH_2C(CH_3)_2OH \rightarrow [HOC(CH_3)_2CH_2OO]_2$	$k = (4 \pm 1) \times 10^8$	[294]
5	$[HOC(CH_3)_2CH_2OO]_2 \rightarrow O_2 + HOC(CH_3)_2\ CH_2OH + HOC(CH_3)_2\ CHO$	$R = 0.2^a$	[295]
6	$[HOC(CH_3)_2CH_2OO]_2 \rightarrow H_2O_2 + 2HOC(CH_3)_2\ CHO$	$R = 0.3^a$	[295]
7	$[HOC(CH_3)_2CH_2OO]_2 \rightarrow O_2 + 2CH_2O + 2^{\bullet}C(CH_3)_2OH$	$R = 0.25^a$	[295]
8	$[HOC(CH_3)_2CH_2OO]_2 \rightarrow O_2 + HOC(CH_3)_2CCH_2OOCH_2C(CH_3)_2OH$	$R = 0.25^a$	[295]
9	$^{\bullet}C(CH_3)_2OH + O_2 \rightarrow {}^{\bullet}OOC(CH_3)_2OH$	2×10^9	[295]
10	$^{\bullet}OOC(CH_3)_2OH \rightarrow (CH_3)_2C{=}O + HO_2^{\bullet}$	6×10^2	[295]
11	$CH_2O + {}^{\bullet}OH \rightarrow {}^{\bullet}HCO$	1×10^9	[296]
12	$CH_2O + O_3 \rightarrow {}^{\bullet}HCO + HO_3^{\bullet}$	0.1	[296]

decay of tetroxide intermediate is assumed to be rapid; a value of $R \times 10^6\ s^{-1}$ was adopted, with the proportions (R) taken Reisz *et al.*[295]

8.3.1.1 Inhibition of ozone decay kinetics

As shown in Figure 8.6a, the presence of TBA impacts ozone self-decay kinetics at pH 7.3 in phosphate buffered solution. In comparison, no significant (p>0.05 using single tailed student's t–test) influence of TBA addition on O_3 self–decay is observed in carbonate–buffered solution (Figure 8.6b). Scavenging of $^{\bullet}OH$ by TBA prevents ozone–$^{\bullet}OH$ interaction (eq. 8.10) and subsequent radical chain reactions, thereby decelerating the ozone self–decay rate in phosphate buffered solution. In carbonate buffered solution, HCO_3^-/CO_3^{2-} rapidly scavenges most of the $^{\bullet}OH$ formed, preventing ozone–$^{\bullet}OH$ interaction and hence no influence of TBA addition was observed on ozone self–decay in carbonate buffered solution. The stabilization of O_3 in the presence of TBA, particularly in systems where $^{\bullet}OH$ scavenging by the matrix is minimal, may facilitate the bulk oxidation of organics via direct interaction with O_3. Such an effect was observed in an earlier study wherein higher removal of sulfamethoxazole (SMX) was observed in the presence of TBA during HCO using a ceria based catalyst due to stabilization of O_3 in solution favouring the reaction between SMX and O_3, which is more selective than $^{\bullet}OH$ for the degradation of SMX.[283]

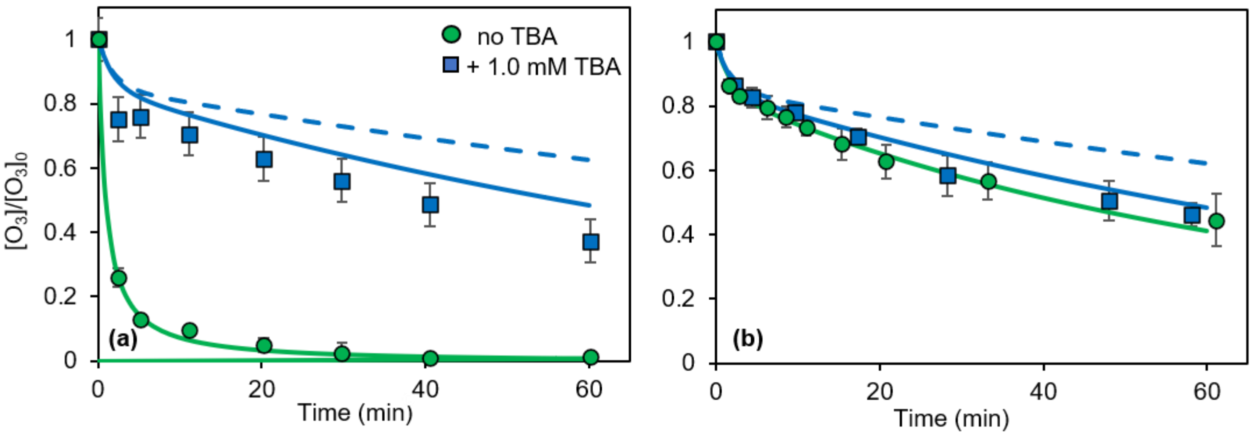

Figure 8.6 Ozone self–decay in the absence (circles) and presence of 1.0 mM TBA (squares) at pH 7.3 buffered using 1.33 mM phosphate solution (a) or 1.33 carbonate solution (b). Experimental conditions: $[O_3]_0$ = 100.0 µM, pH 7.3 using 1.33 mM phosphate/carbonate buffer. Symbols represent experimental data, lines represent model–predicted values. Note that the dashed lines represent model–predicted O_3 self-decay in the presence of 1.0 mM TBA if products formed on TBA–$^{\bullet}OH$ do not participate in any further reaction. Solid lines represent model-predicted O_3 self-decay in the presence of 1.0 mM TBA if products formed on TBA–$^{\bullet}OH$ undergo further reactions as described earlier [295] (see Table 8.3 for these reactions).

While the data presented here is for ozone self–decay kinetics, the stabilization of O_3 in the presence of TBA has previously been reported to occur during HCO employing $CuAl_2O_4$ based mixed oxides [192] and bauxites.[284] The stabilization of dissolved O_3 may facilitate O_3 diffusion and subsequent reaction with active sites on the catalyst surface thereby aiding the surface associated oxidation of organics as reported earlier.[192, 297, 298] Furthermore, as aforementioned, the stabilization of dissolved O_3 in the presence of TBA may also facilitate the bulk oxidation of organics via direct interaction with O_3.

Overall, stabilization of O_3 in the presence of TBA is likely to lead to inconclusive results in the case of ozone reactive compounds, either due to facilitation of surface mediated oxidation and/or bulk oxidation of organics by O_3. However, it may have no impact on the overall validity of TBA addition experiments for ozone-resistant compounds unless surface oxidation of these compounds is facilitated in the presence of TBA. For ozone–resistant compounds, even though TBA addition decreases O_3 decay, TBA addition will still result in inhibition of organic oxidation in agreement with the role of $^{\bullet}OH$ in organic oxidation in this system. The increased concentration of O_3 in the presence of TBA will not have any impact on the oxidation of ozone–resistant organics. Recently, Guo *et al.*[86] suggested that TBA is not a good probe compound to determine the role of $^{\bullet}OH$ in oxidation of 1,3 dichlorobenzene (*m*–DCB; an ozone resistant compound) based on the observation that TBA addition significantly inhibited ozone decay in the presence of MnO_2. However, their underlying assumption that an increase in the steady state dissolved O_3 concentration is problematic is not correct as explained above. Our argument is supported by the observation that $^{\bullet}OH$ is determined to be the main oxidant in *m*–DCB oxidation using other probe compounds in their work,[86] which agrees with the complete inhibition of oxidation of *m*–DCB in the presence of TBA observed in their study. Similarly, even though the presence of TBA resulted in higher residual ozone concentration during ozonation of atrazine (a relatively ozone resistant compound; k_{O_3}=2.3 $M^{-1}\cdot s^{-1}$ [299] and $k_{^{\bullet}OH}$=3.0×10^9 $M^{-1}\cdot s^{-1}$ [300]), TBA addition caused nearly complete inhibition of oxidation of atrazine in accordance with the role of $^{\bullet}OH$ in the oxidation of these organics moieties.[216] Note that if $O_2^{\bullet-}$, formed via chain reactions initiated on $^{\bullet}OH$ mediated oxidation of organics is directly involved in the oxidation of organics, then addition of TBA will inhibit superoxide–mediated oxidation of organics and lead to erroneous conclusions. However, direct oxidation of organics via interaction with $O_2^{\bullet-}$ is unlikely as $O_2^{\bullet-}$ is expected to react with O_3 rather than the organics since (i) the rate constant for O_3 and $O_2^{\bullet-}$ reaction

(1.6×10^{9} $M^{-1}\cdot s^{-1}$)[301] is much higher than the reported rate constants for $O_2^{\bullet-}$ reaction with various organics, and (ii) the concentration of O_3 is usually higher than the micropollutants concentration. As reported in an earlier study, any role of $O_2^{\bullet-}$ in organic oxidation reported in various earlier studies is due to generation of $^{\bullet}OH$ via O_3 and $O_2^{\bullet-}$ reaction and not due to direct oxidation of organics by $O_2^{\bullet-}$.[29]

8.3.1.2 Involvement of TBA derived radicals in O_3 decay

Another important limitation with the use of TBA which has not been carefully considered and may potentially be important is related to the influence of radicals formed on TBA–$^{\bullet}$OH reaction on ozone decay and associated oxidation of organics. Earlier studies have reported that the $^{\bullet}$OH–mediated oxidation of TBA is initiated by hydrogen–atom abstraction with the resultant alkyl radicals transforming to peroxyl radicals on reaction with O_2 (eqs. 8.14 – 16).[258, 295]

$$HO^{\bullet} + (CH_3)_3COH \longrightarrow H_2O + {}^{\bullet}CH_2C(CH_3)_2OH \qquad (8.14)$$

$$2\,{}^{\bullet}CH_2C(CH_3)_2OH \longrightarrow HO(CH_3)_2CH_2CH_2C(CH_3)_2OH \qquad (8.15)$$

$${}^{\bullet}CH_2C(CH_3)_2OH + O_2 \longrightarrow {}^{\bullet}OOCH_2C(CH_3)_2OH \qquad (8.16)$$

$$2\,{}^{\bullet}OOCH_2C(CH_3)_2OH \longrightarrow [HOC(CH_3)_2CH_2OO]_2 \qquad (8.18)$$

$$[HOC(CH_3)_2CH_2OO]_2 \longrightarrow O_2 + HOC(CH_3)_2CH_2OH + HOC(CH_3)_2CHO \qquad (8.18)$$

$$[HOC(CH_3)_2CH_2OO]_2 \longrightarrow H_2O_2 + 2HOC(CH_3)_2CHO \qquad (8.19)$$

$$[HOC(CH_3)_2CH_2OO]_2 \longrightarrow O_2 + 2CH_2O + 2\,{}^{\bullet}C(CH_3)_2OH \qquad (8.20)$$

$$[HOC(CH_3)_2CH_2OO]_2 \longrightarrow O_2 + HOC(CH_3)_2CCH_2OOCH_2C(CH_3)_2OH \qquad (8.21)$$

$$^{\bullet}C(CH_3)_2OH + O_2 \longrightarrow {}^{\bullet}OOC(CH_3)_2OH \qquad (8.22)$$

$$^{\bullet}OOC(CH_3)_2OH \longrightarrow (CH_3)_2C{=}O + HO_2^{\bullet} \qquad (8.23)$$

The peroxyl radicals so formed undergo a series of reactions (eqs. 8.17 – 23) ultimately forming formaldehyde and acetone which oxidize further to form a variety of low molecular weight products.[295] In the presence of ozone, alkyl and peroxyl radicals so formed also undergo reaction with O_3 forming oxyl radicals with earlier report suggesting that ~ 10% of the TBA radicals (alkyl and peroxyl radical) produced are transformed into oxyl radicals.[295]

$$^{\bullet}CH_2C(CH_3)_2OH + O_3 \longrightarrow {}^{\bullet}OCH_2C(CH_3)_2OH + O_2 \qquad (8.24)$$

$$^{\bullet}OOCH_2C(CH_3)_2OH + O_3 \longrightarrow {}^{\bullet}OCH_2C(CH_3)_2OH + 2O_2 \qquad (8.25)$$

These oxyl radicals also undergo rapid rearrangement in aqueous solution ultimately forming second and third generation peroxyl radicals.[258, 295] Though peroxyl radicals have lower reactivity than $^{\bullet}OH$, the lifetime of these radicals is higher than $^{\bullet}OH$ and may play a role in the oxidation of various organic compounds.[302] Furthermore, peroxyl radicals may initiate O_3 decay [295] and/or undergo dismutation forming H_2O_2 and $O_2^{\bullet-}$ (see eqs. 8.17 – 23) [303] which facilitates O_3 decay. While direct and/or indirect measurement of peroxyl radicals in the ozonation system using probe compounds (such as *p*–aminobenzoic acid [302]) and/or scavengers is not feasible due to the rapid reaction of most probe compounds and/or scavengers with O_3 and/or $^{\bullet}OH$, we used the modelling approach developed here to determine the role of TBA–associated radicals in O_3 decay. As shown in Figure 8.6a and b, the model-predicted ozone decay in the presence of TBA, if the radicals/products formed on TBA–$^{\bullet}$OH reaction are inert (shown by the dashed line), slightly underpredicts the ozone decay rate. However, when the decay of TBA radicals (ultimately resulting in formation of formaldehyde and acetone based on the mechanism reported earlier [295] and shown in eqs. 8.14 – 23) is included in the kinetic model, we observe improved description of O_3 self–decay in the presence of TBA, thereby supporting the hypothesis that TBA associated radicals and products slightly influence O_3 decay. While the role of TBA associated radicals in organic oxidation is not clear and will be dependent on the nature of the organics, it is unlikely to exert a strong influence on the oxidation of organics given that only small influence of these radicals on ozone self-decay is observed. Nevertheless, TBA scavenging results should be carefully considered and proper control experiments should be performed to ensure that the role of TBA associated radicals is minimal, particularly if enhancement in the O_3 decay rate and/or organic oxidation is observed in the presence of TBA.

8.3.2 Limitations associated with the use of TBA in HCO

The limitations described in the previous section for ozonation also apply to HCO. In addition, there are several other drawbacks associated with the use of TBA during HCO. These are described in the following sections.

8.3.2.1 No access to surface hydroxyl radicals generated during HCO

One of the major limitations with the use of TBA as $^{\bullet}$OH probe in HCO is that TBA may not scavenge surface generated $^{\bullet}$OH due to the low surface affinity of TBA.[260] As shown in Figures 8.7a and b, the formation of fluorescent 7–HC occurs on the surface of Cu-Al LDHs on HCO of coumarin, even in the presence of TBA, confirming that (i) surface $^{\bullet}$OH are formed during HCO employing Cu-Al LDHs as the catalyst and (ii)

TBA is not able to quench the surface $^{\bullet}OH$. Increasing the TBA concentration to 100.0 mM had no influence on the formation of fluorescent 7–HC (Figure 8.8) confirming that the inability of TBA to scavenge surface $^{\bullet}OH$ is not due to limited TBA concentration. Note that no formation of 7–HC was observed on ozonation of coumarin in the absence and presence of 1.0 mM TBA (Figure 8.9) confirming that 7–HC formation via direct reaction between O_3 (and/or bulk $^{\bullet}OH$) and coumarin is negligible with only surface $^{\bullet}OH$ contributing to 7–HC formation during Cu–Al LDHs-mediated ozonation of coumarin. As explained in detail in chapter 5, minimal contribution of bulk $^{\bullet}OH$ (formed on O_3 self-decay) to 7–HC formation is in agreement with the results of earlier work [29] and was possibly due to (i) limited concentration of bulk $^{\bullet}OH$ formed, (ii) rapid oxidation of coumarin by O_3 (rather than bulk $^{\bullet}OH$) in the absence of catalyst and/or (iii) rapid further oxidation of any 7–HC formed by bulk O_3 and/or $^{\bullet}OH$. We would also like to highlight that the evidence of 7–HC formation in the case of Cu–Al LDHs is not an artefact of sample preparation and/or imaging procedure since no evidence of surface 7–HC formation was observed when CuO was used as the catalyst instead of Cu–Al LDHs (Figure 8.10). Since TBA is not able to quench surface $^{\bullet}OH$, the conclusion regarding insignificance of $^{\bullet}OH$-mediated processes in HCO solely based on TBA quenching experiments reported in many earlier studies[26, 79, 80, 96, 97, 130, 161, 169, 290, 304-311] may not be correct. For example, Ikhlaq and Kasprzyk-Hordern[310] excluded the involvement of $^{\bullet}OH$ in HCO employing zeolites as the catalyst based on the observed lack of influence of TBA on the catalytic ozonation performance even though some other studies have shown that zeolites facilitate the generation of $^{\bullet}OH$ via O_3 decay.[78, 312] Furthermore, the partial inhibition of oxidation of organics by HCO in the presence of TBA observed in some earlier studies may possibly be due to involvement of both surface and bulk $^{\bullet}$OH rather than the hypothesized bulk $^{\bullet}$OH, $O_2^{\bullet-}$ and/or O_3 mediated oxidation in these studies.[169, 282, 313-318] The partial inhibition of oxalate and ketoprofen oxidation by HCO in the presence of TBA in recent studies may possibly be due to involvement of both bulk and surface $^{\bullet}$OH rather than due to reaction with bulk O_3 and $^{\bullet}$OH as proposed.[169, 282] Similarly, in the study by Dai et al[313], surface $^{\bullet}$OH may play a partial role since TBA addition only partially decreases the oxidation of 5–sulfosalicylic acid (SSal) by HCO, however the involvement of surface $^{\bullet}$OH was not considered by these investigators. In view of these potentially compromised results, it is recommended that alternate techniques such as fluorescence microscopy imaging using coumarin be employed to probe the generation of surface $^{\bullet}$OH in case no/partial influence of TBA addition on the catalytic activity in HCO is observed.

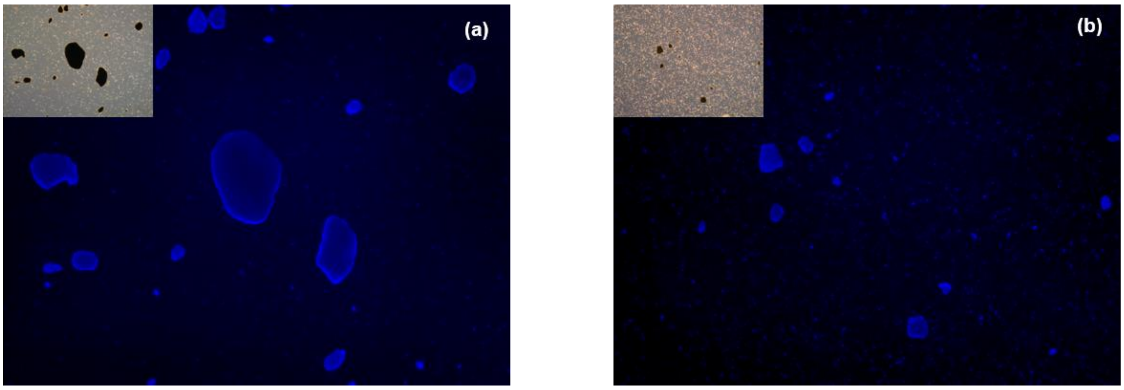

Figure 8.7 Fluorescence microscopy image of samples following HCO of coumarin in the absence (a) and presence (b) of 1.0 mM TBA after 60 min of treatment. Experimental conditions: [Cu–Al LDHs]$_0$ = 0.06 g L^{-1}, $[O_3]_0$ = 100.0 µM, [coumarin]$_0$ = 10.0 µM, pH 7.3 using 2.0 mM $NaHCO_3$.

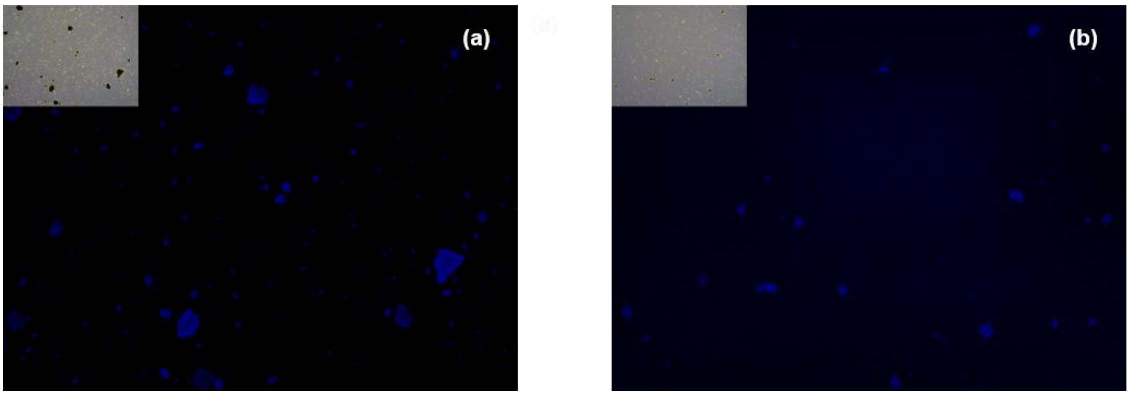

Figure 8.8 Fluorescence microscopy image of samples following HCO of coumarin in the presence of 10.0 mM (a) and 100.0 mM (b) TBA after 60 min of treatment. Experimental conditions: [Cu–Al LDHs]$_0$ = 0.06 g L^{-1}, $[O_3]_0$ = 100.0 µM, [coumarin]$_0$ = 10.0 µM, pH 7.3 using 1.33 mM $NaHCO_3$.

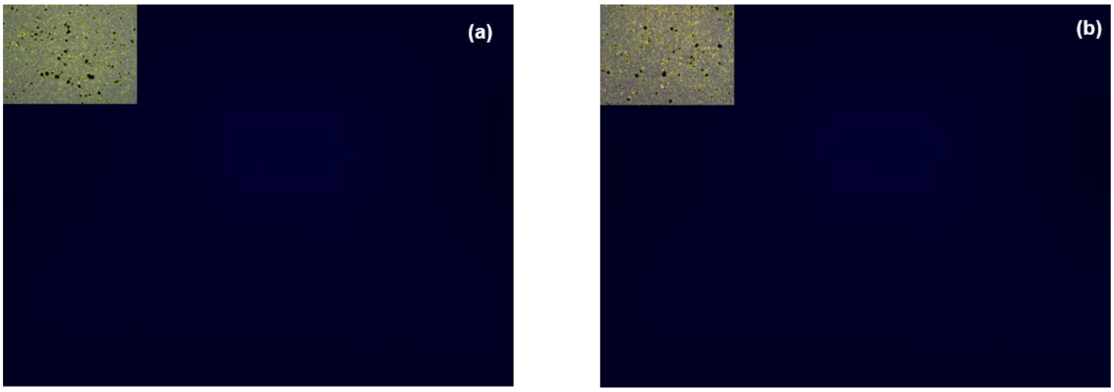

Figure 8.9 Fluorescence microscopy image of samples prepared by ozonation of coumarin in the absence (a) and presence of 1.0 mM TBA (b) for 60 min and then sorbed onto Cu–Al LDHs surface for 60 min. Experimental conditions: $[O_3]_0$ = 100.0 µM, [coumarin]$_0$ = 10.0 µM, pH 7.3 using 1.33 mM $NaHCO_{39}$. [Cu-Al LDHs]$_0$ = 0.06 g L^{-1} during the sorption step.

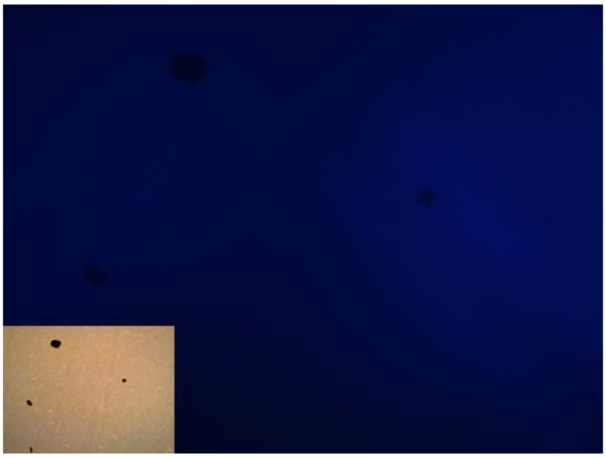

Figure 8.10 Fluorescence microscopy image of samples following HCO of coumarin for 60 min using CuO as the catalyst. Experimental conditions: $[CuO]_0$ = 0.06 g L^{-1}, $[O_3]_0$ = 100.0 µM, [coumarin]$_0$ = 10.0 µM, pH 7.3 using 1.33 mM $NaHCO_3$.

8.3.2.2 Interference with the adsorption of organic compounds during HCO

Though some earlier studies have reported that TBA does not compete with organics for surface adsorption sites,[306, 307, 319] our results show that the presence of TBA may interfere with the adsorption of organics on the catalyst surface. As shown in Figure 8.11a, the addition of 0.1 mM TBA decreased $HCOO^-$ adsorption on the Fe-loaded activated carbon surface at pH 3.0 (note that $HCOO^-$ represents the total formate concentration including both protonated and deprotonated concentrations). Similarly, inhibition of $C_2O_4^{2-}$ sorption on the CuO surface at pH 7.3 was observed in the presence of TBA, albeit at a very high TBA concentration (Figure 8.11b). The inhibition of adsorption of organics in the presence of TBA is likely to influence the surface oxidation (if important) of organics. A similar impact of TBA addition was observed on the adsorption of oxalic acid on the Fe–SBA–15 surface.[149] The effect of TBA addition was also observed on rhodamine B (RhB) adsorption and subsequent degradation by HCO employing an Fe based metal-organic framework as the catalyst.[281] As reported by Yu *et al.*,[281] the presence of TBA at a concentration of 2 $g.L^{-1}$ facilitated RhB adsorption (and subsequent oxidation) on the catalyst surface by increasing the porosity of the catalysts however increasing the TBA concentration to 60 $g.L^{-1}$ led to a decrease in the RhB adsorption due to occupation of surface sites by TBA. The impact of TBA addition on the adsorption of organic compounds suggests that caution should be taken when interpreting the results obtained in the presence of TBA since the impact of TBA observed in the HCO process may not be entirely due to scavenging of $^{\bullet}OH$ but due to decrease in the adsorption and concomitant oxidation of organics via a non–radical mediated pathway.

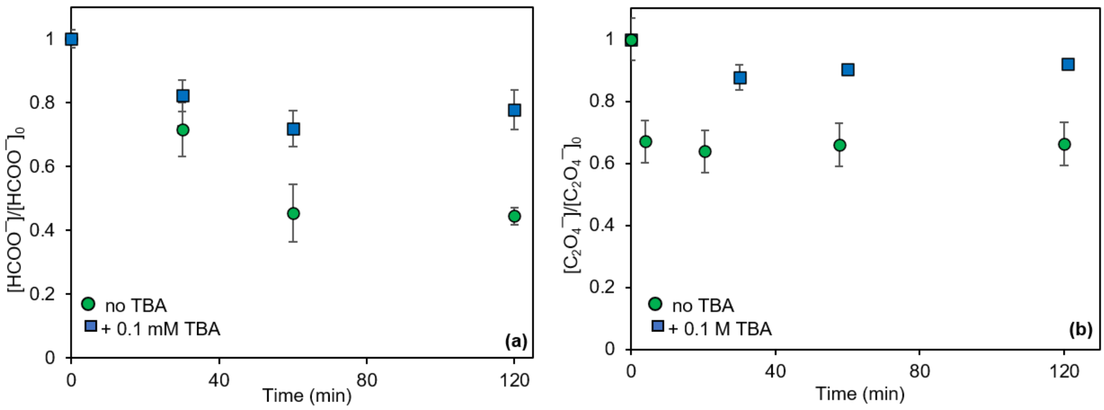

Figure 8.11 (a) $HCOO^{-}$ adsorption on the surface of Fe–AC at pH 3.0 in the absence (circles) and presence (squares) of 0.1 mM TBA. Experimental conditions: $[Fe–AC]_0 = 10.0$ g L^{-1}, $[HCOO^{-}]_0 = 1.0$ μM, pH 3.0. (b) $C_2O_4^{2-}$ adsorption on the surface of CuO at pH 7.3 in the absence (circles) and presence (squares) of 0.1 M TBA. Experimental conditions: $[CuO]_0 = 0.6$ g L^{-1}, $[C_2O_4^{2-}]_0 = 1.0$ μM, pH 7.3.

8.4 Conclusions

The results presented here clearly show that observations of the impact of TBA addition on HCO and/or conventional ozonation may not lead to the correct deduction concerning the contribution of $^{\bullet}OH$ in organic oxidation since TBA (i) may not be able to access surface located $^{\bullet}OH$, (ii) results in alteration of the oxidation pathway from $O_3/^{\bullet}OH$ mediated oxidation in the absence of TBA to O_3 driven oxidation in the presence of TBA, (iii) decreases O_3 decay rate, and (iv) interferes with the adsorption of organic contaminants to the catalyst surface.

We would like to highlight that even though the impact of a single TBA concentration is investigated here, the conclusions presented here are valid at higher TBA concentrations as well. Use of lower TBA concentrations may mitigate some of the effects discussed here though, usually, excess TBA (in the concentration range 0.3 mM - 0.1 M) [169, 320] is used to facilitate scavenging of all $^{\bullet}OH$ present. As such, the TBA concentration used here is reasonably representative of the concentrations used in TBA scavenging studies by other investigators. Note that while we have highlighted the limitations associated with the use of TBA, these limitations also apply, to varying degrees depending on surface affinity, to other organic and/or inorganic scavengers of $^{\bullet}OH$ (such as sodium azide and/or sodium bicarbonate and sodium silicate) used in various earlier studies.

To summarize, the flow chart shown in Figure 8.12 should be used to determine whether TBA addition results can conclusively determine the role of $^{\bullet}OH$ in HCO and/or conventional ozonation processes. As highlighted, the current interpretation of TBA scavenging results in most studies (shown in the inset in Figure 8.12) is significantly flawed with the need for further testing required to convincingly determine the role of $^{\bullet}OH$ in the oxidation of organic compounds. As shown in the flowchart, TBA scavenging results are inconclusive for organic compounds that are ozone reactive and promote decay. Furthermore, if surface sorption of organics decreases in the presence of TBA, TBA scavenging results can be misleading. For the former case, other methods such as R_{ct} approach should be used determine the role of $^{\bullet}OH$ in organic oxidation. For the latter case, further investigation using other probe methods and/or measurement of oxidation products of TBA should be performed to verify if the decreased removal of organics in the presence of TBA is due to the inhibition of oxidation or sorption of organics. TBA scavenging results are inconclusive even for ozone resistant compounds if (i) partial inhibition of oxidation of organics and (ii) decreased ozone decay rate is observed in the presence of TBA. In this case, while on one hand TBA addition inhibits $^{\bullet}OH$–mediated oxidation of organics, it also decreases O_3 decay with the higher O_3 concentration in solution facilitating surface associated oxidation via direct interaction with O_3 and/or other oxidant(s) (generated on O_3 decay) thereby resulting in partial decrease in the oxidation of organics.

Overall, based on the results shown here, TBA is best employed as a bulk •OH scavenger for ozone resistant compounds. Thus, there is an immediate need to develop other simple methods to determine the role of •OH (including both surface and bulk) in organic oxidation during ozonation and HCO. In the interim, TBA scavenging results should be interpreted in conjunction with other measurement including fluorescence imaging method, R_{ct} method and quantification of TBA oxidation products.

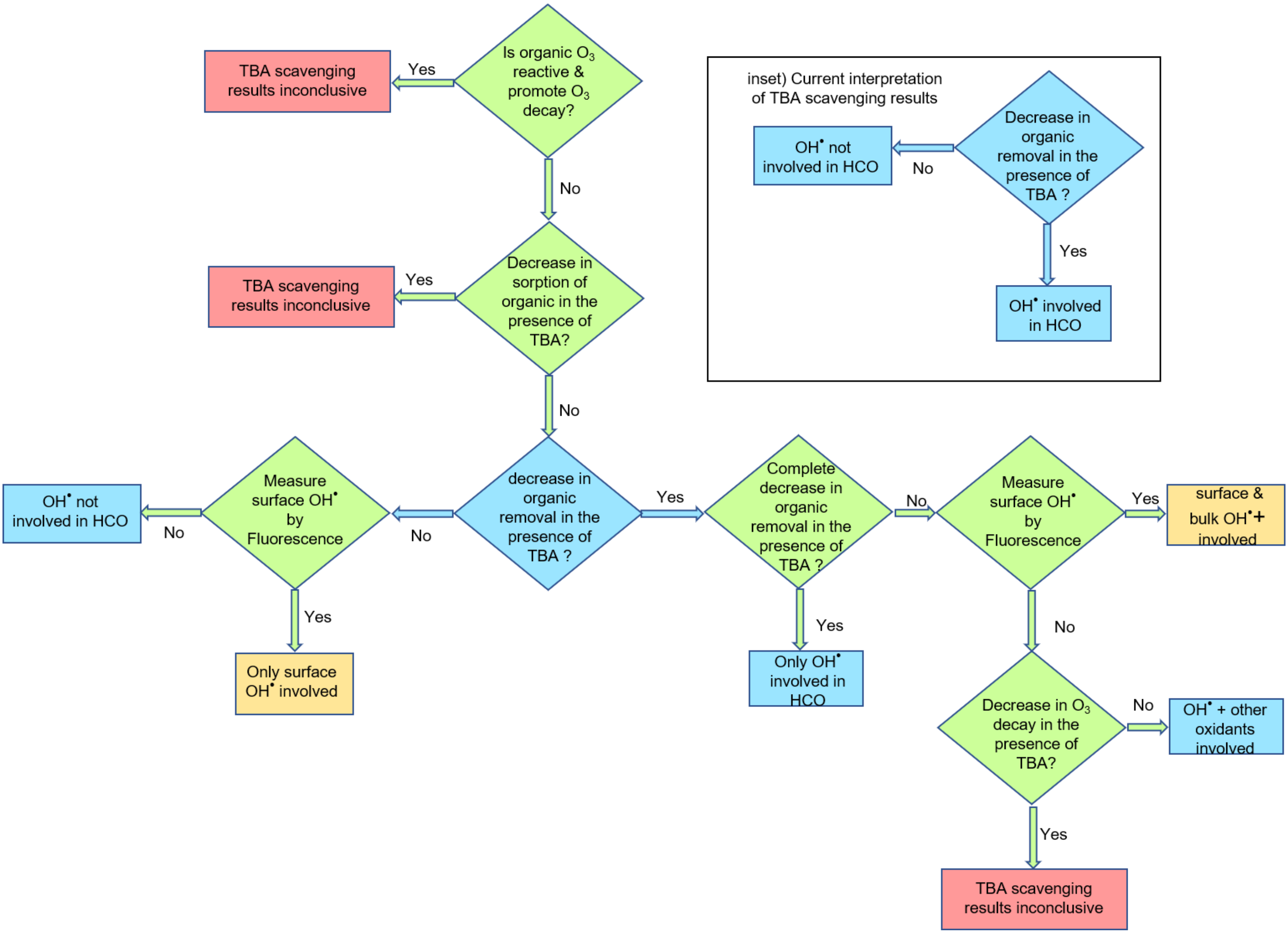

Figure 8.12 Flowchart indicating the steps required following TBA addition experiments to correctly understand the role of •OH in organic oxidation

Chapter 9 Conclusions and implications

This thesis investigated the mechanism of catalytic ozonation using carbon, copper and iron-based catalysts by quantifying the rate of decay of O_3 and oxidation of various organics in the presence of these catalysts. In addition, we have investigated the influence of salinity and matrix on the performance of catalytic ozonation.

Our results show that the presence of iron-impregnated activated carbon enhanced O_3 decay and formate oxidation at pH 3.0 compared to that observed in the presence of O_3 alone due to the generation of oxidants via O_3–Fe oxide interaction. The decrease in the rate and extent of formate oxidation in the presence of TBA and Cl^- (which are known bulk $^{\bullet}OH$ scavengers under acidic conditions) confirmed that the oxidant generated during the catalytic ozonation process employing Fe-oxide/AC catalyst is $^{\bullet}OH$. Moreover, these results confirmed that the oxidation of formate mostly occurs in the solid–liquid interface and/or the bulk solution with surface adsorption of organics playing no role in the overall oxidation of organics. The catalyst was not active at pH 7.3 and 8.5 suggesting that only protonated iron oxide surface sites generate strong oxidant(s) on interaction with O_3. We also developed a mathematical kinetic model which describes the ozone decay and oxidation of formate by this catalyst over a range of conditions.

When CuO and Cu–Al LDHs were employed as the catalyst in the catalytic ozonation process, oxidation of oxalate mostly occurred on the catalyst surface via interaction of surface oxalate complexes with surface–located oxidants. In contrast, the oxidation of formate occurred in the bulk solution as well as on the surface of the catalyst. Measurement of O_3 decay kinetics coupled with fluorescence microscopy image analysis corresponding to 7–hydroxycoumarin formation indicated that while surface hydroxyl groups in Cu−Al LDHs facilitate slow decay of O_3 resulting in the formation of hydroxyl radicals on the surface, CuO rapidly transforms O_3 into surface-located hydroxyl radicals and/or other oxidants. Futile consumption of surface-located oxidants via interaction with the catalyst surface was minimal for Cu−Al LDHs; however, it becomes significant in the presence of higher CuO dosages. Based on the mechanistic insights provided, we have also developed a mathematical kinetic model which describes the O_3 decay kinetics and organic oxidation in the presence of these catalysts very well and can be used to optimize the process conditions such that contaminant degradation by the catalytic ozonation process is maximized.

The influence of the matrix on the performance of ozonation and catalytic ozonation processes employing CuO and Cu–Al LDHs as catalyst was also investigated. Our results reveal that the rate of ozone self-decay was considerably faster in phosphate buffered solution compared to that in carbonate buffered solution with this effect resulting from differing $^{\bullet}OH$ scavenging capacities of the buffering ions. Interestingly, while the nature of the buffers used affected the rate of O_3 self–decay, there was minimal effect on the overall extent of oxidation of the formate and oxalate by conventional ozonation. The results obtained indicated that the carbonate radicals generated as a result of carbonate – $^{\bullet}OH$ reaction are capable of oxidizing the low molecular weight acids such as formate and oxalate however the oxidation of these organics by phosphate radicals appears to be minimal. In the catalytic ozonation process, the presence of phosphate ions affects the surface chemistry of the Cu–based catalysts with phosphate ions inhibiting catalyst mediated O_3 decay and sorption of the target organic compounds on the catalyst surface, thereby decreasing the overall rate and extent of oxidation of target organics. Overall, our results show that the performance of the catalytic ozonation process will be underestimated in phosphate buffered solution particularly if surface reactions play an important role in the oxidation of organics.

We also investigated the performance of commercially available Fe-loaded Al_2O_3 catalyst in treating synthetic reverse osmosis concentrate and measured the influence of salinity on the overall performance. Our results show that the scavenging of aqueous O_3 by chloride ions and/or transformation of organics (particularly humics) to more hydrophobic form as a result of charge shielding between adjacent functional groups and/or intramolecular binding by cations inhibits the bulk oxidation of organics to a measurable extent. While the scavenging of aqueous hydroxyl radicals at the salt concentrations investigated here was minimal, the accumulation of chloride ions in the electric double layer near the catalyst surface, particularly when $pH < pH_{pzc}$, results in more significant scavenging of surface associated hydroxyl radicals. Overall, our results showed that the presence of salts (particularly chloride ions) has a significant influence on the performance of both conventional and catalytic ozonation processes.

We also discussed the caveats associated with use of TBA as a $^{\bullet}OH$ scavenger in the ozonation and catalytic ozonation processes. Our results show that TBA may not be able to access surface located $^{\bullet}OH$ formed during HCO. Furthermore, TBA may also interfere with the adsorption of organics on the catalyst surface and decrease the adsorptive as well as concomitant oxidative removal of organics via non radical mediated pathways (if important). Moreover, TBA scavenging results are inconclusive for mildly ozone reactive compounds due to switching from $O_3/^{\bullet}OH$ mediated oxidation in the absence of TBA to O_3 driven oxidation in the presence of TBA. The presence of TBA may also decrease the rate of ozone decay with the increased stability of O_3 in the presence of TBA facilitating (i) direct oxidation of ozone-reactive organics in the bulk solution and/or (ii) diffusion of O_3 to the surface and subsequent surface-mediated oxidation of organics.

Overall, the results of this study show that the performance of the catalytic ozonation process is highly dependent on the nature of the catalyst as well as the organics as a result of their influence on (i) generation and decay of oxidants, (ii) adsorption of organics on the catalyst surface, and (iii) importance of surface versus bulk oxidation. For example, Fe-impregnated activated carbon drove the oxidation of formate mainly in the solid-liquid interface with adsorption playing no role in formate oxidation. In contrast, CuO and Cu–Al LDHs favoured the oxidation of oxalate on the surface with adsorption enhancing organic oxidation. The bulk oxidation is expected to more sensitive towards the constituents of the matrix (such as Cl^-) compared to surface mediated oxidation of organics. The influence of the nature of the organics on the efficacy of the catalytic ozonation process suggests that the design of the ozonation process should be modified according to the nature of the organic compounds present in the wastewater to be treated. For organic compounds that can be readily oxidized by O_3, a homogeneous ozonation process is expected to be more cost-effective than a catalytic ozonation process. In contrast, a catalytic ozonation process is required for the oxidation of organic compounds that are refractory to direct ozone oxidation. In general, a multistage ozone process employing a separate homogeneous ozone reactor followed by a catalytic ozone process is recommended for the efficient usage of ozone and catalyst for the treatment of wastewaters containing complex organic mixtures.

Careful attention should be paid to the experimental design of the catalytic ozonation process, especially in studies designed to provide insights into the oxidation pathway(s) during the ozonation and catalytic ozonation processes. Moreover, the pH should be well controlled since the difference in pH between ozonation and catalytic ozonation processes will result in erroneous conclusions regarding the efficacy of the catalysts. Lastly, caution should be exercised when selecting the buffer that will be used in investigations of the conventional ozonation and catalytic ozonation processes as a result of varying surface affinity and ROS scavenging capacity of buffering ions.

The mechanism-based mathematical kinetic models developed here are very useful tools for providing important insights into the ozonation and catalytic ozonation processes employing a range of catalysts. While probe methods employing compounds such as *p*–CBA and TBA can be used to investigate the generation of radicals and the rate and extent of organics oxidation for conventional ozonation, quantitative analysis of surface–related reactions with any probe compound is challenging due to the varying surface affinity of probes toward different catalysts and the difficulty in quantifying the extent of oxidation of probe compounds located on the catalyst surface. Hence, for the catalytic ozonation process, where surface-mediated processes are likely to dominate, we are of the opinion that the kinetic modeling approach used here will be of value in providing mechanistic insight, though more careful validation of these kinetic models is needed prior to their application to complex real wastewater matrices. The kinetic models developed in this study can be readily extended to other catalysts though the determination of certain rate constants appropriate to the particular catalyst of interest will be required. Moreover, the kinetic models developed in this thesis can also be used to optimize the full–scale reactor design for ozonation and catalytic ozonation processes by combining these kinetic models with hydrodynamics using modelling tools such as computational fluid dynamics (CFD).

References

1. Beltrán, F. J., *Ozone reaction kinetics for water and wastewater systems*. CRC: Boca Raton, pp.113-149, 2003.
2. Bailey, P. S., The reactions of ozone with organic compounds. *Chemical Reviews* **1958,** *58*, (5), 925-1010.
3. Hoigné, J.; Bader, H., Rate constants of reactions of ozone with organic and inorganic compounds in water—II: Dissociating organic compounds. *Water Research* **1983,** *17*, (2), 185-194.
4. Hoigné, J.; Bader, H., Rate constants of reactions of ozone with organic and inorganic compounds in water—I: Non-dissociating organic compounds. *Water Research* **1983,** *17*, (2), 173-183.
5. Hoigné, J.; Bader, H.; Haag, W. R.; Staehelin, J., Rate constants of reactions of ozone with organic and inorganic compounds in water—III. Inorganic compounds and radicals. *Water Research* **1985,** *19*, (8), 993-1004.
6. Hoigne, J.; Bader, H., Ozonation of water: role of hydroxyl radicals as oxidizing intermediates. *Science* **1975**, 782-784.
7. Fábián, I., Reactive intermediates in aqueous ozone decomposition: A mechanistic approach. *Pure and applied chemistry* **2006,** *78*, (8), 1559-1570.
8. Mizuno, T.; Tsuno, H.; Yamada, H., Development of Ozone Self-Decomposition Model for Engineering Design. *Ozone: Science & Engineering* **2007,** *29*, (1), 55-63.
9. Guo, Y.; Zhan, J.; Yu, G.; Wang, Y., Evaluation of the concentration and contribution of superoxide radical for micropollutant abatement during ozonation. *Water Research* **2021,** *194*, 116927.
10. Yang, Y.; Liu, Z.; Demeestere, K.; Van Hulle, S., Ozonation in view of micropollutant removal from biologically treated landfill leachate: Removal efficiency, OH exposure, and surrogate-based monitoring. *Chemical Engineering Journal* **2021,** *410*, 128413.
11. Thalmann, B.; von Gunten, U.; Kaegi, R., Ozonation of municipal wastewater effluent containing metal sulfides and metal complexes: Kinetics and mechanisms. *Water Research* **2018,** *134*, 170-180.
12. Tentscher, P. R.; Bourgin, M.; von Gunten, U., Ozonation of *Para*-Substituted Phenolic Compounds Yields p-Benzoquinones, Other Cyclic *α, β*-Unsaturated Ketones, and Substituted Catechols. *Environmental science & technology* **2018,** *52*, (8), 4763-4773.
13. Liu, Z.; Yang, Y.; Shao, C.; Ji, Z.; Wang, Q.; Wang, S.; Guo, Y.; Demeestere, K.; Hulle, S. V., Ozonation of trace organic compounds in different municipal and industrial wastewaters: Kinetic-based prediction of removal efficiency and ozone dose requirements. *Chemical Engineering Journal* **2019**, 123405.
14. Reisz, E.; von Sonntag, C.; Tekle-Röttering, A.; Naumov, S.; Schmidt, W.; Schmidt, T. C., Reaction of 2-propanol with ozone in aqueous media. *Water Research* **2018,** *128*, (Supplement C), 171-182.
15. Önnby, L.; Salhi, E.; McKay, G.; Rosario-Ortiz, F. L.; von Gunten, U., Ozone and chlorine reactions with dissolved organic matter - Assessment of oxidant-reactive moieties by optical measurements and the electron donating capacities. *Water Research* **2018,** *144*, 64-75.
16. Chys, M.; Demeestere, K.; Nopens, I.; Audenaert, W. T. M.; Van Hulle, S. W. H., Municipal wastewater effluent characterization and variability analysis in view of

an ozone dose control strategy during tertiary treatment: The status in Belgium. *Science of The Total Environment* **2018,** *625*, 1198-1207.
17. Weng, J.; Jia, H.; Wu, B.; Pan, B., Is ozonation environmentally benign for reverse osmosis concentrate treatment? Four-level analysis on toxicity reduction based on organic matter fractionation. *Chemosphere* **2018,** *191*, 971-978.
18. Hübner, U.; von Gunten, U.; Jekel, M., Evaluation of the persistence of transformation products from ozonation of trace organic compounds–a critical review. *water research* **2015,** *68*, 150-170.
19. Lee, M.; Blum, L. C.; Schmid, E.; Fenner, K.; Von Gunten, U., A computer-based prediction platform for the reaction of ozone with organic compounds in aqueous solution: kinetics and mechanisms. *Environmental Science: Processes & Impacts* **2017,** *19*, (3), 465-476.
20. Lee, M.; Zimmermann-Steffens, S. G.; Arey, J. S.; Fenner, K.; von Gunten, U., Development of prediction models for the reactivity of organic compounds with ozone in aqueous solution by quantum chemical calculations: the role of delocalized and localized molecular orbitals. *Environmental science & technology* **2015,** *49*, (16), 9925-9935.
21. Remucal, C. K.; Salhi, E.; Walpen, N.; von Gunten, U., Molecular-Level Transformation of Dissolved Organic Matter during Oxidation by Ozone and Hydroxyl Radical. *Environmental Science & Technology* **2020,** *54*, (16), 10351-10360.
22. von Sonntag, C.; von Gunten, U., *Chemistry of ozone in water and wastewater treatment*. IWA publishing, London 2012.
23. Zhu, H.; Ma, W.; Han, H.; Han, Y.; Ma, W., Catalytic ozonation of quinoline using nano-MgO: Efficacy, pathways, mechanisms and its application to real biologically pretreated coal gasification wastewater. *Chemical Engineering Journal* **2017,** *327*, 91-99.
24. Sirés, I.; Brillas, E.; Oturan, M. A.; Rodrigo, M. A.; Panizza, M., Electrochemical advanced oxidation processes: today and tomorrow. A review. *Environmental Science and Pollution Research* **2014,** *21*, (14), 8336-8367.
25. Zhang, T.; Li, W.; Croué, J.-P., A non-acid-assisted and non-hydroxyl-radical-related catalytic ozonation with ceria supported copper oxide in efficient oxalate degradation in water. *Applied Catalysis B: Environmental* **2012,** *121-122*, 88-94.
26. Zhang, T.; Li, W.; Croué, J.-P., Catalytic ozonation of oxalate with a cerium supported palladium oxide: an efficient degradation not relying on hydroxyl radical oxidation. *Environmental Science & Technology* **2011,** *45*, (21), 9339-9346.
27. Ernst, M.; Lurot, F.; Schrotter, J.-C., Catalytic ozonation of refractory organic model compounds in aqueous solution by aluminum oxide. *Applied Catalysis B: Environmental* **2004,** *47*, (1), 15-25.
28. Vel Leitner, N. K.; Delouane, B.; Legube, B.; Luck, F., Effects of catalysts during ozonation of salicylic acid, peptides and humic substances in aqueous solution. *Ozone: Science & Engineering* **1999,** *21*, (3), 261-276.
29. Zhang, S.; Quan, X.; Zheng, J.-F.; Wang, D., Probing the interphase “HO zone” originated by carbon nanotube during catalytic ozonation. *Water Research* **2017,** *122*, (Supplement C), 86-95.
30. Legube, B.; Leitner, N. K. V., Catalytic ozonation: a promising advanced oxidation technology for water treatment. *Catalysis Today* **1999,** *53*, (1), 61-72.
31. Wang, J.; Chen, H., Catalytic ozonation for water and wastewater treatment: Recent advances and perspective. *Science of The Total Environment* **2019**, 135249.

32. Kasprzyk-Hordern, B., Chemistry of alumina, reactions in aqueous solution and its application in water treatment. *Advances in Colloid and Interface Science* **2004,** *110*, (1), 19-48.
33. Yang, L.; Hu, C.; Nie, Y.; Qu, J., Catalytic ozonation of selected pharmaceuticals over mesoporous alumina-supported manganese oxide. *Environmental science & technology* **2009,** *43*, (7), 2525-2529.
34. Song, S.; Liu, Z.; He, Z.; Zhang, A.; Chen, J.; Yang, Y.; Xu, X., Impacts of Morphology and Crystallite Phases of Titanium Oxide on the Catalytic Ozonation of Phenol. *Environmental Science & Technology* **2010,** *44*, (10), 3913-3918.
35. Psaltou, S.; Kaprapa, E.; Triantafyllidis, K.; Mitrakas, M.; Zouboulis, A., Heterogeneous catalytic ozonation–The significant contribution of PZC value and wettability of the catalysts. *Journal of Environmental Chemical Engineering* **2021**, 106173.
36. Zhao, L.; Ma, J.; Sun, Z.; Zhai, X., Mechanism of Influence of Initial pH on the Degradation of Nitrobenzene in Aqueous Solution by Ceramic Honeycomb Catalytic Ozonation. *Environmental Science & Technology* **2008,** *42*, (11), 4002-4007.
37. Zhao, L.; Sun, Z.; Ma, J.; Liu, H., Enhancement Mechanism of Heterogeneous Catalytic Ozonation by Cordierite-Supported Copper for the Degradation of Nitrobenzene in Aqueous Solution. *Environmental Science & Technology* **2009,** *43*, (6), 2047-2053.
38. Qi, F.; Xu, B.; Chen, Z.; Ma, J., Catalytic Ozonation for Degradation of 2, 4, 6 - Trichloroanisole in Drinking Water in the Presence of γ - AlOOH. *Water environment research* **2009,** *81*, (6), 592-597.
39. Yuan, L.; Shen, J.; Chen, Z.; Guan, X., Role of Fe/pumice composition and structure in promoting ozonation reactions. *Applied Catalysis B: Environmental* **2016,** *180*, 707-714.
40. Zhao, L.; Sun, Z.; Ma, J., Novel relationship between hydroxyl radical initiation and surface group of ceramic honeycomb supported metals for the catalytic ozonation of nitrobenzene in aqueous solution. *Environmental Science & Technology* **2009,** *43*, (11), 4157-4163.
41. Li, W.; Lu, X.; Xu, K.; Qu, J.; Qiang, Z., Cerium incorporated MCM-48 (Ce-MCM-48) as a catalyst to inhibit bromate formation during ozonation of bromide-containing water: Efficacy and mechanism. *Water research* **2015,** *86*, 2-8.
42. Byun, S.; Davies, S. H.; Alpatova, A. L.; Corneal, L. M.; Baumann, M. J.; Tarabara, V. V.; Masten, S. J., Mn oxide coated catalytic membranes for a hybrid ozonation–membrane filtration: Comparison of Ti, Fe and Mn oxide coated membranes for water quality. *Water Research* **2011,** *45*, (1), 163-170.
43. Wang, J.; Bai, Z., Fe-based catalysts for heterogeneous catalytic ozonation of emerging contaminants in water and wastewater. *Chemical Engineering Journal* **2017,** *312*, 79-98.
44. Bulanin, K.; Lavalley, J.; Tsyganenko, A., IR spectra of adsorbed ozone. *Colloids and Surfaces A: Physicochemical and Engineering Aspects* **1995,** *101*, (2-3), 153-158.
45. Alejandro-Martín, S.; Valdés, H.; Manero, M.-H.; Zaror, C. A., Catalytic Ozonation of Toluene Using Chilean Natural Zeolite: The Key Role of Brønsted and Lewis Acid Sites. *Catalysts* **2018,** *8*, (5), 211.
46. Yu, D.; Wang, L.; Yang, T.; Yang, G.; Wang, D.; Ni, H.; Wu, M., Tuning Lewis acidity of iron-based metal-organic frameworks for enhanced catalytic ozonation. *Chemical Engineering Journal* **2021,** *404*, 127075.

47. Bing, J.; Hu, C.; Nie, Y.; Yang, M.; Qu, J., Mechanism of catalytic ozonation in Fe_2O_3/Al_2O_3@SBA-15 aqueous suspension for destruction of ibuprofen. *Environmental Science & Technology* **2015,** *49*, (3), 1690-1697.
48. Yan, L.; Bing, J.; Wu, H., The behavior of ozone on different iron oxides surface sites in water. *Scientific reports* **2019,** *9*, (1), 1-10.
49. Yang, L.; Hu, C.; Nie, Y.; Qu, J., Surface acidity and reactivity of *β*-FeOOH/Al_2O_3 for pharmaceuticals degradation with ozone: In situ ATR-FTIR studies. *Applied Catalysis B: Environmental* **2010,** *97*, (3), 340-346.
50. Esmailpour, A. A.; Moradi, S.; Yun, J.; Scott, J.; Amal, R., Promoting surface oxygen vacancies on ceria via light pretreatment to enhance catalytic ozonation. *Catalysis Science & Technology* **2019,** *9*, (21), 5979-5990.
51. Afzal, S.; Quan, X.; Lu, S. J. A. C. B. E., Catalytic performance and an insight into the mechanism of CeO_2 nanocrystals with different exposed facets in catalytic ozonation of *p*-nitrophenol. **2019,** *248*, 526-537.
52. Wang, Y.; Chen, L.; Cao, H.; Chi, Z.; Chen, C.; Duan, X.; Xie, Y.; Qi, F.; Song, W.; Liu, J.; Wang, S., Role of oxygen vacancies and Mn sites in hierarchical $Mn_2O_3/LaMnO_{3-\delta}$ perovskite composites for aqueous organic pollutants decontamination. *Applied Catalysis B: Environmental* **2019,** *245*, 546-554.
53. Yan, P.; Shen, J.; Zhou, Y.; Yuan, L.; Kang, J.; Wang, S.; Chen, Z., Interface mechanism of catalytic ozonation in an α-Fe0.9Mn0.1OOH aqueous suspension for the removal of iohexol. *Applied Catalysis B: Environmental* **2020,** *277*, 119055.
54. Nawaz, F.; Cao, H.; Xie, Y.; Xiao, J.; Chen, Y.; Ghazi, Z. A., Selection of active phase of MnO_2 for catalytic ozonation of 4-nitrophenol. *Chemosphere* **2017,** *168*, 1457-1466.
55. Zhang, L. H.; Zhou, J.; Liu, Z. Q.; Guo, J. B., Mesoporous CeO_2 Catalyst Synthesized by Using Cellulose as Template for the Ozonation of Phenol. *Ozone-Sci. Eng.* **2019,** *41*, (2), 166-174.
56. Lee, W. J.; Bao, Y.; Hu, X.; Lim, T.-T., Hybrid Catalytic Ozonation-Membrane Filtration Process with CeOx and MnOx Impregnated Catalytic Ceramic Membranes for Micropollutants Degradation. *Chemical Engineering Journal* **2019**.
57. Ren, Y.; Dong, Q.; Feng, J.; Ma, J.; Wen, Q.; Zhang, M., Magnetic porous ferrospinel $NiFe_2O_4$: A novel ozonation catalyst with strong catalytic property for degradation of di-n-butyl phthalate and convenient separation from water. *Journal of Colloid and Interface Science* **2012,** *382*, (1), 90-96.
58. Pines, D. S.; Reckhow, D. A., Effect of dissolved cobalt (II) on the ozonation of oxalic acid. *Environmental science & technology* **2002,** *36*, (19), 4046-4051.
59. Liu, Y.; Wu, D.; Peng, S.; Feng, Y.; Liu, Z., Enhanced mineralization of dimethyl phthalate by heterogeneous ozonation over nanostructured Cu-Fe-O surfaces: Synergistic effect and radical chain reactions. *Separation and Purification Technology* **2019,** *209*, 588-597.
60. Oulton, R.; Haase, J. P.; Kaalberg, S.; Redmond, C. T.; Nalbandian, M. J.; Cwiertny, D. M., Hydroxyl radical formation during ozonation of multiwalled carbon nanotubes: performance optimization and demonstration of a reactive CNT filter. *Environmental science & technology* **2015,** *49*, (6), 3687-3697.
61. Wepasnick, K. A.; Smith, B. A.; Schrote, K. E.; Wilson, H. K.; Diegelmann, S. R.; Fairbrother, D. H., Surface and structural characterization of multi-walled carbon nanotubes following different oxidative treatments. *Carbon* **2011,** *49*, (1), 24-36.
62. Tessmer, C. H.; Vidic, R. D.; Uranowski, L. J., Impact of Oxygen-Containing Surface Functional Groups on Activated Carbon Adsorption of Phenols. *Environmental Science & Technology* **1997,** *31*, (7), 1872-1878.

63. Kasprzyk-Hordern, B.; Ziółek, M.; Nawrocki, J., Catalytic ozonation and methods of enhancing molecular ozone reactions in water treatment. *Applied Catalysis B: Environmental* **2003,** *46*, (4), 639-669.
64. Rivera-Utrilla, J.; Sánchez-Polo, M., Ozonation of 1, 3, 6-naphthalenetrisulphonic acid catalysed by activated carbon in aqueous phase. *Applied Catalysis B: Environmental* **2002,** *39*, (4), 319-329.
65. Qu, R.; Xu, B.; Meng, L.; Wang, L.; Wang, Z., Ozonation of indigo enhanced by carboxylated carbon nanotubes: Performance optimization, degradation products, reaction mechanism and toxicity evaluation. *Water Research* **2015,** *68*, 316-327.
66. Gonçalves, A. G.; Figueiredo, J. L.; Órfão, J. J. M.; Pereira, M. F. R., Influence of the surface chemistry of multi-walled carbon nanotubes on their activity as ozonation catalysts. *Carbon* **2010,** *48*, (15), 4369-4381.
67. Liu, Z.-Q.; Ma, J.; Cui, Y.-H.; Zhao, L.; Zhang, B.-P., Influence of different heat treatments on the surface properties and catalytic performance of carbon nanotube in ozonation. *Applied Catalysis B: Environmental* **2010,** *101*, (1-2), 74-80.
68. Morales-Lara, F.; Pérez-Mendoza, M. J.; Altmajer-Vaz, D.; García-Román, M.; Melguizo, M.; López-Garzón, F. J.; Domingo-García, M., Functionalization of multiwall carbon nanotubes by ozone at basic pH. Comparison with oxygen plasma and ozone in gas phase. *The Journal of Physical Chemistry C* **2013,** *117*, (22), 11647-11655.
69. Ouyang, C.; Wei, K.; Huang, X.; Zhang, X., Bifunctional Fe for Induced Graphitization and Catalytic Ozonation Based on a Fe/N-Doped Carbon-Al_2O_3 Framework: Theoretical Calculations Guided Catalyst Design and Optimization. *Environmental Science & Technology* **2021**.
70. Jothinathan, L.; Hu, J., Kinetic evaluation of graphene oxide based heterogenous catalytic ozonation for the removal of ibuprofen. *Water Research* **2018,** *134*, 63-73.
71. Bai, Z.; Yang, Q.; Wang, J., Catalytic ozonation of dimethyl phthalate using Fe_3O_4/multi-wall carbon nanotubes. *Environ. Technol.* **2017,** *38*, (16), 2048-2057.
72. Rezaei, F.; Moussavi, G.; Bakhtiari, A. R.; Yamini, Y., Toluene removal from waste air stream by the catalytic ozonation process with MgO/GAC composite as catalyst. *Journal of hazardous materials* **2016,** *306*, 348-358.
73. Fan, X.; Restivo, J.; Órfão, J. J. M.; Pereira, M. F. R.; Lapkin, A. A., The role of multiwalled carbon nanotubes (MWCNTs) in the catalytic ozonation of atrazine. *Chemical Engineering Journal* **2014,** *241*, 66-76.
74. Wei, K.; Cao, X.; Gu, W.; Liang, P.; Huang, X.; Zhang, X., Ni-induced C-Al_2O_3-framework (NiCAF) supported core-multishell catalysts for efficient catalytic ozonation: A Structure-to-performance study. *Environmental Science & Technology* **2019,** *53*, (12), 6917-6926.
75. Yuan, L.; Shen, J.; Yan, P.; Chen, Z., Interface mechanisms of catalytic ozonation with amorphous iron silicate for removal of 4-chloronitrobenzene in aqueous solution. *Environmental Science & Technology* **2018,** *53*, (2), 1429-1434.
76. Fujita, H.; Izumi, J.; Sagehashi, M.; Fujii, T.; Sakoda, A., Adsorption and decomposition of water-dissolved ozone on high silica zeolites. *Water Research* **2004,** *38*, (1), 159-165.
77. Tizaoui, C.; Slater, M., Uses of ozone in a three-phase system for water treatment: ozone adsorption. *Ozone Science & Engineering* **2003,** *25*, (4), 315-322.
78. Kusuda, A.; Kitayama, M.; Ohta, Y., Catalytic activities of zeolite compounds for decomposing aqueous ozone. *Journal of Environmental Sciences* **2013,** *25*, S141-S145.

79. Ikhlaq, A.; Waheed, S.; Joya, K. S.; Kazmi, M., Catalytic ozonation of paracetamol on zeolite A: Non-radical mechanism. *Catalysis Communications* **2018,** *112*, 15-20.
80. Ikhlaq, A.; Brown, D. R.; Kasprzyk-Hordern, B., Mechanisms of catalytic ozonation on alumina and zeolites in water: Formation of hydroxyl radicals. *Applied Catalysis B: Environmental* **2012,** *123-124*, (Supplement C), 94-106.
81. Ikhlaq, A.; Brown, D. R.; Kasprzyk-Hordern, B., Mechanisms of catalytic ozonation: An investigation into superoxide ion radical and hydrogen peroxide formation during catalytic ozonation on alumina and zeolites in water. *Applied Catalysis B: Environmental* **2013,** *129*, (Supplement C), 437-449.
82. Zhang, T.; Croue, J.-P., Catalytic ozonation not relying on hydroxyl radical oxidation: a selective and competitive reaction process related to metal–carboxylate complexes. *Applied Catalysis B: Environmental* **2014,** *144*, 831-839.
83. Pines, D. S.; Reckhow, D. A., Solid phase catalytic ozonation process for the destruction of a model pollutant. *Ozone: Science & Engineering* **2003,** *25*, (1), 25-39.
84. Blesa, M. A.; Weisz, A. D.; Morando, P. J.; Salfity, J. A.; Magaz, G.; Regazzoni, A. E., The interaction of metal oxide surfaces with complexing agents dissolved in water. *Coordination Chemistry Reviews* **2000,** *196*, (1), 31-63.
85. Wu, J.; Ma, L.; Chen, Y.; Cheng, Y.; Liu, Y.; Zha, X., Catalytic ozonation of organic pollutants from bio-treated dyeing and finishing wastewater using recycled waste iron shavings as a catalyst: removal and pathways. *Water research* **2016,** *92*, 140-148.
86. Guo, Y.; Zhang, Y.; Yu, G.; Wang, Y., Revisiting the role of reactive oxygen species for pollutant abatement during catalytic ozonation: The probe approach versus the scavenger approach. *Applied Catalysis B: Environmental* **2021,** *280*, 119418.
87. Park, J.-S.; Choi, H.; Cho, J., Kinetic decomposition of ozone and *para*-chlorobenzoic acid (*p*CBA) during catalytic ozonation. *Water Research* **2004,** *38*, (9), 2285-2292.
88. Park, H.; Kim, Y.; An, B.; Choi, H., Characterization of natural organic matter treated by iron oxide nanoparticle incorporated ceramic membrane-ozonation process. *Water Research* **2012,** *46*, (18), 5861---5870.
89. Elovitz, M. S.; von Gunten, U., Hydroxyl Radical/Ozone Ratios During Ozonation Processes. I. The Rct Concept. *Ozone: Science & Engineering* **1999,** *21*, (3), 239-260.
90. Yong, E. L.; Lin, Y.-P., Incorporation of initiation, promotion and inhibition in the Rct concept and its application in determining the initiation and inhibition capacities of natural water in ozonation. *Water Research* **2012,** *46*, (6), 1990-1998.
91. Pi, Y.; Schumacher, J.; Jekel, M., Decomposition of aqueous ozone in the presence of aromatic organic solutes. *Water Research* **2005,** *39*, (1), 83-88.
92. Davies, M. J., Detection and characterisation of radicals using electron paramagnetic resonance (EPR) spin trapping and related methods. *Methods* **2016,** *109*, 21-30.
93. Wang, Y.; Chen, L.; Chen, C.; Xi, J.; Cao, H.; Duan, X.; Xie, Y.; Song, W.; Wang, S., Occurrence of both hydroxyl radical and surface oxidation pathways in N-doped layered nanocarbons for aqueous catalytic ozonation. *Applied Catalysis B: Environmental* **2019,** *254*, 283-291.
94. Riebel, A. H.; Erickson, R. E.; Abshire, C. J.; Bailey, P. S., Ozonation of carbon-nitrogen double bonds. I. Nucleophilic attack of ozone1. *Journal of the American Chemical Society* **1960,** *82*, (7), 1801-1807.

95. Wang, Y.; Ren, N.; Xi, J.; Liu, Y.; Kong, T.; Chen, C.; Xie, Y.; Duan, X.; Wang, S., Mechanistic Investigations of the Pyridinic N–Co Structures in Co Embedded N-Doped Carbon Nanotubes for Catalytic Ozonation. *ACS ES&T Engineering* **2020**.
96. Wang, Y.; Xie, Y.; Sun, H.; Xiao, J.; Cao, H.; Wang, S., Efficient catalytic ozonation over reduced graphene oxide for *p*-hydroxylbenzoic acid (PHBA) destruction: active site and mechanism. *ACS Applied Materials & Interfaces* **2016,** *8*, (15), 9710-9720.
97. Nawaz, F.; Xie, Y.; Cao, H.; Xiao, J.; Zhang, X.; Li, M.; Duan, F., Catalytic ozonation of 4-nitrophenol over an mesoporous α-MnO_2 with resistance to leaching. *Catalysis Today* **2015,** *258*, 595-601.
98. Bielski, B. H. J.; Cabelli, D. E.; Arudi, R. L.; Ross, A. B., Reactivity of $HO_2^{\bullet}/O_2^{\bullet-}$ radicals in aqueous-solution. *Journal of Physical and Chemical Reference Data* **1985,** *14*, (4), 1041-1100.
99. Cory, R. M.; McNeill, K.; Cotner, J. P.; Amado, A.; Purcell, J. M.; Marshall, A. G., Singlet Oxygen in the Coupled Photochemical and Biochemical Oxidation of Dissolved Organic Matter. *Environmental Science & Technology* **2010,** *44*, (10), 3683-3689.
100. Betterton, E. A.; Craig, D., Kinetics and mechanism of the reaction of azide with ozone in aqueous solution. *Journal of the Air & Waste Management Association* **1999,** *49*, (11), 1347-1354.
101. Salla, J. S.; Padoin, N.; Amorim, S. M.; Li Puma, G.; Moreira, R. F. P. M., Humic acids adsorption and decomposition on Mn_2O_3 and α-Al_2O_3 nanoparticles in aqueous suspensions in the presence of ozone. *Journal of Environmental Chemical Engineering* **2020,** *8*, (2), 102780.
102. Valdés, H.; Zaror, C. A., Heterogeneous and homogeneous catalytic ozonation of benzothiazole promoted by activated carbon: Kinetic approach. *Chemosphere* **2006,** *65*, (7), 1131-1136.
103. Lim, H.-N.; Choi, H.; Hwang, T.-M.; Kang, J.-W., Characterization of ozone decomposition in a soil slurry: kinetics and mechanism. *Water research* **2002,** *36*, (1), 219-229.
104. Kummert, R.; Stumm, W., The surface complexation of organic acids on hydrous γ-Al2O3. *Journal of Colloid and Interface Science* **1980,** *75*, (2), 373-385.
105. Kosmulski, M., *Chemical properties of material surfaces*. CRC press: 2001; Vol. 102.
106. Yuan, Y.; Zhang, H.; Pan, G., Flocculation of cyanobacterial cells using coal fly ash modified chitosan. *Water Research* **2016,** *97*, 11-18.
107. Bader, H.; Hoigné, J., Determination of ozone in water by the indigo method. *Water Research* **1981,** *15*, (4), 449-456.
108. He, D.; Ma, J.; Collins, R. N.; Waite, T. D., Effect of structural transformation of nanoparticulate zero-valent iron on generation of reactive oxygen species. *Environmental Science & Technology* **2016,** *50*, (7), 3820-3828.
109. Ma, J. X.; He, D.; Tang, W. W.; Kovalsky, P.; He, C.; Zhang, C. Y.; Waite, T. D., Development of Redox-Active Flow Electrodes for High-Performance Capacitive Deionization. *Environmental Science & Technology* **2016,** *50*, (24), 13495-13501.
110. Ianni, J. C., Kintecus Version 6.80. www.kintecus.com **2020**.
111. Yuan, Y.; Xing, G.; Garg, S.; Ma, J.; Kong, X.; Dai, P.; Waite, T. D., Mechanistic insights into the catalytic ozonation process using iron oxide-impregnated activated carbon. *Water Research* **2020,** *177*, 115785.
112. Janknecht, P.; Wilderer, P.; Picard, C.; Larbot, A., Ozone–water contacting by ceramic membranes. *Separation and Purification Technology* **2001,** *25*, (1-3), 341-346.

113. Nawrocki, J., Catalytic ozonation in water: controversies and questions. Discussion paper. *Applied Catalysis B: Environmental* **2013,** *142*, 465-471.
114. Zhang, S.; Quan, X.; Wang, D., Catalytic ozonation in arrayed zinc oxide nanotubes as highly efficient mini-column catalyst reactors (MCRs): augmentation of hydroxyl radical exposure. *Environmental Science & Technology* **2018,** *52*, (15), 8701-8711.
115. Sánchez-Polo, M. v.; Von Gunten, U.; Rivera-Utrilla, J., Efficiency of activated carbon to transform ozone into OH radicals: influence of operational parameters. *Water research* **2005,** *39*, (14), 3189-3198.
116. Ikhlaq, A.; Brown, D. R.; Kasprzyk-Hordern, B., Mechanisms of catalytic ozonation on alumina and zeolites in water: formation of hydroxyl radicals. *Applied Catalysis B: Environmental* **2012,** *123*, 94-106.
117. Beltrán, F. J.; García-Araya, J. F.; Giráldez, I., Gallic acid water ozonation using activated carbon. *Applied Catalysis B: Environmental* **2006,** *63*, (3-4), 249-259.
118. Biernacki, W.; Fijołek, L.; Nawrocki, J., Dissolved ozone decomposition in presence of activated carbon at low pH: how experimental parameters affect observed kinetics of the process. *Ozone: Science & Engineering* **2019,** *41*, (4), 296-311.
119. Fijołek, L.; Malaika, A.; Biernacki, W.; Nawrocki, J., H_2O_2 Generation during carbon ozonation – factors influencing the process and their implications. *Ozone: Science & Engineering* **2019,** *41*, (2), 128-136.
120. Gao, G.; Shen, J.; Chu, W.; Chen, Z.; Yuan, L., Mechanism of enhanced diclofenac mineralization by catalytic ozonation over iron silicate-loaded pumice. *Separation and Purification Technology* **2017,** *173*, 55-62.
121. Ernst, M.; Lurot, F.; Schrotter, J. C., Catalytic ozonation of refractory organic model compounds in aqueous solution by aluminum oxide. *Appl. Catal. B-Environ.* **2004,** *47*, (1), 15-25.
122. Zhong, X.; Cui, C.; Yu, S., Identification of Oxidation Intermediates in Humic Acid Oxidation. *Ozone: Science & Engineering* **2018,** *40*, (2), 93-104.
123. Garoma, T.; Gurol, M. D., Modeling aqueous ozone/UV process using oxalic acid as probe chemical. *Environmental Science & Technology* **2005,** *39*, (20), 7964-7969.
124. Flyunt, R.; Schuchmann, M. N.; von Sonntag, C., A common carbanion intermediate in the recombination and proton-catalysed disproportionation of the carboxyl radical anion, $CO_2^{\bullet-}$, in aqueous solution. *Chemistry–A European Journal* **2001,** *7*, (4), 796-799.
125. Kuo, C.-Y., Improved application of ion chromatographic determination of carboxylic acids in ozonated drinking water. *Journal of Chromatography A* **1998,** *804*, (1-2), 265-272.
126. Beltrán, F. J.; Rivas, J.; Alvarez, P.; Montero-de-Espinosa, R., Kinetics of heterogeneous catalytic ozone decomposition in water on an activated carbon. *Ozone: science & engineering* **2002,** *24*, (4), 227-237.
127. Nawrocki, J.; Fijołek, L., Catalytic ozonation—Effect of carbon contaminants on the process of ozone decomposition. *Applied Catalysis B: Environmental* **2013,** *142-143*, 307-314.
128. Sánchez-Polo, M.; Rivera-Utrilla, J.; Von Gunten, U., Metal-doped carbon aerogels as catalysts during ozonation processes in aqueous solutions. *Water research* **2006,** *40*, (18), 3375-3384.
129. Faria, P.; Órfão, J.; Pereira, M., Activated carbon catalytic ozonation of oxamic and oxalic acids. *Applied Catalysis B: Environmental* **2008,** *79*, (3), 237-243.

130. Beltrán, F. J.; Rivas, F. J.; Montero-de-Espinosa, R., Ozone-enhanced oxidation of oxalic acid in water with cobalt catalysts. 2. Heterogeneous catalytic ozonation. *Industrial & engineering chemistry research* **2003,** *42*, (14), 3218-3224.
131. Ferre-Aracil, J.; Cardona, S. C.; Navarro-Laboulais, J., Kinetic Study of Ozone Decay in Homogeneous Phosphate-Buffered Medium. *Ozone: Science & Engineering* **2015,** *37*, (4), 330-342.
132. Ianni, J. C., Enzyme chemical kinetics and equilibrium software. **2003**.
133. Aghaeinejad-Meybodi, A.; Ebadi, A.; Shafiei, S.; Khataee, A.; Kiadehi, A. D., Degradation of Fluoxetine using catalytic ozonation in aqueous media in the presence of nano-γ-alumina catalyst: Experimental, modeling and optimization study. *Separation and Purification Technology* **2019,** *211*, 551-563.
134. Kiadehi, A. D.; Ebadi, A.; Aghaeinejad-Meybodi, A., Removal of methyl *tert*-butyl ether (MTBE) from aqueous medium in the presence of nano-perfluorooctyl alumina (PFOAL): Experimental study of adsorption and catalytic ozonation processes. *Separation and Purification Technology* **2017,** *182*, 238-246.
135. Mitchell, M. B.; Sheinker, V. N.; Cox, W. W., Room temperature reaction of ozone and dimethyl methylphosphonate (DMMP) on alumina-supported iron oxide. *The Journal of Physical Chemistry C* **2007,** *111*, (26), 9417-9426.
136. Gardoni, D.; Vailati, A.; Canziani, R., Decay of ozone in water: a review. *Ozone: Science & Engineering* **2012,** *34*, (4), 233-242.
137. Bezbarua, B. K.; Reckhow, D. A., Modification of the standard neutral ozone decomposition model. *Ozone: science & engineering* **2004,** *26*, (4), 345-357.
138. Logemann, F. P.; Annee, J. H. J., Water treatment with a fixed bed catalytic ozonation process. *Water science and technology* **1997,** *35*, (4), 353.
139. Sui, M.; Sheng, L.; Lu, K.; Tian, F., FeOOH catalytic ozonation of oxalic acid and the effect of phosphate binding on its catalytic activity. *Applied Catalysis B: Environmental* **2010,** *96*, (1-2), 94-100.
140. Reisz, E.; Fischbacher, A.; Naumov, S.; von Sonntag, C.; Schmidt, T. C., Hydride transfer: a dominating reaction of ozone with tertiary butanol and formate ion in aqueous solution. *Ozone: Science & Engineering* **2014,** *36*, (6), 532-539.
141. Buxton, G. V.; Greenstock, C. L.; Helman, W. P.; Ross, A. B., Critical review of rate constants for reactions of hydrated electrons, hydrogen atoms and hydroxyl radicals ($HO^{\bullet}/O^{\bullet-}$ in aqueous solution. *Journal of Physical and Chemical Reference Data* **1988,** *17*, (2), 513-886.
142. Jayson, G.; Parsons, B.; Swallow, A. J., Some simple, highly reactive, inorganic chlorine derivatives in aqueous solution. Their formation using pulses of radiation and their role in the mechanism of the Fricke dosimeter. *Journal of the Chemical Society, Faraday Transactions 1: Physical Chemistry in Condensed Phases* **1973,** *69*, 1597-1607.
143. Yapsakli, K.; Can, Z. S., Interaction of ozone with formic acid: A system which supresses the scavenging effect of HCO_3^-/CO_3^{2-}. *Water Qual. Res. J. Canada* **2004,** *39*, (2), 140-148.
144. Masten, S. J.; Galbraith, M. J.; Davies, S. H., Oxidation of 1, 3, 5 ‐ trichlorobenzene using advanced oxidation processes. *Ozone: science & engineering* **1996,** *18*, (6), 535-547.
145. Zhao, L.; Sun, Z.; Ma, J.; Liu, H., Influencing mechanism of bicarbonate on the catalytic ozonation of nitrobenzene in aqueous solution by ceramic honeycomb supported manganese. *Journal of Molecular Catalysis A: Chemical* **2010,** *322*, (1-2), 26-32.

146. Liu, J.-N.; Chen, Z.; Wu, Q.-Y.; Li, A.; Hu, H.-Y.; Yang, C., Ozone/graphene oxide catalytic oxidation: a novel method to degrade emerging organic contaminant N, N-diethyl-m-toluamide (DEET). *Scientific reports* **2016,** *6*, (1), 1-9.
147. Neta, P.; Huie, R. E.; Ross, A. B., Rate constants for reactions of inorganic radicals in aqueous solution. *Journal of Physical and Chemical Reference Data* **1988,** *17*, (3), 1027-1284.
148. Sun, Y.; Pignatello, J. J., Evidence for a surface dual hole-radical mechanism in the titanium dioxide photocatalytic oxidation of 2, 4-D. *Environmental science & technology* **1995,** *29*, (8), 2065-2072.
149. Yan, H.; Chen, W.; Liao, G.; Li, X.; Ma, S.; Li, L., Activity assessment of direct synthesized Fe-SBA-15 for catalytic ozonation of oxalic acid. *Separation and Purification Technology* **2016,** *159*, 1-6.
150. Masten, S. J., Ozonation of VOC's in the presence of humic acid and soils. **1991**.
151. Von Gunten, U., Ozonation of drinking water: Part I. Oxidation kinetics and product formation. *Water Research* **2003,** *37*, (7), 1443-1467.
152. Taube, H.; Bray, W. C., Chain reactions in aqueous solutions containing ozone, hydrogen peroxide and acid. *Journal of the American Chemical Society* **1940,** *62*, (12), 3357-3373.
153. Huie, R. E., NDRL/NIST Solution kinetics database on the Web. *Journal of Research (NIST JRES)* **2003,** *108*, (2).
154. Duesterberg, C. K.; Cooper, W. J.; Waite, T. D., Fenton-mediated oxidation in the presence and absence of oxygen. *Environmental Science & Technology* **2005,** *39*, (13), 5052-5058.
155. Acero, J. L.; von Gunten, U., Influence of carbonate on the ozone/hydrogen peroxide based advanced oxidation process for drinking water treatment. *Ozone: Science & Engineering* **2000,** *22*, (3), 305-328.
156. Vander Griend, D. A.; Golden, J. S.; Arrington, C. A., Kinetics and mechanism of chromate reduction with hydrogen peroxide in base. *Inorganic chemistry* **2002,** *41*, (26), 7042-7048.
157. Dickson, A.; Whitfield, M., An ion-association model for estimating acidity constants (at 25° C and 1 atm total pressure) in electrolyte mixtures related to seawater (ionic strength< 1 mol kg^{-1} H_2O). *Marine Chemistry* **1981,** *10*, (4), 315-333.
158. Morel, F. M.; Hering, J. G.; Hering, J. G., *Principles and applications of aquatic chemistry*. John Wiley & Sons, pp 157-232: 1993.
159. Andreozzi, R.; Insola, A.; Caprio, V.; Marotta, R.; Tufano, V., The use of manganese dioxide as a heterogeneous catalyst for oxalic acid ozonation in aqueous solution. *Applied Catalysis A: General* **1996,** *138*, (1), 75-81.
160. Karnik, B. S.; Davies, S. H.; Chen, K. C.; Jaglowski, D. R.; Baumann, M. J.; Masten, S., Effects of ozonation on the permeate flux of nanocrystalline ceramic membranes. *Water Research* **2005,** *39*, (4), 728-734.
161. Ma, J.; Sui, M.; Zhang, T.; Guan, C., Effect of pH on MnOx/GAC catalyzed ozonation for degradation of nitrobenzene. *Water Research* **2005,** *39*, (5), 779-786.
162. Karnik, B. S.; Davies, S. H.; Baumann, M. J.; Masten, S. J., Use of Salicylic Acid as a Model Compound to Investigate Hydroxyl Radical Reaction in an Ozonation–Membrane Filtration Hybrid Process. *Environmental Engineering Science* **2007,** *24*, (6), 852-860.
163. Masten, S. J.; Shu, M.; GALBRAITH, M. J.; DAVIES, S. H., Oxidation of chlorinated benzenes using advanced oxidation processes. *Hazardous waste and hazardous materials* **1996,** *13*, (2), 265-282.

164. Hsu, M. I.-Y.; Masten, S. J., The kinetics of the reaction of ozone with phenanthrene in unsaturated soils. *Environmental engineering science* **1997,** *14*, (4), 207-218.
165. Beltrán, F. J.; Rivas, F. J.; Montero-de-Espinosa, R., Iron type catalysts for the ozonation of oxalic acid in water. *Water Research* **2005,** *39*, (15), 3553-3564.
166. Zhang, T.; Li, C.; Ma, J.; Tian, H.; Qiang, Z., Surface hydroxyl groups of synthetic α-FeOOH in promoting OH generation from aqueous ozone: Property and activity relationship. *Applied Catalysis B: Environmental* **2008,** *82*, (1), 131-137.
167. Orge, C. A.; Órfão, J. J.; Pereira, M. F.; de Farias, A. M. D.; Neto, R. C. R.; Fraga, M. A., Ozonation of model organic compounds catalysed by nanostructured cerium oxides. *Applied Catalysis B: Environmental* **2011,** *103*, (1-2), 190-199.
168. Wang, J.; Quan, X.; Chen, S.; Yu, H.; Chen, Y., Performing homogeneous catalytic ozonation using heterogeneous Mn(II)-bonded oxidized carbon nanotube by self-driven pH variation induced reversible desorption and adsorption of Mn(II). *Environmental Science: Nano* **2019**.
169. Yang, W.; Wu, T., Investigation of Matrix Effects in Laboratory Studies of Catalytic Ozonation Processes. *Industrial & Engineering Chemistry Research* **2019,** *58*, (8), 3468-3477.
170. Mizuno, T.; Tsuno, H.; Yamada, H., Effect of inorganic carbon on ozone self-decomposition. *Ozone: Science and Engineering* **2007,** *29*, (1), 31-40.
171. Yuan, Y.; Garg, S.; Ma, J.; Waite, T. D., Kinetic Modeling-Assisted Mechanistic Understanding of the Catalytic Ozonation Process Using Cu–Al Layered Double Hydroxides and Copper Oxide Catalysts. *Environmental Science & Technology* **2021,** *55*, (19), 13274-13285.
172. Wang, R.-X.; Wen, T.; Wu, X.-L.; Xu, A.-W., Highly efficient removal of humic acid from aqueous solutions by Mg/Al layered double hydroxides–Fe_3O_4 nanocomposites. *RSC Advances* **2014,** *4*, (42), 21802-21809.
173. González, M. A.; Pavlovic, I.; Rojas-Delgado, R.; Barriga, C., Removal of Cu^{2+}, Pb^{2+} and Cd^{2+} by layered double hydroxide–humate hybrid. Sorbate and sorbent comparative studies. *Chemical Engineering Journal* **2014,** *254*, 605-611.
174. El Hassani, K.; Beakou, B. H.; Kalnina, D.; Oukani, E.; Anouar, A., Effect of morphological properties of layered double hydroxides on adsorption of azo dye methyl orange: a comparative study. *Applied Clay Science* **2017,** *140*, 124-131.
175. Lin, M.; Klarup, D. G., The effect of ozonation of humic acids on the removal efficiency of humic acid-copper complexes via filtration. *Ozone: Science & Engineering* **2001,** *23*, (1), 41-51.
176. Kefif, F.; Ezziane, K.; Bahmani, A.; Bettahar, N.; Mayouf, S., Evans Blue dye removal from contaminated water on calcined and uncalcined Cu-Al-CO_3 layered double hydroxide materials prepared by coprecipitation. *Bulletin of Materials Science* **2019,** *42*, (1), 1-11.
177. Haraketi, M.; Hosni, K.; Srasra, E., Intercalation behavior of salicylic acid into calcined Cu-Al-layered double hydroxides for a controlled release formulation. *Surface Engineering and Applied Electrochemistry* **2017,** *53*, (4), 360-370.
178. Behrens, M.; Kasatkin, I.; Kühl, S.; Weinberg, G., Phase-pure Cu, Zn, Al hydrotalcite-like materials as precursors for copper rich $Cu/ZnO/Al_2O_3$ catalysts. *Chemistry of Materials* **2009,** *22*, (2), 386-397.
179. Davranche, M.; Lacour, S.; Bordas, F.; Bollinger, J.-C., An Easy Determination of the Surface Chemical Properties of Simple and Natural Solids. *Journal of Chemical Education* **2003,** *80*, (1), 76.

180. Tamura, H.; Tanaka, A.; Mita, K.-y.; Furuichi, R., Surface hydroxyl site densities on metal oxides as a measure for the ion-exchange capacity. *Journal of Colloid and Interface Science* **1999,** *209*, (1), 225-231.
181. Savvina, P.; Apostolis, K.; Manassis, M.; Anastasios, Z., The role of metal ions on p-CBA degradation by catalytic ozonation. *Journal of Environmental Chemical Engineering* **2019,** *7*, (5), 103324.
182. Pi, Y.; Schumacher, J.; Jekel, M., The Use of *para*-Chlorobenzoic Acid (*p*CBA) as an Ozone/Hydroxyl Radical Probe Compound. *Ozone: Science & Engineering* **2005,** *27*, (6), 431-436.
183. Louit, G.; Foley, S.; Cabillic, J.; Coffigny, H.; Taran, F.; Valleix, A.; Renault, J. P.; Pin, S., The reaction of coumarin with the OH radical revisited: hydroxylation product analysis determined by fluorescence and chromatography. *Radiation Physics and Chemistry* **2005,** *72*, (2-3), 119-124.
184. Liu, Z.; Ma, R.; Ebina, Y.; Iyi, N.; Takada, K.; Sasaki, T., General synthesis and delamination of highly crystalline transition-metal-bearing layered double hydroxides. *Langmuir* **2007,** *23*, (2), 861-867.
185. Okamoto, K.; Iyi, N.; Sasaki, T., Factors affecting the crystal size of the MgAl-LDH (layered double hydroxide) prepared by using ammonia-releasing reagents. *Applied Clay Science* **2007,** *37*, (1), 23-31.
186. Ma, S.; Fan, C.; Du, L.; Huang, G.; Yang, X.; Tang, W.; Makita, Y.; Ooi, K., Intercalation of macrocyclic crown ether into well-crystallized LDH: formation of staging structure and secondary host− guest reaction. *Chemistry of Materials* **2009,** *21*, (15), 3602-3610.
187. Shang, S.; Hanif, A.; Sun, M.; Tian, Y.; Ok, Y. S.; Yu, I. K. M.; Tsang, D. C. W.; Gu, Q.; Shang, J., Novel M (Mg/Ni/Cu)-Al-CO_3 layered double hydroxides synthesized by aqueous miscible organic solvent treatment (AMOST) method for CO_2 capture. *Journal of Hazardous Materials* **2019,** *373*, 285-293.
188. Sable, S. S.; Ghute, P. P.; Fakhrnasova, D.; Mane, R. B.; Rode, C. V.; Medina, F.; Contreras, S., Catalytic ozonation of clofibric acid over copper-based catalysts: In situ ATR-IR studies. *Applied Catalysis B: Environmental* **2017,** *209*, 523-529.
189. Bulanin, K. M.; Lavalley, J. C.; Tsyganenko, A. A., IR spectra of adsorbed ozone. *Colloids and Surfaces A: Physicochemical and Engineering Aspects* **1995,** *101*, (2), 153-158.
190. Dhandapani, B.; Oyama, S. T., Gas phase ozone decomposition catalysts. *Applied Catalysis B: Environmental* **1997,** *11*, (2), 129-166.
191. Wu, J.; Su, T.; Jiang, Y.; Xie, X.; Qin, Z.; Ji, H., In situ DRIFTS study of O_3 adsorption on CaO, γ-Al_2O_3, CuO, α-Fe_2O_3 and ZnO at room temperature for the catalytic ozonation of cinnamaldehyde. *Applied Surface Science* **2017,** *412*, 290-305.
192. Xu, Y.; Lin, Z.; Zheng, Y.; Dacquin, J.-P.; Royer, S.; Zhang, H., Mechanism and kinetics of catalytic ozonation for elimination of organic compounds with spinel-type CuAl2O4 and its precursor. *Science of The Total Environment* **2019,** *651*, 2585-2596.
193. Sui, M.; Xing, S.; Sheng, L.; Huang, S.; Guo, H., Heterogeneous catalytic ozonation of ciprofloxacin in water with carbon nanotube supported manganese oxides as catalyst. *Journal of Hazardous Materials* **2012,** *227-228*, 227-236.
194. Qi, F.; Xu, B.; Chen, Z.; Ma, J.; Sun, D.; Zhang, L., Influence of aluminum oxides surface properties on catalyzed ozonation of 2, 4, 6-trichloroanisole. *Separation and Purification Technology* **2009,** *66*, (2), 405-410.

195. Afzal, S.; Quan, X.; Zhang, J., High surface area mesoporous nanocast $LaMO_3$ (M=Mn, Fe) perovskites for efficient catalytic ozonation and an insight into probable catalytic mechanism. *Applied Catalysis B: Environmental* **2017,** *206*, 692-703.
196. Li, Y.; Xu, J.; Qian, M.; Yu, J.; Pan, J.; Guan, B., The role of surface hydroxyl concentration on calcinated alumina in catalytic ozonation. *Environmental Science and Pollution Research* **2019,** *26*, (15), 15373-15380.
197. Wang, D.; Xu, H.; Ma, J.; Giannakis, S.; Lu, X.; Chi, H.; Song, S.; Qi, J., Enhanced mineralization of atrazine by surface induced hydroxyl radicals over light-weight granular mixed-quartz sands with ozone. *Water Research* **2019,** *149*, 136-148.
198. Kung, H. H., Chapter 5 Surface Acidity. In *Transition Metal Oxides Surface Chemistry and Catalysis*, Elsevier: 1989; Vol. 45, pp 72-90.
199. Yoon, T. H.; Johnson, S. B.; Musgrave, C. B.; Brown Jr, G. E., Adsorption of organic matter at mineral/water interfaces: I. ATR-FTIR spectroscopic and quantum chemical study of oxalate adsorbed at boehmite/water and corundum/water interfaces. *Geochimica et Cosmochimica Acta* **2004,** *68*, (22), 4505-4518.
200. Pocostales, J. P.; Sein, M. M.; Knolle, W.; von Sonntag, C.; Schmidt, T. C., Degradation of ozone-refractory organic phosphates in wastewater by ozone and ozone/hydrogen peroxide (peroxone): the role of ozone consumption by dissolved organic matter. *Environmental science & technology* **2010,** *44*, (21), 8248-8253.
201. Sehested, K.; Getoff, N.; Schwoerer, F.; Markovic, V.; Nielsen, S. O., Pulse radiolysis of oxalic acid and oxalates. *Journal of Physical Chemistry* **1971,** *75*, (6), 749-755.
202. Zafiriou, O. C.; Voelker, B. M.; Sedlak, D. L., Chemistry of the superoxide radical (O2-) in seawater: Reactions with inorganic copper complexes. *The Journal of Physical Chemistry A* **1998,** *102*, (28), 5693-5700.
203. Xing, L.; Xie, Y.; Cao, H.; Minakata, D.; Zhang, Y.; Crittenden, J. C., Activated carbon-enhanced ozonation of oxalate attributed to HO radical oxidation in bulk solution and surface oxidation: effects of the type and number of basic sites. *Chemical Engineering Journal* **2014,** *245*, 71-79.
204. Acero, J. L.; Stemmler, K.; von Gunten, U., Degradation Kinetics of Atrazine and Its Degradation Products with Ozone and OH Radicals: A Predictive Tool for Drinking Water Treatment. *Environmental Science & Technology* **2000,** *34*, (4), 591-597.
205. Dodd, M.; Buffle, M.; Von Gunten, U., Moiety-Specific Oxidation of antibacterial molecules by aqueous Ozone. Reaction kinetics and relevance to Ozone-based wastewater treatment. *Environmental Science & Technology* **2006,** *40*, (6), 1969-1977.
206. Lee, Y.; Gerrity, D.; Lee, M.; Bogeat, A.; Salhi, E.; Gamage, S.; Trenholm, R.; Wert, E.; Snyder, S., Prediction of micropollutant elimination during ozonation of municipal wastewater effluents: use of kinetic and water specific information. *Environmental Science & Technology* **2013,** *47*, (11).
207. Yuan, Y.; Mortazavi, M.; Garg, S.; Ma, J.; Waite, T. D., Comparison of Performance of Conventional Ozonation and Heterogeneous Catalytic Ozonation Processes in Phosphate- and Bicarbonate-Buffered Solutions. *ACS ES&T Engineering* **2022,** *2*, (2), 210-221.
208. Nöthe, T.; Fahlenkamp, H.; Sonntag, C. v., Ozonation of wastewater: rate of ozone consumption and hydroxyl radical yield. *Environmental Science & Technology* **2009,** *43*, (15), 5990-5995.

209. Staehelin, J.; Hoigne, J., Decomposition of ozone in water: rate of initiation by hydroxide ions and hydrogen peroxide. *Environmental Science & Technology* **1982,** *16*, (10), 676-681.
210. MA, J.; ZHAO, L., Degradation of nitrobenzene in aqueous solution by ozone-ceramic honeycomb. *Journal of Environmental Sciences* **2005,** *17*, (5), 716-721.
211. Benitez, F. J.; Real, F. J.; Acero, J. L.; Garcia, C., Kinetics of the transformation of phenyl-urea herbicides during ozonation of natural waters: Rate constants and model predictions. *Water Research* **2007,** *41*, (18), 4073-4084.
212. Jin, P.; Jin, X.; Bjerkelund, V. A.; Østerhus, S. W.; Wang, X. C.; Yang, L., A study on the reactivity characteristics of dissolved effluent organic matter (EfOM) from municipal wastewater treatment plant during ozonation. *Water Research* **2016,** *88*, 643-652.
213. Huber, M. M.; Canonica, S.; Park, G.-Y.; von Gunten, U., Oxidation of Pharmaceuticals during Ozonation and Advanced Oxidation Processes. *Environmental Science & Technology* **2003,** *37*, (5), 1016-1024.
214. Santana-Casiano, J. M.; González-Dávila, M.; Millero, F. J., Oxidation of nanomolar levels of Fe (II) with oxygen in natural waters. *Environmental science & technology* **2005,** *39*, (7), 2073-2079.
215. Neal, C.; House, W. A.; Down, K., An assessment of excess carbon dioxide partial pressures in natural waters based on pH and alkalinity measurements. *Science of the Total Environment* **1998,** *210*, 173-185.
216. Ma, J.; Graham, N. J., Degradation of atrazine by manganese-catalysed ozonation—influence of radical scavengers. *Water Research* **2000,** *34*, (15), 3822-3828.
217. Nemes, A.; Fabian, I.; Van Eldik, R., Kinetics and mechanism of the carbonate ion inhibited aqueous ozone decomposition. *The Journal of Physical Chemistry A* **2000,** *104*, (34), 7995-8000.
218. Gurol, M. D.; Singer, P. C., Kinetics of ozone decomposition: a dynamic approach. *Environmental science & technology* **1982,** *16*, (7), 377-383.
219. Fijołek, L.; Nawrocki, J. J. C., Phosphate helps to recover from scavenging effect of chloride in self-enhanced ozonation. **2018,** *212*, 802-810.
220. Morozov, P.; Ershov, B., The influence of phosphates on the decomposition of ozone in water: chain process inhibition. *Russian Journal of Physical Chemistry A* **2010,** *84*, (7), 1136-1140.
221. Pi, Y.; Ernst, M.; Schrotter, J.-C., Effect of phosphate buffer upon CuO/Al_2O_3 and Cu (II) catalyzed ozonation of oxalic acid solution. *Ozone Science & Engineering* **2003,** *25*, (5), 393-397.
222. Zhao, H.; Dong, Y.; Jiang, P.; Wang, G.; Zhang, J.; Li, K., An insight into the kinetics and interface sensitivity for catalytic ozonation: the case of nano-sized $NiFe_2O_4$. *Catalysis Science & Technology* **2014,** *4*, (2), 494-501.
223. Zhao, H.; Dong, Y.; Wang, G.; Jiang, P.; Zhang, J.; Wu, L.; Li, K., Novel magnetically separable nanomaterials for heterogeneous catalytic ozonation of phenol pollutant: $NiFe_2O_4$ and their performances. *Chemical Engineering Journal* **2013,** *219*, 295-302.
224. Lv, A.; Hu, C.; Nie, Y.; Qu, J., Catalytic ozonation of toxic pollutants over magnetic cobalt-doped Fe_3O_4 suspensions. *Applied Catalysis B: Environmental* **2012,** *117*, 246-252.
225. Chen, C.; Jia, N.; Song, K.; Zheng, X.; Lan, Y.; Li, Y., Sulfur-doped copper-yttrium bimetallic oxides: A novel and efficient ozonation catalyst for the degradation of aniline. *Separation and Purification Technology* **2019**, 116248.

226. Dong, Y. M.; Wu, L. N.; Wang, G. L.; Zhao, H.; Jiang, P. P.; Feng, C. Y., Synergistic Effect of Copper and Cobalt in Cu-Co-O Composite Nanocatalyst for Catalytic ozonation. *Bull. Korean Chem. Soc.* **2013,** *34*, (11), 3227-3232.
227. Zhang, H.; Ji, F.; Zhang, Y.; Pan, Z.; Lai, B., Catalytic ozonation of N, N-dimethylacetamide (DMAC) in aqueous solution using nanoscaled magnetic $CuFe_2O_4$. *Separation and Purification Technology* **2018,** *193*, 368-377.
228. Qi, F.; Chu, W.; Xu, B., Comparison of phenacetin degradation in aqueous solutions by catalytic ozonation with $CuFe_2O_4$ and its precursor: surface properties, intermediates and reaction mechanisms. *Chemical Engineering Journal* **2016,** *284*, 28-36.
229. Staehelin, J.; Hoigne, J., Decomposition of ozone in water in the presence of organic solutes acting as promoters and inhibitors of radical chain reactions. *Environmental Science & Technology* **1985,** *19*, (12), 1206-1213.
230. Mao, Y.; Guo, D.; Yao, W.; Wang, X.; Yang, H.; Xie, Y. F.; Komarneni, S.; Yu, G.; Wang, Y., Effects of conventional ozonation and electro-peroxone pretreatment of surface water on disinfection by-product formation during subsequent chlorination. *Water Research* **2018,** *130*, 322-332.
231. Beltrán, F. J.; Rivas, F. J.; Fernández, L. A.; Álvarez, P. M.; Montero-de-Espinosa, R., Kinetics of catalytic ozonation of oxalic acid in water with activated carbon. *Industrial & engineering chemistry research* **2002,** *41*, (25), 6510-6517.
232. Biń, A. K.; Machniewski, P.; Wołyniec, J.; Pieńczakowska, A., Modeling of Ozone Reaction with Benzaldehyde Incorporating Ozone Decomposition in Aqueous Solutions. *Ozone: Science & Engineering* **2013,** *35*, (6), 489-500.
233. Maruthamuthu, P.; Neta, P., Reactions of phosphate radicals with organic compounds. *The Journal of Physical Chemistry* **1977,** *81*, (17), 1622-1625.
234. Tian, S.-Q.; Qi, J.-Y.; Wang, Y.-P.; Liu, Y.-L.; Wang, L.; Ma, J., Heterogeneous catalytic ozonation of atrazine with Mn-loaded and Fe-loaded biochar. *Water Research* **2021**, 116860.
235. Yuan, Y.; Garg, S.; Wang, Y.; Li, W.; Chen, G.; Gao, M.; Zhong, J.; Wang, J.; Waite, T. D., Influence of salinity on the heterogeneous catalytic ozonation process: Implications to treatment of high salinity wastewater. *Journal of Hazardous Materials* **2022,** *423*, 127255.
236. Huang, Y.; Hou, X.; Liu, S.; Ni, J., Correspondence analysis of bio-refractory compounds degradation and microbiological community distribution in anaerobic filter for coking wastewater treatment. *Chemical Engineering Journal* **2016,** *304*, 864-872.
237. Wei, X.; Zhang, Z.; Fan, Q.; Yuan, X.; Guo, D., The effect of treatment stages on the coking wastewater hazardous compounds and their toxicity. *Journal of hazardous materials* **2012,** *239*, 135-141.
238. Gao, M., Research status of coal chemical high － concentrated wastewater treatment and degradation mechanism of characteristic organic pollutant. *Clean Coal Technology* **2020,** *26*, (4).
239. Liu, Z.; Huang, C.; Li, J.; Yang, J.; Qu, B.; Yang, S.; Cui, Y.; Yan, Y.; Sun, S.; Wu, X., Activated carbon catalytic ozonation of reverse osmosis concentrate after coagulation pretreatment from coal gasification wastewater reclamation for zero liquid discharge. *Journal of Cleaner Production* **2021,** *286*, 124951.
240. Liu, Z.; You, L.; Xiong, X.; Wang, Q.; Yan, Y.; Tu, J.; Cui, Y.; Li, X.; Wen, G.; Wu, X., Potential of the integration of coagulation and ozonation as a pretreatment of reverse osmosis concentrate from coal gasification wastewater reclamation. *Chemosphere* **2019,** *222*, 696-704.

241. Cheng, C.; Li, J.; Wen, Y.; Wang, J.; Jin, C.; Sun, C.; Wang, H.; Wei, H.; Yang, X., Deactivation mechanism of Fe/Al_2O_3 catalyst during the ozonation of reverse osmosis concentrates (ROCs): Effect of silicate. *Chemical Engineering Journal Advances* **2020,** *1*, 100003.
242. Yang, L.; Sheng, M.; Li, Y.; Xue, W.; Li, K.; Cao, G., A hybrid process of Fe-based catalytic ozonation and biodegradation for the treatment of industrial wastewater reverse osmosis concentrate. *Chemosphere* **2020,** *238*, 124639.
243. Levanov, A. V.; Isaikina, O. Y.; Gasanova, R. B.; Lunin, V. V., Solubility of ozone and kinetics of its decomposition in aqueous chloride solutions. *Industrial & Engineering Chemistry Research* **2018,** *57*, (43), 14355-14364.
244. Zhang, Y.; Li, L.; Pan, Z.; Zhu, Y.; Shao, Y.; Wang, Y.; Yu, K., Degradation of sulfamethoxazole by UV/persulfate in different water samples: influential factors, transformation products and toxicity. *Chemical Engineering Journal* **2020,** *379*, 122354.
245. Xu, Y.; Wu, Y.; Zhang, W.; Fan, X.; Wang, Y.; Zhang, H., Performance of artificial sweetener sucralose mineralization via UV/O_3 process: Kinetics, toxicity and intermediates. *Chemical Engineering Journal* **2018,** *353*, 626-634.
246. He, C.; Wang, J.; Wang, C.; Zhang, C.; Hou, P.; Xu, X., Catalytic ozonation of bio-treated coking wastewater in continuous pilot- and full-scale system: Efficiency, catalyst deactivation and in-situ regeneration. *Water Research* **2020,** *183*, 116090.
247. Fang, F.; Han, H., Effect of Catalytic Ozonation Coupling with Activated Carbon Adsorption on Organic Compounds Removal Treating RO Concentrate from Coal Gasification Wastewater. *Ozone: Science & Engineering* **2018**, 1-9.
248. Huang, X.; Cui, W.; Yu, J.; Lu, S.; Liao, X., Preparation of Mesoporous MnO_2 Catalysts with Different Morphologies for Catalytic Ozonation of Organic Compounds. *Catalysis Letters* **2021**, 1-10.
249. Moussavi, G.; Alizadeh, R., The integration of ozonation catalyzed with MgO nanocrystals and the biodegradation for the removal of phenol from saline wastewater. *Applied Catalysis B: Environmental* **2010,** *97*, (1-2), 160-167.
250. Yu, L.; Han, P.; Jin, H.; Wei, H.; Liu, W.; Ma, L.; Xu, C., Catalytic ozonation of three isomeric cresols in the presence of NaCl with nano-mesoporous β-molecular sieves. *Process Safety and Environmental Protection* **2019,** *129*, 63-73.
251. Ahmadi, M.; Kakavandi, B.; Jaafarzadeh, N.; Babaei, A. A., Catalytic ozonation of high saline petrochemical wastewater using PAC@FeIIFe$_2$IIIO$_4$: optimization, mechanisms and biodegradability studies. *Separation and Purification Technology* **2017,** *177*, 293-303.
252. Kong, X.; Gao, M.; Yuan, Y.; Li, W.; Liu, X.; Chen, G.; Ma, J.; Garg, S.; Waite, T. D., Application of ozonation to degradation of refractory organic matter present in membrane concentrates: A case study of the contribution of coal chemical wastewater treatment to minimizing liquid discharge. *Journal of Cleaner Production* **In review**.
253. Huber, S. A.; Balz, A.; Abert, M.; Pronk, W., Characterisation of aquatic humic and non-humic matter with size-exclusion chromatography–organic carbon detection–organic nitrogen detection (LC-OCD-OND). *Water research* **2011,** *45*, (2), 879-885.
254. Goslan, E. H.; Fearing, D. A.; Banks, J.; Wilson, D.; Hills, P.; Campbell, A. T.; Parsons, S. A., Seasonal variations in the disinfection by-product precursor profile of a reservoir water. *Journal of Water Supply: Research and Technology—AQUA* **2002,** *51*, (8), 475-482.
255. Malcolm, R. L.; MacCarthy, P., Quantitative evaluation of XAD-8 and XAD-4 resins used in tandem for removing organic solutes from water. *Environment International* **1992,** *18*, (6), 597-607.

256. Dorubet, D.; Mircea, C.; Astarastoaae, V.; Butnaru, E., Validation of a GC/HS method for ethanol quantitative analysis using as internal standard *tert*-butanol. *Farmacia* **2011,** *59*, (5), 721-728.
257. Ianni, J. C., Kintecus - Enzyme Chemical Kinetics and Equilibrium Software. **2003**.
258. Garoma, T.; Gurol, M. D., Degradation of *tert*-butyl alcohol in dilute aqueous solution by an O_3/UV process. *Environmental science & technology* **2004,** *38*, (19), 5246-5252.
259. Barazesh, J. M.; Prasse, C.; Sedlak, D. L., Electrochemical transformation of trace organic contaminants in the presence of halide and carbonate ions. *Environmental science & technology* **2016,** *50*, (18), 10143-10152.
260. Liu, Z.; Ma, J.; Cui, Y.; Zhao, L.; Zhang, B., Factors affecting the catalytic activity of multi-walled carbon nanotube for ozonation of oxalic acid. *Separation and Purification Technology* **2011,** *78*, (2), 147-153.
261. Zhang, K.; Parker, K. M., Halogen radical oxidants in natural and engineered aquatic systems. *Environmental science & technology* **2018,** *52*, (17), 9579-9594.
262. Razumovskii, S.; Konstantinova, M.; Grinevich, T.; Korovina, G.; Zaitsev, V. Y., Mechanism and kinetics of the reaction of ozone with sodium chloride in aqueous solutions. *Kinetics and Catalysis* **2010,** *51*, (4), 492-496.
263. Pham, A. N.; Xing, G.; Miller, C. J.; Waite, T. D., Fenton-like copper redox chemistry revisited: Hydrogen peroxide and superoxide mediation of copper-catalyzed oxidant production. *Journal of catalysis* **2013,** *301*, 54-64.
264. Xing, G.; Pham, A. N.; Miller, C. J.; Waite, T. D., pH-dependence of production of oxidants (Cu (III) and/or HO•) by copper-catalyzed decomposition of hydrogen peroxide under conditions typical of natural saline waters. *Geochimica et Cosmochimica Acta* **2018,** *232*, 30-47.
265. Buxton, G.; Sellers, R., Acid dissociation constant of the carboxyl radical. Pulse radiolysis studies of aqueous solutions of formic acid and sodium formate. *Journal of the Chemical Society, Faraday Transactions 1: Physical Chemistry in Condensed Phases* **1973,** *69*, 555-559.
266. Rischbieter, E.; Stein, H.; Schumpe, A., Ozone solubilities in water and aqueous salt solutions. *Journal of Chemical & Engineering Data* **2000,** *45*, (2), 338-340.
267. Liu, H.; Gao, Y.; Wang, J.; Ma, D.; Wang, Y.; Gao, B.; Yue, Q.; Xu, X., The application of UV/O_3 process on ciprofloxacin wastewater containing high salinity: Performance and its degradation mechanism. *Chemosphere* **2021,** *276*, 130220.
268. Panich, N.; Ershov, B.; Seliverstov, A.; Basiev, A., Ozone solubility in concentrated aqueous solutions of salts. *Russian Journal of Applied Chemistry* **2007,** *80*, (11), 1812-1815.
269. Wang, J.; Liu, H.; Ma, D.; Wang, Y.; Yao, G.; Yue, Q.; Gao, B.; Wang, S.; Xu, X., Degradation of organic pollutants by ultraviolet/ozone in high salinity condition: Non-radical pathway dominated by singlet oxygen. *Chemosphere* **2021,** *268*, 128796.
270. Pérez, A.; Poznyak, T.; Chairez, I.; Guzmán-Zavaleta, Z. J.; Alfaro-Ponce, M., Influence of sodium sulfate on the direct red 28 degradation by ozone in a wastewater recycling process: a stoichiometric and novel image analysis. *Ozone: Science & Engineering* **2020,** *42*, (5), 428-438.
271. Roth, J. A.; Sullivan, D. E., Solubility of ozone in water. *Industrial & Engineering Chemistry Fundamentals* **1981,** *20*, (2), 137-140.
272. Levanov, A.; Kuskov, I.; Antipenko, E.; Lunin, V., The solubility of ozone and kinetics of its chemical reactions in aqueous solutions of sodium chloride. *Russian Journal of Physical Chemistry A, Focus on Chemistry* **2008,** *82*, (12), 2045-2050.

273. Yeatts, L. R. B.; Taube, H., The kinetics of the reaction of ozone and chloride ion in acid aqueous solution. *Journal of the American Chemical Society* **1949,** *71*, (12), 4100-4105.
274. Baalousha, M.; Motelica-Heino, M.; Le Coustumer, P., Conformation and size of humic substances: effects of major cation concentration and type, pH, salinity, and residence time. *Colloids and surfaces A: physicochemical and engineering aspects* **2006,** *272*, (1-2), 48-55.
275. Lutze, H. V.; Kerlin, N.; Schmidt, T. C., Sulfate radical-based water treatment in presence of chloride: Formation of chlorate, inter-conversion of sulfate radicals into hydroxyl radicals and influence of bicarbonate. *Water Research* **2015,** *72*, 349-360.
276. Yan, P.; Shen, J.; Yuan, L.; Kang, J.; Wang, B.; Zhao, S.; Chen, Z., Catalytic ozonation by Si-doped α-Fe_2O_3 for the removal of nitrobenzene in aqueous solution. *Separation and Purification Technology* **2019,** *228*, 115766.
277. Feng, J.; Zhang, X.; Fu, J.; Chen, H., Catalytic ozonation of oxalic acid over rod-like ceria coated on activated carbon. *Catalysis Communications* **2018,** *110*, 28-32.
278. Liu, Y.; Wang, S.; Gong, W.; Chen, Z.; Liu, H.; Bu, Y.; Zhang, Y., Heterogeneous catalytic ozonation of *p*-chloronitrobenzene (*p*CNB) in water with iron silicate doped hydroxylation iron as catalyst. *Catalysis Communications* **2017,** *89*, 81-85.
279. Ikhlaq, A.; Brown, D. R.; Kasprzyk-Hordern, B., Catalytic ozonation for the removal of organic contaminants in water on alumina. *Applied Catalysis B: Environmental* **2015,** *165*, 408-418.
280. Guo, Y.; Xu, B.; Qi, F., A novel ceramic membrane coated with MnO_2–Co_3O_4 nanoparticles catalytic ozonation for benzophenone-3 degradation in aqueous solution: fabrication, characterization and performance. *Chemical Engineering Journal* **2016,** *287*, 381-389.
281. Yu, D.; Wu, M.; Hu, Q.; Wang, L.; Lv, C.; Zhang, L., Iron-based metal-organic frameworks as novel platforms for catalytic ozonation of organic pollutant: Efficiency and mechanism. *Journal of hazardous materials* **2019,** *367*, 456-464.
282. Sun, Z.; Zhao, L.; Liu, C.; Zhen, Y.; Ma, J., Catalytic Ozonation of Ketoprofen with In-situ N-doped Carbon: Novel Synergetic Mechanism of Hydroxyl Radical Oxidation and Intra-electron-transfer Non-radical Reaction. *Environmental Science & Technology* **2019**.
283. Gonçalves, A. G.; Órfão, J. J.; Pereira, M. F., Ceria dispersed on carbon materials for the catalytic ozonation of sulfamethoxazole. *Journal of Environmental Chemical Engineering* **2013,** *1*, (3), 260-269.
284. Qi, F.; Xu, B.; Zhao, L.; Chen, Z.; Zhang, L.; Sun, D.; Ma, J., Comparison of the efficiency and mechanism of catalytic ozonation of 2, 4, 6-trichloroanisole by iron and manganese modified bauxite. *Applied Catalysis B: Environmental* **2012,** *121*, 171-181.
285. Buxton, G. V.; Elliot, A. J., Rate constant for reaction of hydroxyl radicals with bicarbonate ions. *International Journal of Radiation Applications and Instrumentation. Part C. Radiation Physics and Chemistry* **1986,** *27*, (3), 241-243.
286. Leandri, V.; Gardner, J. M.; Jonsson, M., Coumarin as a quantitative probe for hydroxyl radical formation in heterogeneous photocatalysis. *The Journal of Physical Chemistry C* **2019,** *123*, (11), 6667-6674.
287. Nosaka, Y.; Nosaka, A. Y., Comment on “Coumarin as a Quantitative Probe for Hydroxyl Radical Formation in Heterogeneous Photocatalysis”. *The Journal of Physical Chemistry C* **2019**.

288. Buffle, M.-O.; von Gunten, U., Phenols and Amine Induced HO• Generation During the Initial Phase of Natural Water Ozonation. *Environmental Science & Technology* **2006,** *40*, (9), 3057-3063.
289. Han, S.-K.; Ichikawa, K.; Utsumi, H., Quantitative analysis for the enhancement of hydroxyl radical generation by phenols during ozonation of water. *Water Research* **1998,** *32*, (11), 3261-3266.
290. Zhang, F.; Wu, K.; Zhou, H.; Hu, Y.; Sergei, P.; Wu, H.; Wei, C., Ozonation of aqueous phenol catalyzed by biochar produced from sludge obtained in the treatment of coking wastewater. *Journal of Environmental management* **2018,** *224*, 376-386.
291. Wang, Y.; Yang, W.; Yin, X.; Liu, Y., The role of Mn-doping for catalytic ozonation of phenol using Mn/γ-Al2O3 nanocatalyst: performance and mechanism. *Journal of Environmental Chemical Engineering* **2016,** *4*, (3), 3415-3425.
292. Wu, J.; Rudy, K.; Spark, J., Oxidation of aqueous phenol by ozone and peroxidase. *Advances in Environmental Research* **2000,** *4*, (4), 339-346.
293. Caprio, V.; Insola, A.; Silvestre, A., The ozonation of glyoxylic acid in aqueous solution: chemical products and kinetics evolution. **1987**.
294. Simic, M.; Neta, P.; Hayon, E., Pulse radiolysis study of alcohols in aqueous solution. *The Journal of Physical Chemistry* **1969,** *73*, (11), 3794-3800.
295. Reisz, E.; Schmidt, W.; Schuchmann, H.-P.; von Sonntag, C., Photolysis of ozone in aqueous solutions in the presence of tertiary butanol. *Environmental science & technology* **2003,** *37*, (9), 1941-1948.
296. Can, Z. S.; Gurol, M., Formaldehyde formation during ozonation of drinking water. *Ozone: science & engineering* **2003,** *25*, (1), 41-51.
297. Orge, C.; Órfão, J.; Pereira, M., Composites of manganese oxide with carbon materials as catalysts for the ozonation of oxalic acid. *Journal of hazardous materials* **2012,** *213*, 133-139.
298. He, K.; Dong, Y. M.; Li, Z.; Yin, L.; Zhang, A. M.; Zheng, Y. C., Catalytic ozonation of phenol in water with natural brucite and magnesia. *Journal of hazardous materials* **2008,** *159*, (2-3), 587-592.
299. Xiong, F.; Graham, N. J., Rate constants for herbicide degradation by ozone. **1992**.
300. Hoigné, J., Inter-calibration of OH radical sources and water quality parameters. *Water Science and Technology* **1997,** *35*, (4), 1-8.
301. Buehler, R. E.; Staehelin, J.; Hoigné, J., Ozone decomposition in water studied by pulse radiolysis. 1. Perhydroxyl (HO_2)/hyperoxide (O_2-) and HO_3/O_3-as intermediates. *The Journal of Physical Chemistry* **1984,** *88*, (12), 2560-2564.
302. Guclu, K.; Kıbrıslıoğlu, G. l. a.; Ozyurek, M.; Apak, R., Development of a fluorescent probe for measurement of peroxyl radical scavenging activity in biological samples. *Journal of agricultural and food chemistry* **2014,** *62*, (8), 1839-1845.
303. von Sonntag, C.; Dowideit, P.; Fang, X.; Mertens, R.; Pan, X.; Schuchmann, M. N.; Schuchmann, H.-P., The fate of peroxyl radicals in aqueous solution. *Water Science and Technology* **1997,** *35*, (4), 9-15.
304. Bernat-Quesada, F.; Espinosa, J. C.; Barbera, V.; Alvaro, M.; Galimberti, M.; Navalon, S.; Garcia, H., Catalytic ozonation using edge-hydroxylated graphite-based materials. *ACS Sustainable Chemistry & Engineering* **2019,** *7*, (20), 17443-17452.
305. He, C.; Wang, Y.; Li, Z.; Huang, Y.; Liao, Y.; Xia, D.; Lee, S., Facet engineered α-MnO_2 for efficient catalytic ozonation of odor CH_3SH: oxygen vacancy-induced active centers and catalytic mechanism. *Environmental Science & Technology* **2020,** *54*, (19), 12771-12783.

306. He, Z.; Zhang, A.; Song, S.; Liu, Z.; Chen, J.; Xu, X.; Liu, W., γ-Al_2O_3 modified with praseodymium: an application in the heterogeneous catalytic ozonation of succinic acid in aqueous solution. *Industrial & engineering chemistry research* **2010,** *49*, (24), 12345-12351.
307. Beltran, F. J.; Rivas, F. J.; Montero-de-Espinosa, R., A TiO_2/Al_2O_3 catalyst to improve the ozonation of oxalic acid in water. *Applied Catalysis B: Environmental* **2004,** *47*, (2), 101-109.
308. Shen, T.; Zhang, X.; Lin, K.-Y. A.; Tong, S., Solid base Mg-doped ZnO for heterogeneous catalytic ozonation of isoniazid: Performance and mechanism. *Science of The Total Environment* **2020,** *703*, 134983.
309. Liu, D.; Wang, C.; Song, Y.; Wei, Y.; He, L.; Lan, B.; He, X.; Wang, J., Effective mineralization of quinoline and bio-treated coking wastewater by catalytic ozonation using $CuFe_2O_4$/Sepiolite catalyst: Efficiency and mechanism. *Chemosphere* **2019,** *227*, 647-656.
310. Ikhlaq, A.; Kasprzyk-Hordern, B., Catalytic ozonation of chlorinated VOCs on ZSM-5 zeolites and alumina: formation of chlorides. *Applied Catalysis B: Environmental* **2017,** *200*, 274-282.
311. Martins, R. C.; Quinta-Ferreira, R. M., Catalytic ozonation of phenolic acids over a Mn-Ce-O catalyst. *Appl. Catal. B-Environ.* **2009,** *90*, (1-2), 268-277.
312. Valdés, H.; Farfán, V. J.; Manoli, J. A.; Zaror, C. A., Catalytic ozone aqueous decomposition promoted by natural zeolite and volcanic sand. *Journal of Hazardous Materials* **2009,** *165*, (1), 915-922.
313. Dai, Q.; Zhang, Z.; Zhan, T.; Hu, Z.-T.; Chen, J., Catalytic Ozonation for the Degradation of 5-Sulfosalicylic Acid with Spinel-Type $ZnAl_2O_4$ Prepared by Hydrothermal, Sol–Gel, and Coprecipitation Methods: A Comparison Study. *ACS Omega* **2018,** *3*, (6), 6506-6512.
314. Xia, D.; Xu, W.; Wang, Y.; Yang, J.; Huang, Y.; Hu, L.; He, C.; Shu, D.; Leung, D. Y. C.; Pang, Z., Enhanced Performance and Conversion Pathway for Catalytic Ozonation of Methyl Mercaptan on Single-Atom Ag Deposited Three-Dimensional Ordered Mesoporous MnO2. *Environmental Science & Technology* **2018**.
315. Pelalak, R.; Alizadeh, R.; Ghareshabani, E., Enhanced heterogeneous catalytic ozonation of pharmaceutical pollutants using a novel nanostructure of iron-based mineral prepared via plasma technology: A comparative study. *Journal of Hazardous Materials* **2020**, 122269.
316. Zhang, H.; He, Y.; Lai, L.; Yao, G.; Lai, B., Catalytic ozonation of Bisphenol A in aqueous solution by Fe_3O_4–MnO_2 magnetic composites: Performance, transformation pathways and mechanism. *Separation and Purification Technology* **2020,** *245*, 116449.
317. Wei, X.; Shao, S.; Ding, X.; Jiao, W.; Liu, Y., Degradation of phenol with heterogeneous catalytic ozonation enhanced by high gravity technology. *Journal of Cleaner Production* **2020,** *248*, 119179.
318. Tong, S.-P.; Shi, R.; Zhang, H.; Ma, C.-a., Kinetics of Fe_3O_4–CoO/Al_2O_3 catalytic ozonation of the herbicide 2-(2, 4-dichlorophenoxy) propionic acid. *Journal of hazardous materials* **2011,** *185*, (1), 162-167.
319. Ye, G.; Luo, P.; Zhao, Y.; Qiu, G.; Hu, Y.; Preis, S.; Wei, C., Three-dimensional Co/Ni bimetallic organic frameworks for high-efficient catalytic ozonation of atrazine: Mechanism, effect parameters, and degradation pathways analysis. *Chemosphere* **2020,** *253*, 126767.
320. Beltrán, F. J.; Gómez-Serrano, V.; Durán, A., Degradation kinetics of *p*-nitrophenol ozonation in water. *Water Research* **1992,** *26*, (1), 9-17.